Effective Field Theory for Lepton Flavour Violation

Marco Ardu

THÈSE POUR OBTENIR LE GRADE DE DOCTEUR DE L'UNIVERSITÉ DE MONTPELLIER

En Physique

École doctorale: Information, Structures, Systèmes

Unité de recherche: Laboratoire Univers et Particules de Montpellier

Effective Field Theory for Lepton Flavour Violation

Présentée par Marco Ardu
le 18 juillet 2023

Sous la direction de Sacha Davidson

Devant le jury composé de

Jean-Loïc KNEUR, Directeur de recherche CNRS, L2C Montpellier	Président
Sacha Davidson, Directrice de recherche CNRS, LUPM Montpellier	Directrice de Thèse
Paride Paradisi, Professeur, Univesità degli Studi di Padova	Rapporteur
Alejandro Ibarra, Professeur, Technical University of Munich (TUM)	Rapporteur
Olcyr Sumensari, Chargé de recherche CNRS, IJCLab Orsay	Examinateur

UNIVERSITÉ DE MONTPELLIER

Acknowledgments

First of all, I would like to deeply thank my advisor, Sacha Davidson, for her never-ending support during the last three years. It was a pleasure to be supervised by such a brilliant, knowledgeable and skilled physicist, and at the same time by an extremely fair, thoughtful and kind person. I wish to thank her for everything that I have learned working with her and the constant help she provided in the path of becoming a more mature researcher.

I would like to thank all the professors and permanent researchers of the IFAC team at the LUPM and L2C (in random order): Felix, Vivian, Michele, Julien Lavalle, Julien Larena, Jean-Loic, Gilbert. Many thanks to Michele for the many interesting discussions and nice moments (despite his questionable preferences in tennis players). I wish to thank Jean-Loic for agreeing to be the president of the committee for the defense of this thesis. I extend this gratitude to all the members of the thesis committee and in particular to the reviewers that agreed to review this manuscript.

Special thanks to the current and past non-permanents of the LUPM (and some of L2C): Guillermo, MJ, Gaetan, Alice, Mihael, Riccardo, Giacomo, Khalil, Theo S., Hugo, Theo D., Francesca, Chadi, Karim, Loic. Thank you for all the lunches, physics discussions, nights out, riddles/puzzles solving, the CAF+CPAM+CDI+... calls, and the political/philosophical debates[1]. You really made Montpellier I place I could home for the last three years, and I hope our friendships will last despite being scattered around the world.

I am greateful to all the scientific collaborators I had during my PhD. Many thanks to Martin Gorbahn for his collaboration on one the projects featured in this thesis. His expertise on SMEFT calculations was extremely insightful. I wish to thank Gino Isidori for hosting me for three months at the University of Zurich. I felt warmly welcomed by everyone there, I learned a lot and had a lot of fun. Many thanks to Marko Pesut in particular, with whom I collaborated during my stay in Zurich. I also want to thank Fiona Kirk for the fun project we worked on together and the thought-provoking conversations (to not forget the countless dinners offered while I was in Zurich).

I will keep fond memories of all the PhD students and postdocs I met at schools (especially the wonderful attendees of the Les Houches Summer School in 2021), conferences and seminars. I hope we will meet again.

Un grazie alle persone care che ho lasciato dietro in Italia. Ai miei amici di sempre, Giacomo, Raffaele, Francesco, Eleonora, Sara, Silvia, Ludovica, Filippo, perché nonostante viva lontano da tanti anni sono accolto con lo stesso affetto ogni volta che ritorno. Un ringraziamento speciale alla famiglia ed in particolare ai miei genitori che non hanno mai smesso di motivarmi e supportarmi. Senza il vostro sostegno ed i vostri insegnamenti non avrei avuto i mezzi per superare questo traguardo.

Infine, grazie infinite ad Eleonora, la mia persona preferita da quasi 10 anni. Grazie per esserci sempre stata nonostante i chilometri che ci separano e grazie per essere con me a condividere la conclusione di questo percorso.

[1] I am especially greatful to have avoided the non-permanent day organization for three years straight.

Contents

List of Acronyms

Chapter 1

Introduction

The Standard Model (SM) of particle physics has been remarkably successful in explaining the interactions of the known elementary particles. The electroweak sector has been tested with exquisite precision, while perturbative calculations, effective approaches and lattice results crowned QCD as the description of the strong force. The Standard Model predicted the existence and the properties of several particles, including most recently the Higgs boson, which was discovered at the Large Hadron Collider in 2012.

Despite its successes, several observations and theoretical considerations call for an extension of the Standard Model. Neutrino masses and oscillations, dark matter, and the asymmetry between matter and antimatter are among the observations that require new physics. These unresolved puzzles motivate the search for physics Beyond the Standard Model (BSM), which could shed light on these fundamental questions and pave the way for a deeper understanding of nature.

Neutrino oscillations are a well-established experimental phenomenon that calls for beyond-standard-model physics, as they break the lepton flavor symmetries of the Standard Model Lagrangian. A minimal way to extend the SM to agree with observations is by introducing light right-handed chiral fermions to give neutrinos Dirac masses. However, this scenario is difficult to test because it leads to extremely suppressed lepton flavor changing neutral currents.

New states and interactions are required if neutrinos are Majorana fermions and/or if neutrino masses are connected to other open questions[1], leading to potentially observable processes that change the flavour of charged leptons. This possibility has prompted a great experimental effort to look for lepton flavor violating transitions, which are now among the best-measured processes in particle physics and are expected to improve further in the near future. Lepton Flavour Violation (LFV) is a promising smoking gun signal of new physics, which could shed light on the mechanism behind the neutrino masses. Moreover, it is a powerful tool in directing the model-building of generic new physics, since accidental symmetries of the SM are easily violated once new states and interactions are introduced. Models that attempt to solve various puzzles are often constrained by the requirement of agreeing with the experimental results on LFV.

The null-results obtained by the energy and intensity frontier experiments may suggest that we are at the presence of a mass gap, with the new physics appearing at a largely separated scale $\Lambda_{\text{NP}} \gg v$. If this is the case, the Standard Model may be the renormalizable Lagrangian of an Effective Field Theory where the heavy states have been removed. The effect of the heavy physics at low-energies can be parametrized in terms of contact interactions among the light degrees of freedom, suppressed by powers of the heavy scale according to the operator dimension. Observables can be calculated in the effective theory as functions of operator coefficients, and experiments can look for evidence of their presence.

[1] The generation of the Baryon Asymmetry from Leptogenesis is one notable example

In this thesis, we analyze the current and upcoming experimental results of LFV searches in the Standard Model Effective Field Theory (SMEFT). The goal is to obtain as much theoretical guidance as possible on the viable landscape of LFV new physics.

EFT calculations can be envisaged from a top-down or a bottom-up perspective. In top-down, the heavy degrees of freedom are removed from the theory and the UV couplings and masses parametrise the size of the operator coefficients. Observables are calculated with the effective operators and reproduce the model predictions within the truncation error of the EFT. In bottom-up, observables are calculated in the most general effective theory that is consistent with the symmetries, including every operator contribution that could be within reach of the experiments. In doing so, we identify the region of coefficient space where beyond standard models should sit. In both perspectives, with the exceptional improvement in the sensitivities that are expected for the next generation of experiments (especially for $\mu \to e$ transitions), theoretical calculations should follow the level precision of LFV observables, potentially including often-neglected contributions in the effective theory calculations. These may include higher-loop diagrams, as well as operators at higher order in the EFT expansion. We aim to identify all the contributions that are within the reach of future experiments to have a complete effective parametrisation of lepton flavour changing transitions. We motivate and perform challenging SMEFT calculations, and use them to obtain novel limits on LFV operator coefficients.

The thesis is organised as follows. In Chapter 2 we give a brief introduction to the Standard Model, lay down the notation for the rest of the text and discuss the evidence and observations that require going beyond the SM.

In Chapter 3 we give an overview on lepton flavour violation. We discuss models that explain neutrino masses and consider other popular models that predict sizable and potentially observable LFV signals. We also review the experimental status of LFV searches and the improvements that are expected in the upcoming years. Chapter 3 is largely based on the publication:

- [1]: M. Ardu and G. Pezzullo, Introduction to Charged Lepton Flavor Violation, Universe 8 (2022) 299

In Chapter 4 we give an introduction to effective field theories. We discuss general aspects of the EFT machinery and provide examples of explicit calculations. Then, we present the effective theory for LFV that is extensively used in Chapter 5 and Chapter 6.
Chapter 5 and Chapter 6 are respectively based on the following publications:

- [2]: M. Ardu and S. Davidson, What is Leading Order for LFV in SMEFT?, JHEP 08 (2021) 002

- [3]: M. Ardu, S. Davidson and M. Gorbahn, Sensitivity of $\mu \to e$ processes to τ flavour change, Phys. Rev. D 105 (2022) 096040

In Chapter 5 we organise the perturbative expansions in SMEFT in terms of small parameter λ to systematically estimate the contributions of the effective operators to LFV processes. We argue that a complete effective parametrisation of LFV observables requires calculations that are currently missing or are partially available in the literature.

In Chapter 6 we build on the result of Chapter 5 to show that $\mu \to e$ observables could be sensitive to the product of $\tau \leftrightarrow \mu$, $\tau \leftrightarrow e$ flavour changing interactions beyond the reach of dedicated

τ LFV searches. We calculate at next-to-leading order in the SMEFT expansion to find new limits on the product of $\tau \leftrightarrow e(\mu)$ operators. Finally, in Chapter 7 we summarize the results and discuss the prospects.

During my PhD I have also authored the following works that are not covered in this thesis:

- [4]: M. Ardu and F. Kirk, A viable $L_e - L_\mu$ model with $\mu \to e$ violation, Eur. Phys. J. C 83(2023) 394
- [5]: M. Ardu, G. Isidori and M. Pesut, Semi-inclusive Lepton Flavor Universality ratio in $b \to s\ell^+\ell^-$ transitions, Phys. Rev. D 106 (2022) 093008

Chapter 2

The Standard Model and Beyond

Contents

2.1 A brief hystory of the Standard Model

The SM of particle physics is the theoretical framework that describes the currently known particles and their interactions. It successfully accounts for three of the fundamental forces of Nature: the electromagnetic, weak and strong interactions.

After the breakthroughs of Quantum Electrodynamics (QED) [6], which followed from a systematic understanding of renormalization [7], physicists sought to develop a Quantum Field Theory (QFT) that could describe the other fundamental forces. Enrico Fermi proposed a four-fermion interaction involving the neutron, proton, electron and (at the time) hypothetical neutrino that accurately described the nuclear β decays [8]. Similar interactions with the same coupling constant were successful in explaining various processes, including the muon decay and several semi-leptonic transitions of strongly interacting particles. The electron neutrino emitted in β decays was discovered in 1956 [9], whereas the muonic neutrino involved in the muon decay was observed a few years later [10].

While the Fermi theory was extremely useful at the leading order, it was found to be non-renormalizable. The attempts to describe the weak interactions as mediated by a massive vector coupled to a $V - A$ (vector minus axial) current, which was observed in experiments, encountered similar unremovable infinities [11–15]. Weinberg was the first[1] to propose a renormalizable model of the electro-weak interactions. The theory featured a local symmetry group $\mathrm{SU}(2)_L \times \mathrm{U}(1)_Y$ which is spontaneously broken down into the QED gauge group $\mathrm{U}(1)_{\mathrm{e.m}}$ [16]. Upon the spontaneous breaking of the gauge symmetry, the weak gauge bosons, namely the charged $W^{\pm}$ and the neutral Z, acquire their mass from the Brout-Englert-Higgs mechanism [17, 18], leaving the photon γ

[1] Salam and Glashow proposed the same gauge group to describe the electroweak interactions. However, the weak gauge bosons masses were added by hand, making the theory non-renormalizable

massless. Neutral weak currents, although not yet observed, had been postulated long before Weinberg's model, but his theory predicted that semi-leptonic neutral current transitions would occur at rates comparable to those of already known charged current processes. This prediction was soon confirmed by experimental observations at CERN [19]. Weinberg's model also predicted the existence of a neutral scalar, which was not discovered until 40 years later.

Around the same time, physicists were searching for a theory of the strong interactions. The first particles known to interact strongly were the constituents of nuclei: protons and neutrons. Little was known in the 1930s, but Heisenberg introduced the concept of Isospin to explain the observed symmetry of the nuclear interactions, which seemed identical between protons and neutrons. Neutrons and protons also have very similar masses, and were therefore regarded as the components of a SU(2) isotopic spin doublet, which is an approximate symmetry of the strong force. The charged pion was discovered by observing cosmic-ray tracks [20] and had the correct mass to mediate Yukawa-like strong interactions at a range compatible with observations and it was initially believed to be the mediator of the strong force. In the same year, the "strangely" long-lived Kaon was discovered [21], and shortly thereafter the neutral pion was also observed [22]. This was followed by a plethora of newly discovered strongly interacting particles (hadrons), shading doubt on the fundamental nature of the observed "particle zoo". Certain particles (like the Kaons) that decay electro-weakly were found to be more long-lived than others, and for this reason, were dubbed "strange". Since strange particles appeared in pairs whenever they were produced by strong processes, it was hypothesized that strangeness is a quantum number, conserved in strong transitions but violated by weak interactions with a suppressed Fermi constant [23]. Gell-Mann observed that the hadrons could be arranged in multiplets of a SU(3) symmetry, generalizing the SU(2) isotopic spin to include strangeness. The SU(3) group was later understood to be acting on three different flavours of the fundamental constituents of hadrons, the u (up), d (down) and s (strange) quarks [24,25]. The suppression of strange particle decay rate was explained by Cabibbo assuming the weak eigenstate $d' = \cos\theta_c d + \sin\theta_c s$, which couples to the u flavour, to be a superposition of the flavour eigenstates d and s, suppressing processes that change $s \to u$ by $\sin\theta_c \sim 0.22$ but leaving approximately unaffected the $d \to u$ transitions [26].

In order to have the correct wave function symmetry for certain fermionic baryons (hadrons composed of three quarks), it was understood that each flavour of quark should come in three colors [27]. Evidence of the three colors was later collected from the decay of the neutral pion and from the deep inelastic scattering $e^+e^- \to hadrons$. This led to the formulation of Quantum Chromodynamics (QCD) as the underlying $SU(3)_c$ gauge theory that describes the strong interactions. Gross, Politzer and Wilczek demonstrated that the QCD gauge coupling becomes weaker at high energies, allowing perturbative calculations to be used to test QCD in that regime [28,29]. The coupling's behavior is reversed at low energies, resulting in strong interactions at a scale of approximately $\Lambda_{\mathrm{QCD}} \sim 200$ MeV. The Gell-Mann SU(3) was understood to be an approximate symmetry of QCD when neglecting the u, d, s quark masses with respect to Λ_{QCD}, scoring another major success for the theory.

Despite the progress in understanding the strong and electroweak interactions, the theory was still incomplete. The oscillation between the neutral Kaons, $K^0 - \overline{K^0}$, which changes strangeness by two units ($\Delta S = 2$), could occur by the exchange of pairs of W bosons at a higher rate than what experimentally allowed. Glashow, Iliopoulos, and Maiani (GIM) proposed a solution to this problem by introducing a fourth flavor of quark, the charm c, coupled to the weak eigenstate

Field	$\mathrm{SU}(3)_c$	$\mathrm{SU}(2)_L$	$\mathrm{U}(1)_Y$
$q = \begin{pmatrix} u_L \\ d_L \end{pmatrix}$	$\underline{3}$	$\underline{2}$	$\frac{1}{6}$
$u \equiv u_R$	$\underline{3}$	$\underline{1}$	$\frac{2}{3}$
$d \equiv d_R$	$\underline{3}$	$\underline{1}$	$-\frac{1}{3}$
$\ell = \begin{pmatrix} \nu_L \\ e_L \end{pmatrix}$	$\underline{1}$	$\underline{2}$	$-\frac{1}{2}$
$e \equiv e_R$	$\underline{1}$	$\underline{1}$	-1
H	$\underline{1}$	$\underline{2}$	$\frac{1}{2}$

Table 2.1: Matter content of the Standard Model (one generation). We specify the representation that each field fills under the SM gauge group $\mathrm{SU}(3)_c \times \mathrm{SU}(2)_L \times \mathrm{U}(1)_Y$. Fermions are chiral and written in the Dirac notation: $\psi_X = P_X \psi$, where $P_{L,R}$ are the left-handed and right-handed chiral projectors. The electric charge is conventionally defined as $Q = T^3 + Y$, where Y is the hypercharge and T^3 the diagonal generator of $\mathrm{SU}(2)_L$

$s' = -\sin\theta_c d + \cos\theta_c s$ [30]. The latter is orthogonal to the $d' = \cos\theta_c d + \sin\theta_c s$ mixture introduced by Cabibbo, and the charm contribution cancels against the diagram with a virtual u, up to terms suppressed by the charm quark's mass. The mass was estimated to be $m_c \sim 1.5$ GeV to agree with the observations, and a $\bar{c}c$ bound state (the J/ψ) with a mass $\sim 2 \times 1.5$ GeV was discovered a few years later [31,32].

The need for the charm quark also became apparent for the consistency of the gauge invariance of the theory, as it was required to cancel the gauge anomalies [33]. At this stage, fundamental particles were organized into two families or generations, each containing a set of fermions filling anomaly-free representations under the gauge group $\mathrm{SU}(3)_c \times \mathrm{SU}(2)_L \times \mathrm{U}(1)_Y$. The first generation comprised the u and d quarks, the electron e, and the electron neutrino ν_e. The second family included the c and s quarks, the muon μ, and its neutrino ν_μ. With the discovery of the tau τ lepton [34], the bottom quark b [35] and the top quark t [36], a third generation of fermions was added to the SM. Kobayashi and Maskawa expanded the quark mixing matrix first introduced by Cabibbo to account for the third generation, and found a source of CP violation in the irreducible phase of the resulting 3×3 matrix [37]. The GIM mechanism that prevented large contributions to the $K^0 - \overline{K^0}$ mixing operates as a consequence of the unitarity of the quark mixing matrix, complemented with a small mixing between the first and the heavy third generation.

The successes of the SM continued with the discovery of the W and Z bosons [38,39], and finally, the Higgs boson predicted by Weinberg was detected in 2012 at the Large Hadron Collider [40,41], providing the last missing piece.

2.2 The Standard Model Lagrangian

The Standard Model is a gauge theory based on the gauge group $\mathrm{SU}(3)_c \times \mathrm{SU}(2)_L \times \mathrm{U}(1)_Y$, with the field content summarised in Table 2.1. The fermions are divided into three generations or flavours.

The gauge interactions are flavour-blind and described by the kinetic Lagrangian

$$\mathcal{L}_{\text{kin}} = -\frac{1}{4}B^{\alpha\beta}B_{\alpha\beta} - \frac{1}{4}W^{a\alpha\beta}W^a_{\alpha\beta} - \frac{1}{4}G^{b\alpha\beta}G^b_{\alpha\beta} + (D^\alpha H)^\dagger(D_\alpha H) + \sum_f \bar{f}i\not{D}f \tag{2.1}$$

where $B_{\alpha\beta}, W^a_{\alpha\beta}, G^b_{\alpha\beta}$, with $a = 1,2,3$ and $b = 1,\cdots 8$, are the tensor field strength of the gauge group $\mathrm{U}(1)_Y, \mathrm{SU}(2)_L$, and $\mathrm{SU}(3)_c$ respectively. The sum in the second term is over all fermions, and the covariant derivative acting on the representation $\mathcal{R} \sim (\underline{3},\underline{2})_Y$ is defined as

$$D_\alpha = \partial_\alpha + ig'YB_\alpha + ig\frac{\tau^a}{2}W^a_\alpha + ig_s\frac{\lambda^b}{2}G^b_\alpha \tag{2.2}$$

where τ^a are the Pauli matrices, and λ^b the Gell-mann matrices.

The only flavour-defining couplings in the SM are the Yukawa interactions of the fermions with the Higgs doublet

$$-\mathcal{L}_{\text{Yuk}} = [Y_u]_{nm}\bar{q}_n\tilde{H}u_m + [Y_d]_{nm}\bar{q}_nHd_m + [Y_e]_{ij}\bar{\ell}_iHe_j + \text{h.c} \tag{2.3}$$

where $\tilde{H} \equiv \varepsilon H^*$, with ε being the anti-symmetric and invariant $\mathrm{SU}(2)_L$ tensor, and $Y_{u,d,e}$ are 3×3 complex matrices. Any complex matrix can be diagonalised with a bi-unitary transformation

$$Y_u = V_{q_u}\hat{Y}_uV_u^\dagger \qquad Y_d = V_{q_d}\hat{Y}_dV_d^\dagger \qquad Y_e = V_\ell\hat{Y}_eV_e^\dagger \tag{2.4}$$

where $\hat{Y}_f$ are diagonal matrices with non-negative entries. Since the quark doublet fields couple both with the up and the down singlets, the up and down Yukawas are not simultaneously diagonalisable. In a basis where the up Yukawa matrix is diagonal, the down Yukawa can be cast in the following form

$$Y_d = V_{q_u}^\dagger V_{q_d}\hat{Y}_d \equiv V_{\text{CKM}}\hat{Y}_d \tag{2.5}$$

where V_{CKM} is the Cabibbo-Kobayashi-Masukawa (CKM) unitary matrix. In this basis, the Yukawa couplings are the following

$$-\mathcal{L}_{\text{Yuk}} = [\hat{Y}_u]_{nn}\bar{q}_n\tilde{H}u_n + [V_{\text{CKM}}\hat{Y}_d]_{nm}\bar{q}_nHd_m + [\hat{Y}_e]_{ii}\bar{\ell}_iHe_i + \text{h.c} \tag{2.6}$$

The kinetic terms respect a flavour symmetry that corresponds to independent rotations in flavour space of each fermion field. This symmetry is broken by the Yukawa Lagrangian

$$\mathrm{U}(3)_q \times \mathrm{U}(3)_u \times \mathrm{U}(3)_d \times \mathrm{U}(3)_\ell \times \mathrm{U}(3)_e \xrightarrow{\mathcal{L}_{\text{Yuk}}} \mathrm{U}(1)_B \times \mathrm{U}(1)_{L_e} \times \mathrm{U}(1)_{L_\mu} \times \mathrm{U}(1)_{L_\tau} \tag{2.7}$$

leaving accidentally unbroken a flavour-independent $\mathrm{U}(1)_B$ phase rotation of the colored field $\psi \to e^{i\alpha/3}\psi$, where $\psi = q_i, u_i, d_i$ for every i, and a phase rotation $\mathrm{U}(1)_{L_i}$ of each individual lepton flavour $i = e, \mu\,\tau$, $\ell_i \to e^{i\alpha_i}\ell_i$, $e_i \to e^{i\alpha_i}e_i$. The corresponding conserved charges associated with these global symmetries are respectively the Baryon Number (B) and Lepton Flavour (LF). While the former is compatible with the non-observation of proton decay [42], non-zero neutrino masses require an extension of the Standard Model that necessarily breaks the lepton flavor symmetries (see section 2.3.1). These classical symmetries are broken at the quantum level by the triangle anomalies [43, 44], such that the quantum Noether's currents are not conserved

$$\partial_\alpha j^\alpha_B = 3 \times \partial_\alpha j^\alpha_{L_i} = \frac{3g^2}{32\pi^2}\varepsilon^{\alpha\beta\gamma\delta}W^a_{\alpha\beta}W^a_{\gamma\delta}. \tag{2.8}$$

Since the term $\varepsilon^{\alpha\beta\gamma\delta}W^a_{\alpha\beta}W^a_{\gamma\delta}$ can be written as a total derivative [45], the anomalous effects are absent in perturbative calculations, while they appear via non-perturbative topological solutions to the gauge field equation of motion known as instantons [46]. As a consequence, the $B/3+L_i$ charge can be violated via non-perturbative effects[2], while the difference $B/3-L_i$ is strictly conserved in the SM.

The spontaneous symmetry breaking of the electroweak symmetry $\mathrm{SU}(2)_L \times \mathrm{U}(1)_Y \to \mathrm{U}(1)_{\mathrm{e.m}}$, where $\mathrm{U}(1)_{\mathrm{e.m}}$ is the QED gauge group, is triggered by the Vacuum Expectation Value (VEV) of the Higgs doublet. The Higgs potential

$$V(H) = -\mu_H^2(H^\dagger H) + \frac{\lambda_H}{4}(H^\dagger H)^2 \tag{2.9}$$

is minimized when

$$\left\langle H^\dagger H \right\rangle = \frac{2\mu_H^2}{\lambda_H} \equiv v^2 \tag{2.10}$$

where $v \sim 174$ GeV. Defining the electric charge as $Q = T^3 + Y$, the QED preserving vacuum

$$\langle H \rangle = \begin{pmatrix} 0 \\ v \end{pmatrix} \tag{2.11}$$

is responsible for the mass of the weak gauge bosons

$$|D_\alpha H|^2 \supset \frac{v^2}{4}\begin{pmatrix} B_\alpha & W^3_\alpha \end{pmatrix}\begin{pmatrix} g'^2 & g'g \\ g'g & g^2 \end{pmatrix}\begin{pmatrix} B^\alpha \\ W^{3\alpha} \end{pmatrix} + m_W^2 W^+_\alpha W^{-\alpha} \tag{2.12}$$

where $W^\pm = (W^1 \mp iW^2)/\sqrt{2}$ are the charged W bosons, with a mass $m_W^2 = g^2v^2/2 \sim (80.4\ \mathrm{GeV})^2$ [47]. The neutral gauge bosons mass matrix is diagonalised after the rotation

$$\begin{pmatrix} A_\alpha \\ Z_\alpha \end{pmatrix} = \begin{pmatrix} \cos\theta_W & \sin\theta_W \\ -\sin\theta_W & \cos\theta_W \end{pmatrix}\begin{pmatrix} B_\alpha \\ W^3_\alpha \end{pmatrix} \tag{2.13}$$

where $\tan\theta_W = g/g'$, A_α is the massless photon field and Z_α has a mass $m_Z^2 = g^2v^2/(2\cos^2\theta_W) = m_W^2/\cos^2\theta_W$. Upon spontaneous symmetry breaking all fermions apart from the neutrinos acquire a mass from the Yukawa interactions of Eq. (2.6)

$$-\mathcal{L}_{\mathcal{M}} = m_{u_n}\bar{u}_n P_R u_n + [V_{\mathrm{CKM}}]_{nm} m_{d_m}\bar{d}_n P_R d_m + m_{e_i}\bar{e}_i P_R e_i + \mathrm{h.c} \qquad \text{where } m_{f_i} = [\hat{Y}_f]_{ii}v.$$

The down-type quark gauge (d_L) and mass (d'_L) eigenstates are misaligned by a CKM rotation

$$d'_L = V^\dagger_{\mathrm{CKM}} d_L \tag{2.14}$$

The neutral currents, that do not mix up-type and down-type fields, are unaffected by a unitary flavour rotation, while the $W^\pm$ couplings are modified:

$$\begin{aligned}\mathcal{L}_{\mathrm{gauge}} = &-\frac{g}{\sqrt{2}}\left[W^+_\alpha(\bar{u}_n\gamma^\alpha[V_{\mathrm{CKM}}]_{nm}P_L d'_m + \bar{\nu}_i\gamma^\alpha P_L e_i) + \mathrm{h.c}\right] - g\sin\theta_W A_\alpha J^\alpha_{\mathrm{e.m}} + \\ &- \frac{g}{2\cos\theta_W}Z_\alpha(J^\alpha_{ZL} + J^\alpha_{ZR})\end{aligned} \tag{2.15}$$

[2] This has no consequence at zero temperature, as the sphalerons (electroweak instantons) transitions are not effective at low energies. However, they could have important consequences in the Early Universe for the generation of the baryon asymmetry, as we discuss in section 2.3.3

where $g \sin\theta_W = g' \cos\theta_W \equiv e$ is the QED coupling and

$$\begin{aligned} J^\alpha_{\text{e.m}} &= \sum_f Q_f \bar{f}\gamma^\alpha f \\ J^\alpha_{ZL} &= \bar{u}_n \gamma^\alpha P_L u_n + \bar{\nu}_i \gamma^\alpha P_L \nu_i - \bar{d}_n \gamma^\alpha P_L d_n - \bar{e}_i \gamma^\alpha P_L e_i \\ J^\alpha_{ZR} &= -2\sin^2\theta_W \sum_f Q_f \bar{f}\gamma^\alpha P_R f, \end{aligned} \tag{2.16}$$

with Q_f being the electric charge of the fermion f. The unitarity of CKM not only prevents the appearance of tree level Flavour Changing Neutral Currents (FCNC), but it is also responsible for the GIM suppression $\sim m_q^2/m_W^4$ of FCNC at the loop-level[3] [30]. The suppression of FCNC is in excellent agreement with the experimental observations.

CKM can be parametrised in terms of three angles and one phase[4]. Introducing the short-hand notation $c_{ij} = \cos\theta_{ij}, s_{ij} = \sin\theta_{ij}$, the canonical parametrisation reads

$$V_{\text{CKM}} = \begin{pmatrix} V_{ud} & V_{us} & V_{ub} \\ V_{cd} & V_{cs} & V_{cb} \\ V_{td} & V_{ts} & V_{tb} \end{pmatrix} = \begin{pmatrix} 1 & 0 & 0 \\ 0 & c_{23} & s_{23} \\ 0 & -s_{23} & c_{23} \end{pmatrix} \times \begin{pmatrix} c_{13} & 0 & s_{13}e^{i\delta} \\ 0 & 1 & 0 \\ -s_{13}e^{i\delta} & 0 & c_{13} \end{pmatrix} \times \begin{pmatrix} c_{12} & s_{12} & 0 \\ -s_{12} & c_{12} & 0 \\ 0 & 0 & 1 \end{pmatrix} \tag{2.17}$$

The mixing angles in the CKM matrix exhibit a distinct hierarchy, where $s_{13} \ll s_{23} \ll s_{12} \ll 1$, which can be best appreciated in the Wolfenstein parametrisation [48–50]. Introducing the small parameter λ, we write

$$s_{12} = \lambda, \qquad s_{23} = A\lambda^2 \tag{2.18}$$

$$s_{13}e^{i\delta} = A\lambda^3(\rho + i\eta) = \frac{A\lambda^3(\bar{\rho} + i\bar{\eta})\sqrt{1 - A^2\lambda^4}}{\sqrt{1-\lambda^2}(1 - A^2\lambda^4(\bar{\rho} + i\bar{\eta}))} \tag{2.19}$$

having defined $\bar{\rho}, \bar{\eta}$ such that the matrix written in terms of $A, \bar{\rho}, \bar{\eta}$ is unitary to all orders in λ. The CKM matrix can be expanded up to λ^4 order

$$V_{\text{CKM}} = \begin{pmatrix} 1 - \lambda^2/2 & \lambda & A\lambda^3(\rho - i\eta) \\ -\lambda & 1 - \lambda^2/2 & A\lambda^2 \\ A\lambda^3(1 - \rho - i\eta) & -A\lambda^2 & 1 \end{pmatrix} + \mathcal{O}(\lambda^4) \tag{2.20}$$

with the following best-fit values for the parameters [50–52]

$$\lambda = 0.22650 \pm 0.000048, \qquad A = 0.790^{+0.018}_{-0.015} \tag{2.21}$$

$$\bar{\rho} = 0.159 \pm 0.010, \qquad \bar{\eta} = 0.348 \pm 0.010 \tag{2.22}$$

Since under CP the charged gauge bosons W are exchanged $W^+ \overset{\text{CP}}{\longleftrightarrow} W^-$, it is clear from Eq. (2.15) that a non-zero phase of the CKM matrix implies CP violation. Whether a matrix is real or complex is a basis-dependent statement, while physical observables should depend on basis-invariants. If

[3] The top contribution to tightly constrained processes, such as $K^0 - \overline{K^0}$ mixing, does not overshoot the rate despite $m_t \sim v$ because of the small mixing between the first and third generation.

[4] A unitary 3×3 matrix can be parametrised with three angles and six phases. Out of the six phases, five can be absorbed in field redefinitions, leaving a single physical one

the up and down Yukawas were simultaneously diagonalizable, CKM would be the identity and no CP violation would be present. It is thus natural to parametrise CP violation with the commutator $[Y_u, Y_d]$. The determinant is invariant under flavour space rotations and reads

$$\det([Y_u, Y_d]) = \frac{2i}{v^2}(m_t - m_c)(m_t - m_u)(m_c - m_u)(m_b - m_s)(m_b - m_d)(m_s - m_d) \times J \tag{2.23}$$

where, writing $V_{\text{CKM}} \equiv V$ to avoid cluttering, for any i, j, k and l

$$\text{Im}(V_{ij} V_{kl} V_{il}^* V_{kj}^*) = J \times \sum_{m,n} \varepsilon_{ikm} \varepsilon_{jln}. \tag{2.24}$$

J parametrise the magnitude of CP violation and is known as Jarlskog invariant [53]. Considering the best-fit values for the CKM elements reported above, its value is $J = (3.08^{+0.15}_{-0.13}) \times 10^{-5}$.

2.3 The need for Beyond Standard Model Physics

Despite being an incredibly successful theory in explaining a wide variety of phenomena, the Standard Model is incomplete. Several experimental observations and theoretical conundrums call for its extension. In this section, we discuss the evidence and hints of physics Beyond the Standard Model.

2.3.1 Neutrino masses and oscillations

As we discussed in the previous section, the SM predicts massless neutrinos. Since the so-called "solar neutrino problem" of the 1960s, a deficit [54–59] in the number of electron neutrinos compared to the prediction of the standard solar model [60–62], neutrino oscillations have been confirmed by many observations [63–67] firmly establishing non-zero masses for at least two neutrinos. Neutrino oscillations are direct evidence of lepton flavour change, violating the SM symmetry of Eq. (2.7). Some SM extensions that account for neutrino masses are discussed in Chapter 3. Regardless of the model details, neutrino masses provide an additional flavour-choosing basis for the leptons and thus the weak eigenstates ν_{Li} $(i = e, \mu, \tau)$ are a superposition of the mass eigenstates ν_s, with $s = 1, \ldots, n$ [68, 69]

$$\nu_{Li} = U_{is} \nu_s \tag{2.25}$$

where U is $3 \times n$ lepton mixing matrix, satisfying $UU^\dagger = 1_{3\times3}$. As a consequence, lepton flavour change appears in the charged weak lepton currents

$$\mathcal{L}_{\text{CC}} \supset -\frac{g}{\sqrt{2}} W_\alpha^- \bar{e}_i \gamma^\alpha P_L U_{is} \nu_s + \text{h.c} \tag{2.26}$$

If the massive neutrinos are $n = 3$, U is the lepton analogue of CKM and is known as the Pontecorvo-Maki-Nakagawa-Sakata (PMNS) matrix [70, 71]. It can be parametrised similarly to CKM as

$$U = \begin{pmatrix} 1 & 0 & 0 \\ 0 & c_{23} & s_{23} \\ 0 & -s_{23} & c_{23} \end{pmatrix} \times \begin{pmatrix} c_{13} & 0 & s_{13} e^{i\delta} \\ 0 & 1 & 0 \\ -s_{13} e^{i\delta} & 0 & c_{13} \end{pmatrix} \times \begin{pmatrix} c_{12} & s_{12} & 0 \\ -s_{12} & c_{12} & 0 \\ 0 & 0 & 1 \end{pmatrix} \times P \tag{2.27}$$

where the matrix P is the identity if neutrinos have Dirac masses, while it contains two extra phases for Majorana neutrinos $P = \mathrm{diag}\left(1 \quad e^{i\alpha_1} \quad e^{i\alpha_2}\right)$. This is because, with self-conjugate left-handed neutrinos, fewer relative field re-definitions can absorb the matrix phases.

Whenever a weak eigenstate is produced via the interactions of Eq. (2.26), the resulting state is a U weighted superposition of the mass eigenstates

$$|\nu_{Li}\rangle = U_{is}\,|\nu_s\rangle\,. \tag{2.28}$$

The state evolves as the neutrino travels a distance L, and if the mass eigenstates are assumed to be plane waves, the evolution is $|\nu_s(t)\rangle = e^{-iE_s t}\,|\nu_s(0)\rangle$[5], where $t \sim L$ for relativistic neutrinos. Then, the probability of producing a weak flavour eigenstate ν_{Lj} with a charged current interaction in the detector is

$$P(\nu_{Li} \to \nu_{Lj}) = |\langle \nu_{Lj}|\nu_{Li}(t)\rangle|^2 = \left|U^*_{jl}U_{is}e^{-iE_s t}\,\langle \nu_l|\nu_s\rangle\right|^2. \tag{2.29}$$

We use the orthogonality condition $\langle \nu_l|\nu_s\rangle = \delta_{ls}$, expand the energy in the relativistic limit $E_s \sim p_s + m_s^2/(2E_s)$ and assume that $E \simeq E_s \sim p_s$ for every s, to arrive at the oscillation probability [51]

$$\begin{aligned} P(\nu_{Li} \to \nu_{Lj}) = \delta_{ij} &- 4\sum_{l<s} \mathrm{Re}(U^*_{jl}U_{il}U_{js}U^*_{is}) \sin^2\left(\frac{(m_s^2 - m_l^2)L}{4E}\right) \\ &+ 2\sum_{l<s} \mathrm{Im}(U^*_{jl}U_{il}U_{js}U^*_{is}) \sin\left(\frac{(m_s^2 - m_l^2)L}{2E}\right). \end{aligned} \tag{2.30}$$

If the neutrinos travel through matter, the interactions with the particles in the medium can modify the effective neutrino energy. Although the weak scattering cross sections are small, neutrinos can scatter coherently with the medium constituents, giving rise to an effective mass that depends on the medium density and composition [74]. These effects are particularly relevant when neutrinos propagate in dense mediums, such as the Earth and the sun. Since the oscillation probability is sensitive to the energy difference, only the charged current interactions are relevant for the matter effects, while the neutral current interactions are flavour universal and do not give rise to an observable phase difference in the neutrino evolution. Considering for instance a medium composed of ordinary matter, the coherent scattering $e\nu_e \to e\nu_e$ modifies the effective Hamiltonian of the electron neutrino by

$$V_e = \sqrt{2}G_F n_e, \tag{2.31}$$

where n_e is the electron number density and G_F the Fermi constant $G_F = g^2/(4\sqrt{2}m_W^2) \simeq 1.16 \times 10^{-5}\ (\mathrm{GeV})^{-2}$. Note that the effective potential for anti-neutrinos scattering off ordinary matter is $-V_e$. The sign of the medium effective potential can be particularly important in determining the sign of neutrino mass differences. The Sun produces electron-neutrinos in its core via thermonuclear reactions. Solar neutrino oscillations exhibit distinct matter effects that require a resonant behavior possible only for a positive difference $\Delta m^2_{\mathrm{solar}} = m_2^2 - m_1^2$ [75]. The squared mass difference $\Delta m^2_{\mathrm{atm}}$, which is $\Delta m^2_{\mathrm{solar}} \ll \left|\Delta m^2_{\mathrm{atm}}\right| \sim \left|m_3^2 - m_2^2\right| \sim \left|m_3^2 - m_1^2\right|$, can be observed in the oscillation of neutrinos coming from the decays of particles produced by cosmic rays interacting with Earth's

[5] Several subtleties in the quantum mechanical derivation followed here are being overlooked for brevity. We refer the reader to more detailed discussions in [72, 73]

atmosphere. The observations are compatible with either sign for Δm^2_{atm}, leading to two possible scenarios: $m_1 < m_2 < m_3$ or $m_3 < m_1 < m_2$, respectively known as Normal Ordering (NO) and Inverted Ordering (IO). In the 3ν picture, the lepton matrix mixing angles, the mass squared

		Normal Ordering (Best Fit)		Inverted Ordering ($\Delta\chi^2 = 2.6$)	
		bfp $\pm 1\sigma$	3σ Range	bfp $\pm 1\sigma$	3σ Range
without SK atmospheric data	$\sin^2\theta_{12}$	$0.304^{+0.013}_{-0.012}$	$0.269 \to 0.343$	$0.304^{+0.012}_{-0.012}$	$0.269 \to 0.343$
	$\theta_{12}/^\circ$	$33.44^{+0.77}_{-0.74}$	$31.27 \to 35.86$	$33.45^{+0.77}_{-0.74}$	$31.27 \to 35.87$
	$\sin^2\theta_{23}$	$0.573^{+0.018}_{-0.023}$	$0.405 \to 0.620$	$0.578^{+0.017}_{-0.021}$	$0.410 \to 0.623$
	$\theta_{23}/^\circ$	$49.2^{+1.0}_{-1.3}$	$39.5 \to 52.0$	$49.5^{+1.0}_{-1.2}$	$39.8 \to 52.1$
	$\sin^2\theta_{13}$	$0.02220^{+0.00068}_{-0.00062}$	$0.02034 \to 0.02430$	$0.02238^{+0.00064}_{-0.00062}$	$0.02053 \to 0.02434$
	$\theta_{13}/^\circ$	$8.57^{+0.13}_{-0.12}$	$8.20 \to 8.97$	$8.60^{+0.12}_{-0.12}$	$8.24 \to 8.98$
	$\delta_{\text{CP}}/^\circ$	194^{+52}_{-25}	$105 \to 405$	287^{+27}_{-32}	$192 \to 361$
	$\frac{\Delta m^2_{21}}{10^{-5}\,\text{eV}^2}$	$7.42^{+0.21}_{-0.20}$	$6.82 \to 8.04$	$7.42^{+0.21}_{-0.20}$	$6.82 \to 8.04$
	$\frac{\Delta m^2_{3\ell}}{10^{-3}\,\text{eV}^2}$	$+2.515^{+0.028}_{-0.028}$	$+2.431 \to +2.599$	$-2.498^{+0.028}_{-0.029}$	$-2.584 \to -2.413$
		Normal Ordering (Best Fit)		Inverted Ordering ($\Delta\chi^2 = 7.0$)	
		bfp $\pm 1\sigma$	3σ range	bfp $\pm 1\sigma$	3σ range
with SK atmospheric data	$\sin^2\theta_{12}$	$0.304^{+0.012}_{-0.012}$	$0.269 \to 0.343$	$0.304^{+0.013}_{-0.012}$	$0.269 \to 0.343$
	$\theta_{12}/^\circ$	$33.45^{+0.77}_{-0.75}$	$31.27 \to 35.87$	$33.45^{+0.78}_{-0.75}$	$31.27 \to 35.87$
	$\sin^2\theta_{23}$	$0.450^{+0.019}_{-0.016}$	$0.408 \to 0.603$	$0.570^{+0.016}_{-0.022}$	$0.410 \to 0.613$
	$\theta_{23}/^\circ$	$42.1^{+1.1}_{-0.9}$	$39.7 \to 50.9$	$49.0^{+0.9}_{-1.3}$	$39.8 \to 51.6$
	$\sin^2\theta_{13}$	$0.02246^{+0.00062}_{-0.00062}$	$0.02060 \to 0.02435$	$0.02241^{+0.00074}_{-0.00062}$	$0.02055 \to 0.02457$
	$\theta_{13}/^\circ$	$8.62^{+0.12}_{-0.12}$	$8.25 \to 8.98$	$8.61^{+0.14}_{-0.12}$	$8.24 \to 9.02$
	$\delta_{\text{CP}}/^\circ$	230^{+36}_{-25}	$144 \to 350$	278^{+22}_{-30}	$194 \to 345$
	$\frac{\Delta m^2_{21}}{10^{-5}\,\text{eV}^2}$	$7.42^{+0.21}_{-0.20}$	$6.82 \to 8.04$	$7.42^{+0.21}_{-0.20}$	$6.82 \to 8.04$
	$\frac{\Delta m^2_{3\ell}}{10^{-3}\,\text{eV}^2}$	$+2.510^{+0.027}_{-0.027}$	$+2.430 \to +2.593$	$-2.490^{+0.026}_{-0.028}$	$-2.574 \to -2.410$

Table 2.2: Best-fit values for the neutrino mixing parameters and mass difference [76]

differences (up to the atmospheric sign) and the Dirac phase δ can be determined by fitting the neutrino oscillation data [76, 77]. The Dirac phase contributes to the CP violating difference in the oscillation probability $P(\nu_{Li} \to \nu_{Lj})$ and $P(\overline{\nu}_{Li} \to \overline{\nu}_{Lj})$ [78–80]. The best-fit values for the neutrino parameters are shown in Tab. 2.2.

If the neutrinos are Majorana fermions, the Majorana phases contribute as a source of CP violation in processes that depend linearly on the neutrino masses, hence not in oscillation where the dependence is quadratic. Whether neutrinos are Dirac or Majorana could be determined with the observation of lepton number violating transitions. The most sensitive of such processes is the neutrinoless double β decay ($0\nu2\beta$)

$$(A, Z) \to (A, Z + 2) + 2e^-. \tag{2.32}$$

The corresponding Feynman diagram is shown in Fig. (2.1), where a Majorana mass insertion is

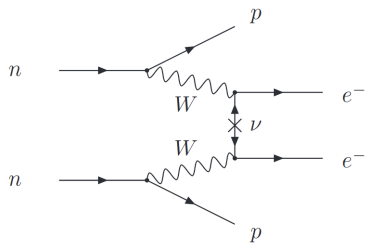

Figure 2.1: Feynman diagram for the neutrinoless double β decay mediated by Majorana neutrinos

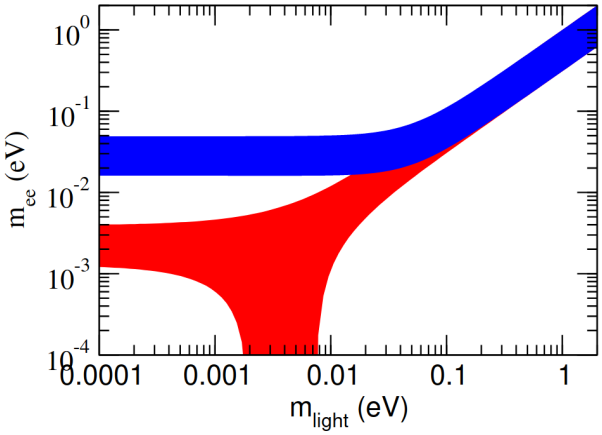

Figure 2.2: Allowed values for the matrix element m_{ee} defined in Eq. (2.34) entering in the neutrinoless double beta decay rate. The red and blue regions correspond to NO and IO respectively. Figure taken from [51], with ranges obtained projecting the results of the analysis in [83]

necessary to close the virtual neutrino line. The squared amplitude takes the following form

$$|\mathcal{A}_{0\nu2\beta}|^2 \sim |\mathcal{M}_{0\nu2\beta}|^2 \times m_{ee}^2 \qquad m_{ee} = \left|\sum_s m_s U_{es}^2\right| \tag{2.33}$$

where $\mathcal{M}_{0\nu2\beta}$ is the nuclear matrix element. The effective Majorana mass m_{ee} depends on the neutrino parameters, including the Majorana phases

$$m_{ee} = \left|c_{13}^2 c_{12}^2 m_1 + e^{i\alpha_1} c_{13}^2 s_{12}^2 m_2 + e^{i(\alpha_2 - 2\delta)} s_{13}^2 m_3\right| \tag{2.34}$$

We show in Figure 2.2 the allowed ranges for m_{ee} for the two different ordering. Since in the NO scenario m_{ee} can vanish for specific choices of the lightest neutrino mass m_1 and phases, the non-observation of $0\nu2\beta$ cannot rule out the possibility of Majorana neutrinos, while a positive signal may disprove the Dirac nature. On the other hand, inverted ordering could be ruled out by $0\nu2\beta$ searches, given that $m_{ee}^{(\mathrm{IO})} > 0.016$ eV. The most stringent bounds on the neutrinoless double beta decay are given by the GERDA (^{76}Ge) and KamLAND-Zen (^{136}Xe) collaborations, respectively setting the lower bounds on the half-lives $T_{1/2}^{0\nu2\beta}(^{76}\mathrm{Ge}) > 1.8{\times}10^{26}$ yr and $T_{1/2}^{0\nu2\beta}(^{136}\mathrm{Xe}) > 1.07{\times}10^{26}$ yr [81, 82].

2.3.2 Dark Matter

The need for physics BSM is also supported by the observation of Dark Matter (DM). Cosmological and astrophysical data are consistent with the standard model of cosmology (ΛCDM), which is based on Einstein's theory of general relativity and parametrises the Universe's composition with a cosmological constant Λ, the abundance of ordinary matter (baryonic and radiation), and of cold dark matter. The presence of a non-baryonic and non-relativistic (cold) matter component has been evident since 1933, when Zwicky calculated the total mass of galaxy clusters using the Virial Theorem. He found that the mass was greater than the contribution of baryonic matter, which can be estimated via its luminosity [84].

Evidence of dark matter also comes from the observed circular velocities of stars in spiral galaxies. Under the effect of gravity, velocities should experience a Keplerian fall-off $v_c \sim r^{-1/2}$ at large distances r from the galactic centre. Instead, the circular velocity plateaus to a roughly constant value [85,86], which can be explained by an invisible halo of dark matter surrounding the galaxy.

Another strong motivation for dark matter comes from measurements on the Cosmic Microwave Background (CMB). The density fluctuations of baryonic matter observed from the CMB are too small to account for the observed matter power spectrum, which is consistent with the presence of a dominant cold dark matter component. Planck results are compatible with an abundance of DM comprising $\sim 84\%$ of the total matter density, which accounts for 31.5% of the energy budget of the Universe, with the cosmological constant accounting for the remaining 68.5% [87]. Despite the gravitational effects of DM provide conclusive evidence of its existence, and many BSM theories and production mechanisms have been proposed to account for the observed abundance, DM has never been detected in a particle physics experiment [51].

2.3.3 Baryogenesis

Observations show that our Universe is primarily composed of ordinary matter, mainly protons and neutrons, with a negligible presence of antimatter. The matter-antimatter asymmetry is measured by the η parameter, defined as

$$\eta \equiv \frac{n_b - n_{\bar{b}}}{n_\gamma} \sim 6.1 \times 10^{-10} \tag{2.35}$$

where $n_b, n_{\bar{b}}$ and n_γ are the number densities of baryons, anti-baryons and photons respectively. η can be measured via the CMB temperature fluctuations or via the abundance of light elements that are produced during the Big Bang Nucleosynthesis (BBN) [87,88].

The possibility of having a fine-tuned primordial excess of baryons over anti-baryons that would give rise to the asymmetry is disfavored by inflation, as it tends to erase any initial condition. To generate dynamically the Baryon Asymetry of the Universe (BAU), three conditions must be satisfied [89]:

1. Baryon number is violated;
2. C and CP are violated;
3. Departure from thermal equilibrium.

While these conditions are met in the Standard Model, they are still insufficient for successful baryogenesis. The CP violation in the SM arising from the CKM matrix phase and parametrised by the Jarlksog invariant of Eq. (2.24), is too small to account for the observed asymmetry [90–93]. Furthermore, the electroweak phase transition is shown to be a smooth cross-over [94–98] for a Higgs mass $m_H \sim 125$ GeV [99, 100], while electroweak baryogenesis would require a strong first-order transition. Several extensions of the SM have been proposed to achieve baryogenesis [101]. The BAU can be connected to the neutrino mass problem if the baryon asymmetry is obtained via Leptogenesis, where a lepton asymmetry is given by the out-of-equilibrium decay of a sterile neutrino and transferred to the baryons via the electroweak sphalerons [102].

2.3.4 Hints of New Physics

Beyond the experimental evidence of New Physics (NP) that we discussed so far, many theoretical considerations and puzzles can hint towards BSM physics. These include:

- **The hierarchy problem**

  The Higgs boson in the SM is a fundamental scalar and its mass is potentially sensitive to unknown UV physics. The hierarchy problem is not a problem of the SM, but it is of generic models with heavy states that couple with the Higgs. Corrections to the Higgs mass can arise via loops of heavy particles, having the schematic form

  $$\delta m_H^2 \sim \frac{\Lambda^2}{16\pi^2} \tag{2.36}$$

  where Λ is the mass scale of the UV physics. If $\Lambda \gg v$, observations would require that the tree-level bare mass of the Higgs m_H^2 cancel almost exactly with the loop corrections, leaving a remnant small mass close to the electroweak scale

  $$(m_H^{\text{obs}})^2 \sim m_H^2 + \delta m_H^2 \sim v^2. \tag{2.37}$$

  If the UV physics lies at the Planck scale $\Lambda \sim M_{\text{Pl}} = 1.9 \times 10^{19}$ GeV, the scale separation is $v/M_{\text{Pl}} \sim 10^{-17}$ and the fine-tuning required in the cancellation is extreme. Fermion masses do not suffer from similar dangerous UV contributions because they are only logarithmically sensitive to the UV physics, given that the chiral symmetry forces the loop corrections to be proportional to the tree-level mass. Small fermion masses are therefore technical natural[6]. The hierarchy problem motivates the expectation of finding NP close to the electroweak scale and has led to a variety of proposals to protect the Higgs mass from UV physics contributions. Most notably, Supersymmetry (SUSY) is a space-time symmetry that relates bosons and fermions [104–108], making the bosons inherit the protection mechanism provided by the chiral symmetry. Some supersymmetric extensions of the SM are discussed in Chapter 3. For a more detailed discussion on the possible BSM directions to address the Hierarchy problem, we refer the reader to [109] and references therein.

[6] We refer to technical naturalness as defined by t'Hooft [103], which states that a small parameter c is technically natural whenever the limit $c \to 0$ enhances the symmetry of the theory.

- **Strong CP problem**

  The apparent absence of CP violation in strong interactions constitutes another puzzle. The QCD gauge invariance allows for the following CP odd terms involving the gluon fields

$$\mathcal{L}_\theta = \theta \frac{g_s^2}{32\pi^2} \varepsilon^{\alpha\beta\gamma\delta} G^b_{\alpha\beta} G^b_{\gamma\delta} \tag{2.38}$$

  whose non-trivial effects are given at the non-perturbative level by the instanton solutions. The θ parameter is necessary for a gauge invariant definition of the QCD vacuum [110] and the Lagrangian term of Eq. (2.38) is also a consequence of a building block of QFT, i.e the cluster decomposition principle [111].

  Imaginary mass terms are additional sources of CP violation[7], and since a chiral transformation acting on a quark field q

$$q \to e^{i\alpha\gamma_5} q \tag{2.41}$$

  affect both the mass phase and the θ term via the chiral anomaly, the physical basis-independent parameter $\bar{\theta}$ is a combination of the QCD vacuum parameter and the mass phases. In the SM, the invariant CP angle is equal to

$$\bar{\theta} = \theta + \arg\det(Y_u Y_d). \tag{2.42}$$

  The most sensitive observables to CP violation in the strong interactions is the electric dipole moment of the neutron d_n, which is yet to be observed $d_n < 2.2 \times 10^{-26}$ e cm (95 % CL) [112]. The contribution to d_n sensitive to $\bar{\theta}$ is calculated in Chiral Perturbation Theory to be [113, 114]

$$d_n \sim 6 \times 10^{-16}\ \bar{\theta}\ e\ \text{cm} \tag{2.43}$$

  requiring $\bar{\theta} \lesssim 10^{-10}$. Why should $\bar{\theta}$ be so small and potentially zero is the essence of the Strong CP problem. Arguably, the most popular solution to the Strong CP problem is the one proposed by Peccei and Quinn [115, 116]. They showed that in the presence of an extra chiral symmetry $\mathrm{U(1)_{PQ}}$ acting on some quark fields, CP would be conserved. It was later realized by Weinberg and Wilczeck that the Peccei-Quinn solution would require the spontaneous symmetry breaking of the $\mathrm{U(1)_{PQ}}$ to allow for massive quarks, predicting a light pseudo-goldstone boson, dubbed 'axion' [8] [117, 118]. The axion solution relies on the QCD anomaly of the $\mathrm{U(1)_{PQ}}$ chiral symmetry, which generates an axion-gluon-gluon coupling with the same structure of the θ term in Eq. (2.38), effectively promoting θ to a dynamical field. As a consequence of the Vafa-Witten theorem [119], the axion expectation value conserves CP.

  In the original Peccei-Quinn model, the breaking scale f_a of $\mathrm{U(1)_{PQ}}$ coincided with the electroweak scale, a possibility that was soon ruled out by experiments. The so-called invisible

[7] The mass Lagrangian

$$m_q \bar{q}_L q_R + m_q^* \bar{q}_R q_L \tag{2.39}$$

can be written as

$$\left(\frac{m_q + m_q^*}{2}\right) \bar{q} q + \left(\frac{m_q - m_q^*}{2}\right) \bar{q} \gamma_5 q. \tag{2.40}$$

The second term, non-zero only if $m_q - m_q^* \neq 0$, is CP-odd.

[8] After a brand of laundry detergent

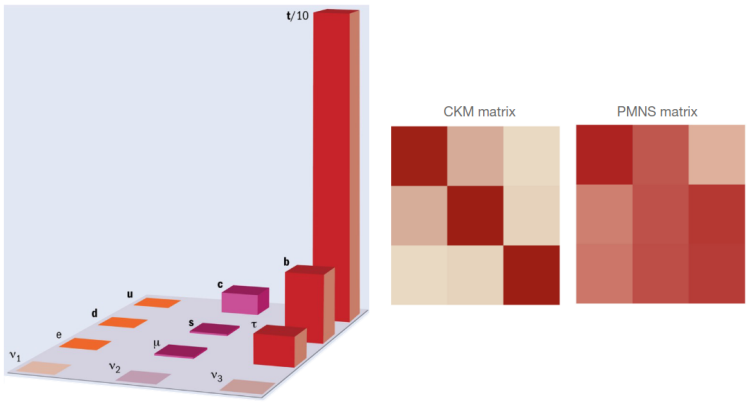

Figure 2.3: Observed hierarchy in the fermion masses and the flavour mixing matrices in the SM minimally extended to account for neutrino masses. In the CKM and PMNS elements, the color shade represents the magnitude (darker colors correspond to larger values)

axion models [120–122], where $f_a \gg v$, are still viable. Invisible axions are also excellent DM candidates [123–125]. For a detailed theoretical and experimental review on invisible QCD axion models, see [126].

Other solutions to the strong CP problem assume CP to be a symmetry in the UV, which is spontaneously broken and communicated to the SM via messenger fields. The main difficulty is in generating a large CKM angle while having a small θ QCD, leading to involved model-building. The first proposals in this direction were put forward by Nelson and Barr [127–129]

- **Flavour Puzzle**

  The SM exhibits a highly non-generic pattern in the observed fermion masses and flavour mixing matrices, as represented in Figure 2.3. The SM fermion masses span 12 orders of magnitude, ranging from the neutrino mass scale $m_\nu \lesssim 0.1$ eV to the top mass $m_t \sim 172$ GeV, displaying a distinct hierarchy between the generations. Quark flavour mixing is parametrised by a nearly diagonal CKM, with a small mixing between heavy and light quarks. PMNS, which parametrises the lepton mixing introduced by the neutrino masses, features a "democratic" hierarchy, with mostly large angles except for θ_{13}.

  The SM flavour structure may be the hint of an underlying flavour symmetry of BSM physics. Froggatt and Nielsen famously proposed to explain the quark masses and CKM elements hierarchies as being controlled by powers of the breaking parameter of a $\mathrm{U}(1)_{\mathrm{FN}}$ flavour symmetry [130]. The 'flavon' scalar field S acquire a VEV $\langle S \rangle$ that breaks spontaneously the abelian flavour symmetry. The $\mathrm{U}(1)_{\mathrm{FN}}$ breaking is communicated to the SM fermions integrating out Froggatt-Nielsens states with a mass M_{FN}, contributing to the fermion masses and mixing angles as $\sim \varepsilon^n$, where $\varepsilon = \langle S \rangle / M_{\mathrm{FN}}$ is taken to be close to the Cabibbo angle $\varepsilon \sim \lambda \sim 0.2$ and n depends on the FN charges. Charge assignments that lead to realistic quark (lepton) masses and mixing angles are for example discussed in [131].

  The peculiar flavour structure of the SM is also responsible for the suppression of a variety

of processes in excellent agreement with the observations, most notably regarding FCNC. The experimental picture surrounding FCNC suggests that generic flavour structure for BSM would require a scale of NP in some cases many orders of magnitude larger than the electroweak scale, in contrast with the naturalness expectation motivated by the observed Higgs mass. Inspired by this problem, the Minimal Flavour Violation (MFV) hypothesis postulates that any flavour change of BSM physics must be linked to the known structure of the Yukawa matrices [132]. Other models attempting to solve the flavour puzzle can be found in [133].

In addition to these theoretical puzzles, some yet not conclusive experimental observations provide hints of new physics and have inspired several BSM proposals.

- **$\mathbf{g_\mu - 2}$**
  A long-standing discrepancy is observed between the experimental value and the SM prediction for the anomalous magnetic moment of the muon. The muon magnetic moment is defined as
  $$\vec{\mu}_\mu = g_\mu \left(\frac{e}{2m_\mu}\right) \vec{S}_\mu \tag{2.44}$$
  where $\vec{S}_\mu$ is the muon spin. Quantum effects correct the prediction $g_\mu^{\text{tree}} = 2$ given by the tree-level Dirac equation, which are calculated in the SM to yield [134]
  $$a_\mu^{\text{SM}} \equiv \frac{1}{2}(g_\mu^{\text{SM}} - 2) = 116591810(43) \times 10^{-11}. \tag{2.45}$$
  The muon magnetic moment has been recently measured at the Fermilab National Accelerator Laboratory (FNAL) Muon g-2 Experiment [135], which, combined with the previous result obtained at the Brookhaven National Laboratory [136], gives a 4.2σ discrepancy with the theoretical prediction
  $$a_\mu^{\text{exp}} - a_\mu^{\text{SM}} = (251 \pm 59) \times 10^{-11} \tag{2.46}$$
  Although an impressive number of new physics models have been proposed to explain the discrepancy, the SM prediction is debated. The main source of uncertainty is the contribution of the hadronic vacuum polarization a_μ^{HPV} to the muon anomalous magnetic moment, which can be extracted via $\sigma(e^+e^- \to \text{hadrons})$ data and dispersive relations, but can also be calculated on the lattice. The lattice results predict a milder deviation from the experimental value [137–139].

- **B meson anomalies**
  A series of deviations from the SM predictions have been observed in the semi-leptonic decays of B mesons. These include discrepancies in the ratio of processes controlled by the underlying charged-current quark transitions $b \to c\ell\nu$,
  $$R_{D^{(*)}} = \frac{Br(B \to D^{(*)}\tau\nu)}{Br(B \to D^{(*)}l\nu)} \tag{2.47}$$
  where l can be e or μ. The SM prediction does not suffer from hadronic uncertainties because they largely cancel in the ratio. Including the latest measurements, the observed discrepancy in $R_{D^{(*)}}$ amount to a 3.1σ deviation [140]. Anomalies with a similar statistical significance are

observed in the neutral current transitions $b \to s\mu\mu$, however, the theoretical predictions are contaminated by the hadronic uncertainties. The ratios of neutral current transitions $b \to sll$

$$R_{K^{(*)}} = \frac{Br(B \to K^{(*)}\mu\mu)}{Br(B \to K^{(*)}ee)}, \tag{2.48}$$

have also shown deviations from the lepton flavour universal prediction of the SM, but they were not confirmed by the latest results [141].

Chapter 3

Charged Lepton Flavour Violation

Contents

3.1 Introduction

As we discussed in the previous chapter, the Standard Model defined with left-handed neutrinos conserves the lepton flavour. The observation of neutrino oscillations provided clear evidence of non-zero neutrino masses and mixing angles, demonstrating that lepton flavour is not a symmetry of nature.

Charged Lepton Flavour Violation (CLFV) (or LFV), defined as a short-range interaction among the charged leptons that change flavour, is therefore expected to occur but it is yet to be observed. If neutrinos get Dirac masses via the renormalizable Yukawa interactions with the Higgs, the predicted rates for CLFV are typically GIM suppressed $G_F^2 m_\nu^4 \sim 10^{-50}$ and are practically unobservable. A detection of CLFV would thus be a clear signature of new physics that could shed a light on the origin of neutrino masses.

Additionally, lepton flavor is an accidental symmetry of the SM that is respected by the most general Lagrangian with gauge invariant renormalizable interactions. Thus, SM extensions that are motivated independently from neutrino masses can easily introduce extra sources of lepton flavour violation and lead to sizeable CLFV rates.

For these reasons, experimental searches of CLFV attract great interest and are a valuable tool in identifying viable BSM scenarios. CLFV searches can pinpoint theories at energy scales currently not directly accessible by the collider facilities. Null results from the current experiments significantly constrain the parameter space of new physics models, and the improvements in sensitivity by several orders of magnitude, especially in the $\mu \to e$ sector, will further probe BSM physics.

In this chapter, we present an overview of the theoretical and experimental status of CLFV, mostly based on [1]. Excellent reviews on the topic can be found in the literature [142–146]. In Section 3.2, we discuss several SM extensions that could be potentially probed in the upcoming CLFV experimental searches. We only review heavy new physics models, as this is the focus of the original work discussed in this thesis. We discuss the LFV phenomenology of models that generate neutrino masses at tree and loop level, and we present the CLFV signatures of different BSM scenarios, such as the two Higgs doublets model and the supersymmetric SM.

In Section 3.3, the state of the art and the upcoming experiments looking for CLFV processes are discussed. A particular emphasis is given to those looking for rare muon CLFV decays. Several facilities around the world (Fermilab, PSI and J-PARC) already started building or commissioning new generation experiments with improved sensitivity on the muon CLFV searches (up to four orders of magnitude). This is possible thanks to improvements in the acceleration techniques, necessary to deliver beam with intensity $\sim 10^{10}$ μ/s, and novel detector technologies. The same section also provides an overview of the current best limits achieved on the tau CLFV branching ratios set by general-purpose experiments at e^+e^- and pp colliders. Also on the tau front, an improved sensitivity on several searches is expected thanks to the unprecedented luminosity of the Large Hadron Collider at CERN and the SuperKEKB collider at KEK laboratory

3.2 Theory review

3.2.1 CLFV in models that generate neutrino masses at Tree Level

If we assume the presence of three right-handed neutrinos ν_{Ri} which are singlets of the SM gauge group, gauge invariance allows for Yukawa couplings between the lepton and the Higgs doublets that generate Dirac masses for neutrinos when electroweak symmetry is spontaneously broken

$$-\mathcal{L}_\nu = [Y_\nu]_{ij}\bar{\ell}_i\tilde{H}\nu_{Rj} + \text{h.c.} \tag{3.1}$$

To obtain neutrino masses that are compatible with cosmological constraints $\sum m_\nu \lesssim 0.12$ eV [87], neutrino Yukawa couplings must be $Y_\nu \lesssim \mathcal{O}(10^{-12})$. Although small Yukawas are technically natural, Dirac masses require a strong hierarchy between the charged and neutral lepton Yukawa sector.

Analogously to CKM, the PMNS matrix is the result of the misalignment between charged lepton and neutrino mass basis, as the neutrino and charged lepton Yukawas cannot be simultaneously diagonalized respecting the electroweak gauge symmetry. Flavour violation is parameterized by presence of the PMNS matrix in the charged lepton current

$$\mathcal{L}_{\text{CC}} \supset -\frac{g}{\sqrt{2}}W^-_\alpha U_{ij}\bar{e}_{iL}\gamma^\alpha\nu'_{jL} + \text{h.c} \tag{3.2}$$

where ν'_L are the neutrino mass eigenstates. Charged lepton flavor violation is consequently mediated by the flavor-changing interactions in Equation (3.2). In Figure 3.1, we show a representative diagram for the decay $\mu \to e\gamma$. The amplitude of this process can be generically cast in the following

form[1]:

$$\begin{aligned}\mathcal{M}(\mu \to e\gamma) &= \bar{u}_e(p_e)(m_\mu(A_R P_R + A_L P_L) i\sigma_{\alpha\beta} q^\beta + (B_R P_R + B_L P_L) q_\alpha + \\ &+ (C_R P_R + C_L P_L)\gamma_\alpha) u_\mu(p_e + q)\varepsilon^{*\alpha}(q) \\ &= \mathcal{M}_\alpha \varepsilon^{*\alpha}(q)\end{aligned} \tag{3.3}$$

where A_X, B_X and C_X are complex numbers. As a consequence of QED gauge invariance, the amplitude satisfies the Ward identity $q^\alpha \mathcal{M}_\alpha = 0$. On-shell spinors obey the equation of motion $(\not{p} - m)u(p) = 0$, and the Ward identity requires

$$m_\mu(C_R P_R + C_L P_L) - m_e(C_R P_L + C_L P_R) + q^2(B_R P_R + B_L P_L) = 0 \tag{3.4}$$

which, for on-shell photons $q^2 = 0$, has the unique solution $C_R = C_L = 0$. The only relevant term is a dipole transition

$$\mathcal{M}(\mu \to e\gamma) = \bar{u}_e(p_e)\left[i\sigma_{\alpha\beta} q^\beta m_\mu (A_R P_R + A_L P_L)\right] u_\mu(p_e + q)\varepsilon^{*\alpha}(q) \tag{3.5}$$

which is chirality-flipping and, thus, proportional to the muon mass (if we neglect the electron mass). Equation (3.5) yields the following decay rate [142]:

$$\Gamma(\mu \to e\gamma) = \frac{m_\mu^5}{16\pi}(|A_L|^2 + |A_R|^2) \tag{3.6}$$

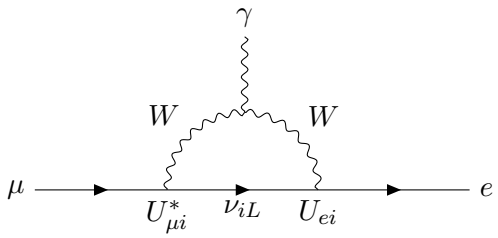

Figure 3.1: $\mu \to e\gamma$ mediated by massive neutrinos ν_{iL}.

In the diagram of Figure 3.1, the outgoing electrons are left-handed and only A_R is non-zero[2]. The amplitude is proportional to the internal neutrino propagator, which can be expanded for small neutrino masses as

$$\sum_i \frac{U^*_{ei} U_{\mu i}}{(k^2 - m_i^2)} = \sum_i \frac{U^*_{ei} U_{\mu i}}{k^2} + \sum_i \frac{U^*_{ei} U_{\mu i}}{k^2}\left(\frac{m_i^2}{k^2}\right) + \mathcal{O}\left(\frac{m_i^4}{k^4}\right). \tag{3.7}$$

We see that the leading term vanishes due to PMNS unitarity, and the amplitude is GIM suppressed by the square of neutrino masses. Indeed, the process is analogous to a flavor-changing neutral current in the quark sector, which features a similar GIM suppression by CKM unitarity. The calculation is done in [148] in the R_ξ gauge, where additional diagrams replacing W with the

[1] see, for instance, Chapter 6, Section 6.2 of [147]

[2] A_L is zero in taking the limit $m_e \to 0$

charged Goldstones must be included. All diagrams are finite and in the unitary gauge limit $\xi \to \infty$; only the diagram of Figure 3.1 is non-zero. Dividing by the rate $\Gamma(\mu \to e\nu\bar{\nu}) = G_F^2 m_\mu^5/192\pi^3$ of the dominant LF conserving three-body decay, the resulting branching ratios for $\mu \to e\gamma$ is [149–153]

$$Br(\mu \to e\gamma) = \frac{3\alpha_e}{32\pi}\left|\sum_i U_{ei}^* U_{\mu i}\frac{m_i^2}{M_W^2}\right|^2 . \tag{3.8}$$

Rewriting the sum as

$$\sum_i U_{ei}^* U_{\mu i}\frac{m_i^2}{M_W^2} = U_{e2}^* U_{\mu 2}\frac{\Delta m_{21}^2}{M_W^2} + U_{e3}^* U_{\mu 3}\frac{\Delta m_{31}^2}{M_W^2} \tag{3.9}$$

and substituting the best-fit values of the mass differences and mixing parameters, the predicted branching ratios for the LFV $\mu \to e\gamma$ is $Br(\mu \to e\gamma) = 10^{-54} - 10^{-55}$, which lie beyond any foreseeable experimental reach. In models with Dirac neutrino masses, rates of other LFV processes are similarly GIM suppressed and, thus, too small to be observable.

The right-handed neutrinos are *sterile*, i.e., neutral under the SM gauge group, so SM gauge invariance allows for a lepton number violating Majorana mass term

$$-\mathcal{L}_\nu = [Y_\nu]_{ij}\bar{\ell}_i\tilde{H}\nu_{Rj} + \frac{1}{2}[M_R]_{ij}\overline{\nu^c}_{iR}\nu_{jR} + \text{h.c.} \tag{3.10}$$

having defined $\nu^c = C\bar{\nu}^T$, where C is the Dirac charge conjugation matrix [154]. Majorana mass matrices are symmetric because fermion fields are anti-commuting and the charge conjugation matrix C is antisymmetric. Upon electroweak symmetry breaking, the mass Lagrangian can be cast in the following form (suppressing generation indices)

$$-\mathcal{L}_\nu = \frac{1}{2}\overline{N^c}M_N N + \text{h.c} \qquad \text{where } M_N = \begin{pmatrix} 0 & M_D \\ M_D^T & M_R \end{pmatrix} \tag{3.11}$$

where $N = \begin{pmatrix}\nu_L^c & \nu_R\end{pmatrix}^T$ and $M_D = vY_\nu$. If we assume that the Majorana masses M_R are much larger than the Dirac masses (symbolically $M_R \gg M_D$), the matrix can be put in block diagonal form that disentangles the light and heavy neutrinos [155]

$$W^T M_N W = \begin{pmatrix} M_\nu & 0 \\ 0 & M_{heavy} \end{pmatrix}, \qquad \begin{pmatrix}\nu_L^c \\ \nu_R\end{pmatrix} = W\begin{pmatrix}\nu_{light}^c \\ \nu_{heavy}\end{pmatrix} \tag{3.12}$$

where W is a unitary matrix. At leading $M_D M_R^{-1}$ order, the mass matrices are

$$M_{heavy} = M_R \qquad M_\nu = -M_D M_R^{-1} M_D^T \tag{3.13}$$

Assuming $\sim \mathcal{O}(1)$ Yukawas, light neutrinos masses can be explained by Majorana masses close to the grand unification scale $M_R \sim 10^{15}$ GeV. This is the celebrated seesaw mechanism [156], specifically known as type I when the SM is extended with singlet right-handed fermions.

A unitary U^* diagonalizes the symmetric Majorana matrix M_ν with a congruence transformation $U^{*T} M_\nu U^* = \hat{M}_\nu = \text{diag}\begin{pmatrix} m_1 & m_2 & m_3 \end{pmatrix}$, but U is not the matrix that appears in the charged currents. Defining $U \equiv U \otimes 1_{heavy}$ as acting on the light neutrinos subspace, gauge interaction and mass basis are related by

$$\begin{pmatrix} \nu_L^c \\ \nu_R \end{pmatrix} = W U^* \begin{pmatrix} \nu_{light}^c \\ \nu_{heavy} \end{pmatrix}, \tag{3.14}$$

where the matrix W can be expanded at second order as [155]

$$W = \begin{pmatrix} 1 - \frac{1}{2} B_1 B_1^\dagger & B_1 \\ -B_1^\dagger & 1 - \frac{1}{2} B_1^\dagger B_1 \end{pmatrix} \qquad \text{with } B_1 = (M_R^{-1} M_D^T)^\dagger = v (M_R^{-1} Y_\nu^T)^\dagger. \tag{3.15}$$

The left-handed weak eigenstates are related to the light mass eigenstates via a non-unitary matrix U'

$$\nu_L = U' \nu_{light} = \left(1 - \frac{1}{2}(B_1 B_1^\dagger)^*\right) U \nu_{light} = \left(1 - \frac{v^2}{2} Y_\nu \frac{1}{M_R^\dagger M_R} Y_\nu^\dagger\right) U \nu_{light} \tag{3.16}$$

Lacking unitarity, the GIM suppression no longer operates substituting the U' matrix in Equation (3.7), and the rate of $\mu \to e\gamma$ becomes [148, 157]

$$\frac{\Gamma(\mu \to e\gamma)}{\Gamma(\mu \to e\nu\bar{\nu})} = \frac{3\alpha_e}{32\pi} \frac{\left|\sum_i U'^*_{ei} U'_{\mu i} F(x_i)\right|^2}{(U'U'^\dagger)_{ee} (U'U'^\dagger)_{\mu\mu}} \tag{3.17}$$

where $x_i = m_i^2/M_W^2$ and $F(x_i)$ is a loop function that can be expanded for $x_i \ll 1$ as $F(x_i) \simeq 10/3 - x_i$. CLFV processes can thus constrain departures from the unitarity of the PMNS matrix [158]. Substituting the typical value $y_\nu^2 \simeq m_\nu M_R / v^2$, GIM suppression is replaced by the ratio m_ν / M_R, which for GUT scale sterile neutrinos predict rates that are nonetheless well below future experimental sensitivity. Seesaw models can predict sizeable CLFV rates if the Majorana right-handed masses are closer to the electroweak scale. In the non-supersymmetric seesaw, this is also desirable to avoid large correction to the Higgs mass [159]. However, in a generic setup with TeV scale M_R and unsuppressed CLFV rates, fine-tuned cancellations are required in Equation (3.13) to explain neutrino masses. Fine-tuning is, of course, avoided if a symmetry principle forces the neutrino mass to be small despite having large Yukawa couplings. Observe that neutrino masses are a lepton number violating effect $\sim Y_\nu M_R^{-1} Y_\nu^T$, while the non-unitary matrix that governs CLFV rates is lepton number conserving $\sim Y_\nu M_R^{-2} Y_\nu^\dagger$. It is possible to suppress neutrino masses by invoking a small breaking of lepton number conservation while keeping the masses of the sterile neutrinos sufficiently close to the electroweak scale and with no need for small Yukawa couplings. This is, for example, achieved in the inverse seesaw [160, 161], naturally leading to quasi-degenerate pairs of sterile neutrinos [162–164].

The seesaw formula can be understood as the result of integrating out the heavy neutrinos. A more general discussion on Effective Field Theories can be found in Chapter 4. The relevant s and t channel diagrams are shown in Figure 3.2 and match onto the dimension five Weinberg operator

$$\mathcal{L}_{d=5} = \frac{1}{2} C_{ij}^5 (\bar{\ell}_i \tilde{H})(\ell_j^c \tilde{H}) + \text{h.c} \tag{3.18}$$

with the coefficient $C^5 = Y_\nu M_R^{-1} Y_\nu^T$. When the Higgs doublet gets a VEV, neutrinos acquire Majorana masses via the Weinberg operator $M_\nu \equiv -v^2 C^5 = -M_D M_R^{-1} M_D^T$, which agree with Equation (3.13). Moreover, the following dimension six operator is generated

$$\mathcal{L}_{d=6} = C^6_{ij} (\bar{\ell}_i \tilde{H}) i\not{\partial} (\tilde{H}^\dagger \ell_j), \tag{3.19}$$

with a coefficient $C_6 = Y_\nu M_R^{-1\dagger} M_R^{-1} Y_\nu^\dagger$, which corrects the light neutrinos kinetic terms. The redefinition needed to canonically normalize the fields introduce a non-unitary matrix in the charged currents [165]

$$\nu_L \to (\delta_{ij} + v^2 C^6_{ij})^{-1/2} \nu_L \;\to\; \mathcal{L}_{\rm CC} = -\frac{g}{\sqrt{2}} W^-_\alpha \sum_{\substack{i=e,\mu,\tau \\ j=1,2,3}} \left(\delta_{ik} - \frac{v^2}{2} C^6_{ik}\right) U_{kj} \bar{e}_{iL} \gamma^\alpha \nu_{jL} + \text{h.c} \tag{3.20}$$

which again agrees with Equation (3.16). The advantage of an effective field theory description is that different seesaw scenarios can be described at low energy in a common framework. In Figure 3.3, we show how extending the Standard Model with particles transforming in different representations of the SM gauge group can generate Majorana neutrino masses via the Weinberg operator. Recent effective field theory analysis of type I and type II seesaw models include the complete one-loop matching onto effective operators [166, 167], providing useful resources to study the low-energy CLFV signatures. For more complete reviews on the CLFV phenomenology of seesaw models, we refer the reader to [165, 168].

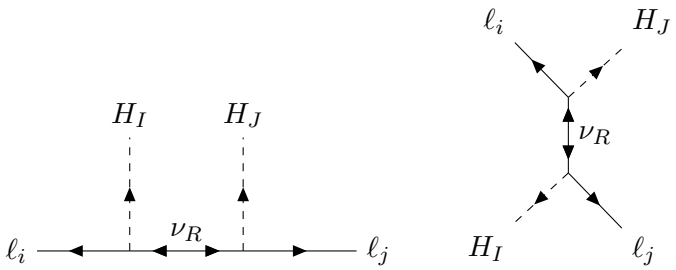

Figure 3.2: Matching contributions to the Weinberg operator in type I seesaw.

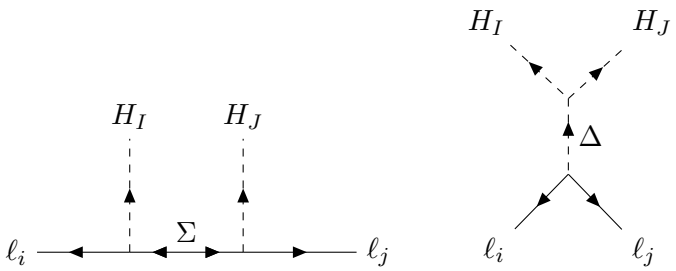

Figure 3.3: Seesaw Majorana neutrino masses generated by integrating out a heavy scalar triplet Δ (type II) or a heavy fermion triplet Σ (type III).

3.2.2 CLFV in models that generate neutrino masses at loop level

New physics not too far from the electroweak scale can account for small neutrino masses if they are generated radiatively via loop diagrams. As a specific example, the so-called scotogenic model [169] extends the SM with an additional scalar doublet η (with hypercharge $Y_\eta = 1/2$) and three generations of sterile neutrinos N. The new particles are assumed to be odd under a discrete Z_2 symmetry, which forbids Yukawa couplings with the SM Higgs between lepton doublets and the sterile neutrinos, as well as constraining the possible interactions in the scalar potential. The Z_2 is also responsible for keeping stable the lightest new particle, which, if neutral, provides a potential dark matter candidate. Omitting the kinetic terms, the scotogenic Lagrangian reads [3]

$$\mathcal{L}_{sc} = \mathcal{L}_{\rm SM} + \left([Y_\eta]_{ij} \bar{\ell}_i \tilde{\eta} N_j - \frac{M_{Ni}}{2} \overline{N^c}_i N_i + \text{h.c} \right) - V(H, \eta) \tag{3.21}$$

where the scalar potential is

$$\begin{aligned} V(H,\eta) = {} & m_h^2 H^\dagger H + m_\eta^2 \eta^\dagger \eta + \frac{\lambda_1}{2}(H^\dagger H)^2 + \frac{\lambda_2}{2}(\eta^\dagger \eta)^2 + \lambda_3 (H^\dagger H)(\eta^\dagger \eta) \\ & + \lambda_4 (H^\dagger \eta)(\eta^\dagger H) + \frac{\lambda_5}{2}\left[(H^\dagger \eta)^2 + (\eta^\dagger H)^2 \right]. \end{aligned} \tag{3.22}$$

To preserve the Z_2 symmetry when the electroweak symmetry is spontaneously broken, the potential parameters must be such that the η field does not acquire a VEV. We also assume that all parameters in the potential are real and CP is conserved. With this assumption, the real and imaginary parts of the uncharged component $\eta_0 = (\eta_R + i\eta_I)/\sqrt{2}$ do not mix. The mass splitting between the two neutral scalars is proportional to $\lambda_5 v^2$, consequently $\eta_{R,I}$ are approximately degenerate in the limit $\lambda_5 \ll 1$. Note that the lepton number is conserved if λ_5 is zero so that small values are technically natural.

The Z_2 symmetry prevents the appearance of tree-level Majorana masses for the left-handed neutrinos, but it can generate them at the one-loop level via the λ_5 mixing of η with the SM Higgs doublet, as shown in the diagram of Figure 3.4. The resulting neutrino mass matrix is calculable, and, for $\lambda_5 \ll 1$ ($m_0 = m_{\eta_R} \sim m_{\eta_I}$), can be approximated as [169]

$$[M_\nu]_{ij} \simeq \frac{2\lambda_5 Y_{\eta ik} Y_{\eta jk} v^2}{16\pi^2 M_{N_i}} \left[\frac{M_{N_k}^2}{m_0^2 - M_{N_k}^2} + \frac{M_{N_k}^4}{(m_0^2 - M_{N_k}^2)^2} \log\left(\frac{M_{N_k}^2}{m_0^2} \right) \right]. \tag{3.23}$$

Contrary to the traditional seesaw scenario, the extra suppression $\sim \lambda_5/(16\pi^2)$ can predict small values of m_ν with TeV scale sterile neutrinos and unsuppressed Yukawa couplings. The CLFV signature of the scotogenic model has been studied with particular attention to $l_i \to l_j \gamma$ processes [170–172], while the phenomenology of $l_i \to l_j l_k l_m$ and $\mu \to e$ conversion in nuclei have also been discussed [173]. In Figure 3.5, we show a selection of diagrams giving contributions to CLFV processes at the one-loop level.

[3] it always possible to diagonalize the symmetric Majorana mass matrix of the sterile neutrinos with no loss of generality

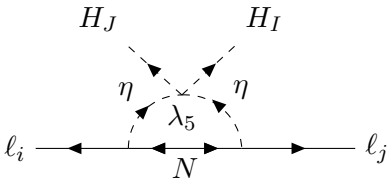

Figure 3.4: Radiative neutrino mass in the scotogenic model. The loop and λ_5 suppression allow for TeV−scale new physics and small neutrino masses.

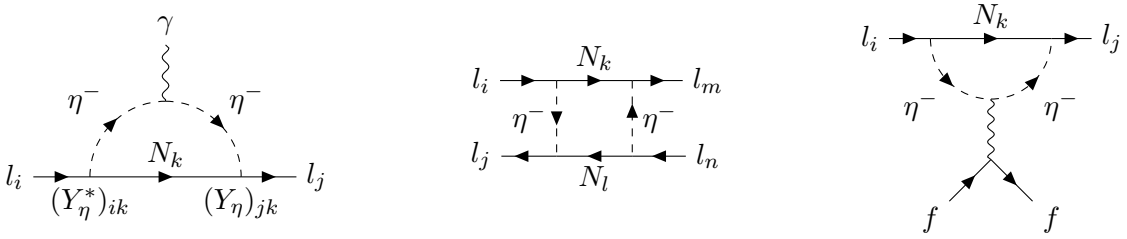

Figure 3.5: CLFV processes in the scotogenic model. From left-to-right: (**a**) Diagrams contributing to the $l_i \to l_j\gamma$ rate. (**b**) Box diagrams contributing to the $l_i \to l_m l_n l_j$ rate. (**c**) Penguin diagrams contributing to the $l_i \to l_j l_k l_k$ rate and $\mu \to e$ conversion rate (f can be a quark or a lepton).

Part of the parameter space of the scotogenic model is excluded by the current experimental LFV searches, while the viable region can give branching ratios within upcoming experimental sensitivities and will be probed in the near future. It is often the case that $l_i \to l_j\gamma$ is the most constraining LFV channel because the dipole (Figure 3.5a) contribution to the photon penguin (Figure 3.5c) can dominate the amplitude of $l_i \to l_j \bar{f} f$, leading to the following relation [174]

$$Br(l_i \to 3l_j) \sim \frac{\alpha_e}{3\pi}\left(2\log\left(\frac{m_{l_i}}{m_{l_j}}\right) - \frac{11}{4}\right) Br(l_i \to l_j\gamma) \tag{3.24}$$

However, the box contribution (Figure 3.5b) can be larger than the photon penguin diagram for a mass of the lightest neutrino close to the cosmological upper limit ~ 0.1 eV (Figure 3.6) so that upcoming $\mu \to 3e$ searches can constrain the model orthogonally to the MEG bound on $\mu \to e\gamma$. In addition, the penguin diagram of Figure 3.5c mediates LFV interactions with quarks, contributing to the rate of $\mu \to e$ conversion in nuclei (we briefly review the $\mu \to e$ conversion rate calculation in Appendix A). When the dipole dominates the penguin amplitude, $\mu \to e$ conversion experimental reach is not competitive with $\mu \to e\gamma$ searches[4], given that

$$\frac{Br(\mu \to e\gamma)}{Br(\mu N(A,Z) \to eN(A,Z))} \sim f(A,Z) \times 10^2 \tag{3.25}$$

where $f(A,Z)$ is a nucleus dependent factor that is $\sim \mathcal{O}(1)$ for the targets used in experiments [142]. As shown in the right plot of Figure 3.6, the scaling of Equation (3.25) is satisfied for small m_N/m_η ratios, while the non-dipole penguin amplitude can come to dominate for larger m_N/m_η values.

[4] although with the future branching ratios sensitivity $Br(\mu A \to eA) \sim 10^{-16}$, $\mu \to e$ conversion might be able to probe smaller dipole coefficients than MEG II with $Br(\mu \to e\gamma) \sim 6 \times 10^{-14}$

The upcoming $\mu \to e$ conversion searches will be a valuable probe for this region of parameter space [175].

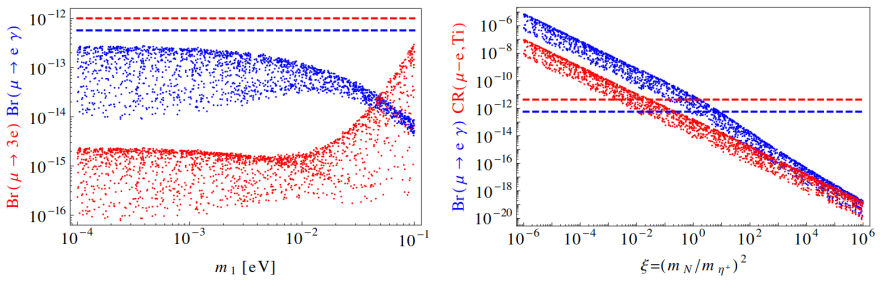

Figure 3.6: The plots show some CLFV branching fractions in the scotogenic model: in the left plot the prediction for $Br(\mu \to e\gamma)$ and $Br(\mu \to 3e)$ for degenerate sterile neutrino masses $m_N = 4$ TeV and $m_{\eta^+} = 1$ TeV, varying the mass of the lightest neutrino (normal ordering); in the right figure $Br(\mu \to e\gamma)$ and $Br(\mu \to e)$ conversion as a function of $(m_N/m_{\eta^+})^2$. The dashed lines correspond to the current experimental upper limit. Yukawas Y_η compatible with neutrino parameters are randomly generated (Figure from [173]).

Another popular model that can generate neutrino masses at loop level is the Zee-Babu Model [176, 177], where the SM is extended with two SU(2) singlet and charged scalars k^+, k^{++} and allow for the Lagrangian terms

$$\mathcal{L}_{ZB} \supset f^{+}_{ij}\overline{\ell^c}_{iI}\varepsilon_{IJ}\ell_{jJ}k^{+} + f^{++}_{ij}\overline{e^c}_i e_j k^{++}, \tag{3.26}$$

where ε_{IJ} is the anti-symmetric $SU(2)$ tensor. Lepton number is not conserved and neutrino masses are generated at the two-loop level, while the interactions also violate lepton flavor. The CLFV phenomenology of the Zee-Babu model has been studied in [178–180]. For other models that generate neutrino masses at the loop level and their CLFV signatures, we refer the reader to [181].

3.2.3 Two Higgs Doublet Model

One simple extension of the Standard Model features an additional scalar doublet H_2, which is commonly known as the Two-Higgs Doublet Model (2HDM) (for a review see [182]). A second Higgs is strongly motivated by supersymmetry, where one Higgs cannot give masses to all fermions and the second Higgsino, the superpartner of the second doublet, is necessary to cancel the gauge anomalies. Although supersymmetry imposes precise relations among the Higgs masses and couplings, supersymmetry breaking terms lead to modifications, such that, at low energy, it is suitable to describe the two Higgs with generic couplings. A general 2HDM (type III) predicts LFV couplings that must be sufficiently suppressed to satisfy the current experimental constraint. Often, additional symmetries are assumed to avoid the appearance of flavor-changing neutral current at the tree level. In Type I 2HDM, the SM fermions only couple to one Higgs, while, in the type II, the up quarks couple to a different Higgs than leptons and down quarks, which is the case for supersymmetric SM.

The 2HDM scalar Lagrangian is the following

$$\begin{aligned}-\mathcal{L}_{\text{2HDM}} &= [Y_e]_{ij}\bar{\ell}_i H_1 e_j + [Y_u]_{nm}\bar{q}_n \tilde{H}_1 u_m + [Y_d]_{nm}\bar{q}_n H_1 d_m + \text{h.c} \\ &+ [K_e]_{ij}\bar{\ell}_i H_2 e_j + [K_u]_{nm}\bar{q}_n \tilde{H}_2 u_m + [K_d]_{nm}\bar{q}_n H_2 d_m + \text{h.c} \\ &+ V(H_1, H_2)\end{aligned} \tag{3.27}$$

where the potential reads

$$\begin{aligned}V(H_1,H_2) &= m_{11}^2 H_1^\dagger H_1 + m_{22}^2 H_2^\dagger H_2 - m_{21}^2(H_1^\dagger H_2 + \text{h.c}) + \frac{\lambda_1}{2}(H_1^\dagger H_1)^2 + \frac{\lambda_2}{2}(H_2^\dagger H_2)^2 \\ &+ \lambda_3(H_1^\dagger H_1)(H_2^\dagger H_2) + \lambda_4(H_1^\dagger H_2)(H_2^\dagger H_1) \\ &+ \left(\frac{\lambda_5}{2}(H_1^\dagger H_2)^2 + \lambda_6(H_1^\dagger H_1)(H_1 H_2^\dagger) + \lambda_7(H_2^\dagger H_2)(H_1 H_2^\dagger) + \text{h.c}\right).\end{aligned} \tag{3.28}$$

In a region of the potential parameters, the Higgs can acquire a VEV that spontaneously breaks the electroweak gauge symmetry, and it is always possible to rotate in a basis where only one has a non-zero expectation value $\langle H_1\rangle = \begin{pmatrix}0 & v\end{pmatrix}^T$, $\langle H_2\rangle = 0$. The doublets are written as

$$H_1 = \begin{pmatrix} G^+ \\ v + \frac{1}{\sqrt{2}}(\rho_1 + iG^0)\end{pmatrix} \qquad H_2 = \begin{pmatrix}\phi^+ \\ \frac{1}{\sqrt{2}}(\rho_2 + iA)\end{pmatrix}. \tag{3.29}$$

Once the Goldstones G are eaten by the gauge bosons, the scalar spectrum contains one ϕ^+ complex scalar, two CP even neutral scalar $\rho_{1,2}$ and one CP odd scalar A. If the potential parameters are real, only the two CP even scalars mix, and we identify two mass eigenstates h, H [183, 184]

$$h = \sin(\beta-\alpha)\rho_1 + \cos(\beta-\alpha)\rho_2 \equiv s_{\beta\alpha}\rho_1 + c_{\beta\alpha}\rho_2 \tag{3.30}$$

$$H = \cos(\beta-\alpha)\rho_1 - \sin(\beta-\alpha)\rho_2 \equiv c_{\beta\alpha}\rho_1 - s_{\beta\alpha}\rho_2 \tag{3.31}$$

where $\beta-\alpha$ is the angle that diagonalizes the neutral scalar mass matrix, and h, H have masses $m_h < m_H$, respectively. We identify the lighter scalar with the 125−GeV Higgs boson. In a basis where the two doublets Φ_i both have VEVs v_i, a rotation with angle α diagonalizes the neutral scalar mass matrix, while the angle β such that $\tan\beta \equiv v_1/v_2$ allows us to rotate into the H_i basis. In the Type III 2HDM, there is no unambiguous way to identify β and α because the two doublets are not distinguishable. On the other hand, $\beta-\alpha$ is calculable in terms of the potential parameters [184]

$$\cos(\beta-\alpha)\sin(\beta-\alpha) = -\frac{2\lambda_6 v^2}{(m_H^2 - m_h^2)} \tag{3.32}$$

In the fermion mass basis, the Yukawa matrices Y_f are diagonalized, while the K_f couplings with H_2 are, in general, non-diagonal. The Yukawa interactions between the fermions and the uncharged scalar sector read

$$\begin{aligned}-\mathcal{L}_Y &= \frac{h}{\sqrt{2}}\bar{f}_{iL}\left(\frac{[m_f]_i\delta_{ij}}{v}s_{\beta\alpha} + [K_f]_{ij}c_{\beta\alpha}\right)f_{jR} + \text{h.c} \\ &\quad \frac{H}{\sqrt{2}}\bar{f}_{iL}\left(\frac{[m_f]_i\delta_{ij}}{v}c_{\beta\alpha} - [K_f]_{ij}s_{\beta\alpha}\right)f_{jR} + \text{h.c} \\ &\quad \sum_{f=d,e} i\frac{A}{\sqrt{2}}\bar{f}_{iL}[K_f]_{ij}f_{jR} - i\frac{A}{\sqrt{2}}\bar{u}_{iL}[K_u]_{ij}u_{jR} + \text{h.c}\end{aligned} \tag{3.33}$$

The LHC measures a $h \to \tau^+\tau^-, \mu^+\mu^-$ rate compatible with the Standard Model prediction [185, 186], requiring $s_{\beta\alpha} \sim 1$. Substituting this approximation in Equation (3.32) gives

$$c_{\beta\alpha} \simeq -2\lambda_6 v^2/(m_H^2 - m_h^2) \ll 1 \;\to\; c_{\beta\alpha} \simeq \frac{-2\lambda_6 v^2}{m_H^2}. \tag{3.34}$$

In the decoupling limit $\lambda_i v^2 \ll m_{22}^2$ [187] that we have assumed to justify $m_H^2 \gg m_h^2$, the mass splitting $m_H^2 - m_A^2 \sim \lambda_5 v^2$ is small, and in the following, we consider $M^2 \sim m_H^2 \sim m_A^2$. The off-diagonal interaction $K_e c_{\beta\alpha}$ can mediate LFV Higgs boson decay with a rate [188, 189]

$$\Gamma(h \to l_i l_j) = \frac{|K_e|_{ij}^2 + |K_e|_{ji}^2}{16\pi} c_{\beta\alpha}^2 m_h \qquad \text{where} \;\; l_i l_j = l_i^+ l_j^- + l_i^- l_j^+ \tag{3.35}$$

Non-observation of LFV decay modes of the Higgs boson at LHC set the upper limits on the branching fractions reported in Table 3.1 and directly constrain the size of flavor violating coupling.

Process	Bound on Br
$h \to \mu e$	6.1×10^{-5} [190]
$h \to \tau\mu$	1.5×10^{-3} [191]
$h \to \tau e$	2.2×10^{-3} [191]

Table 3.1: Lepton flavor violating decay of the SM Higgs boson with the current experimental bounds set by ATLAS and CMS.

Off-diagonal Yukawas are also indirectly bounded by other LFV processes, as they can mediate $l_i \to l_j \gamma$ through the loop diagrams shown in Figure 3.7. The two-loop diagrams of Figure 3.7b,c are relevant and can be numerically larger than one-loop contributions [192] because, in the former, the Higgs line is attached to a heavy particle running in the loop and Yukawa suppression is avoided. In the $\mu \to e$ sector, $\mu \to e\gamma$ is the most sensitive process to LFV Yukawas, which has been extensively studied in the context of 2HDM [184, 193–196]. For the $\tau \leftrightarrow l$ sector, the bound on the radiative decay $Br(\tau \to l\gamma) <$ few $\times 10^{-8} \to 10^{-9}$ is less stringent and the Higgs LFV decays are sensitive to smaller off-diagonal Yukawas. In a simplified scenario where only the SM Higgs is present, the author of [197] computed several processes in terms of generic LFV couplings $hY_{ij}\bar{e}_{Li}e_{Rj}$, and Figure 3.8 shows the current bounds (sensitivity) set by LFV observables. In 2HDM, there are also contributions from the heavy scalars, which are parametrically of similar size of light Higgs LFV; while they do not suffer from the small mixing angle $c_{\beta\alpha} \sim v^2/M^2$, the propagator yields a similar suppression $\sim 1/M^2$.

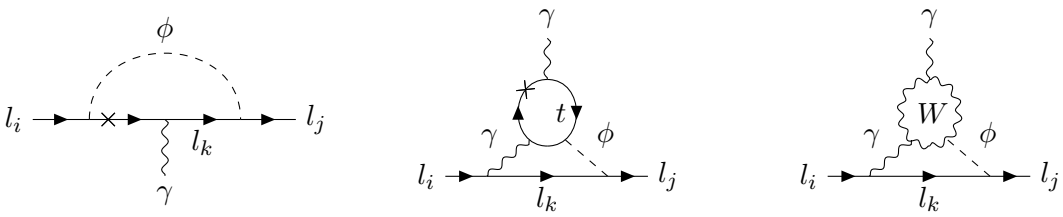

Figure 3.7: Diagrams for $l_i \to l_j\gamma$ in the 2HDM, where $\phi = h, H, A$. Two-loop Bar-Zee diagrams with a Z exchange also exist. From left-to-right: (**a**) One loop contribution to the $l_i \to l_j\gamma$ rate in the 2HDM with LFV Yukawa couplings. (**b**) Two loop Barr-Zee diagram with a top loop contributing to $l_i \to l_j\gamma$ in the 2HDM with LFV Yukawa couplings. (**c**) Two loop Barr-Zee diagram with a W loop contributing to $l_i \to l_j\gamma$ in the 2HDM with LFV Yukawa couplings.

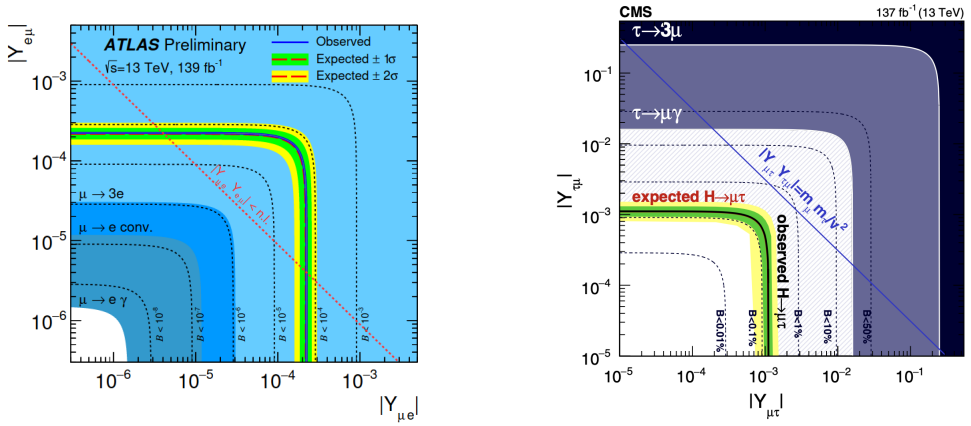

Figure 3.8: Left figure from [190]: constraint on LFV Yukawa couplings $Y_{\mu e}, Y_{e\mu}$ from the limits on $Br(h \to e\mu)$ (observed limit corresponds to the solid blue line, while the expected one is the dashed red line). Shaded regions show the sensitivity of $\mu \to 3e, \mu \to e\gamma$ and $\mu \to e$ conversion on the LFV Yukawas, from the calculations of [197]. Right figure from [191]: same plot for the $\tau \leftrightarrow \mu$ sector. The diagonal line shows the natural limit $|Y_{ij}Y_{ji}| < m_i m_j / 2v^2$ (note that for us $v = 174$ GeV, while in the plot $v = 246$ GeV) [198].

Contribution to $l_i \to l_j l_k l_k$ and $l_i \to l_j qq$ also appear at tree level in the 2HDM. The same processes also receive relevant contributions attaching a $l_j l_j$ (qq) current to the photon of the diagrams in Figure 3.7.

3.2.4 CLFV in Supersymmetry

Supersymmetry (SUSY) is a space-time symmetry that extends Poincare invariance by adding fermionic generators that satisfy the anti-commutation relations of the supersymmetry algebra [199–201]. SUSY is the largest space-time symmetry that the $S-$matrix can have given a set of physical assumptions such as unitarity, locality and causality [202, 203]. Since fermionic operators Q are added to the algebra, irreducible SUSY representation (supermultiplets) contain particles of different spin that are related by the action of Q on one-particle states. The simplest supersymmetric extension of the Poincare group is $N = 1$ SUSY, i.e., with only one pair of conjugate

Weyl spinor generators $Q, \bar{Q}$. In the Minimal Supersymmetric Standard Model (MSSM), for every quark q and lepton ℓ, there is a corresponding complex scalar in the same gauge representation, commonly known as the squark $\tilde{q}$ and slepton $\tilde{\ell}$. Similarly, the gauginos $\tilde{B}, \tilde{W}^I, \tilde{G}^a$ are the fermion superpartner of the gauge bosons, which transforms in the adjoint of the gauge group, while the higgsinos $\tilde{H}_u, \tilde{H}_d$ are the spin-1/2 particles that belong to the supermultiplets of the Higgs doublets. As already discussed in the previous section, a supersymmetric version of the SM requires at least two Higgs doublets.

Degenerate partners of the known SM particles with opposite statistics have never been observed; therefore, SUSY, if realized at all, must be broken at some scale m_0. To avoid the reappearance of the hierarchy problem, m_0 should not be too far from the Higgs mass and explicit SUSY breaking terms must be soft, i.e., have to contain only terms with strictly positive mass dimension. The solution to the hierarchy problem is also preserved if SUSY is spontaneously broken by the expectation value $\sim m_0$ of some scalar field. In models of spontaneous breaking, soft breaking terms appear in the low energy non-supersymmetric description. Null results from the LHC rule out SUSY breaking scales below few $\times$ TeV [204–206], although the bounds on superpartners' masses are not completely model-independent.

In the MSSM, the SUSY breaking sector can be a source of lepton flavor violation. The soft breaking terms contain masses for the sleptons and trilinear couplings with the Higgs

$$-\mathcal{L}_{\text{soft}} \supset [\tilde{m}_R^2]_{ij}\tilde{e}_i^\dagger \tilde{e}_j + [\tilde{m}_L^2]_{ij}\tilde{\ell}_i^\dagger \tilde{\ell}_j + m_0[A]_{ij}\tilde{\ell}_i^\dagger H_d \tilde{e}_j \tag{3.36}$$

that introduce LFV if the off-diagonal entries are non-zero in the lepton mass eigenstate basis. For $\sim$ 100 GeV$-$TeV soft terms, the current bounds on LFV, and more generally on flavor-changing neutral current in the SM, call for a suppression mechanism of sfermions mass mixing. This is known as the SUSY flavor problem. The spontaneous symmetry breaking of SUSY cannot be triggered by the scalar fields in the MSSM supermultiplets, as this would lead to an unacceptable spectrum. Supersymmetry breaking may occur in an hidden sector that have very small coupling with the MSSM particle. This is know as the mediation paradigm. If SUSY breaking is communicated via supergravity couplings of the hidden sector to matter, it results in universal and flavor conserving soft terms at the Planck scale [207,208]. Nonetheless, this does not strictly forbid LFV, since mass mixing can still be radiatively generated. In the minimal SU(5) Grand Unified Theory (GUT), the matter content of SM is reproduced by three generations of two fermion fields: one in the anti-fundamental $\bar{\mathbf{5}}$ of SU(5) ($\bar{F}$), which contains the lepton doublet and the right-handed down-type quark, and one that fills the **10** representation of SU(5) (T), which contains the quark doublet, the right-handed up-type quark and the right-handed charged lepton. They are coupled in the Yukawa sector to two Higgs scalar fields transforming in the $\bar{\mathbf{5}}$ and **5** representation.

$$-\mathcal{L}_{\text{SU(5),Yuk}} = [Y_u]_{ij}T_i H T_j + [Y_d]_{ij}\bar{F}_i \bar{H} T_j + \text{h.c} \tag{3.37}$$

In SUSY GUT, the above equation corresponds to the superpotential W, where $T, \bar{F}, H, \bar{H}$ are the superfields that contain the SM particles and the superpartners. Assuming gravity-mediated SUSY breaking, the soft terms at M_{Pl} are flavor blind and characterised by a common mass scale m_0

$$-\mathcal{L}_{\text{SU(5),soft}} = m_0^2(\tilde{T}_i^\dagger \tilde{T}_i + \tilde{\bar{F}}_i^\dagger \tilde{\bar{F}}_i) + m_0 a_0([Y_u]_{ij}\tilde{T}_i H \tilde{T}_j + [Y_d]_{ij}\tilde{\bar{F}}_i \bar{H}\tilde{T}_j + \text{h.c}) \tag{3.38}$$

The top Yukawa is large and loop correction to third generation masses can be sizeable. In a basis where the up Yukawa matrix is diagonalized and neglecting first and second generation couplings, the leading-log correction in the renormalization of the $\tilde{T}_3$ mass is [142,209]

$$\Delta\tilde{m}_{T,33} \simeq -\frac{3}{8\pi^2}|Y_u|^2_{33} m_0^2 (3+|a_0|^2) \log\left(\frac{M_{\rm Pl}}{M_{\rm GUT}}\right) \tag{3.39}$$

where $M_{\rm GUT} \sim 10^{16}$ GeV is the GUT scale. The $\tilde{T}$ fields contain the right-handed charged sleptons that have a diagonal but non-universal mass matrix. In the mass eigenstate basis for the charged leptons, the right-handed slepton mass matrix acquires non-diagonal entries

$$[\Delta\tilde{m}_R]_{ij} \simeq -\frac{3}{8\pi^2}[V_e^*]_{i3}[V_e]_{j3}|Y_u|^2_{33} m_0^2 (3+|a_0|^2) \log\left(\frac{M_{\rm Pl}}{M_{\rm GUT}}\right) \qquad \text{with } Y_e = V_\ell \hat{Y}_e V_e^\dagger \tag{3.40}$$

where $\hat{Y}_e$ is the diagonal lepton Yukawa. In SU(5) GUT, the down and lepton Yukawa are unified $Y_e = Y_d^T$, and V_e correspond to the transpose CKM matrix. In the diagrams of Figure 3.9, we show how slepton mass mixing can mediate $l_i \to l_j\gamma$ at loop level, that in most SUSY setups is the largest LFV signal. Box diagrams exist for $l_i \to l_j l_k l_k$ and $l_i \to l_j qq$, but the processes are often dominated by the penguin diagrams, where a flavor diagonal current is attached to an off-shell photon in the diagrams of Figure 3.9. The rate of $\mu \to e\gamma$ in minimal SU(5) GUT has been calculated in [209,210]. A potentially detectable signal for the upcoming experiments is predicted, although the values considered for the sparticles masses are in tension with more recent LHC data [211].

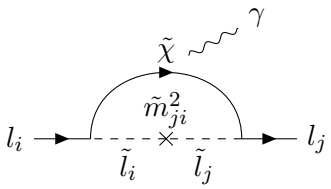

Figure 3.9: $l_i \to l_j\gamma$ in SUSY through sleptons mass mixing. $\tilde{\chi}$ correspond to charginos and neutralinos (mass eigenstates of electroweak gauginos and higgsinos).

LFV can be sizeable in the context of GUT theories with right-handed sterile neutrinos, which has been studied in [210,212–220]. In SO(10), right-handed neutrinos naturally appear in the **16** spinor representation that a SM generation fills, and neutrino masses can be explained with a supersymmetric seesaw mechanism. Considering heavy right-handed neutrinos, the superpotential in the lepton sector reads

$$W_L = [Y_e]_{ij}\bar{L}_i H_d E_j + [Y_\nu]_{ij}\bar{L}_i H_u N_j + \frac{1}{2}[M_R]_{ij} N_i N_j \tag{3.41}$$

where the notation for the SM superfields is self-explanatory, and N is the superfield that contains sterile neutrinos. As in Equation (3.13), for large Majorana masses M_R, the light neutrino mass matrix is

$$m_\nu = -Y_\nu M_R^{-1} Y_\nu^T v^2 \sin^2\beta \qquad \text{where } \tan\beta = \frac{\langle H_u\rangle}{\langle H_d\rangle},\ v = 174 \text{ GeV} \tag{3.42}$$

The gravity-mediated soft breaking terms involving the sleptons are the following

$$-\mathcal{L}_{soft} = m_0^2(\tilde{\ell}_i^\dagger \tilde{\ell}_i + \tilde{e}_i^\dagger \tilde{e}_i) + m_0 a_0([Y_e]_{ij}\tilde{\ell}_i^\dagger H_d \tilde{e}_j + [Y_\nu]_{ij}\tilde{\ell}_i^\dagger H_u \tilde{N}_j + \text{h.c}) \tag{3.43}$$

and the left-handed sleptons mass matrix is renormalized in the leading-log approximation as [212]

$$[\Delta \tilde{m}_L^2]_{ij} = -\frac{1}{8\pi^2}[Y_\nu^\dagger Y_\nu]_{ij} m_0^2(3 + |a_0|^2) \log\left(\frac{M_{\text{Pl}}}{M_R}\right) \tag{3.44}$$

The typical size of $l_i \to l_j\gamma$ branching fraction is [215]

$$Br(l_i \to l_j\gamma) \sim \frac{\alpha_{em}^3}{G_F^2} \frac{\left|\Delta \tilde{m}_{Lji}^2\right|^2}{m_{SUSY}^8} \tan^2\beta \times Br(l_i \to l_j \bar{\nu}_j \nu_i) \tag{3.45}$$

where m_{SUSY} is the sparticles mass scale. In general, even knowing neutrino masses and mixing angles, the neutrino Yukawa Y_ν is not uniquely defined [221]. In a basis where the Majorana masses $\hat{M}_R$ are diagonal, we can use the Casas-Ibarra parametrization [215] for Y_ν

$$Y_\nu \sim (U\sqrt{\hat{m}_\nu} R \sqrt{\hat{M}_R})/(v \sin\beta)^2 \tag{3.46}$$

where U is PMNS and R is an unknown orthogonal complex matrix. The matrix that controls the slepton mixing is then

$$Y_\nu^\dagger Y_\nu \sim \sqrt{\hat{M}_R} R^\dagger \hat{m}_\nu R \sqrt{\hat{M}_R} \tag{3.47}$$

and depends on R. Assuming specific mass hierarchy and degenerate patterns for neutrinos, the free parameters in R are reduced, and the predicted LFV signals are studied when the parameters are varied [222]. In SO(10) GUT, the neutrino and up Yukawa are unified at the GUT scale, and different breaking scenarios can lead to lepton flavor change dominated by the CKM or PMNS mixing with the third generation [216,217]. The PMNS angles are large and lead to an insufficiently suppressed $\mu \to e\gamma$ rate, larger than the current upper limit $Br(\mu \to e\gamma) < 4.2 \times 10^{-13}$ [223]. In the scenario where LFV amplitudes are proportional to CKM matrix elements, the rate is compatible with the current experimental upper bound and part of the parameter space could be probed by the upcoming searches $Br(\mu \to e\gamma) \sim 6 \times 10^{-14}$ [224]. The model predicts a correlation between the branching ratios of $\tau \to l\gamma$ and $\mu \to e\gamma$ which is

$$Br(\tau \to \mu\gamma) \sim \frac{|V_{33}V_{23}|^2}{|V_{13}V_{23}|^2} Br(\mu \to e\gamma) \times 10^{-1} \lesssim 10^{-10} \tag{3.48}$$

where V is the CKM matrix. Assuming no detection from MEGII $Br(\mu \to e\gamma) < 6 \times 10^{-14}$, an observation of $Br(\tau \to \mu\gamma) \sim 10^{-9}$ at Belle II [225] can disfavor the model. In the context of sleptons mixing and LFV, several simplified SUSY scenarios have been more recently studied, complemented with the bounds of the null results of the LHC [226].

The soft-breaking sector is not the only possible source of LFV in supersymmetric SM. Gauge and SUSY invariance allow for the following terms in the superpotential:

$$W_{RPV} = \frac{\lambda_{ijk}}{2} L_i L_j \bar{E}_k + \lambda'_{ijk} L_i Q_j \bar{D}_k + \lambda''_{ijk} \bar{U}_i \bar{D}_j \bar{D}_k + \mu_i L_i H_u \tag{3.49}$$

The λ'' term is baryon number violating and can lead to prompt proton decay. To avoid this disastrous outcome, $R-$parity is often assumed. The $R-$parity of a particle is defined as $(-1)^R \equiv (-1)^{3(B-L)+2S}$, where B, L are the baryon and lepton number, while S is the particle spin. It follows that any SM particle is $RP-$even and the superpartners are $RP-$odd. $RP-$invariance automatically forbids all terms in the superpotential of Equation (3.49), but other discrete symmetries such as baryon parity [227] can allow for lepton flavor violation while conserving the baryon number. The first two terms in the superpotential leads to the Lagrangian terms [228]

$$\begin{aligned}\mathcal{L}_{RPV} = \lambda_{ijk}(\overline{\nu^c}_{Li} e_{Lj} \tilde{e}^{\dagger}_{Rk} + \bar{e}_{Rk}\nu_{Li}\tilde{e}_{Lj} + \bar{e}_{Rk} e_{Lj}\tilde{\nu}_{iL}) \\ +\lambda'_{ijk}(V_{jm}\bar{d}_{Rk} d_{Lm}\tilde{\nu}_{iL} + V_{jm}\bar{d}_{Rk}\nu_{Li}\tilde{d}_{mL} + V_{jm}\overline{\nu^c}_{Li} d_{Lm}\tilde{d}^{\dagger}_{Rk} + \\ -\bar{d}_{Rk}u_{Lj}\tilde{e}_{Li} - \bar{d}_{Rk}e_{Li}\tilde{u}_{Lj} - \overline{e^c}_{Li}u_{Lj}\tilde{d}^{\dagger}_{Rk}) + \text{h.c}\end{aligned} \tag{3.50}$$

that can allow for several LFV processes already at tree level. In Figure 3.10a, we show a diagram for the LFV K^0 decay $K^0_L \to \mu e$, whose branching fraction is constrained by the current upper limit $Br(K^0_L \to \mu e) < 4.7 \times 10^{-12}$ [229]. Assuming only one non-zero pair of R-parity violating coupling $\lambda'^*_{ik1}\lambda'_{jk2}$, the bound implies (adapted from [230])

$$\left|\lambda'^*_{1k1}\lambda'_{2k2}\right| \times \left(\frac{100\ \text{GeV}}{m_{\tilde{u}_k}}\right)^2 < 1.3 \times 10^{-7} \qquad \to \qquad \left|\lambda'^*_{1k1}\lambda'_{2k2}\right| \lesssim 10^{-4} \tag{3.51}$$

where we have assumed $m_{\tilde{u}_k} \sim$ few $\times$ TeV. Similarly, $Br(\mu \to 3e) < 10^{-12} \to 10^{-16}$ [231, 232] can set the following constraint on the coupling products $|\lambda_{n21}\lambda^*_{n11}|$ (λ is anti-symmetric in the first two indices and $n \neq 1$) from the diagrams of Figure 3.10b:

$$|\lambda_{n21}\lambda^*_{n11}| \times \left(\frac{100\ \text{GeV}}{m_{\tilde{\nu}_n}}\right)^2 < 6.6 \times 10^{-7}\ (6.6 \times 10^{-9}) \tag{3.52}$$

$\lambda\lambda'$ diagram give tree-level contributions to $\mu \to e$ conversion, and at one loop $l_i \to l_j\gamma$ is sensitive to $\lambda\lambda, \lambda'\lambda'$ couplings. For a more complete discussion on LFV in R-parity violating theories, we refer the reader to [233–238].

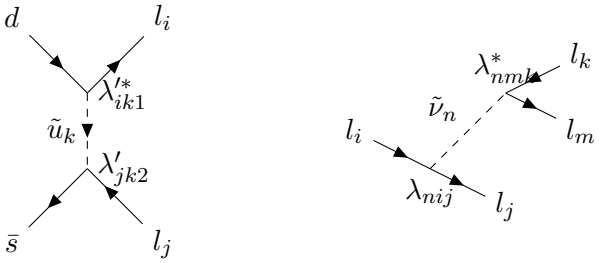

Figure 3.10: Examples of LFV tree-level diagrams in the supersymmetric SM with R-parity violation. (**a**) Diagrams contributing to the LFV meson decay $K^0 \to l_i l_j$. (**b**) Diagrams contributing to the $l_i \to l_j l_k l_m$ rate.

3.3 Experimental Searches

Searches for CLFV signals span a broad range of experimental techniques thanks to the large variety of processes one could be looking for, such as rare muon and tau decays ($\mu^+ \to e^+\gamma$, $\mu^\pm \to e^\pm e^- e^+$,

$\tau^{\pm} \to \mu^{\pm}\gamma$, $\tau^{\pm} \to e^{\pm}\gamma$, $\tau \to 3l$), rare mesons and bosons decays, and direct conversions of a lepton in a nuclear field ($\mu^{-}\mathrm{N} \to e^{-}\mathrm{N}$, $\mu^{-}\mathrm{N} \to e^{+}\mathrm{N}'$). Table 3.2 summarizes the current best limits on the various channels. The CLFV searches based on muons have been performed with dedicated experiments, usually highly tuned for a specific channel, which took advantage of the facilities capable of delivering a high intensity muon beam (see next section). For all the other cases (tau, mesons and bosons), with the only exception made for the Kaons, it is not possible to deliver a dedicated beam; thus, general purpose detector systems have been used. As discussed in the previous sections, the most stringent constraints on various BSM models are set by the direct searches of CLFV decays of muons and taus decays. In the following sections, we describe the most recent and the coming experimental efforts for these two categories: (i) searches using muons, (ii) searches using taus. For each search, a discussion of the peculiarities of the signal topology and of the various experimental challenges is provided.

3.3.1 CLFV Searches Using Muons

In the history of CLFV experiments, muons have been, so far, the most popular. Historically, the first experiment looking for CLFV using muons was performed by Hinks and Pontecorvo using atmospheric muons [261]. Since then, the advancements in the muon beam production/acceleration technology at different facilities (PSI, TRIUMPH, LANL, etc.) made available high-intensity muon beams at the level of $10^{8}(10^{7})\mu^{+}(\mu^{-})/s$ [144, 262], enabling the possibility to search for rare CLFV processes. Facilities under construction at Fermilab (USA) and J-PARC (Japan) [143], or planned, like the High Intensity Muon Beam project at the PSI (Switzerland) [263], have been designed to provide muon beams with an intensity of about 10^{10} μ/s. This planned intensity corresponds to 2–3 orders of magnitude improvement with respect to the current state-of-the-art technology. The J-PARC and Fermilab muon experiments will use a novel method for creating the muon beam. A prototype muon beamline, the Muon Science Innovative Channel (MuSIC), was set up at the Research Center for Nuclear Physics (Osaka, Japan) to prove the conceptual idea. The production of an intense muon beam relies on the efficient capture of pions (from proton-target interactions), which subsequently decay to muons, using a novel superconducting solenoid magnet system [264]. The current best limits on the muon-CLFV processes come from experiments that performed dedicated searches for the following processes: $\mu^{+} \to e^{+}\gamma$, $\mu^{\pm} \to e^{\pm}e^{-}e^{+}$, $\mu^{-}\mathrm{N} \to e^{-}\mathrm{N}$ and $\mu^{-}\mathrm{N} \to e^{+}\mathrm{N}'$. Table 3.2 summarizes these results. One thing to notice is that all the searches, except the $\mu^{-}\mathrm{N} \to e^{-}\mathrm{N}$ and $\mu^{-}\mathrm{N} \to e^{+}\mathrm{N}'$, were performed using μ^{+} rather than μ^{-}. This choice is motivated by several advantages: (i) μ^{+} cannot get captured in nuclei, while μ^{-} can undergo nuclear capture events, which produce protons, neutrons, photons and, thus, increase the activity in the detector deteriorating its performance, (ii) the muon beam is obtained from charged pions decay, which are produced in proton-target interactions where π^{+} production is larger; thus, the resulting μ^{+} beam intensity is higher. The following sections offer a more detailed description of each of these experimental searches.

3.3.1.1 $\mu^{+} \to e^{+}\gamma$

In the $\mu^{+} \to e^{+}\gamma$ decay, the final state consists of a back-to-back positron and photon with an energy of 52.8 MeV. The background sources for this search can be factorized into two main

Table 3.2: Current experimental upper limits on the branching ratios of CLFV processes for muons, taus, mesons (π, J/ψ, B, K) and bosons (Z^0, h).

Process	Experiment	Limit	C.L.
$\mu^+ \to e^+\gamma$	MEG	4.2×10^{-13} [223]	90%
$\mu^+ \to e^+e^-e^+$	SINDRUM	1.0×10^{-12} [239]	90%
$\mu^-\mathrm{N} \to e^-\mathrm{N}$	SINDRUM-II	$6.1(7.1) \times 10^{-13}$ Ti (Au) [240,241]	90%
$\mu^-\mathrm{N} \to e^+\mathrm{N}'$	SINDRUM-II	5.7×10^{-13} [242]	90%
$\tau^\pm \to e^\pm\gamma$	BaBar	3.3×10^{-8} [243]	90%
$\tau^\pm \to \mu^\pm\gamma$	BaBar	4.4×10^{-8} [243]	90%
$\tau \to eee$	Belle	2.7×10^{-8} [244]	90%
$\tau \to \mu\mu\mu$	Belle	2.1×10^{-8} [244]	90%
$\tau \to \mu ee$	Belle	1.8×10^{-8} [244]	90%
$\tau \to e\mu\mu$	Belle	2.7×10^{-8} [244]	90%
$\tau \to \pi^0 e$	Belle	8.0×10^{-8} [245]	90%
$\tau \to \pi^0 \mu$	BaBar	1.1×10^{-7} [246]	90%
$\tau \to \eta e$	Belle	9.2×10^{-8} [245]	90%
$\tau \to \eta \mu$	Belle	6.5×10^{-8} [245]	90%
$\tau \to \rho^0 e$	Belle	1.8×10^{-8} [247]	90%
$\tau \to \rho^0 \mu$	Belle	1.2×10^{-8} [247]	90%
$\pi^0 \to \mu e$	kTeV	3.6×10^{-10} [248]	90%
$K_L^0 \to \pi^0\mu^+e^-$	kTeV	7.6×10^{-11} [248]	90%
$K_L^0 \to \mu e$	BNL E871	4.7×10^{-12} [229]	90%
$K^+ \to \pi^+\mu^+e^-$	BNL E865	1.3×10^{-11} [249]	90%
$J/\psi \to \mu e$	BESIII	1.5×10^{-7} [250]	90%
$J/\psi \to \tau e$	BESIII	7.5×10^{-8} [251]	90%
$J/\psi \to \tau\mu$	BESII	2.6×10^{-6} [252]	90%
$B^0 \to \mu e$	LHCb	2.8×10^{-9} [253]	95%
$B^0 \to \tau e$	BaBar	2.8×10^{-5} [254]	90%
$B^0 \to \tau\mu$	LHCb	1.4×10^{-5} [255]	95%
$B \to K\mu e$	BaBar	3.8×10^{-8} [256]	90%
$B \to K^*\mu e$	BaBar	5.1×10^{-7} [256]	90%
$B^+ \to K^+\tau e$	BaBar	4.8×10^{-5} [257]	90%
$B^+ \to K^+\tau\mu$	BaBar	3.0×10^{-5} [257]	90%
$B_s^0 \to \mu e$	LHCb	1.1×10^{-8} [253]	90%
$B_s^0 \to \tau\mu$	LHCb	4.2×10^{-5} [255]	95%
$Z^0 \to \mu e$	ATLAS	7.5×10^{-7} [258]	95%
$Z^0 \to \tau e$	OPAL	9.8×10^{-6} [259]	95%
$Z^0 \to \tau\mu$	DELPHI	1.2×10^{-5} [260]	95%
$h \to \mu e$	ATLAS	6.1×10^{-5} [190]	95%
$h \to \tau e$	CMS	2.2×10^{-3} [191]	95%
$h \to \tau\mu$	CMS	1.5×10^{-3} [191]	95%

categories: (i) an intrinsic physics background from the Radiative Muon Decay (RMD) process $\mu^+ \to e^+\gamma\nu_e\bar{\nu}_\mu$, where the neutrinos carry off small momenta, and (ii) an "accidental" background where a positron from the Michel decay $\mu^+ \to e^+\nu_e\bar{\nu}_\mu$, together with a photon from an RMD event or an electron-positron annihilation in flight or an $e-N$ nucleus scattering, recreate the topology of the $\mu^+ \to e^+\gamma$ decay. While signal and RMD rates are proportional to the muon stopping rate R_μ, the accidental background rate is proportional to R_μ^2 because both particles come from the beam; the accidental background is, therefore, the dominant enemy of this search. Thus, a continuous muon beam is better suited than a pulsed beam to avoid stripping particles in short bunches, and R_μ must be carefully chosen to optimize the sensitivity. The $\mu^+ \to e^+\gamma$ searches from the last decades confirmed that the accidental background is dominant, while the intrinsic background accounts for about 10% of the total background budget. Two different strategies have been applied for designing the experimental apparatus for the $\mu^+ \to e^+\gamma$ search: (i) a tracking-only system equipped with a converter to convert the photon in an e^+e^- pair, or (ii) a tracker combined with a calorimeter for the photon detection. The tracking-only solution has a much better resolution but a cost of a loss in acceptance because converting the photon requires material that spoils the resolution (due to energy loss and multiple scattering) but too little limits the size of the data sample.

One of the first experiments to adopt the calorimetric solution for the photon detection was the Crystal Box experiment at Los Alamos Meson Physics Facility (LAMPF) [265]. The experiment, shown in Figure 3.11, used a surface muon beam at LAMPF with an average intensity of 300 kHz. The detector consists of a cylindrical drift chamber surrounded by 396 NaI(Tl) crystals. A layer of scintillation counters in front of the crystals provided a timing measurement for the electrons and a veto for photons. The energy resolution for electrons and photons was ∼6% (FWHM). The position resolution of the drift chamber was 350 µm, while the time resolution was ∼400 ps for the scintillators and ∼ 1 ns for the crystals.

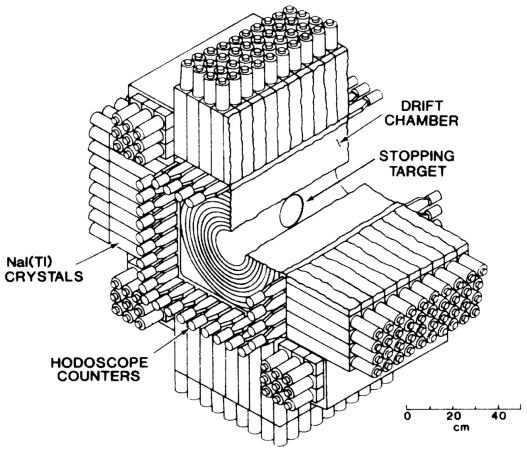

Figure 3.11: Schematic of the Crystal Box experiment (Figure from [265]).

A total of 3×10^{12} muon were stopped in a thin polystyrene stopping target. A maximum likelihood analysis established a 90% C.L. upper limit of 4.9×10^{-11} [265].

The next-generation experiment, MEGA [266], was also performed at LAMPF. The MEGA experimental apparatus, shown in Figure 3.12, used a surface muon beam at the stopped muon channel

at LAMPF that was stopped in a 76 µm Mylar foil centered in the 1.5 T magnetic field of a superconducting solenoid. The MEGA detector consisted of a magnetic spectrometer for the positron and three spectrometers for the photon, therefore sacrificing the signal acceptance and efficiency for a better resolution and background rejection. In total, 1.2×10^{14} muons were stopped during the life of the experiment, and the overall efficiency for the observation of the $\mu^+ \to e^+\gamma$ event was $\sim 3.9 \times 10^{-3}$. The small efficiency was due to the photon conversion probability (∼2.5%) and to the reduced capability of reconstructing the positron tracks in the solenoidal field compared to the design value. For these reasons, the final sensitivity reached by the MEGA experiment, 1.2×10^{-11} @ 90% C.L. [266], was ∼35 times worse than the design value, proving how challenging it is to deliver progress in this type of search.

The current best limit for the $\mu^+ \to e^+\gamma$ branching ratio, 4.2×10^{-13} @ 90% C.L., comes from the MEG experiment [223]. The detector system, shown in Figure 3.13, covers ∼10% of the solid angle and surrounds a 205 µm-thick polyethylene muon stopping target. The apparatus consists of a positron spectrometer and a liquid-xenon (LXe) calorimeter.

MEG opted for no converter for the photon detection, the opposite of MEGA. This choice avoids the pileup problem in the pattern recognition that limited MEGA but, at the same time, limits the geometrical acceptance. Table 3.3 summarizes the detector performance measured during the MEG operation [224]. A key feature of MEG is the magnetic field design. MEG adopted a graded solenoidal field, set at ∼1.1 T near the center of the apparatus, that sweeps out the positrons emitted at ∼90 deg and provides a constant bending radius for the signal positron essentially independent of the angle of emission. This feature helps in achieving a uniform and efficient signal track reconstruction. Another technological breakthrough from the MEG experiment is the development of the liquid Xe (LXe) calorimeter. The MEG LXe calorimeter is the first application of a large volume of LXe for particle detection and, so far, it proved to have the best performance for the electromagnetic calorimetry detection in the energy range below 100 MeV [267].

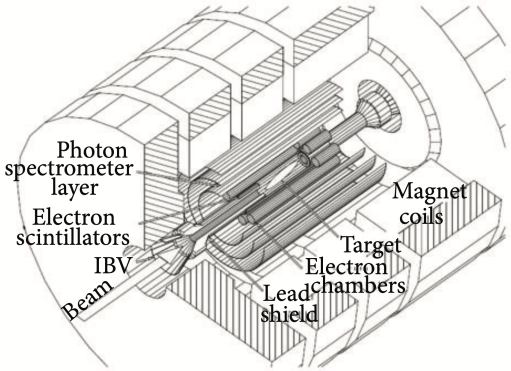

Figure 3.12: Schematic of the MEGA experiment (Figure from [266]).

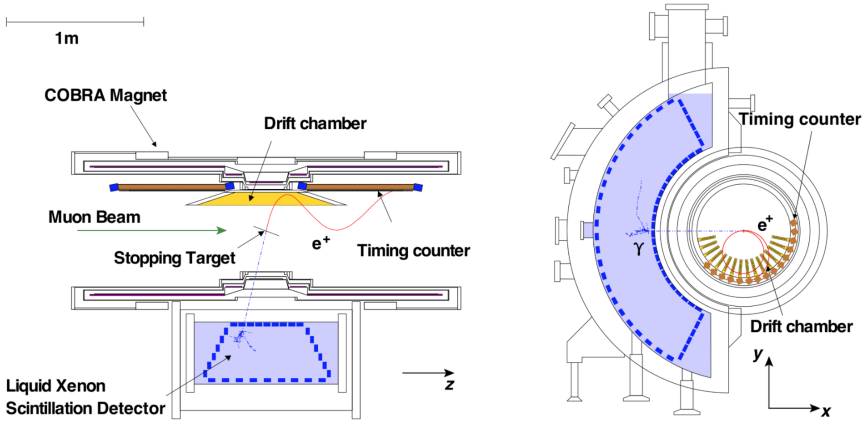

Figure 3.13: Schematic of the MEG experiment (Figure from [223]).

Table 3.3: Summary of detector performance for the MEG and MEG-II experiments [224]. σ_X indicates the resolution of the observable X, ε_X the detection efficiency for the particle X. For the case of the photon energy resolution σ_{E_γ}, the two values refer to the shallow (<2 cm)/deep (>2 cm) events. $\sigma_{t_{e^+\gamma}}$ is the time resolution on the $e^+ - \gamma$ time residual. The reported values for the MEG-II case refer to the updated results from the engineering runs reported in [224].

	$\sigma_{p_e^+}$	$\sigma_{\theta_e^+}$	σ_{E_γ}	σ_{x_γ}	$\sigma_{t_{e^+\gamma}}$	ε_{e^+}	ε_γ
MEG	380 keV/c	9.4 mrad	2.4%/1.7%	5 mm	122 ps	30%	63%
MEG-II	100 keV/c	6.7 mrad	1.7%/1.7%	2.4 mm	70 ps	65%	69%

Recently, the MEG collaboration worked on the upgrade of the experiment (MEG II), which aims to reach a sensitivity of 6×10^{-14} 90% C.L. [224]. Various improvements on the detector were delivered. The positron spectrometer was replaced with a low-mass single-volume cylindrical drift chamber with high rate capability. This increased the acceptance of the spectrometer with respect to the MEG configuration by more than a factor of 2. The LXe calorimeter was also upgraded by replacing the MEG photomultiplier tubes (PMTs) with smaller vacuum-ultraviolet sensitive silicon photomultipliers (SiPMs). A novel timing detector for an active suppression of the accidental background was also introduced. The results of the engineering runs showed a fast degradation of the wires of the drift chamber and of the SiPMs [224]. Table 3.3 compares the new detector performance with the previous ones reported for the MEG detector. The MEG-II collaboration plans to build a new chamber to replace the existing one, and they will take advantage of the coming engineering runs to study more carefully the degradation of the SiPMs. Preliminary results show that they can adjust the operation conditions to achieve the desired level of sensitivity [224].

3.3.1.2 $\mu^\pm \to e^\pm e^- e^+$

In the $\mu^\pm \to e^\pm e^- e^+$ decay, the final state consists of two positrons and one electron emerging from the same vertex with an invariant mass that matches the muon rest mass. In a three-body decay, the energy associated to each product is not a fixed amount. Simple relativistic kinematics consideration show that the maximum energy of one of the decay products is about $m_\mu/2$ and that

the decay can be described by two independent variables. The energy distribution of each daughter particle depends on the exact dynamics of the underlying unknown physics. In general, the highest energy particle is expected to have a momentum larger than 35 MeV/c, while the distribution of the lowest energy particle peaks near zero and decreases quickly as its energy tends to its upper limit so that only about one half have an energy larger than 15 MeV [144]. The background sources for this search can be factorized in two main categories: a physical background coming from the $\mu^+ \to e^+\bar{\nu}_\mu\nu_e e^- e^+$ process, and an uncorrelated component coming from the accidental coincidence of a positron from a Michel decay and a positron-electron pair produced by the interactions of other positrons or muon with the target or the detector material. The accidental background component scales quadratically with the muon beam intensity. As in the $\mu^+ \to e^+\gamma$ case, it is more convenient to design an experimental apparatus that uses positive muons.

The current best limit on $\mu^\pm \to e^\pm e^- e^+$, 1.0×10^{-12} [239] at 90% C.L., was set by the SINDRUM experiment at PSI [239] based on $\sim 10^6$ stopped μ^+. The SINDRUM apparatus, shown in Figure 3.14, consisted of a double cone-shaped stopping target in the middle of five concentric multi-wire proportional chambers surrounded by an array of plastic scintillator counters inside a solenoidal magnetic field. For a 50 MeV electron/positron, the detector apparatus had a momentum resolution at the level of $\sim$1 MeV/c, a timing resolution ≤ 1 ns and a vertex resolution of $\sim$1 cm. The data reduction was achieved with a multiple stage trigger, taking advantage of track and charge pre-filters that were requiring at least one negatively and two positively charged tracks within a time window of 7 ns. Then, a track-correlator was used to limit the total transverse momentum of the $e^+e^-e^+$ triplet below 17 MeV/c. In the statistical analysis, the event candidates were determined from the two-dimensional distribution of $\sum E_i$ vs. $\hat{p}^2$, where $\hat{p} = (p_L/\sigma_L)^2 + (p_T/\sigma_T)^2$ (L and T denote the longitudinal and transverse components with respect to the beam axis). This parametrization is particularly convenient because the signal candidates satisfy $\sum E_i = m_\mu$ and $\hat{p}^2$ is expected to peak near 0. A new effort to improve the sensitivity on $\mu^\pm \to e^\pm e^- e^+$ search is underway at PSI by the Mu3e collaboration [231]. The Mu3e experiment aims for a 10^{-16} single-event sensitivity, which would correspond to an improvement by four orders of magnitude compared to the limit set by the SINDRUM experiment. Such a leap in sensitivity is enabled by: (i) the availability of high-intensity muon beams, (ii) the use of silicon pixel detectors instead of multi-wire proportional chambers to track the decay products, and (iii) a modern data-acquisition system able to handle the vast amount of data produced by the detector. A first phase of the experiment is currently under construction at the πE5 beamline at PSI, where the intense DC surface muon beam of $10^8 \mu^+/s$ will be exploited to achieve a single event sensitivity of 2×10^{-15} in about 300 days of data taking [232]. The Mu3e experimental setup is shown in Figure 3.15. It is designed to track the two positrons and one electron from the positive muon decaying at rest with a light-weight tracker placed inside a 1 T magnetic field, thereby reconstructing the decay vertex and invariant mass.

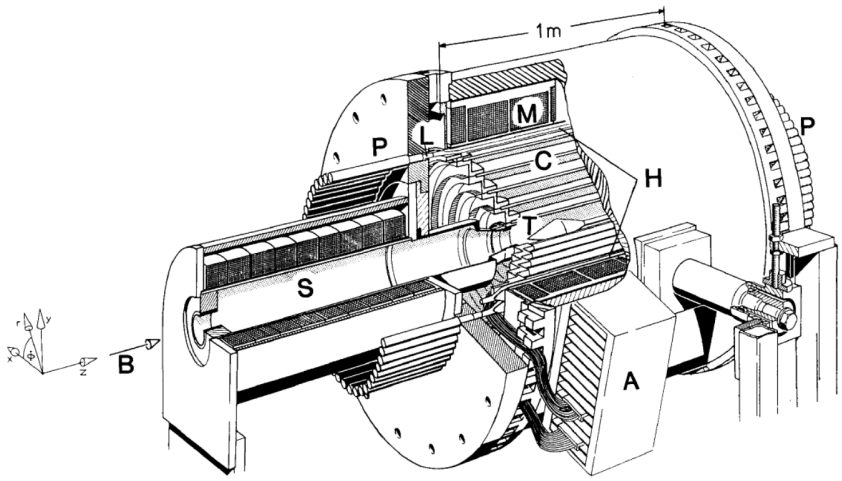

Figure 3.14: Schematic of the SINDRUM experiment. B, muon beam; S, focussing solenoid; T, target; C, five cylindrical multi-wire proportional chambers; H, hodoscope of 64 scintillators; L, light guides for the hodoscope; P, 128 photomultipliers; A, preamplifiers for the cathode strips and amplifier/discriminators for the anode wires; M, normal conducting coil of the magnet. Figure and caption from [268].

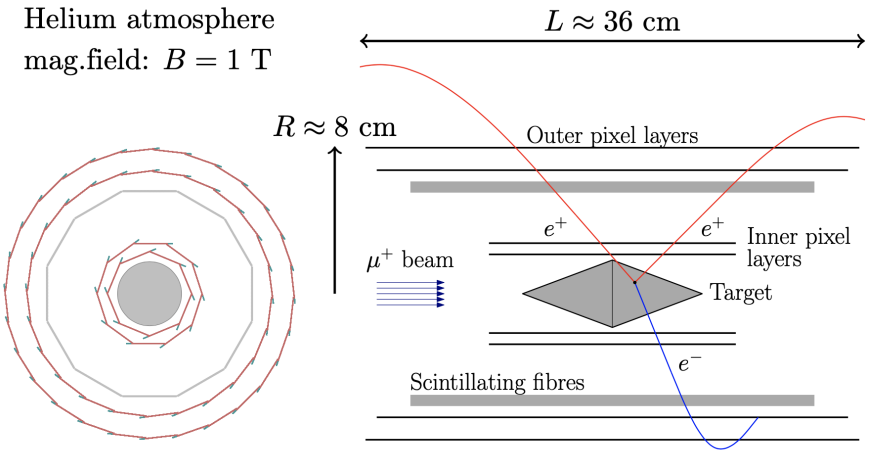

Figure 3.15: Schematic of the Mu3e experiment (Figure from [232]).

The muon beam is stopped in a hollow double-cone target placed at the center of the Mu3e solenoid. This allows for the spread out of the decay vertices in z and minimizes the amount of target material traversed by the decay particles. The target is surrounded by the cylindrical central tracker, which consists of an inner silicon pixel detector, a scintillating fiber tracker for time measurements, and an outer silicon pixel detector. A momentum resolution of better than 1 MeV/c at @ 50 MeV/c is achieved by letting the positrons (electrons) re-curl in the magnetic field, either crossing the central tracker again or hitting the outer tracking stations surrounding the upstream and downstream beam pipe. These stations consist of a silicon pixel tracker and a scintillating tile

detector mounted on the inside of the pixel tracker. The 5 mm thick tiles enable a time resolution for the tracks reaching these outer stations of better than 100 ps. The material budget, which must be minimized to reduce the multiple scattering and thus deliver the required momentum resolution, was minimized by means of custom High-Voltage Monolithic Active Pixel Sensor (HV-MAPS) [269] based on a commercial 180 nm HV-CMOS process. Together with its support structure, the entire silicon tracking module has a thickness of ∼0.12% radiation lengths, with a single-hit efficiency $> 99\%$ and a time resolution of $O(10$ ns). A gaseous helium cooling system allows the experiment to dissipate 250 mW/cm^2 of power generated by the MAPS modules. A time resolution of about 10 ns is insufficient to determine the direction and thus the charge of the decay particles. A scintillating fiber detector is, therefore, placed between the inner and outer layer of the central silicon-pixel tracker, consisting of a dozen 30 cm long ribbons made from three staggered layers of 250 µm diameter multi-clad round fibers, read out by Silicon Photomultipliers (SiPM) arrays on both sides. Located at the very end of the re-curling particle trajectories hitting the upstream or downstream tracker, where the constraints on the material budget are less stringent, the tile detector provides the needed precise timing information of the particle tracks, in conjunction with the fiber detector, significantly reducing the accidental background. Each tile is read out by a single SiPM. For the tile and fiber detector, a time resolution of <50 ps and <400 ps is achieved, respectively. Mu3e had a successful integration run campaign from May to July 2021 with a reduced detector: 2 pixel layers + fiber detector.

3.3.1.3 $\mu^-\mathrm{N} \to e^-\mathrm{N}$

$\mu^-\mathrm{N} \to e^-\mathrm{N}$ conversion is the process where a muon converts into an electron in the field of a nucleus without producing neutrinos in the final state. This process has the same dynamic of a two-body decay and, therefore, results with a monochromatic electron with an energy $E_{\mu e}$:

$$E_{\mu e} = m_\mu - E_b - \frac{E_\mu^2}{2m_N},$$

where m_μ is the muon mass, $E_b \sim Z^2\alpha^2 m_\mu/2$ is the muonic binding energy and the last term is from nuclear recoil energy up to terms of order $1/m_N^2$, neglecting variations of the weak-interaction matrix element with energy [143], where $E_\mu = m_\mu - E_b$ and m_N is the atomic mass. In the case of Al, which is the selected material for the current experiments under construction, $E_{\mu e} \sim$ 104.96 MeV. In muon conversion experiments, the quantity

$$R_{\mu e} = \frac{\Gamma(\mu^-\mathrm{N} \to e^-\mathrm{N})}{\Gamma(\mu^- + N \to all - capture)}$$

is measured. The normalization to captures simplifies calculations as many details of the nuclear wavefunction cancel in the ratio [270]. The coherent conversion leaves the nucleus intact, and there is only one detectable particle in the final state. As we will see, the resulting electron energy stands out from the background, hence muon-electron conversion does not suffer from accidental background, and extremely high rates can be used. Negative muons stopped in the stopping target can undergo a nuclear capture. Particles generated in the muon capture (n, p and γ) may reach the detector system and create extra activity that can either obscure a conversion electron (CE) track or create spurious hits. As a result, some specific shielding is required to reduce this background.

Electrons from the high momentum tail of the muon decay-in-orbit (DIO) represent the intrinsic background source for the $\mu^-\mathrm{N} \to e^-\mathrm{N}$ search. Figure 3.16 shows the energy spectrum of DIO electrons [271].

The main features of the DIO energy spectrum can be summarized as follows:

- the endpoint of the spectrum corresponds to the energy of the electrons from $\mu^-\mathrm{N} \to e^-\mathrm{N}$ conversion (CE);
- the overall spectrum is falling as $(E_\mu - E)^5$, where E is the DIO energy;
- about 10^{-17} of the spectrum is within the last MeV from the endpoint.

Therefore, to reach a high sensitivity at the level $O(10^{-17})$, the detector resolution is crucial. As the muon beam is generated from charged pions, another relevant background comes from the radiative pion capture (RPC) process $\pi^- N \to \gamma N^*$, followed by the electron-positron pair conversion of the photon. Unfortunately, not all pions decay in the transport line, and, consequently, the muon beam is contaminated by pions. This source of background is reduced by taking advantage of the difference between the pion and the muonic atom lifetimes. The pion has a decay constant $\tau <$ few tens of ns, while the bound muon has a τ of the order of several hundreds of ns (depending on the Z of the material). Therefore, using a pulsed beam structure, it is possible to set a live gate delayed with respect to the beam arrival, reducing the RPC contribution to the desired level. Other beam-related sources of background are: remnant electrons in the beam that scatter in the stopping target, muon decays in flight and antiprotons interacting in the apparatus. Atmospheric muons can also represent a significant source of background because these particles can interact in the apparatus and eventually generate a signature very similar to the CE. An active shielding is thus required to detect the incoming cosmic muons crossing the apparatus and veto the event candidates on time. Moreover, the detector system has to provide particle identification (PID) capabilities to reject un-vetoed muons that can mimic the CE due to a mis-reconstruction.

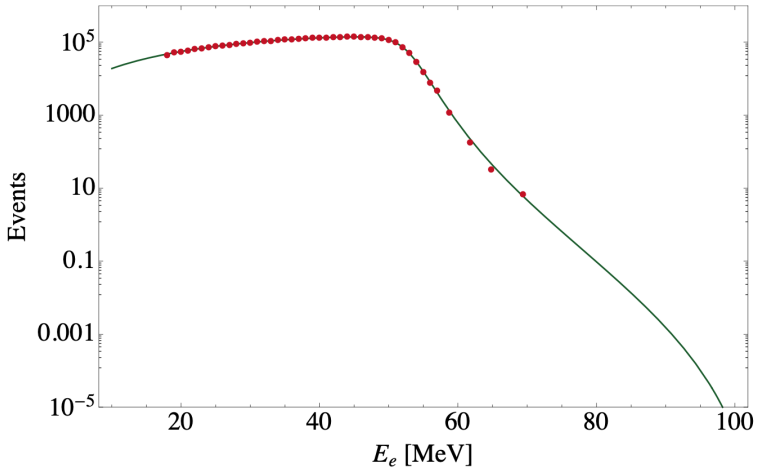

Figure 3.16: Energy spectrum of the DIO electrons (solid line) fitted to TWIST data (dots) [272]. Figure from [271].

The current best limit on the $\mu^- \mathrm{N} \to e^- \mathrm{N}$ measurement comes from the SINDRUM-II experiment at PSI [241]. In SINDRUM-II, a high intensity muon beam was stopped in a target that was surrounded by the detector elements housed in a superconducting solenoid. Figure 3.17 shows a sketch of the SINDRUM-II apparatus. The detector consisted of two drift chambers, to reconstruct the trajectories of the charged particles, and Cerenkov hodoscopes, to measure the timing of the reconstructed tracks and for providing PID capabilities.

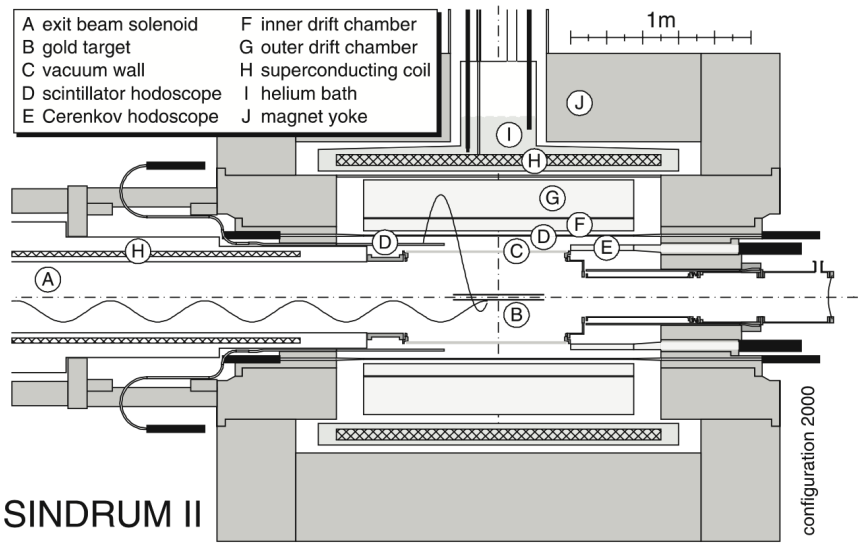

Figure 3.17: The SINDRUM-II experimental setup. Figure from [241].

With a total of $\sim 10^{14}$ stopped muons, SINDRUM-II reached a sensitivity at the level of $\sim 10^{-13}$ on the $\mu^- \mathrm{N} \to e^- \mathrm{N}$ process using different target materials [241].

New experimental concepts have been proposed and are currently under construction at Fermilab (USA) and J-PARC (Japan) to search for $\mu^- \mathrm{N} \to e^- \mathrm{N}$ with unprecedented sensitivity at the level of $\sim 10^{-17}$. The Mu2e experiment at Fermilab had its genesis back in the 1980s, behind the Iron Curtain. In a way, Mu2e was born in the Soviet Union. In 1989, the Soviet Journal of Nuclear Physics published a letter to the editor from physicists Vladimir Lobashev and Rashid Djilkibaev, where they proposed an experiment that would perform the most thorough search yet for muon-to-electron flavor violation. In 1992, they proposed the MELC experiment at the Moscow Meson Factory [273], but in 1995, due to the political and economic crisis, the experiment shut down. The same overall scheme was subsequently adopted in the Brookhaven National Laboratory MECO proposal in 1997 [274] and then in the Mu2e and COMET experiments.

The Mu2e apparatus [275], shown in Figure 3.18, consists of three main superconducting solenoids. The first two, named production and transport solenoid in Figure 3.18, are used to generate a high-intensity, low-momentum muon beam starting from a 8 GeV proton beam. The third solenoid, named "Detector Solenoid" in Figure 3.18, contains an Al stopping target, where the muons are stopped to generate the muonic atoms, and downstream to it, we have a low-mass straw-tube tracker [276], followed by a pure-CsI crystal calorimeter [277]. Both detectors are left un-instrumented in the inner 38 cm to avoid any interaction with the largest majority (>99%) of

the low momenta electrons coming from the muon DIO processes in the stopping target. In Mu2e, the stopping target is not placed in the middle of the tracker as it was done in SINDRUM-II to limit the flux of protons, photons and neutrons (from the muon nuclear captures) in the detector. A graded magnetic field around the stopping target increases the detector geometrical acceptance by reflecting the electrons that initially were emitted in the direction opposite to the detector. The whole detector solenoid and half of the transport solenoid are covered with a cosmic ray veto system designed to detect atmospheric muons with an efficiency $\geq$99.99%.

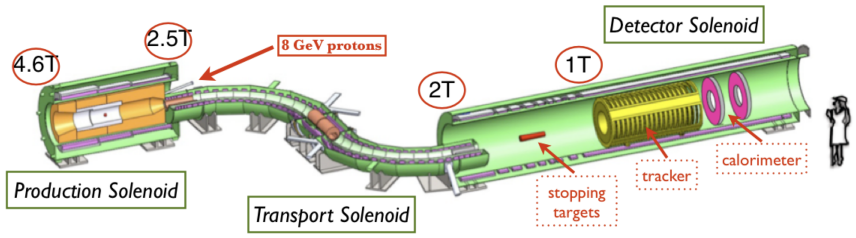

Figure 3.18: Schematic of the Mu2e experiment.

The design of the COMET experiment at J-PARC, shown in Figure 3.19, is based on a similar concept. A 8 GeV pulsed proton beam is used to produce pions, which are then captured and transported by a series of superconducting solenoids. The pions decay into muons as they travel along the muon transport channel. The toroidal field of the muon transport channel selects muons with negative charge and momentum less than 75 MeV/c. The major difference with respect to the Mu2e design is that a second transport line is installed between the muon stopping target and the detector regions to select charged particles of momentum centered around 100 MeV/c. The detector system consists of a straw-tube tracker followed by a LYSO crystal calorimeter [278].

COMET plans to operate in two stages: Phase-I and Phase-II. Phase-I will allow the experiment to characterize the beam and the key backgrounds as well as provide enough statistic to reach a 90% C.L. sensitivity at the level of 7×10^{-15} [278]. During Phase-I, COMET will operate with a smaller apparatus that consists of half of the first C-shaped muon transport line directly connected to a solenoid that houses the muon stopping target surrounded by the detector system. For Phase-I, the detector consists of a cylindrical drift chamber and a set of trigger hodoscope counters.

Another experiment, named DeeMe [279], aims to search for the $\mu^-\mathrm{N} \to e^-\mathrm{N}$ process with a single event sensitivity of 1×10^{-13} using a graphite target. The experiment is conducted at the Materials and Life Science Experimental Facility (MLF) of the J-PARC. Muonic atoms are produced in a primary-proton target itself, which is hit by pulsed proton beams from the Rapid Cycling Synchrotron (RCS) of J-PARC. To detect the electron and measure its momentum, a magnetic spectrometer, consisting of a dipole magnet and four sets of multi-wire proportional chambers (MWPCs) [280], is employed. The spectrometer is expected to reach a resolution of $\sigma_p < 0.5$ MeV/c at 100 MeV/c. The resolution is needed to reject the DIO background, which is the dominant source of high energy electrons for this search. The number of charged particles hitting the detectors is estimated with Monte Carlo simulation to be approximately 10^8 particles per proton-bunch with an RCS power of 1 MW. The construction of the secondary beamline for DeeMe, the H Line, is now in progress. Meanwhile, the collaboration measured the momentum

spectrum of the DIO electrons in the momentum region 48–62 MeV/c at the D2 area at MLF. This measurement will be important for validating the theoretical models used to model the DIO background and characterize the detector performance. Three sets of measurements were performed between the year 2017 and 2019 [279], and the analysis is now underway.

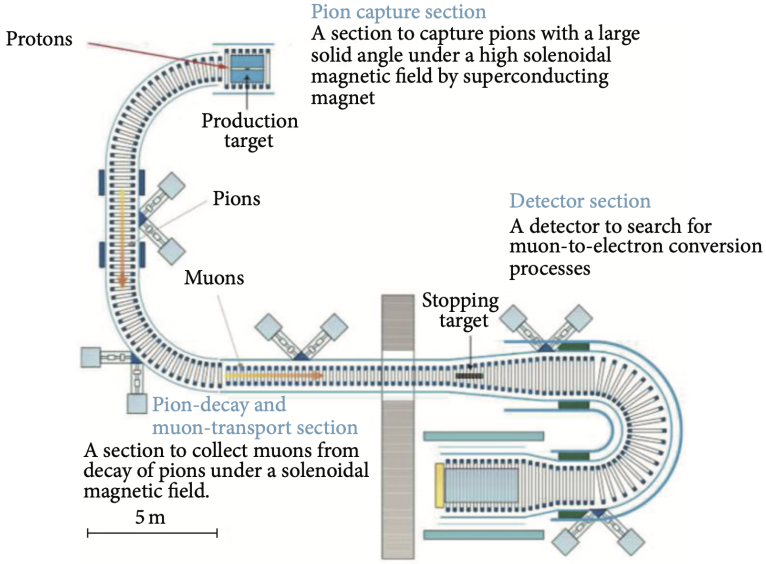

Figure 3.19: Schematic layout of COMET Phase-II (Figure from [278]).

3.3.1.4 $\mu^-\mathrm{N} \to e^+\mathrm{N}'$

$\mu^-\mathrm{N} \to e^+\mathrm{N}'$ conversion is the process where a muon converts into an positron in the field of a nucleus that undergoes a nuclear transition. This process violates the lepton number ($\Delta L = 2$) and the lepton flavor conservation. The experiments looking for the $\mu^-\mathrm{N} \to e^-\mathrm{N}$ process can typically search for the $\mu^-\mathrm{N} \to e^+\mathrm{N}'$ as well. The current best limit on the $\mu^-\mathrm{N} \to e^+\mathrm{N}'$ process comes from the SINDRUM-II experiment [242] that set a limit at 5.7×10^{-13} at 90% C.L. The major background source is the radiative muon capture, where the photon can generate (via asymmetric conversion) a positron with an energy close to the signal region.

The search for the $\mu^-\mathrm{N} \to e^+\mathrm{N}'$ complements the $0\nu\beta\beta$ decay searches and is sensitive to potential flavor effects in the neutrino mass-generation mechanism. We refer the reader to [281] for additional information about the current status and future prospects offered by the COMET and Mu2e experiments.

3.3.2 CLFV Searches Using Taus

The tau lepton is, in principle, a very promising source of CLFV decays. Thanks to the large tau mass ($m_\tau \approx 1.777$ GeV), many CLFV channels can be investigated: $\tau^\pm \to \mu^\pm\gamma$, $\tau^\pm \to e^\pm\gamma$, $\tau \to 3l$, $\tau \to l + h$, ... ($l = e,\ \mu$ and h is a light hadron). Table 3.2 lists the current best limits on the tau CLFV searches, and Figure 3.20 shows the individual results from the BaBar [282], Belle [283] and the LHCb [284] experiments, together with their combination.

From the experimental point of view, however, a difficulty immediately arises: the tau is an unstable particle, with a very short lifetime ($\tau = 2.91 \times 10^{-13}$ s). As a result, tau beams cannot be realized, and large tau samples must be obtained in intense electron or proton accelerators, operating in an energy range where the tau production cross section is large.

At e^+e^- and pp collider machines, the majority of the tau particles are not produced at rest, which means that, unlike the muon searches discussed before, here we need to deal with decays-in-flight. Thanks to the boost, the decay products could get energy values up to several GeV, which experimentally poses the challenge to deliver wide-range calibrations for the detectors (from a few hundreds of MeV to several GeV). For all these searches, events contain a pair of taus in which one tau undergoes SM decay (tag side), while the signal side is selected on the basis of the appropriate topology of each individual channel. The tagging side accepts the leptonic ($\tau \to l\nu\bar{\nu}$) and 1-prong hadronic decays, while on the signal side, CLFV candidates are selected on the basis of the appropriate topology of each individual channel.

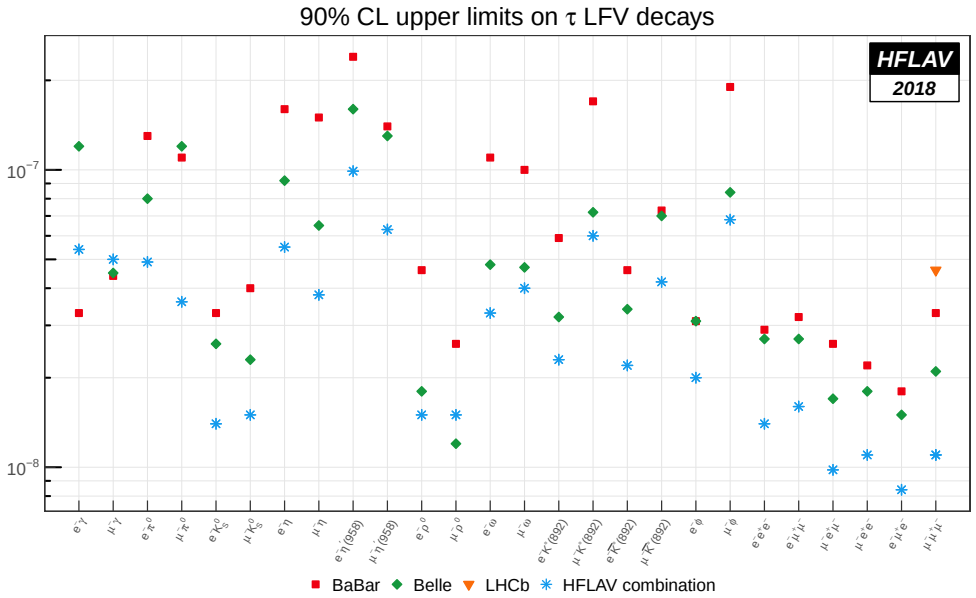

Figure 3.20: Tau lepton-flavor-violating branching fraction upper limits combinations summary plot. For each channel, we report the HFLAV combined limit and the experimental published limits. In some cases, the combined limit is weaker than the limit published by a single experiment. This arises since the CLs method used in the combination can be more conservative compared to other legitimate methods, especially when the number of observed events fluctuates below the expected background [285].

The following paragraphs discuss the current best limits for some of these experimental searches from experiments at B-factories and pp colliders.

3.3.2.1 $\tau \to l\gamma$

The $\tau \to l\gamma$ decay, where l is a light lepton (e, μ), has been one of the most popular CLFV tau channels. The signal is characterized by a $l^{\pm} - \gamma$ pair with an invariant mass and total energy

in the center-of-mass (CM) frame (E_{CM}) close to $m_\tau = 1.777$ GeV and $\sqrt{s}/2$, respectively. The dominant irreducible background comes from τ-pair events containing hard photon radiation and one of the τ leptons decaying to a charged lepton. The remaining backgrounds arise from the relevant radiative processes, $e^+e^- \to e^+e^-\gamma$ and $e^+e^- \to \mu^+\mu^-\gamma$ and from hadronic τ decays where a pion is misidentified as an electron or muon. For this decay channel, the current best limits comes from the BaBar and the Belle collaborations. BaBar collected $(963 \pm 7) \times 10^6$ τ decays near the $\Upsilon(4S)$, $\Upsilon(3S)$ and$\Upsilon(2S)$ resonances. In the BaBar detector [282], charged particles are reconstructed as tracks with a 5-layer silicon vertex tracker and a 40-layer drift chamber inside a 1.5 T solenoidal magnet. A CsI(Tl) electromagnetic calorimeter is used to identify electrons and photons. A ring-imaging Cherenkov detector is used to identify charged pions and kaons. The flux return of the solenoid, instrumented with resistive plate chambers and limited streamer tubes, is used to identify muons. Signal decays are identified by two kinematic variables: the energy difference $\Delta E = E_{CM} - \sqrt{s}/2$ and the beam energy constrained τ mass obtained from a kinematic fit after requiring the CM τ energy to be $\sqrt{s}/2$ and after assigning the origin of the γ candidate to the point of closest approach of the signal lepton track to the e^+e^- collision axis (m_{BC}). Figure 3.21 shows the distributions of the events for the two decay channels in m_{BC} vs. ΔE. The red dots are experimental points, the black ellipses are the 2σ signal contours and the yellow and green regions contain 90% and 50% of MC signal events.

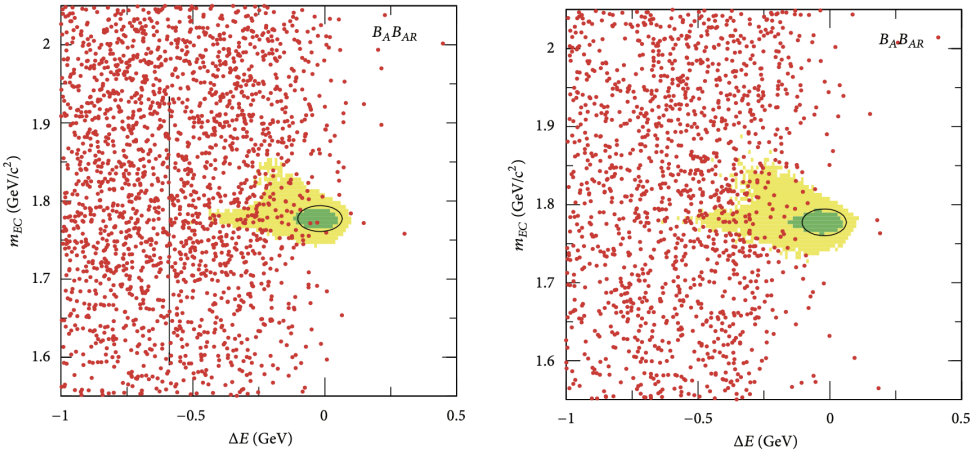

Figure 3.21: The Grand Signal Box and the 2σ ellipse for $\tau^\pm \to e^\pm\gamma$ (**left**) and $\tau^\pm \to \mu^\pm\gamma$ (**right**) decays in the m_{BC} vs. ΔE plane. Data are shown as dots, and contours containing 90% (50%) of signal MC events are shown as light-shaded (dark-shaded) regions (Figure and caption from [243]).

The searches yield no evidence of signals, and the experiment set upper limits on the branching fractions of $B(\tau^\pm \to e^\pm\gamma) < 3.3 \times 10^{-8}$ and $B(\tau^\pm \to \mu^\pm\gamma) < 4.4 \times 10^{-8}$ at 90% confidence level [243].

The Belle experiment [283] reported comparable limits using a data analysis based on 988 fb^{-1} and a strategy similar to that of BaBar. Kinematical selections on missing momentum and opening angle between particles are used to clean the sample. Figure 3.22 shows the two-dimensional distribution of$\Delta E/\sqrt{s}$ vs. m_{BC}. The signal events have $m_{BC} \sim m_\tau$ and $\Delta E/\sqrt{s} \sim 0$. The most dominant background in the $\tau^\pm \to \mu^\pm\gamma$ ($\tau^\pm \to e^\pm\gamma$) search arises from $\tau^+\tau^-$ events decaying to

$\tau^{\pm} \to \mu^{\pm}\nu_{\mu}\nu_{\tau}$ ($\tau^{\pm} \to e^{\pm}\nu_{e}\nu_{\tau}$) with a photon coming from initial-state radiation or beam background. The $\mu^{+}\mu^{-}\gamma$ and $e^{+}e^{-}\gamma$ events are subdominant, with their contributions falling below 5%. Other backgrounds such as two-photon and $e^{+}e^{-} \to q\bar{q}$ ($q = u,\ d,\ s,\ c$) are negligible in the signal region.

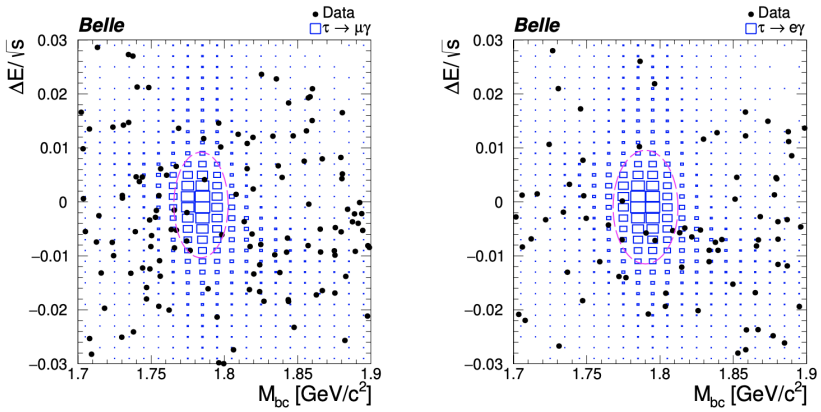

Figure 3.22: Two-dimensional distributions of $\Delta E/\sqrt{s}$ vs. M_{BC} for $\tau^{\pm} \to \mu^{\pm}\gamma$ (**left**) and $\tau^{\pm} \to e^{\pm}\gamma$) (**right**) events. Black points are data, blue squares are $\tau^{\pm} \to l^{\pm}\gamma$ signal MC events, and magenta ellipses show the $\pm 2\sigma$ signal regions used in this analysis (Figure and caption from [286]).

No significant excess over background predictions from the Standard Model is observed, and the 90% C.L. upper limits on the branching fractions are set at $B(\tau^{\pm} \to \mu^{\pm}\gamma) \leq 4.2 \times 10^{-8}$ and $B(\tau^{\pm} \to e^{\pm}\gamma) \leq 5.6 \times 10^{-8}$ [286]. With the full dataset expected for the Belle II experiment [287] (the upgrade of Belle), 50 ab^{-1}, the upper limit for the branching fraction of LFV decays τ will be reduced by two orders of magnitude.

3.3.2.2 $\tau \to 3l$

The signature for $\tau \to 3l$ ($l = e,\ \mu$) is a set of three charged particles, each identified as either an e or a μ, with an invariant mass and energy equal to that of the parent τ lepton.

In the BaBar [288] and Belle [244] analyses, all the six different combinations were explored. Events are preselected requiring four reconstructed tracks and zero net charge, selecting only tracks pointing toward a common region consistent with $\tau^{+}\tau^{-}$ production and decay. The polar angles of all four tracks in the laboratory frame are required to be within the calorimeter acceptance range, to ensure good particle identification. The search strategy consists of forming all possible triplets of charged leptons with the required total charge and of looking at the distribution of events in the (m_{BC} , ΔE) plane (m_{BC} and ΔE are defined as in the previous section). The backgrounds contaminating the sample can be divided in three broad categories: low multiplicity $e^{+}e^{-} \to q\bar{q}$ ($q = u,\ d,\ s,\ c$) events, QED events (Bhabha or $\mu^{+}\mu^{-}$ depending on the specific channel) and SM $\tau^{+}\tau^{-}$ events. These background classes have distinctive distributions in the (m_{BC}, ΔE) plane. The $e^{+}e^{-} \to q\bar{q}$ ($q = u,\ d,\ s,\ c$) events tend to populate the plane uniformly, while QED backgrounds fall in a narrow band at positive values of ΔE, and $\tau^{+}\tau^{-}$ backgrounds are restricted to negative values of both ΔE and m_{BC} due to the presence of at least one undetected

neutrino. Figure 3.20 shows the resulting limit for all the combinations to be at the level of a few 10^{-8} for both collaborations.

Even if the results are not yet competitive to those from B-factories, it is interesting to note that experiments at the LHC have also been looking for the $\tau \to 3\mu$ decay. The ATLAS experiment [289] performed a search for the neutrinoless decay $\tau^- \to \mu^-\mu^+\mu^-$ using a sample of $W^- \to \tau^-\bar{\nu}_\tau$ decays from a dataset corresponding to an integrated luminosity of 20.3 fb^{-1} collected in 2012 at a center-of-mass energy of 8 TeV. The LHCb experiment [290] performed the same search using a sample of tau from b and c-hadron decays from a dataset corresponding to an integrated luminosity of 3.0 fb^{-1} collected by the LHCb detector in 2011 and 2012 at center-of-mass energies of 7 and 8 TeV, respectively. The CMS experiment [291] recently delivered the results for the same search using a sample of τ leptons produced in both W boson and heavy-flavor hadron decays from a dataset cooresponding to an integrated luminosity of 33.2 fb^{-1} recorded by the CMS experiment in 2016 [291]. ATLAS, CMS and LHCb reported a 90% C.L. upper limit on the branching ratio of 3.76×10^{-7}, 8.0×10^{-8} and 4.6×10^{-8}, respectively. The Belle-II collaboration studied prospects for the expected sensitivity on this search. This channel has a purely leptonic final state, thus it is expected to be free of background. This allows to scale the experimental uncertainties linearly with the luminosity, which means that at least an improvement of a factor $\times 50$ is expected for Belle-II after accumulating a luminosity of 50 ab^{-1} [225].

Chapter 4

Effective Field Theories

Contents

4.1 Introduction to Effective Field Theories

Effective theories are based on the idea that specific phenomena can be accurately described without knowing all the details of the potentially unknown fundamental theory. This occurs whenever the physical observables of the problem being described are well approximated by a limit in the wider range of validity of the full theory. For instance, although special relativity is a more fundamental description of reality, slow-moving objects follow to great precision the laws of Newtonian mechanics. The success of Newtonian mechanics arises from the fact that it is a limit of special relativity for small velocities, i.e., $v \ll 1$. Similarly, when describing the electromagnetic field of a charge and current distribution at far distances r, the small distance details of the distribution may not be important, and an expansion in the small parameter $r/L \ll 1$, where L is the typical size of the charged object, can be performed. This approach lies at the heart of the multipole expansion in classical electrodynamics. Effective descriptions are central to the progress of physics because they enable to remove unnecessary complications from the problem at hand.

In QFT what we consider relevant is determined by the energy scale of the processes we wish to describe. The Fermi Theory of the weak interactions

$$-2\sqrt{2}G_F(\overline{\nu_\mu}\gamma P_L\mu)(\bar{e}\gamma P_L\nu_e) \tag{4.1}$$

is successful in describing the muon decay because the relevant scale of the process $E \sim m_\mu$ is much smaller than the mass of the W. More concretely, in the SM the tree-level muon decay amplitude is (in the Feynman gauge)

$$i\mathcal{M} = -\left(\frac{g^2}{2}\right)\frac{-ig_{\alpha\beta}}{p^2 - m_W^2}(\overline{\nu_\mu}\gamma^\alpha P_L\mu)(\bar{e}\gamma^\beta P_L\nu_e) \tag{4.2}$$

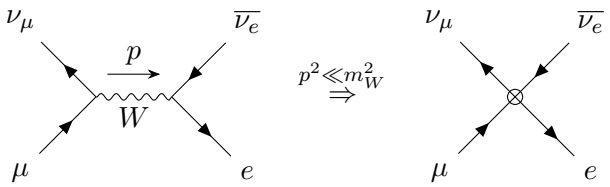

Figure 4.1: Integrating out the W in the SM muon decay to obtain the contact interaction of the Fermi theory.

which can be expanded for small $p^2/m_W^2 \ll 1$ as

$$i\mathcal{M} = -i\left(\frac{g^2}{2m_W^2}\right)(\overline{\nu_\mu}\gamma^\alpha P_L \mu)(\bar{e}\gamma_\alpha P_L \nu_e) + \mathcal{O}\left(\frac{p^2}{m_W^2}\right). \tag{4.3}$$

By identifying the Fermi constant $G_F = g^2/(4\sqrt{2}m_W^2)$ in terms of SM parameters, we can see that the four-fermion interaction of Eq. (4.2) reproduces the leading order term of the propagator expansion (see Fig. 4.1). The W boson, whose mass lies well above the scale of the transitions, is integrated out, and $G_F = g^2/(4\sqrt{2}m_W^2)$ is an example of a matching condition between the full theory and the effective one. Corrections to the leading order can be systematically computed by expanding the propagator in higher powers of the small parameter $\delta \equiv p^2/m_W^2$, which results in a tower of higher-dimensional operators. This process of removing heavy degrees of freedom in the low-energy theory is quite general and relies on the Appelquist-Carrazone theorem [292], which proves that the effects of the integrated-out heavy fields can be parameterized by local operators suppressed by the heavy mass scale. Note that the resulting theory is non-renormalizable in the usual sense, but this is not a problem as long as we want to compute the amplitude at a given accuracy (at fixed order in δ).

EFTs are not only useful to integrate out heavy fields from perturbative models, but can also describe unknown non-perturbative dynamics. At low energy, the QCD coupling grows and quarks and gluons are confined in hadrons. Although the underlying QCD dynamics is non-perturbative, the lightest hadrons can be described by means of Chiral Perturbation Theory (χPT), which is an EFT derived by the symmetry properties of QCD. The π, K, η of the pseudoscalar meson octet are understood to be the pseudo-Goldstone bosons of the spontaneously broken chiral symmetry and their interactions are derived from global symmetry considerations as a systematic expansion in powers of p/Λ_χ, where p is the meson momentum and $\Lambda_\chi \sim 1$ GeV. Other examples of effective field theories that approximate the QCD behaviour include the Heavy Quark Effective Field Theory (HQEFT) and Soft-Collinear Effective Theory (SCET). HQEFT describes the dynamics of hadrons that contain heavy quarks by performing an expansion in powers of $\Lambda_{\rm QCD}/m_Q$, with m_Q being the heavy quark mass. The SCET describes QCD processes where the center-of-mass energy of the collision is much larger than the final state invariant mass, which is the case for jet production at colliders. In general, we can summarise the main ingredients of an EFT as follows:

1. **Degrees of freedom**
   The first step is to identify the relevant degrees of freedom for the physics we wish to describe. At energies below the W mass, the muon decay is described by an interaction between the

electron, the muon and their respective neutrinos. In χPT, the dynamical fields are the light hadrons.

2. **Power counting**
   Secondly, we identify the small parameter in which we perform the expansion. This can be the ratio of light and heavy masses, a small velocity or the ratio between separated energy scales.

3. **Simmetries**
   It is also important to understand the symmetries of the problem in question, as this can constrain the interactions of effective theories. These can be gauge or global symmetries, and may also arise as approximate symmetries of the limit we study with the EFT.

4.2 Generalities on Effective Field Theories

In most of the following discussion, we will have in mind an effective field theory following the removal of heavy degrees of freedom from a weakly coupled theory. The exposition is largely influenced by the EFT introductions presented in [293–297]. An EFT Lagrangian takes the following general form

$$\mathcal{L}_{\text{EFT}} = \mathcal{L}_{d\leq 4} + \sum_{n>4} \frac{C_n \mathcal{O}_n}{\Lambda^{n-4}} \tag{4.4}$$

where $\mathcal{L}_{d\leq 4}$ contains the renormalizable terms and the sum runs over the tower of dimension n operators $\mathcal{O}_n$ compatible with the symmetries of the theory, suppressed by increasing power of the heavy physics scale Λ. The coefficient C_n of the non-renormalizable operators are known as Wilson Coefficient (WC) and are functions of the UV parameters. The factorization of the dynamic into UV-dependent coefficient multiplying local operators constructed out of light fields lies at the heart of the EFT parametrisation. The reason why the factorization holds is due to the analytical properties of the Green functions in the full theory. Amplitudes are functions of complexified kinematical variables that can contain singularities in the real axis that are simple poles or branch cuts associated with the virtual particles going on-shell. When the energy scale E of the processes is well below the heavy particle mass, the amplitude is analytic in the variable E/Λ, while it is in general non-analytic in the IR parameters (light-masses, momenta, etc.). The non-analytic behavior in the low-energy parameter is reproduced by the EFT, while the UV dependence can be absorbed in the Wilson coefficients definition when matching the two theories.

Amplitudes computed with multiple insertions of higher dimensional operators contribute to processes as[1]

$$\sum_n \frac{\delta\mathcal{A}^{(n)}}{\mathcal{A}} \tag{4.5}$$

where the term $\delta\mathcal{A}^{(n)}/\mathcal{A}$ correspond to k_i insertions of n_i dimensional operators such that $\sum_i (n_i - 4) \times k_i = n$

$$\frac{\delta\mathcal{A}^{(n)}}{\mathcal{A}} \sim \left(\frac{E}{\Lambda}\right)^{\sum_i (n_i-4)\times k_i} = \left(\frac{E}{\Lambda}\right)^n \tag{4.6}$$

[1] We factorize the renormalizable amplitude $\mathcal{A}$ to obtain a dimensionless quantity

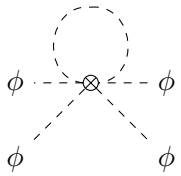

Figure 4.2: Renormalization of the ϕ^4 quartic coupling from the insertion of the higher dimensional operator ϕ^6.

If we want to compute the amplitude at a given accuracy $\delta = (E/\Lambda)^n$, we should keep only the operator with dimensions $d \leq n+4$. Note that this holds even when considering loops in the EFT, as long as we properly regularize the divergent diagrams. Naively, one may worry that the EFT expansion breaks down in the high-momentum region of the loop integral. For instance, we can consider the following EFT with a real scalar field ϕ

$$\mathcal{L}_{\rm EFT} = \frac{1}{2}(\partial_\mu\phi\partial^\mu\phi - m^2\phi^2) - \frac{\lambda}{4!}\phi^4 + \frac{C_6}{\Lambda^2}\phi^6 + \mathcal{O}\left(\frac{1}{\Lambda^4}\right). \tag{4.7}$$

The loop diagram of Figure 4.2 with the insertion of the C_6 operator gives a ϕ^4 amplitude

$$i\mathcal{A} = i\frac{C_6}{2\Lambda^2}\int\frac{d^4k}{(2\pi)^4}\frac{i}{k^2-m^2} \tag{4.8}$$

If we regulate the divergence with a cut-off, $k < \Lambda_c$, the integral gives (neglecting the terms involving the light mass m)

$$i\mathcal{A} \sim i\frac{C_6}{32\pi^2}\frac{\Lambda_c^2}{\Lambda^2} \tag{4.9}$$

Taking the cut-off scale to be around the UV scale $\Lambda_c \sim \Lambda$, we manifestly violate the power counting of the EFT expansion. However, this is not a problem of the EFT, but rather of the bad regulator that we chose. In addition to violating gauge and chiral symmetries, hard cutoffs break the EFT expansion and are not used in the EFT context. Instead, in mass-independent regularizations, such as Dimensional Regularization (DR), the power divergences are absent and all divergences are local functions of the low-energy theory parameters (masses, momenta, couplings), which can then be removed via counterterms that respect the power counting. The integral of Eq. (4.8) in $D = 4-2\varepsilon$ space-time dimensions is the following (see Appendix B)

$$\begin{aligned} i\mathcal{A} &= i\mu^{4\varepsilon}\frac{C_6}{2\Lambda^2}\int\frac{d^Dk}{(2\pi)^D}\frac{i}{k^2-m^2} = \mu^{4\varepsilon}\frac{C_6}{\Lambda}\frac{m^{D-2}}{2^{D+1}\pi^{D/2}}\Gamma\left(1-\frac{D}{2}\right) \\ &= -\mu^{2\varepsilon}\frac{C_6}{32\pi^2}\frac{m^2}{\Lambda^2}\left[\frac{1}{\varepsilon} - \gamma_E + \log\left(\frac{\mu^2}{m^2}\right) + \log 4\pi + 1 + \mathcal{O}(\varepsilon)\right] \end{aligned} \tag{4.10}$$

where we have factorized the power of the renormalization scale $\mu^{4\varepsilon}$ to have C_6 dimensionless in $4-2\varepsilon$ space-time dimensions. We can conveniently define the $\overline{\rm MS}$ renormalization scale $\mu \to \mu(4\pi)^{-1/2}e^{\gamma_E/2}$ to absorb the constant factors that are paired with the $1/\varepsilon$ poles

$$i\mathcal{A} = -\mu^{2\varepsilon}\frac{C_6}{32\pi^2}\frac{m^2}{\Lambda^2}\left[\frac{1}{\varepsilon} + \log\left(\frac{\mu^2}{m^2}\right) + 1 + \mathcal{O}(\varepsilon)\right] \tag{4.11}$$

The $1/\varepsilon$ pole can be removed by a local counterterm proportional to ϕ^4, and the contribution of the dimension six operators is suppressed by m^2/Λ^2, respecting the power counting. Since in DR the cut-off scale cannot appear in the numerator and the renormalization scale is only in logs, the EFT expansion is respected at any loop order. If we then truncate the higher-dimensional operators to a certain order in the $1/\Lambda$ expansion, the divergences can be renormalized with the surviving operators. The renormalization of effective operators will be discussed in section 4.2.2 and plays a crucial role in the EFT calculations.

4.2.1 Matching

Effective theories should reproduce the result of the full theory in their range of validity. The weakest possible requirement is that observables calculated in the UV model and the EFT should be the same up to the truncation error of the EFT expansion. We may require that all S matrix elements involving external light particles are reproduced in the effective theory

$$\langle q_1 \dots q_m | \, S_{\rm UV} \, | p_1 \dots p_k \rangle = \langle q_1 \dots q_m | \, S_{\rm EFT} \, | p_1 \dots p_k \rangle + \mathcal{O}(\delta^n) \tag{4.12}$$

where δ is the expansion parameter. Most of the time we deal with a stronger requirement that automatically implies the one above, that is to impose the equality of the Green functions with external light particles in the two theories. It follows that the scattering amplitudes are the same, as they are calculated from the green functions putting the external legs on their mass shell. In a QFT the correlation functions are obtained from the derivative of the functional integral with respect to the field source

$$Z_{\rm UV}[J] \equiv \int [d\Phi_{\rm UV}] e^{iS_{\rm UV}[\Phi_{\rm UV}] + i\int d^4x J(x)\mathcal{F}[\Phi^{\rm light}_{\rm UV}(x)]} \tag{4.13}$$

$$Z_{\rm EFT}[J] \equiv \int [d\Phi_{\rm EFT}] e^{iS_{\rm EFT}[\Phi_{\rm EFT}] + i\int d^4x J(x)F[\Phi_{\rm EFT}(x)]} \tag{4.14}$$

where $\mathcal{F}[\Phi^{\rm light}_{\rm UV}]$ and $F[\Phi_{\rm EFT}]$ are the fields that excite the light degrees of freedom in the UV and the EFT respectively. The matching requirement is hence

$$Z_{\rm UV}[J] = Z_{\rm EFT}[J] + \mathcal{O}(\delta^n) \tag{4.15}$$

The simplest case is the one that we will mostly interested in: the light degrees of freedom are the same in the EFT and the full theory, while the heavy fields are integrated out from the path integral

$$\int [d\Phi^{\rm heavy}_{\rm UV}] \exp\Big(iS_{\rm UV}[\Phi^{\rm light}_{\rm UV}, \Phi^{\rm heavy}_{\rm UV}]\Big) \equiv \exp\Big(iS_{\rm EFT}[\Phi^{\rm light}_{\rm EFT}]\Big) \tag{4.16}$$

The functional approach is more complicated in cases like QCD and χPT, since the UV theory contains quarks and gluons while the degrees of freedom of the effective Lagrangian are the pions. We will not discuss this issue further as this does not apply to the results of this thesis. In most cases the matching is performed diagrammatically: diagrams with light external fields are calculated in the UV model and the EFT. If we relax the assumption that the external legs are on-shell, we get the equality for the Green functions.

4.2.1.1 Equation of Motion and field redefinitions

We should stress that the correlation functions change under field redefinitions while scattering amplitudes with on-shell particles do not. S-matrix elements are computed with any interpolating field that excites the correct one-particle state out of the vacuum (see [298] for a detailed discussion). We thus have a basis ambiguity when we equate the Green functions. A field redefinition in an EFT can be a generic functional of the field

$$\Phi \to \Phi = F[\Phi'] \tag{4.17}$$

and does not need to be restricted to linear transformation (which is the case if we want to keep a renormalizable model at dimension $\leq$ four). We could for instance have a scalar field ϕ redefined as

$$\phi = \phi' + \frac{1}{\Lambda}\phi'^2 \tag{4.18}$$

Since the EFT Lagrangian is written as a sum of terms with increasing dimensionality

$$\mathcal{L}_{\text{EFT}} = \mathcal{L}^{d\leq 4} + \mathcal{L}^{d=5} + \mathcal{L}^{d=6} + \dots \tag{4.19}$$

a field redefinition $\Phi = \Phi' + \delta\Phi'$ changes the Lagrangian as[2]

$$\begin{aligned}\mathcal{L}_{\text{EFT}}(\Phi', \partial\Phi') = \mathcal{L}^{d\leq 4}(\Phi', \partial\Phi') \\ + \mathcal{L}^{d=5}(\Phi', \partial\Phi') + \left(\frac{\delta\mathcal{L}^{d\leq 4}}{\delta\Phi'} - \partial_\mu \frac{\delta\mathcal{L}^{d\leq 4}}{\delta(\partial_\mu\Phi')}\right)\delta\Phi' \\ + \delta\mathcal{L}^{d=5} + \mathcal{L}^{d=6} + \dots\end{aligned} \tag{4.20}$$

up to total derivatives. If the field redefinition is the one of Eq. (4.18), the second line of the above equation is the dimension five Lagrangian in the new basis. We see that we can always remove operators that are proportional to the renormalizable Equation of Motion (EOM). For instance, in the following EFT for a real scalar field ϕ

$$\mathcal{L}_{\text{EFT}} = \frac{1}{2}(\partial_\mu\phi\partial^\mu\phi - m^2\phi^2) - \frac{\mu}{3!}\phi^3 - \frac{\lambda}{4!}\phi^4 + \frac{C_5}{\Lambda}\phi^5 + \frac{C_5'}{\Lambda}\phi^2\Box\phi + \mathcal{O}\left(\frac{1}{\Lambda^2}\right) \tag{4.21}$$

the renormalizable EOM reads

$$\left(\Box + m^2 + \frac{\mu}{2}\phi + \frac{\lambda}{3!}\phi^2\right)\phi = 0. \tag{4.22}$$

The operator $\phi^2\Box\phi$ is equivalent to

$$\phi^2\Box\phi \leftrightarrow -m^2\phi^3 - \frac{\mu}{2}\phi^4 - \frac{\lambda}{3!}\phi^5 \tag{4.23}$$

given that their difference is proportional to the classical EOM and can be removed with a field redefinition. The operator $\phi^2\Box\phi$ is said to be redundant because the physics can be equivalently described when it is removed from the Lagrangian. Note that it may be convenient in some cases

[2] If the field redefinition involves chiral fermions, the path integral measure may also change, giving rise to anomalous contributions

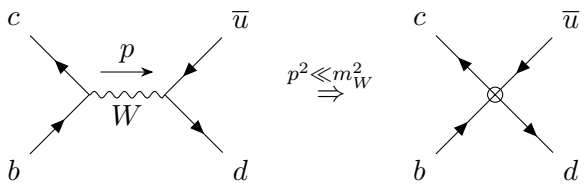

Figure 4.3: Tree-level leading order matching of the SM decay $b \to c\bar{u}d$ onto the operator $\mathcal{O}_1$ defined in the text.

to work with a redundant basis at intermediate steps of matching calculations or when computing the operator's renormalization. It is also interesting to point out that a field redefinition aimed at removing a redundant operator at a certain dimension affects the higher orders in the EFT expansion. This is not a problem when we identify the physical non-redundant basis at a given mass dimension, but can have a consequence when we compute amplitudes at higher orders. We review this case in section 6.2.4 of Chapter 6.

4.2.1.2 A matching example: $b \to c\bar{u}d$

As an illustrative example, we discuss here the matching of the SM onto the Four-Fermi theory for the quark transitions $b \to c\bar{u}d$. We remind that the Fermi theory results from integrating out the W boson from the SM.

Tree-level matching

The tree-level amplitude, given by the diagram of Figure 4.3, is analogous to the one calculated in the first section for the muon decay

$$i\mathcal{A}_{\text{tree}} = -\left(\frac{g^2}{2}\right)\frac{-ig_{\alpha\beta}}{p^2 - m_W^2}(V_{cb}\bar{c}\gamma^\alpha P_L b)(V_{ud}^*\bar{d}\gamma^\beta P_L u) \tag{4.24}$$

where the color indices are contracted in the fermion bilinears. Expanding the propagator for $p^2 \ll m_W^2$, the leading order term is reproduced by the higher dimensional operator

$$\mathcal{O}_1 = (\bar{c}\gamma^\alpha P_L b)(\bar{d}\gamma^\beta P_L u) \tag{4.25}$$

with a coefficient

$$C_1 = -2\sqrt{2}G_F V_{cb}V_{ud}^\star \tag{4.26}$$

where we recall that the Fermi constant is identified in terms of SM parameters as $G_F = \sqrt{2}g^2/(8m_W^2)$.

One-loop (QCD) matching

Suppose that we want to include the QCD corrections to the $b \to c\bar{u}d$ transitions and match onto an effective theory where the W is removed. The diagrams that decorate the W exchange with a gluon loop are shown in Figure 4.4. Given that we want to impose the equality of the Green functions in the two theories, we will keep the external legs off-shell and pick a convenient kinematical point where all external momenta vanish. This may introduce IR divergences that would be

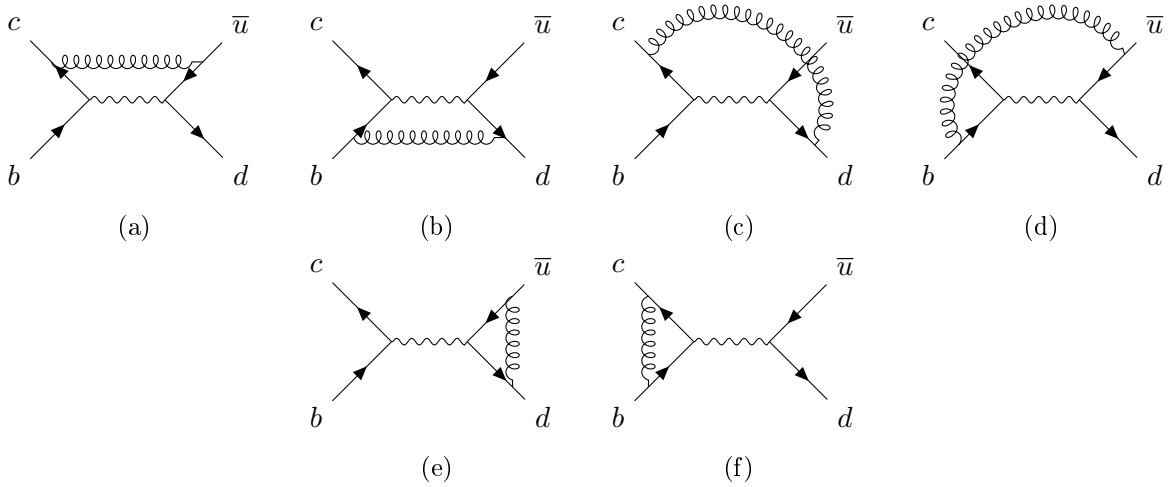

Figure 4.4: One-loop QCD correction to the SM decay $b \to c\bar{u}d$. It is sufficient to calculate only the one-light-particle irreducible diagrams (1LPI: graphs that remain connected when cutting one light particle line) to obtain the equality for all Green functions

otherwise regulated, but since the EFT reproduce the full theory IR behavior, they should cancel in matching. We calculate in the Feynman Gauge for both the W and gluon propagator, while to shorten the notation we define

$$\tilde{G}_F \equiv 2\sqrt{2} G_F V_{ud}^\star V_{cb} \tag{4.27}$$

More details on the DR regularized integrals and spinor identities that are later used can be found in Appendix B. The first diagram amplitude is

$$i\mathcal{A}_a = \left(m_W^2 \tilde{G}_F\right) g_s^2 \mu^{2\varepsilon} \int \frac{d^D k}{(2\pi)^D} \frac{-i}{k^2} \frac{-i}{k^2 - m_W^2} \left(\bar{c}\gamma^\nu T^a \frac{i\not{k}}{k^2}\gamma^\mu P_L b\right) \left(\bar{d}\gamma_\nu T^a \frac{i\not{k}}{k^2}\gamma_\mu P_L u\right) \tag{4.28}$$

where the T^a are the color $\mathrm{SU}(3)_c$ generators in the fundamental representation, satisfying the identity

$$T^a_{ij} T^a_{kl} = \frac{1}{2}\left(\delta_{il}\delta_{kj} - \frac{1}{3}\delta_{ij}\delta_{kl}\right) \tag{4.29}$$

When color indices are not specified they are understood to be contracted implicitly in the fermion bilinear. Due to Lorentz invariance the product $k^\alpha k^\beta$ can be replaced by $g^{\alpha\beta}k^2/D$ under the integral sign, leading to

$$= \left(m_W^2 \tilde{G}_F\right) \frac{g_s^2}{D} \mu^{2\varepsilon} \int \frac{d^D k}{(2\pi)^D} \frac{1}{k^4(k^2 - m_W^2)} \left(\bar{c}\gamma_\nu T^a \gamma_\alpha \gamma_\mu P_L b\right) \left(\bar{d}\gamma^\nu T^a \gamma^\alpha \gamma^\mu P_L u\right) \tag{4.30}$$

Similarly, the second to fourth diagrams give

$$i\mathcal{A}_b = i\mathcal{A}_a \tag{4.31}$$

$$i\mathcal{A}_c = i\mathcal{A}_d = -\left(m_W^2 \tilde{G}_F\right) \frac{g_s^2}{D} \mu^{2\varepsilon} \int \frac{d^D k}{(2\pi)^D} \frac{1}{k^4(k^2 - m_W^2)} \left(\bar{c}\gamma_\nu T^a \gamma_\alpha \gamma_\mu P_L b\right) \left(\bar{d}\gamma^\mu T^a \gamma^\alpha \gamma^\nu P_L u\right) \tag{4.32}$$

The integral is UV finite but has an IR divergence that would be regulated by an external momentum or a quark mass. Since there is no UV divergence, we can compute the diagram non-ambiguously in DR taking $\varepsilon_{\rm IR} < 0$. In the $\overline{\rm MS}$ scheme, we find

$$\frac{g_s^2}{D}\mu^{2\varepsilon}\int\frac{d^Dk}{(2\pi)^D}\frac{1}{k^4(k^2-m_W^2)} = \frac{ig_s^2}{64\pi^2 m_W^2}\left(\frac{1}{\varepsilon_{\rm IR}}+\log\frac{\mu^2}{m_W^2}+\frac{3}{2}\right) \tag{4.33}$$

while Eq. (4.29) and the Fierz identities (see Appendix B) give

$$(\bar c\gamma_\nu T^a\gamma_\alpha\gamma_\mu P_L b)\left(\bar d\gamma^\nu T^a\gamma^\alpha\gamma^\mu P_L u\right) = 4\,(\bar c\gamma_\nu T^a\gamma_\alpha\gamma_\mu P_L b)\left(\bar d\gamma^\mu T^a\gamma^\alpha\gamma^\nu P_L u\right) \tag{4.34}$$

$$= 8\left[(\bar c\gamma^\mu P_L u)\left(\bar d\gamma^\mu P_L b\right) - \frac{1}{3}(\bar c\gamma^\mu P_L b)\left(\bar d\gamma^\mu P_L u\right)\right] \tag{4.35}$$

Combining the results, the sum of the first four diagrams is thus

$$i(\mathcal{A}_a+\mathcal{A}_b+\mathcal{A}_c+\mathcal{A}_d) = \tilde G_F\frac{3i\alpha_s}{4\pi}\left(\frac{1}{\varepsilon_{\rm IR}}+\log\frac{\mu^2}{m_W^2}+\frac{3}{2}\right)\times \tag{4.36}$$

$$\left[(\bar c\gamma^\mu P_L u)\left(\bar d\gamma^\mu P_L b\right) - \frac{1}{3}(\bar c\gamma^\mu P_L b)\left(\bar d\gamma^\mu P_L u\right)\right] \tag{4.37}$$

The last two diagrams contain scaleless integrals that vanish in DR

$$\int\frac{d^Dk}{(2\pi)^D}\frac{1}{(k^2)^2} = 0 \tag{4.38}$$

We may explicitly split the IR and UV divergences by writing the integral as

$$\int\frac{d^Dk}{(2\pi)^D}\frac{1}{(k^2)^2} = \int\frac{d^Dk}{(2\pi)^D}\left[\frac{1}{k^2(k^2-m^2)}-\frac{m^2}{k^4(k^2-m^2)}\right] \tag{4.39}$$

where we have introduced a fictitious mass m to have terms that are separately UV and IR divergent. Each of them can be respectively computed taking $\varepsilon_{\rm UV} > 0$ and $\varepsilon_{\rm IR} < 0$, and we find

$$\int\frac{d^Dk}{(2\pi)^D}\frac{1}{(k^2)^2} = \frac{i}{16\pi^2}\left(\frac{1}{\varepsilon_{\rm UV}}-\frac{1}{\varepsilon_{\rm IR}}\right) \tag{4.40}$$

The analytic continuation would require $\varepsilon = \varepsilon_{\rm UV} = \varepsilon_{\rm IR}$ which is why in DR the integral vanishes. The UV poles are cancelled by the theory counterterms, leading to

$$i\mathcal{A}_e + \text{c.t} = i\mathcal{A}_f + \text{c.t} = -\tilde G_F C_F\frac{\alpha_s}{4\pi}\frac{i}{\varepsilon_{\rm IR}}(\bar c\gamma^\mu P_L b)\left(\bar d\gamma^\mu P_L u\right) \tag{4.41}$$

where $C_F = 4/3$ is the Casimir coefficient $T^aT^a = C_F\times 1_{3\times3}$ of SU(3). The full theory result, including the tree-level diagram, is thus

$$i\mathcal{A}_{\rm tot} + i\mathcal{A}_{\rm c.t} = -i\tilde G_F\left[1-\frac{\alpha_s}{4\pi}\left(\frac{11}{3}\frac{1}{\varepsilon_{\rm IR}}+\log\frac{\mu^2}{m_W^2}+\frac{3}{2}\right)\right](\bar c\gamma^\mu P_L b)\left(\bar d\gamma^\mu P_L u\right)$$

$$-i\tilde G_F\frac{3\alpha_s}{4\pi}\left(\frac{1}{\varepsilon_{\rm IR}}+\log\frac{\mu^2}{m_W^2}+\frac{3}{2}\right)(\bar c\gamma^\mu P_L u)\left(\bar d\gamma^\mu P_L b\right) \tag{4.42}$$

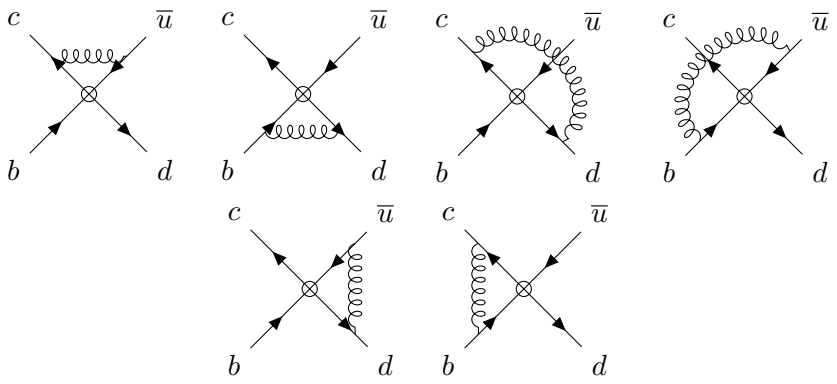

Figure 4.5: One-loop QCD correction to the effective interactions mediating the decay $b \to c\bar{u}d$. Each diagram contains the insertion of the operators $\mathcal{O}_1, \mathcal{O}_2$ defined in the text

The effective operators that are needed to reproduce the amplitude are the following

$$\mathcal{O}_1 = (\bar{c}\gamma^\alpha P_L b)(\bar{d}\gamma^\beta P_L u) \qquad \mathcal{O}_2 = (\bar{c}\gamma^\alpha P_L u)(\bar{d}\gamma^\beta P_L b) \tag{4.43}$$

and we conventionally add them to the Lagrangian as

$$\mathcal{L}_{\text{EFT}} \supset -\sum_i C_i \mathcal{O}_i \tag{4.44}$$

The corresponding diagrams in the low energy effective theory decorated by gluon loops are shown in Figure 4.5. Every diagram contains the insertion of both operators in Eq. (4.43). All EFT loop integrals are scaleless, while the fermion and color structure can be read off from the equivalent full theory diagram. The result, which can be easily computed from the above calculations, is

$$\begin{aligned} i\mathcal{A}_{\text{tot}}^{\text{EFT}} = & \, i\left[-C_1 + \frac{\alpha_s}{4\pi}\left(\frac{1}{\varepsilon_{\text{UV}}} - \frac{1}{\varepsilon_{\text{IR}}}\right)\left(3C_2 - \frac{11}{3}C_1\right)\right](\bar{c}\gamma^\alpha P_L b)(\bar{d}\gamma^\beta P_L u) \\ & + i\left[-C_2 + \frac{\alpha_s}{4\pi}\left(\frac{1}{\varepsilon_{\text{UV}}} - \frac{1}{\varepsilon_{\text{IR}}}\right)\left(3C_1 - \frac{11}{3}C_2\right)\right](\bar{c}\gamma^\alpha P_L u)(\bar{d}\gamma^\beta P_L b) \end{aligned} \tag{4.45}$$

The UV divergences are cancelled via counterterms proportional to $\mathcal{O}_1$ and $\mathcal{O}_2$ as

$$i\mathcal{A}_{\text{c.t}}^{\text{EFT}} = -\frac{\alpha_s}{4\pi}\frac{i}{\varepsilon_{\text{UV}}}\left(3C_2 - \frac{11}{3}C_1\right)(\bar{c}\gamma^\alpha P_L b)(\bar{d}\gamma^\beta P_L u) - \frac{\alpha_s}{4\pi}\frac{i}{\varepsilon_{\text{UV}}}\left(3C_1 - \frac{11}{3}C_2\right)(\bar{c}\gamma^\alpha P_L b)(\bar{d}\gamma^\beta P_L u) \tag{4.46}$$

Note that the UV divergences of the EFT are different from the one of the full theory, but they are closely related to the model IR behaviour. The reason is quite general. If we expand the integrands of the full theory in powers of the IR parameters (masses, external momenta, etc.), the expansion coefficients take the following general form

$$i\mathcal{A}_{\text{full}} = \frac{A}{\varepsilon_{\text{UV}}} + \frac{B}{\varepsilon_{\text{IR}}} + C \tag{4.47}$$

where C is finite, the IR divergences are a consequence of the expansion and the A poles are canceled by the full theory counterterms. Performing the same expansion in the EFT, the loop integrals are

all scaleless and vanish in DR, which means that, separating the IR and UV poles, the amplitude is

$$i\mathcal{A}_{\rm EFT} = -B_{\rm EFT}\left(\frac{1}{\varepsilon_{\rm UV}} - \frac{1}{\varepsilon_{\rm IR}}\right). \tag{4.48}$$

Since the EFT must reproduce the IR behavior of the full theory we have that $B_{\rm EFT} = B$, which connects the UV divergences that are renormalized in the EFT to the IR of the full theory. After the UV poles are separately removed, we find that the loop matching contribution amount to the finite part of the full theory diagram expanded out in the low-energy parameters. Indeed, including the counterterms, the total EFT amplitude of our example is

$$\begin{aligned} i\mathcal{A}^{\rm EFT}_{\rm tot} + i\mathcal{A}^{\rm EFT}_{\rm c.t} = &-\frac{\alpha_s}{4\pi}\frac{i}{\varepsilon_{\rm IR}}\left(3C_2 - \frac{11}{3}C_1\right)(\bar{c}\gamma^\alpha P_L b)(\bar{d}\gamma^\beta P_L u) \\ &-\frac{\alpha_s}{4\pi}\frac{i}{\varepsilon_{\rm IR}}\left(3C_1 - \frac{11}{3}C_2\right)(\bar{c}\gamma^\alpha P_L u)(\bar{d}\gamma^\beta P_L b) \end{aligned} \tag{4.49}$$

which reproduces the theory result if the Wilson coefficients are

$$C_1(\mu) = \tilde{G}_F\left[1 - \frac{\alpha_s}{4\pi}\left(\log\frac{\mu^2}{m_W^2} + \frac{3}{2}\right)\right], \quad C_2(\mu) = \tilde{G}_F\left[\frac{3\alpha_s}{4\pi}\left(\log\frac{\mu^2}{m_W^2} + \frac{3}{2}\right)\right] \tag{4.50}$$

A check for the correctness of the calculations is given by the cancellation of the IR poles. An important observation is in order. The matching conditions contain logs of the ratio between the renormalization scale and the mass of the heavy particle, in this case, m_W. If the energy scales are largely separated, the logs can become dangerously large, invalidating perturbation theory despite having a small QCD coupling

$$\mu \ll m_W \to \left(\frac{\alpha_s}{4\pi}\log\frac{m_W^2}{\mu^2}\right) \sim 1 \tag{4.51}$$

Large logs can be avoided in matching by choosing a renormalization scale as close as possible to the heavy scale $\mu \sim m_W$. However, the EFT calculation with on-shell quarks will contain logs of the ratio between the renormalization scale and the low energy masses or external momenta, which suggests that the EFT result is reliable for $\mu \sim m_b$, potentially reintroducing the large logs problem. The EFT UV behavior saves the day. The EFT counterterms define a renormalization group evolution for the Wilson coefficient that can be solved to re-sum these large logs. This is one of the reasons why the EFT is so useful even when the full theory is known: converting the IR logs of the fundamental theory into UV logs of the EFT allows for their resummation by integrating the renormalization group equations.

4.2.2 Renormalization Group Evolution

We argued in the first section that an EFT is as renormalizable as any QFT if we are happy with a finite accuracy in the calculation. Loops with single insertions of dimension d operators $\mathcal{O}_i^{(d)}$ yield amplitudes that are proportional to $1/\Lambda^{d-4}$ and can be renormalized by dimension d counterterms. In general, the counterterms can be proportional to dimension d operators different from the inserted ones, giving rise to operator mixing

$$\mathcal{L}_{\rm EFT} \supset \frac{1}{\Lambda^{d-4}} C_i^{(d)} Z_{ij}^{(d\to d)} \mathcal{O}_j^{(d)} \tag{4.52}$$

where the contact interactions $\mathcal{O}_j$ contain the renormalized fields. A dimension d counter term may be necessary to renormalize the divergence of a loop diagram with multiple insertions of lower dimension operators having mass dimensions that satisfy $[\sum_i (d_i - 4)] \equiv d - 4$. For example, the double insertion of a dimension five operator gives a dimension six amplitude $(1/\Lambda)\times(1/\Lambda) = 1/\Lambda^2$. We thus expect in the renormalized Lagrangian terms like

$$\mathcal{L}_{\rm EFT} \supset \frac{1}{\Lambda^{d-4}} C_{i_1}^{(d_1)} \times \cdots \times C_{i_k}^{(d_k)} Z_{i_1\cdots i_k, j}^{(d_1\cdots d_k \to d)} \mathcal{O}_j^{(d)} \qquad \left[\sum_i (d_i - 4)\right] \equiv d - 4 \tag{4.53}$$

Moreover, if the EFT has dimensionful parameters in the renormalizable Lagrangian, an operator of dimension $d' = d + n$ can mix into one of dimension d with n insertion of a mass. This is for instance the case for the loop diagram calculated in Eq. (4.11), where the ϕ^6 operator mixes with the renormalizable quartic coupling via two powers of the scalar mass m^2. Therefore, the renormalized Lagrangian may also contain

$$\mathcal{L}_{\rm EFT} \supset \frac{m_{\rm EFT}^n}{\Lambda^{d+n-4}} C_i^{(d+n)} Z_{ij}^{(d+n\to d)} \mathcal{O}_j^{(d)} \tag{4.54}$$

where m_{EFT} is a mass parameter of the $d < 4$ Lagrangian.

To illustrate the renormalization group evolution of the Wilson coefficients we focus on the first case, that is the mixing between operators of the same dimension. The second case will be the main subject of Chapter 6. The Renormalization Group Equations (RGEs) follow from the independence of the bare Lagrangian from the renormalization scale μ. We drop the dimension upper indices to avoid cluttering and write

$$\mathcal{L}_{\rm EFT} \supset C_i Z_{ij} \mathcal{O}_j \tag{4.55}$$

The operators constructed out bare fields $\mathcal{O}_{j,\rm bare} = Z_{\mathcal{O}_j}\mathcal{O}_j$ are μ independent, hence we factorize the field renormalization constant $Z_{\mathcal{O}_j}$ to have

$$0 = \mu\frac{d}{d\mu}\left(C_i \frac{Z_{ij}}{Z_{\mathcal{O}_j}} \mathcal{O}_{j,\rm bare}\right) = \mu\frac{d}{d\mu}\left(C_i \frac{Z_{ij}}{Z_{\mathcal{O}_j}}\right). \tag{4.56}$$

Defining

$$\tilde{Z}_{ij} \equiv \frac{Z_{ij}}{Z_{\mathcal{O}_j}} \tag{4.57}$$

we arrive at

$$\mu\frac{d}{d\mu} C_i = C_j \gamma_{ji} \quad \text{where } \gamma = -\frac{d\tilde{Z}}{d\log\mu}\tilde{Z}^{-1} \equiv -\frac{d\log\tilde{Z}}{d\log\mu}. \tag{4.58}$$

The matrix γ is known as the anomalous dimension matrix and it parametrises how the dimension d operators scale and mix in the renormalization group evolution. To connect to the $b \to c\bar{u}d$ example, let us suppose that we are interested in the QCD loop corrections. At n-loops, we expand the anomalous dimension matrix in powers of the QCD coupling constant

$$\gamma = \sum_{k=0}^{n-1} \left(\frac{\alpha_s}{4\pi}\right)^{k+1} \gamma^{(k)} + \mathcal{O}\left(\left(\frac{\alpha_s}{4\pi}\right)^{n+1}\right) \tag{4.59}$$

while the renormalization constants $\tilde{Z}$ contain increasingly singular ε poles

$$\tilde{Z} = 1 + \sum_{k=1}^{n} \frac{1}{\varepsilon^k} Z_k(\alpha_3) \tag{4.60}$$

The anomalous dimension matrix definition implies the equality

$$\gamma \left(1 + \frac{1}{\varepsilon} Z_1 + \mathcal{O}\left(\frac{1}{\varepsilon^2}\right)\right) = -\frac{1}{\varepsilon} \frac{dZ_1}{d\log\mu} + \mathcal{O}\left(\frac{1}{\varepsilon^2}\right) \tag{4.61}$$

and the renormalized QCD coupling beta function in $4 - 2\varepsilon$ space-time dimension is the following

$$\beta(\alpha_s, \varepsilon) \equiv \frac{d\alpha_s(\mu)}{d\log\mu} = -2\varepsilon\alpha_s + \beta(\alpha_s) \tag{4.62}$$

where $\beta(\alpha_s)$ is

$$\beta(\alpha_s) = -2\alpha_s \left[\sum_{k=0}^{n-1} \left(\frac{\alpha_s}{4\pi}\right)^{k+1} \beta_k + \mathcal{O}\left(\left(\frac{\alpha_s}{4\pi}\right)^{n+1}\right)\right] \tag{4.63}$$

Applying the chain rule to the right-hand side of Eq. (4.61) and substituting the QCD beta function

$$\gamma \left(1 + \frac{1}{\varepsilon} Z_1 + \mathcal{O}\left(\frac{1}{\varepsilon^2}\right)\right) = -\frac{1}{\varepsilon} \frac{dZ_1}{d\alpha_s} (-2\varepsilon\alpha_s + \beta(\alpha_s)) + \mathcal{O}\left(\frac{1}{\varepsilon^2}\right) \tag{4.64}$$

we find that the anomalous dimension matrix is obtained by the single $1/\varepsilon$ poles of the counterterms

$$\gamma = 2\alpha_s \frac{dZ_1}{d\alpha_s} \tag{4.65}$$

4.2.2.1 Solving the RGEs in $b \to c\bar{u}d$

In the example of the previous section we computed the QCD one-loop corrections to the effective operators relevant for the quark transitions $b \to c\bar{u}d$. We have found that the UV divergences are cancelled by the counterterms

$$\mathcal{L}_{\text{c.t}} = -\frac{\alpha_s}{4\pi} \frac{1}{\varepsilon} \left(3C_2 - \frac{11}{3} C_1\right) \mathcal{O}_1 - \frac{\alpha_s}{4\pi} \frac{1}{\varepsilon} \left(3C_1 - \frac{11}{3} C_2\right) \mathcal{O}_2 \tag{4.66}$$

which can be absorbed in the renormalization constants Z

$$\mathcal{L}_{\text{EFT}} \supset -C_i Z_{ij} \mathcal{O}_j \quad \text{with } Z = 1_{2\times 2} + \frac{\alpha_s}{4\pi\varepsilon} \begin{pmatrix} -11/3 & 3 \\ 3 & -11/3 \end{pmatrix} \tag{4.67}$$

The wave function renormalization (in Feynman gauge) of the two operators is the same and equal to $Z_{\mathcal{O}_{1,2}} = 1 - \alpha_s/(3\pi\varepsilon)$ and can be subtracted to obtain $\tilde{Z}$ as defined in Eq. (4.57). Applying Eq. (4.65), we find the one-loop anomalous dimension matrix

$$\mu \frac{dC_i}{d\mu} = C_j \gamma_{ji} \quad \text{with } \gamma = \frac{\alpha_s}{2\pi} \begin{pmatrix} -1 & 3 \\ 3 & -1 \end{pmatrix} \tag{4.68}$$

The RGEs can be easily solved in a basis where the anomalous dimension matrix is diagonal. The matrix is diagonalised by the linear combinations

$$C_\pm = C_1 \pm C_2 \qquad \mu \frac{dC_\pm}{d\mu} = C_\pm \gamma_\pm \tag{4.69}$$

where

$$\gamma_+ = \frac{\alpha_s}{\pi} \qquad \gamma_- = -2\frac{\alpha_s}{\pi} \tag{4.70}$$

In the diagonal basis, the RGEs are readily integrated

$$C_\pm(\mu_f) = C_\pm(\mu_i) \exp\left\{ \int_{\alpha_s(\mu_i)}^{\alpha_s(\mu_f)} d\alpha \frac{\gamma_\pm(\alpha)}{\beta(\alpha)} \right\} \tag{4.71}$$

where $\beta(\alpha)$ is the QCD beta function of Eq. (4.63). With $n_f = 5$, the one-loop coefficient is $\beta_0 = 11 - 2/3 n_f = 23/3$ and the solution reads

$$C_+(\mu_f) = C_+(\mu_i) \left(\frac{\alpha_3(\mu_f)}{\alpha_3(\mu_i)} \right)^{-6/23} \qquad C_-(\mu_f) = C_-(\mu_i) \left(\frac{\alpha_3(\mu_f)}{\alpha_3(\mu_i)} \right)^{12/23} \tag{4.72}$$

We can substitute the tree-level matching values, which to avoid large logs should be taken at $\mu \sim m_W$, and run down to the scale of the $b \to c\bar{u}d$ transitions $\mu \sim m_b$. We find

$$C_+(m_b) \sim 0.85 C_+(m_W) = 0.85 \tilde{G}_F \qquad C_-(m_b) \sim 1.38 C_-(m_W) = 1.38 \tilde{G}_F \tag{4.73}$$

Even though we started with a vanishing $C_2(m_W)$, the renormalization group evolution sizably generates it at low energy $C_2(m_b) \sim -0.27 \tilde{G}_F$. The effects of the large logs are relevant and have been re-summed in integrating the RGEs. Note that if we run with the one-loop anomalous dimension matrix, it would be inconsistent with the order of the calculation to include the $\mathcal{O}(\alpha_s)$ correction in matching. In Leading Order (LO) calculations where we match at $\mathcal{O}\left(\alpha_s^0\right)$ and run at $\mathcal{O}(\alpha_s)$, we resum terms like

$$\text{LO}: \qquad \sum_n \left(\frac{\alpha_s}{4\pi} \log \frac{m_W}{m_b} \right)^n \tag{4.74}$$

If we include $\mathcal{O}(\alpha_s)$ terms in matching, the one-loop running will be contaminated with $\frac{\alpha_s}{4\pi} \sum_n \left(\frac{\alpha_s}{4\pi} \log \frac{m_W}{m_b} \right)^n$ terms that are of the same order of the $\mathcal{O}\left(\alpha_s^0\right)$ two-loop running. A consistent treatment of Next-to-Leading-Order (NLO) would thus require the two-loop RGEs. More generally, in a N^{m}LO calculation we resum

$$\text{N}^m\text{LO}: \qquad \left(\frac{\alpha_s}{4\pi} \right)^m \sum_n \left(\frac{\alpha_s}{4\pi} \log \frac{m_W}{m_b} \right)^n \tag{4.75}$$

by computing the matching at m loops and running at $m+1$ loops.

4.3 The Standard Model Effective Field Theory

In Chapter 2, we discussed the evidence and observations that suggest an extension of the Standard Model is necessary. If we assume that the physics responsible for these observations is much heavier

than the electroweak scale, we can describe it using an effective field theory. We can view the SM as the renormalizable Lagrangian of an effective theory in which the heavy particles have been integrated out. We can include higher-dimensional operators constructed from the SM fields that respect the standard model gauge symmetry, and investigate the distinct signals predicted by these novel operators. By including every possible operator that is not forbidden by symmetries and searching for evidence of their presence in experiments, we can probe a wide range of different models with the sole assumption that the new states are heavy. This effective field theory is known as the Standard Model Effective Field Theory or SMEFT, and the Lagrangian has the following schematic form

$$\mathcal{L}_{\text{SMEFT}} = \mathcal{L}_{\text{SM}} + \sum_{d=5} \frac{1}{\Lambda^{d-4}} \sum_{i=1}^{n_d} C_i^{(d)} \mathcal{O}_i^{(d)}, \tag{4.76}$$

where n_d is the number of independent operators at dimension d. If we assume that no right-handed neutrino is present at low energy, we have solid evidence for a non-zero Weinberg operator at dimension five[3] [299]:

$$\mathcal{L}_5 = \frac{1}{2\Lambda} C_{\text{W}}^{ij} (\bar{\ell}_i \tilde{H})(\ell_j^c \tilde{H}) + \text{h.c} \tag{4.77}$$

which breaks the lepton number symmetry and gives Majorana neutrino masses when the electroweak symmetry is spontaneously broken by the Higgs VEV

$$m_\nu = C_W \frac{v^2}{\Lambda} \tag{4.78}$$

where $\langle H^0 \rangle = v$. For an $\mathcal{O}(1)$ Weinberg operator coefficient, the upper limit on neutrino masses suggest a new physics scale $\Lambda \gtrsim 10^{15}$ GeV. We already discussed models in Chapter 3 that sufficiently suppress the dimension five coefficient to allow for new physics closer to the electroweak scale.

The leading order contributions to a wide variety of BSM processes appear at dimension six. Not accounting for the different flavours, there are 84 independent (non-redundant) operators at dimension six. Redundancies can appear whenever two operators differ by a total derivative or by an operator proportional to the renormalizable equation of motion, which can always be removed with a field redefinition and do not contribute to observables (see section 4.2.1.1). The Hilbert series method provides an elegant way to count the number of independent operators for each mass dimension [300–303]. Part of the dimension six SMEFT Lagrangian appeared in the 80s [304], and was later completed in what is commonly known as the Warsaw basis [305]. We reproduce the dimension six operator basis in Table 4.1. Although numerous potentially interesting BSM signatures are expected when we include the dimension six operators in the Lagrangian, experimental data are yet to show a clear deviation that suggests the presence of a non-zero operator. So far, observations are compatible with the predictions of the renormalizable SMEFT Lagrangian, and can be used to infer upper limits on the size of the operator coefficients.

Complete basis for the operators of dimensions seven and eight have also been classified [306–309]

[3] The Weinberg operator is the only non-zero operator at dimension five that respects the SM gauge symmetry.

$\mathbf{1:X^3}$	
Q_G	$f^{ABC}G_\mu^{A\nu}G_\nu^{B\rho}G_\rho^{C\mu}$
$Q_{\widetilde{G}}$	$f^{ABC}\widetilde{G}_\mu^{A\nu}G_\nu^{B\rho}G_\rho^{C\mu}$
Q_W	$\epsilon^{IJK}W_\mu^{I\nu}W_\nu^{J\rho}W_\rho^{K\mu}$
$Q_{\widetilde{W}}$	$\epsilon^{IJK}\widetilde{W}_\mu^{I\nu}W_\nu^{J\rho}W_\rho^{K\mu}$

$\mathbf{2:H^6}$	
Q_H	$(H^\dagger H)^3$

$\mathbf{3:H^4D^2}$	
$Q_{H\Box}$	$(H^\dagger H)\Box(H^\dagger H)$
Q_{HD}	$\left(H^\dagger D^\mu H\right)^*\left(H^\dagger D_\mu H\right)$

$\mathbf{5:\psi^2H^3+h.c.}$	
Q_{eH}	$(H^\dagger H)(\bar{l}_p e_r H)$
Q_{uH}	$(H^\dagger H)(\bar{q}_p u_r \widetilde{H})$
Q_{dH}	$(H^\dagger H)(\bar{q}_p d_r H)$

$\mathbf{4:X^2H^2}$	
Q_{HG}	$H^\dagger H\, G^A_{\mu\nu}G^{A\mu\nu}$
$Q_{H\widetilde{G}}$	$H^\dagger H\, \widetilde{G}^A_{\mu\nu}G^{A\mu\nu}$
Q_{HW}	$H^\dagger H\, W^I_{\mu\nu}W^{I\mu\nu}$
$Q_{H\widetilde{W}}$	$H^\dagger H\, \widetilde{W}^I_{\mu\nu}W^{I\mu\nu}$
Q_{HB}	$H^\dagger H\, B_{\mu\nu}B^{\mu\nu}$
$Q_{H\widetilde{B}}$	$H^\dagger H\, \widetilde{B}_{\mu\nu}B^{\mu\nu}$
Q_{HWB}	$H^\dagger\tau^I H\, W^I_{\mu\nu}B^{\mu\nu}$
$Q_{H\widetilde{W}B}$	$H^\dagger\tau^I H\, \widetilde{W}^I_{\mu\nu}B^{\mu\nu}$

$\mathbf{6:\psi^2XH+h.c.}$	
Q_{eW}	$(\bar{l}_p\sigma^{\mu\nu}e_r)\tau^I H W^I_{\mu\nu}$
Q_{eB}	$(\bar{l}_p\sigma^{\mu\nu}e_r)H B_{\mu\nu}$
Q_{uG}	$(\bar{q}_p\sigma^{\mu\nu}T^A u_r)\widetilde{H}\, G^A_{\mu\nu}$
Q_{uW}	$(\bar{q}_p\sigma^{\mu\nu}u_r)\tau^I\widetilde{H}\, W^I_{\mu\nu}$
Q_{uB}	$(\bar{q}_p\sigma^{\mu\nu}u_r)\widetilde{H}\, B_{\mu\nu}$
Q_{dG}	$(\bar{q}_p\sigma^{\mu\nu}T^A d_r)H\, G^A_{\mu\nu}$
Q_{dW}	$(\bar{q}_p\sigma^{\mu\nu}d_r)\tau^I H\, W^I_{\mu\nu}$
Q_{dB}	$(\bar{q}_p\sigma^{\mu\nu}d_r)H\, B_{\mu\nu}$

$\mathbf{7:\psi^2H^2D}$	
$Q^{(1)}_{Hl}$	$(H^\dagger i\overleftrightarrow{D}_\mu H)(\bar{l}_p\gamma^\mu l_r)$
$Q^{(3)}_{Hl}$	$(H^\dagger i\overleftrightarrow{D}^I_\mu H)(\bar{l}_p\tau^I\gamma^\mu l_r)$
Q_{He}	$(H^\dagger i\overleftrightarrow{D}_\mu H)(\bar{e}_p\gamma^\mu e_r)$
$Q^{(1)}_{Hq}$	$(H^\dagger i\overleftrightarrow{D}_\mu H)(\bar{q}_p\gamma^\mu q_r)$
$Q^{(3)}_{Hq}$	$(H^\dagger i\overleftrightarrow{D}^I_\mu H)(\bar{q}_p\tau^I\gamma^\mu q_r)$
Q_{Hu}	$(H^\dagger i\overleftrightarrow{D}_\mu H)(\bar{u}_p\gamma^\mu u_r)$
Q_{Hd}	$(H^\dagger i\overleftrightarrow{D}_\mu H)(\bar{d}_p\gamma^\mu d_r)$
Q_{Hud} + h.c.	$i(\widetilde{H}^\dagger D_\mu H)(\bar{u}_p\gamma^\mu d_r)$

$\mathbf{8:(\bar{L}L)(\bar{L}L)}$	
Q_{ll}	$(\bar{l}_p\gamma^\mu l_r)(\bar{l}_s\gamma_\mu l_t)$
$Q^{(1)}_{qq}$	$(\bar{q}_p\gamma^\mu q_r)(\bar{q}_s\gamma_\mu q_t)$
$Q^{(3)}_{qq}$	$(\bar{q}_p\gamma^\mu\tau^I q_r)(\bar{q}_s\gamma_\mu\tau^I q_t)$
$Q^{(1)}_{lq}$	$(\bar{l}_p\gamma^\mu l_r)(\bar{q}_s\gamma_\mu q_t)$
$Q^{(3)}_{lq}$	$(\bar{l}_p\gamma^\mu\tau^I l_r)(\bar{q}_s\gamma_\mu\tau^I q_t)$

$\mathbf{8:(\bar{R}R)(\bar{R}R)}$	
Q_{ee}	$(\bar{e}_p\gamma^\mu e_r)(\bar{e}_s\gamma_\mu e_t)$
Q_{uu}	$(\bar{u}_p\gamma^\mu u_r)(\bar{u}_s\gamma_\mu u_t)$
Q_{dd}	$(\bar{d}_p\gamma^\mu d_r)(\bar{d}_s\gamma_\mu d_t)$
Q_{eu}	$(\bar{e}_p\gamma^\mu e_r)(\bar{u}_s\gamma_\mu u_t)$
Q_{ed}	$(\bar{e}_p\gamma^\mu e_r)(\bar{d}_s\gamma_\mu d_t)$
$Q^{(1)}_{ud}$	$(\bar{u}_p\gamma^\mu u_r)(\bar{d}_s\gamma_\mu d_t)$
$Q^{(8)}_{ud}$	$(\bar{u}_p\gamma^\mu T^A u_r)(\bar{d}_s\gamma_\mu T^A d_t)$

$\mathbf{8:(\bar{L}L)(\bar{R}R)}$	
Q_{le}	$(\bar{l}_p\gamma^\mu l_r)(\bar{e}_s\gamma_\mu e_t)$
Q_{lu}	$(\bar{l}_p\gamma^\mu l_r)(\bar{u}_s\gamma_\mu u_t)$
Q_{ld}	$(\bar{l}_p\gamma^\mu l_r)(\bar{d}_s\gamma_\mu d_t)$
Q_{qe}	$(\bar{q}_p\gamma^\mu q_r)(\bar{e}_s\gamma_\mu e_t)$
$Q^{(1)}_{qu}$	$(\bar{q}_p\gamma^\mu q_r)(\bar{u}_s\gamma_\mu u_t)$
$Q^{(8)}_{qu}$	$(\bar{q}_p\gamma^\mu T^A q_r)(\bar{u}_s\gamma_\mu T^A u_t)$
$Q^{(1)}_{qd}$	$(\bar{q}_p\gamma^\mu q_r)(\bar{d}_s\gamma_\mu d_t)$
$Q^{(8)}_{qd}$	$(\bar{q}_p\gamma^\mu T^A q_r)(\bar{d}_s\gamma_\mu T^A d_t)$

$\mathbf{8:(\bar{L}R)(\bar{R}L)+h.c.}$	
Q_{ledq}	$(\bar{l}^j_p e_r)(\bar{d}_s q_{tj})$

$\mathbf{8:(\bar{L}R)(\bar{L}R)+h.c.}$	
$Q^{(1)}_{quqd}$	$(\bar{q}^j_p u_r)\epsilon_{jk}(\bar{q}^k_s d_t)$
$Q^{(8)}_{quqd}$	$(\bar{q}^j_p T^A u_r)\epsilon_{jk}(\bar{q}^k_s T^A d_t)$
$Q^{(1)}_{lequ}$	$(\bar{l}^j_p e_r)\epsilon_{jk}(\bar{q}^k_s u_t)$
$Q^{(3)}_{lequ}$	$(\bar{l}^j_p\sigma_{\mu\nu}e_r)\epsilon_{jk}(\bar{q}^k_s\sigma^{\mu\nu}u_t)$

$\mathbf{8:(\not{B})+h.c.}$	
Q_{duql}	$\epsilon_{\alpha\beta\gamma}\epsilon_{jk}(d_p^\alpha C u_r^\beta)(q_s^{j\gamma}C l_t^k)$
Q_{qque}	$\epsilon_{\alpha\beta\gamma}\epsilon_{jk}(q_p^{j\alpha}C q_r^{k\beta})(u_s^\gamma C e_t)$
Q_{qqql}	$\epsilon_{\alpha\beta\gamma}\epsilon_{mn}\epsilon_{jk}(q_p^{m\alpha}C q_r^{j\beta})(q_s^{k\gamma}C l_t^n)$
Q_{duue}	$\epsilon_{\alpha\beta\gamma}(d_p^\alpha C u_r^\beta)(u_s^\gamma C e_t)$

Table 4.1: Dimension six operators in the Warsaw Basis [305]. The subscripts p, r, s, t label the flavour indices. The lepton doublet is indicated with l rather than ℓ as in the rest of the text. For non-Hermitian operators, one should include the h.c.

4.3.1 Low Energy Effective Field Theory (LEFT)

The SMEFT is the appropriate effective theory to use when the energy scale of the process we want to describe is above the electroweak scale. It is the EFT we should match onto when we integrate

out the heavy particles of a new physics model. However, the precisely measured processes aimed at probing NP contributions often occur at energy scales much smaller than v, as is the case for most LFV processes. Calculations of low-energy transitions are best parameterized by an EFT in which the heavy particles of the SM, including the W, the Z, the top quark t, and the Higgs boson h, are removed, and the electroweak symmetry is spontaneously broken. The resulting contact interactions should respect the surviving gauge symmetries, i.e. QED and QCD.

Low-energy calculations are connected to high-energy SMEFT coefficients, which are functions of the UV parameters at the NP scale, via the renormalization group evolution. In a top-down perspective, a new physics model is matched onto the SMEFT, and the RGE evolution down to the low-energy scale yields observables in terms of the parameters of the model, which are then compared with experimental results. A bottom-up calculation proceeds in the opposite direction, starting with the observables calculated with low-energy coefficients that respect the experimental constraints and running them up in energy scale. This maps a low-energy experimental bound onto a combination of high-energy coefficients that can be used to identify the region of coefficient space where BSM physics should reside. Since the bottom-up perspective does not consider any particular model, the calculations should, in principle, contain every operator that could be within experimental sensitivity. The effort may be repaid by the fact that any model could be checked against a properly organized bottom-up treatment, which only needs to be updated when new experimental results appear (which is not very often).

Both in top-down and bottom-up calculations, when the electroweak scale is crossed in the running, we should match the low energy and the SM EFT. The matching conditions for dimension six operators have been calculated at one loop [310,311], while the complete tree-level matching up to $1/\Lambda^4$ order has also been computed [312].

SMEFT and LEFT operators running is known up to $1/\Lambda^2$ order, which include the running of dimension five and six operators, as well as the mixing of two dimension five operators with a dimension six one [313–317]. Anomalous dimensions at $1/\Lambda^4$ order are only partially known [318–321], and in Chapter 6 we present previously unknown renormalization group equations for a subset of dimension eight operators.

4.3.2 Effective Field Theory for $\mu \to e$ LFV

In this section, we present an effective analysis of $\mu \to e$ processes that are otherwise flavour diagonal, i.e $\mu \to e\gamma(\gamma)$, $\mu \to 3e$ and $\mu \to e$ conversion in nuclei but not processes like $K \to e\mu$. As we have discussed in Chapter 3, these constitute the best-constrained processes and expect the most significant sensitivity improvements in the upcoming years.

Below the electroweak scale, the operators relevant for $\mu \to e$ transitions are a subset of the QCD and QED invariant contact interactions of the low energy effective theory. These include operators of dimensions five to eight that have three and four external legs. We follow the conventions of [322] and add the operators to the Lagrangian as

$$\mathcal{L}_{\text{EFT}}^{\mu\to e} = \mathcal{L}_{\text{QCD}\times\text{QED}} + \frac{1}{v^2}\sum_{\zeta,\text{Lor}} C_{\text{Lor}}^{\zeta}\mathcal{O}_{\text{Lor}}^{\zeta} \tag{4.79}$$

where ζ represent the flavour indices, while "Lor" indicates the chirality and Lorentz structure of the operator. The observables we want to describe, $\mu \to e\gamma(\gamma)$, $\mu \to 3e$ and $\mu \to e$ conversion in

nuclei, are sensitive to the operators of Table 4.2.

$2l$ operators	
$\mathcal{O}_{D,Y}$	$m_\mu(\bar{e}\sigma^{\alpha\beta}P_Y\mu)F_{\alpha\beta}$
$\mathcal{O}_{XX,Y}$	$\frac{1}{v}(\bar{e}P_Y\mu)X_{\alpha\beta}X^{\alpha\beta}$
$\mathcal{O}_{X\tilde{X},Y}$	$\frac{1}{v}(\bar{e}P_Y\mu)X_{\alpha\beta}\tilde{X}^{\alpha\beta}$
$\mathcal{O}_{XXV,Y}$	$\frac{1}{v^2}(\bar{e}\gamma_\sigma P_Y\mu)X_{\alpha\beta}\partial^\beta X^{\alpha\sigma}$
$\mathcal{O}_{X\tilde{X}V,Y}$	$\frac{1}{v^2}(\bar{e}\gamma_\sigma P_Y\mu)X_{\alpha\beta}\partial^\beta \tilde{X}^{\alpha\sigma}$

$2l2q$ operators	
$\mathcal{O}^{qq}_{V,YZ}$	$(\bar{e}\gamma^\alpha P_Y\mu)(\bar{q}\gamma_\alpha P_Z q)$
$\mathcal{O}^{qq}_{S,YZ}$	$(\bar{e}P_Y\mu)(\bar{q}P_Z q)$
$\mathcal{O}^{qq}_{T,YY}$	$(\bar{e}\sigma^{\alpha\beta}P_Y\mu)(\bar{q}\sigma_{\alpha\beta}P_Y q)$
$4l$ operators	
$\mathcal{O}^{ll}_{V,YZ}$	$(\bar{e}\gamma^\alpha P_Y\mu)(\bar{l}\gamma_\alpha P_Z l)$
$\mathcal{O}^{ll}_{S,YY}$	$(\bar{e}P_Y\mu)(\bar{l}P_Y l)$
$\mathcal{O}^{\tau\tau}_{S,Y\bar{Y}}$	$(\bar{e}P_Y\mu)(\bar{\tau}P_{\bar{Y}}\tau)$
$\mathcal{O}^{\tau\tau}_{T,YY}$	$(\bar{e}\sigma^{\alpha\beta}P_Y\mu)(\bar{\tau}\sigma_{\alpha\beta}P_Y\tau)$

Table 4.2: Low-energy QCD⊗QED invariant EFT for $\mu \to e\gamma(\gamma)$, $\mu \to 3e$ and $\mu \to e$ conversion in nuclei, in the notation of [322]. The experiments can be sensitive to three, four-point functions that correspond to operators of dimensions five to eight. $X_{\alpha\beta} = F_{\alpha\beta}, G_{\alpha\beta}$ are the field tensors of photon and gluons respectively. The chiral projector $P_{Y,Z}$ can be $Y, Z \in \{L, R\}$, $\overline{L} = R, \overline{R} = L$, while $q \in \{u, d, s, b, c\}$ and $l \in \{e, \mu, \tau\}$

Let us consider $\mu \to e\gamma$ as an illustrative example. We can compute at the tree-level in the EFT the branching ratio [142]

$$Br(\mu \to e\gamma) = 384\pi^2(|C_{D,L}|^2 + |C_{D,R}|^2) < 4.2 \times 10^{-13} \to |C_{D,Y}| < 1.05 \times 10^{-8} \tag{4.80}$$

where the dipole operator coefficient $C_{D,Y}(m_\mu)$ are at m_μ to avoid large logs. If we assume that the dipole coefficient is $\sim 1/16\pi^2$ if normalized at the new physics scale, Equation (4.80) implies $\Lambda_{\rm NP} \sim 1.3 \times 10^3$ TeV. The bound can be satisfied with lighter UV physics if the dipole coefficient appears at higher loops and/or is suppressed by a small coupling.

To use the bound on EFT operator coefficients to constrain generic BSM heavy physics, we should determine the upper limit on coefficients at the new physics scale, where the heavy degrees of freedom are integrated out. This is done by solving the renormalization group equations of the Wilson coefficients, which requires dressing the operator basis with QED and QCD loops. The one-loop RGEs can be written as

$$\mu\frac{d\vec{C}}{d\mu} = \frac{\alpha_s(\mu)}{4\pi}\vec{C}\Gamma^s + \frac{\alpha_e(\mu)}{4\pi}\vec{C}\Gamma^e \tag{4.81}$$

having aligned the Wilson coefficient in the row vector $\vec{C}$. The QCD renormalization matrix Γ^s is diagonal, while QED (Γ_e) can mix operators with different legs and Lorentz structure. We would like to resum the numerically relevant QCD effects and expand the QED loop effects in powers of α_e, neglecting its running. The formal solution of the matrix equation $dU/dt = HU$ is a t ordered

exponential $U(t) = (T\exp\int_{t_0}^{t} dt' H(t))U(t_0)$ [4], which in our case can be expanded at $\mathcal{O}(\alpha_e)$ to be

$$C_I(\mu_f) = C_I(\mu_i)\delta_{IJ}\left(\frac{\alpha_s(\mu_f)}{\alpha_s(\mu_i)}\right)^{-a_J}\left[\delta_{JK} + \frac{\alpha_e}{4\pi}f_{JK}\Gamma^e_{JK}(\mu_f)\log\left(\frac{\mu_f}{\mu_i}\right)\right] + \mathcal{O}(\alpha_e)^2 \tag{4.82}$$

where $a_J = \Gamma^s_{JJ}/2\beta_0$ parametrises the QCD running of two-lepton two-quark operators. Vector operators do not run $a_V = 0$, while the scalar and tensor coefficients are respectively $a_S = 12/23$ and $a_T = -4/23$. Defining $\lambda \equiv (\alpha_s(\mu_f)/\alpha_s(\mu_i))$, the coefficients f_{JK} read

$$f_{JK} = \frac{1}{1-\lambda}\frac{1-\lambda^{a_J - a_K - a_d + 1}}{a_J - a_K - a_d + 1} \tag{4.83}$$

with a_d parametrising, if present, the running of QCD parameters in the QED anomalous dimension (for instance, the tensor to dipole mixing for two-lepton two-quark tensors is proportional to the mass of the virtual quark in the loop). QED renormalization, although not as numerically relevant as the QCD coefficient rescaling, plays a crucial role because it mixes operators. Operator mixing allows probing an operator coefficient which is difficult to detect via its mixing with a tightly constrained one. For instance, the tensor operator $\mathcal{O}^{\tau\tau}_{T,Y} = (\bar{e}\sigma^{\alpha\beta}P_Y\mu)(\bar{\tau}\sigma_{\alpha\beta}P_Y\tau)$ mixes into the dipole by closing the tau legs in a loop and attaching a photon. The contribution to the dipole coefficient is one-loop suppressed (and log enhanced), but, to close the loop, a chirality flip is necessary, and a τ mass insertion enhances the mixing by m_τ/m_μ. Complemented with a large anomalous dimension, the mixing is $\sim \mathcal{O}(1)$. The (sensitivity) bound that $\mu \to e\gamma$ sets on the tensor coefficient at m_W is then [322]

$$C^{\tau\tau}_{T,Y}(m_W) \lesssim 1.07 \times 10^{-8} \tag{4.84}$$

We should stress that this is not an exclusion bound, but rather an experimental sensitivity. In coefficient space, $\mu \to e\gamma$ constrains one direction that corresponds to the dipole coefficient at the experimental scale m_μ. The RGEs can tell us how this direction rotates in the coefficient space at higher energies, but the experiment still imposes a bound in one direction only. In other words, the bound will apply to a single combination of operator coefficients at the high scale; namely, solving the RGEs up to m_W,

$$|C_{D,Y}|(m_\mu) = \left|0.938C_{D,Y}(m_W) + 0.981C^{\tau\tau}_{T,Y}(m_W) + \ldots\right| < 1.05 \times 10^{-8}. \tag{4.85}$$

The upper limit in Equation (4.84) corresponds to the case where only $C^{\tau\tau}_{T,Y}(m_W)$ is non-zero and is commonly known as one-operator-at-a-time bound or sensitivity. A sensitivity corresponds to the smallest absolute value which is experimentally detectable, but larger values are possible if cancellations with other contributions occur. Indeed, we can see that if the dipole and the tensor are of similar size and opposite sign, an accidental cancellation can occur in Equation (4.85). This is an example of a flat direction in coefficient space. Flat directions are a general feature of bottom-up EFT analyses of LFV, because the operator basis contains more operators than observables, and the few operators constrained by experiments mix with the rest in the RGEs. Nonetheless, identifying operator coefficients to which observables are most sensitive is a useful guide for model building. The sensitivities of $\mu \to 3e, \mu \to e\gamma$ and $\mu N \to eN$ to Wilson coefficients at m_W in the low energy EFT has been extensively studied [322–326]. Spin-dependent $\mu \to e$ conversion in

[4] This is the solution for time evolution operator in Quantum Mechanics.

nuclei [324,325,327,328], although less constraining than the spin-independent searches, allows to probe different combinations of coefficients and, thus, reduce the number of flat directions.

Leptonic and semi-leptonic rare meson decays such as $K_L^0 \to \mu e$, $K^+ \to \pi^+ \mu e$ are systematically studied in the EFT by adding to the operator basis quark flavor-changing operators, and the sensitivities to Wilson coefficient can be similarly determined [329]. Concerning $\tau \leftrightarrow l$ processes, EFT analysis can be found in [322,330].

To extend the bottom-up analysis above the electroweak scale, one should solve the RGEs of SMEFT lepton-flavour-changing operators and identify all the contributions to which observables could be sensitive. As we explore in Chapter 5, is not obvious what one should include, and we argue that some challenging calculations are required to fully parametrise LFV in the SMEFT.

Chapter 5

What is leading order for LFV in SMEFT?

5.1 Introduction

Perturbation theory is a widely used tool in the Standard Model, New Physics models and many other areas. In a given perturbative expansion, the first non-vanishing term, sometimes called the leading order contribution, is often simple to compute. However, when a calculation simultaneously involves many perturbative expansions, it can be more challenging to identify the "leading" or dominant contribution.

In this chapter, we study perturbative expansions in the lepton flavour changing part of the Lagrangian of the Standard Model Effective Field Theory. We restrict to LFV operators for two reasons ; firstly, they must exist because the observations of neutrino oscillations demonstrate that leptons change flavour, as we discussed in Chapter 3. And secondly, LFV operators are simpler than generic operators, because SM loop effects, included via renormalisation group equations, cannot change lepton flavour, so the flavour of at least two legs of each operator remains fixed.

There are many perturbative expansions in SMEFT: the EFT expansion in the ratio of weak to New Physics scales v^2/Λ_{NP}^2, as well as the SM expansions in loops, in the $\mathcal{O}(1)$ gauge and Higgs self-couplings and in the exceptionally hierarchical Yukawa couplings, and also in mixing angles. So it is not obvious to find the leading effects. For example, it was noticed long ago by Bjorken and Weinberg [192], in the SM extended with a second Higgs H with LFV couplings $Y_{\mu e}\bar{\ell}_\mu H P_R e$, that the one-loop amplitude for $\mu \to e\gamma$ is suppressed by two lepton Yukawas, so is *smaller* than two-loop "Barr-Zee" contribution:

$$\mathcal{A}_{1-loop} \propto \frac{e y_\mu Y^*_{\mu\mu} Y_{\mu e}}{16\pi^2 M_H^2} \quad , \quad \mathcal{A}_{2-loop} \propto \frac{e y_t g^3 Y_{\mu e}}{(16\pi^2)^2 M_H^2} \quad .$$

However, this leading (although two-loop) contribution was missed in part of the subsequent literature.

Various powercounting schemes have been introduced to organise perturbative calculations in flavour physics. For instance, in the quark flavour sector below the weak scale, the Wolfenstein parametrisation of the CKM matrix [48] in powers of Cabibbo's $\lambda \sim 0.22$, allows to guess the order of diagrams [294, 297]. And above the weak scale, there are schemes such as Frogatt-Nielsen charges [130] and Minimal Flavour Violation [132] (see also the more general framework introduced in [331] for B-anomalies). Below the weak scale, a powercounting recipe for flavour is sufficient to organise a calculation, because the mass scales for the EFT are known, and the remaining couplings are few: in the RGEs for four-quark operators, QED effects can be included at appropriate subleading order in the expansion in $\alpha_e \log$ [294, 332]. For LFV below the weak scale, the "leading

order" operators and RGEs have been assembled: observables can be parametrised with three and four-point functions, which correspond to operators of dimensions five to eight (see section 4.3.2), and the "leading order" RGEs, which include two-loop vector to dipole mixing, are given in [323]. However, above the weak scale, the situation is complicated by the dynamical Higgs and SU(2) gauge bosons, which introduce more particle mixing in the RGEs, and also by our ignorance of the mass scale of new particles, $\Lambda_{\rm NP}$.

In this chapter, we suppose that New Physics is "beyond the LHC", which is taken to mean $\Lambda_{NP} > 4$ TeV, and introduce in Section 5.2 a generalisation of the Wolfenstein counting that parametrises the expansions in all the SM parameters of SMEFT, as well as the scale ratio $v/\Lambda_{\rm NP}$, in terms of a single power-counting parameter $\lambda \sim 0.2$. For any operator, this scheme allows to identify the "leading" contribution to a given process among those that could arise at different orders in the multiple perturbative expansions. It also allows to classify the contributions of various operators to a process according to the order in λ, and estimate when a process can have sensitivity to an operator. So in section 5.3, the power-counting scheme is used to address four questions:

1. Are dimension six operators sufficient to parametrise LFV, or can observables be sensitive to dimension eight operators?

2. Does one need two-loop anomalous dimensions in the RGEs?

3. Are LFV observables sensitive to the effects of CKM angles in the RGEs, or can the quark Yukawa matrices be approximated as diagonal?

4. If the dimension six operator $H^\dagger H \bar{\ell} H e$ is present, it contributes to the charged lepton mass matrix when the Higgs has a vev, so the lepton mass eigenstates are not the eigenstates of the lepton Yukawa matrix Y_e that appears in the RGEs. How should this be accounted for?

The results are summarised in section 5.4. The powercounting suggests that in the $\mu \leftrightarrow e$ sector, upcoming data could be sensitive to some dimension eight operators, and some $\mathcal{O}(\log/(16\pi^2)^2)$ effects, for $\Lambda_{\rm NP} \lesssim 50 \to 100$ TeV (see the estimates [1] in tables 5.5 and 5.6). The relevant dimension eight operators are listed in Appendix C, and their (tree-level) matching onto the EFT below m_W is given in Appendix C.2. For $\Lambda_{\rm NP} \gtrsim 50(\to 100)$ TeV in the $\mu \leftrightarrow e$ sector, and for all considered scales in the $\tau \leftrightarrow \ell$ sector ($\Lambda_{\rm NP} \gtrsim 4$ TeV), the powercounting suggests that the one-loop RGEs for dimension six operators are sufficient

5.2 Power-counting

We want to connect low-energy LFV processes with the operator coefficients in the SMEFT. In a top-down sense, this means we want to estimate the "leading" or largest contribution of each operator coefficient to each observable, or equivalently from a bottom-up perspective, the best sensitivity of each observable to each operator.

[1] Only a few $\mu \to e$ operators involving $\bar{t}t$, such as $H^\dagger H(\bar{\mu}\sigma P_R e)(\bar{q}_t \sigma P_R t)$, could contribute up to $\Lambda_{\rm NP} \lesssim 100$ TeV.

5.2.1 Notation

We write the SM Lagrangian in the notation of Chapter 2. Operators that change lepton flavour (but not number) arise at dimension ≥ 6 in SMEFT, and are added to the Lagrangian in the basis of [304,305], with coefficients written as a dimensionless C divided by appropriate factors of a mass scale Λ:

$$\mathcal{L}_{SMEFT} = \mathcal{L}_{SM} + \left\{ \frac{1}{\Lambda^2} \sum_I C_I^\zeta \mathcal{O}_I^\zeta + \frac{1}{\Lambda^4} \sum_K {}^{(8)}C_K^\zeta \mathcal{O}_K^{(8)\ \zeta} + h.c. + ... \right\} \tag{5.1}$$

where Λ is $v = 174$ GeV in the experimental constraints on coefficients ($1/v^2 = 2\sqrt{2}G_F$), but it is sometimes convenient in the powercounting to take Λ to be the scale $\Lambda_{\rm NP}$ of New LFV Physics. So for $\Lambda = v$, the powers of $v^2/\Lambda_{\rm NP}^2$ are included the coefficients C. The coefficient subscripts label the gauge structure, and the superscript ζ is the flavour of the fermions composing the operator in order of appearance(sometimes the LFV indices are suppressed when they are obvious). The dimension six and eight operators are respectively labelled and normalised as in [305][2] and [308].

The operators $\{\mathcal{O}_I\}$ represent LFV contact interactions among SM particles. Loop corrections to the operators generically diverge, so after renormalisation in $\overline{\rm MS}$, the operator coefficients depend on the renormalisation scale μ and satisfy the RGEs. These can be written for dimension six operators as

$$\mu \frac{\partial}{\partial \mu} \vec{C} = \frac{1}{16\pi^2} \vec{C} \widetilde{\Gamma} + ... \tag{5.2}$$

where the operator coefficients are lined up in the row vector $\vec{C}$, and the matrix elements of $\widetilde{\Gamma}$ are the anomalous dimensions multiplied by SM couplings, currently known at one-loop. The matrix $\widetilde{\Gamma}$ can be improved by including higher-loop contributions to the anomalous dimensions, and the equation can be extended by adding higher-dimensional operators (which changes its structure [333]). Eqn(5.2) can be solved numerically, or solved analytically as a "scale-ordered" exponential, or approximated by neglecting the running of SM couplings and exponentiating $\widetilde{\Gamma}$:

$$\vec{C}(\mu_2) \simeq \vec{C}(\mu_1) + \vec{C}(\mu_1) \frac{\widetilde{\Gamma}}{16\pi^2} \ln\left(\frac{\mu_2}{\mu_1}\right) + ... \tag{5.3}$$

This last approximation can be improved by including the running of some SM couplings, and selected $\mathcal{O}(\ln^2/(16\pi^2)^2)$ terms. The power-counting scheme introduced below is diagrammatic, so makes estimates in the spirit of an improved eqn (5.3), and aims to assist in determining which improvements should be included in the RGEs.

5.2.2 The power-counting scheme

The aim here is to construct a power-counting scheme allowing to organise the perturbative expansions that arise in Renormalisation Group running in the SMEFT above m_W. The input to this power-counting scheme should be the experimental sensitivities of one or several observables, and a list of operator coefficients. But since one of the expansion parameters, $v^2/\Lambda_{\rm NP}^2$, is unknown, we only bound it from above, and quantify the order of a coefficients contribution to an observable, as the scale up to which an $\mathcal{O}(1)$ coefficient could be probed.

[2] The hermitian operators are here defined with a 1/2, since the hermitian conjugates are included in eqn 5.1.

We introduce a small parameter

$$\lambda \simeq 0.2 \tag{5.4}$$

by analogy to the λ parameter of the CKM matrix. The numerical value of powers λ^k is given in table 5.1. The various dimensionless expansion parameters that occur in SMEFT can be associated to powers of λ as discussed below (the recipe is summarised in table 5.2).

$k=$	1	3	4	5	6	7	8	10	12
$\lambda^k=$	.2	.008	1.6×10^{-3}	3.2×10^{-4}	6.4×10^{-5}	1.28×10^{-5}	2.56×10^{-6}	1.02×10^{-7}	4×10^{-9}
$\Lambda_{\rm NP}$(TeV)			4.3		22		109	540	2700

Table 5.1: The second line gives the numerical value of λ^k, for $\lambda = 0.2$ and k from the first line. The third line gives the value of $\Lambda_{\rm NP}$, in TeV, such that $(v/\Lambda_{\rm NP})^2 = \lambda^k$ (where $v = 174$ GeV).

1. the gauge couplings g_s, g and g' (of respectively QCD, SU(2) and hypercharge) are counted $\sim \mathcal{O}(1)$, and sometimes retained in the estimates (because $e^3 \sim \lambda^2$).

2. With a Lagrangian normalised as eqn (5.1) with $\Lambda = v = 174$ GeV, the ratio $v^{n-4}/\Lambda_{\rm NP}^{n-4}$ is absorbed into the coefficients (where n is the operator dimension). In discussing dimension eight operators, we assume a New Physics scale beyond the reach of the LHC:

$$\Lambda_{\rm NP} \gtrsim 4 \text{ TeV} \qquad \Rightarrow \frac{v^2}{\Lambda_{\rm NP}^2} \lesssim \lambda^4$$

   however we leave $\Lambda_{\rm NP} > v$ undetermined in estimating the relevance of two-loop or CKM effects.

3. to each loop is attributed a factor

$$\frac{1}{16\pi^2} \sim \lambda^3 \quad , \quad \frac{\log}{16\pi^2} \sim \lambda^2$$

   where the loops that appear in the RGEs are accompanied by a log, so counted with one less power. (For reference, $\ln \frac{m_W}{m_{\mu,\tau}} \simeq 6.7, 3.85$, and $\ln \frac{4\text{TeV}}{m_W} \simeq 3.91$.)

4. anomalous dimensions are counted as $\mathcal{O}(1)$, despite that some can be large (this may sometimes compensate for counting gauge couplings ~ 1).

5. In the lepton sector, we work in the mass eigenstate basis for charged leptons. This would be the eigenbasis of Y_e in the SM, but can differ in the presence of non-renormalisable operators [334]. For instance, the operator $[C_{eH}]^{ij}/\Lambda_{\rm NP}^2\ H^\dagger H \bar{\ell}_i H e_j$ contributes to the charged lepton mass matrix

$$[m_e]^{ij} = [Y_e]^{ij} v - [C_{eH}]^{ij} \frac{v^3}{\Lambda_{\rm NP}^2} \quad . \tag{5.5}$$

   However, there is a factor of 3 in the Feynman rule of $\mathcal{O}_{eH}$, such that the coupling of leptons to the SM Higgs is

$$[\widetilde{Y}]^{ij} = \frac{1}{\sqrt{2}v}\left([m]^{ij} - 2[C_{eH}]^{ij}\frac{v^3}{\Lambda_{NP}^2}\right) \tag{5.6}$$

so in the charged lepton mass basis, flavour-changing higgs decays probe the off-diagonal coefficients of C_{eH}.

The LHC measures the yukawas of the τ and the μ to be consistent with SM expectations [185, 186, 335, 336], and constrains the $\tau \to \ell$ flavour-changing interactions of the 125-GeV Higgs [337, 338]:

$$\frac{v^2}{\Lambda^2_{\rm NP}}\sqrt{\left|C^{\mu\tau}_{eH}\right|^2+\left|C^{\tau\mu}_{eH}\right|^2} < 1.00\times10^{-3} \quad , \quad \frac{v^2}{\Lambda^2_{\rm NP}}\sqrt{\left|C^{e\tau}_{eH}\right|^2+\left|C^{\tau e}_{eH}\right|^2} < 1.60\times10^{-3} \quad . \tag{5.7}$$

For $\mu \to e$ flavour change, the MEG bound [223] on BR($\mu \to e\gamma$) could probe couplings as small as [322]

$$\frac{v^2}{\Lambda^2_{\rm NP}}C^{\mu e}_{eH} \quad , \quad \frac{v^2}{\Lambda^2_{\rm NP}}C^{e\mu}_{eH} \sim 7.5\times10^{-7} \tag{5.8}$$

(larger values could be allowed if they cancel against other contributions). These bounds imply that in the charged lepton mass eigenstate basis, the off-diagonal elements of Y_e are small (they are comparable to the the LFV coefficients $C^{ij}_{eH}v^2/\Lambda^2_{\rm NP}$ —see eqn 6.87), so the two largest eigenvalues of Y_e can approximately be obtained from m_τ and m_μ. Assuming that the magnitude of the electron Yukawa is $\leq y_e|_{max} = m_e/v$, one obtains that in the mass eigenstate basis,

$$[Y_e] = \begin{bmatrix} \leq 2.9\times10^{-6} & < 10^{-6} & < 10^{-3} \\ < 10^{-6} & 6.0\times10^{-4} & < 10^{-3} \\ < 10^{-3} & < 10^{-3} & 1.0\times10^{-2} \end{bmatrix} \approx \begin{bmatrix} \lambda^8 & \lambda^9 & \lambda^4 \\ \lambda^9 & 2\lambda^5 & \lambda^4 \\ \lambda^4 & \lambda^4 & \lambda^3 \end{bmatrix} \tag{5.9}$$

6. In the quark flavour sector, the mass and Yukawa matrices select eigenbases when they are diagonalised in the generation spaces of the SM fermions. Since this chapter is focussed on LFV, operators such as $H^\dagger H\bar{q}Hd$ or $H^\dagger H\bar{q}\tilde{H}u$ are not considered, and the quark masses are assumed to arise from Yukawa couplings. So the eigenvalues of Y_d and Y_u, evaluated at m_W, are taken as:

$$\begin{aligned} (y_b, y_s, y_d) &\approx (1.7\times10^{-2}, 3.5\times10^{-4}, 1.7\times10^{-5}) \approx (\lambda^2/2, \lambda^5, \lambda^7) \\ (y_t, y_c, y_u) &\approx (1.0, 4.0\times10^{-3}, 6.7\times10^{-6}) \approx (1, \lambda^3/2, \lambda^7/2) \quad . \end{aligned} \tag{5.10}$$

where $y_f \equiv m_f(m_W)/v$, with $m_f(m_W)$ obtained from one-loop RGEs — *eg* for quarks:

$$m(m_W) = m(\mu)\left[\frac{\alpha_s(m_W)}{\alpha_s(\mu)}\right]^{4/\beta}$$

with $\beta = (33-2N_f)/3 \simeq 8$, and $m(\mu)$ is from the PDB [47] with $\mu = m_b, m_c$ for the b, c and 2 GeV otherwise[3].

The CKM matrix is approximated in terms of λ in usual way:

$$V_{\rm CKM} = \begin{bmatrix} V_{ud} & V_{us} & V_{ub} \\ V_{cd} & V_{cs} & V_{cb} \\ V_{td} & V_{ts} & V_{tb} \end{bmatrix} = \begin{bmatrix} 0.974 & 0.224 & -0.004 \\ -0.22 & 0.99\pm0.02 & 0.042 \\ 0.008 & -0.04 & 1.0 \end{bmatrix} \simeq \begin{bmatrix} 1 & \lambda & \lambda^3/2 \\ -\lambda & 1 & \lambda^2 \\ \lambda^3/2 & -\lambda^2 & 1 \end{bmatrix}$$

[3] At m_W, this gives $m_b = 3.0$ GeV, $m_c = 0.7$ GeV, $m_s = 62$ MeV, $m_d = 3.0$ MeV, $m_u = 1.2$ MeV.

We will always work in the mass eigenstate bases of the singlet quarks, and the u-type components of the doublet quarks. So in the RGEs, the up Yukawa is a diagonal matrix D_u, and $Y_d = V_{\rm CKM} D_d$. We choose the $\{u_L\}$ basis for quark doublets above m_W for two reasons. First, flavour change in the RGEs is therefore suppressed by CKM and the small d-type Yukawas. Secondly, at dimension six in SMEFT, there is only a tensor operator for us ($\mathcal{O}_{\ell equ(3)}$), so this basis diagonalises the large mixing of this tensor to the dipole operator.

The CKM matrix is included also in matching at m_W, when the low-energy operators involving d-type quarks are expressed as SMEFT operators.

The above power-counting scheme is summarised in table 5.2, and should allow to estimate the contribution of any operator coefficient to any observable. The accuracy of the scheme is discussed at the end of the next subsection, by comparing to the solutions of the RGEs.

loop	$\frac{1}{16\pi^2}$	λ^3
loop*log	$\frac{\log}{16\pi^2}$	λ^2
lepton yukawas	y_τ, y_μ, y_e	$\lambda^3, 2\lambda^5, \lambda^8$
ℓ flavour change	see eqn 5.9	
d-quark yukawas	y_b, y_s, y_d	$\lambda^2/2, \lambda^5, \lambda^7$
u-quark yukawas	y_t, y_c, y_u	$1, \lambda^3/2, \lambda^7/2$
q flavour change	see eqn 5.11	

Table 5.2: power-counting scheme for the perturbative expansion of the SMEFT

5.2.3 Examples

This section gives explicit examples of how the powercounting estimates are made, and compares them to the solutions of the RGEs.

We first consider $\mu \to e$ processes because the most restrictive experimental constraints on LFV arise in this sector, and upcoming experiments aim to improve the sensitivities by several orders of magnitude (see table 5.3; indeed, there plans to reach a conversion ratio $\lesssim 10^{-18}$ for $\mu A \to eA$ [342]). The Branching Ratios can be expressed (see *eg* [142, 322, 329]) in terms of the coefficients, evaluated at the experimental scale, of operators which contribute at tree level. For instance, the low-energy operators

$$\delta\mathcal{L} = 2\sqrt{2} G_F (C_{D,L} m_\mu \bar{e}\sigma \cdot F P_L \mu + C_{D,R} m_\mu \bar{e}\sigma \cdot F P_R \mu) \tag{5.11}$$

contribute to $\mu \to e\gamma$ as

$$BR(\mu \to e\gamma) = 384\pi^2 (|C_{D,R}|^2 + |C_{D,L}|^2) < 4.2 \times 10^{-13} \tag{5.12}$$

which gives the experimental bounds, translated into our power counting parameter ($\Lambda \sim v$ in eqn (5.1)

$$|C_{D,R}|, |C_{D,L}| < 1.05 \times 10^{-8} \sim \lambda^{11} \quad . \tag{5.13}$$

process	bound on BR	sensitivity to C
$\mu \to e\gamma$	$< 4.2 \times 10^{-13}$ [223] $\to 6 \times 10^{-14}$ [224]	$C_D \sim \lambda^{11} \to \lambda^{12}$
$\mu \to e\bar{e}e$	$< 1.0 \times 10^{-12}$ [239] $\to 10^{-16}$ [231]	$C_S \sim \lambda^{8} \to \lambda^{11}$
		$C_V \sim \lambda^{8.5} \to \lambda^{11.5}$
$\mu A \to eA$	$< 7 \times 10^{-13}$ [339] $\to 10^{-16}$ [275,340]	$C_{V,D} \sim \lambda^{9.5} \to \lambda^{12}$
		$C_S \sim \lambda^{10.5} \to \lambda^{14}$
$\overline{K^0_L} \to \mu\bar{e}$	$< 4.7 \times 10^{-12}$	$C_P \sim \lambda^{11.5}$
		$C_A \sim \lambda^{9.5}$
$B^0_d \to \mu^\pm e^\mp$	$< 1 \times 10^{-9}$	$C_P \sim \lambda^{7.5}$
$B^+_d \to \pi^+ \bar{\mu} e$	$< 1.7 \times 10^{-7}$	$C_V \sim \lambda^{7}$
$B^0_s \to \mu^\pm e^\mp$	$< 5.4 \times 10^{-9}$	$C_P \sim \lambda^{7.5}$
$B^+ \to K^+ \bar{\mu} e$	$< 9.1 \times 10^{-8}$	$C_V \sim \lambda^{6.5}$
$D^0 \to \mu^\pm e^\mp$	$< 1.3 \times 10^{-8}$	$C_P \sim \lambda^{6}$
$D^+ \to \pi^+ \bar{\mu} e$	$< 1.7 \times 10^{-7}$	$C_V \sim \lambda^{4}$
$\tau \to \ell\gamma$	$< 3.3 \times 10^{-8}$ [243]	$C_D \sim \lambda^{7.5}$
$\tau \to \ell\bar{\ell}\ell$	$\lesssim 2 \times 10^{-8}$ [244] $\to\lesssim 10^{-9}$ [341]	$C_V \sim \lambda^{5} \to \lambda^{5.5}$
		$C_S \sim \lambda^{4.5} \to \lambda^{5}$
$\tau \to \ell\pi^0$	$< 8.0 \times 10^{-8}$ [245]	$C_S \sim \lambda^{4.5}$
$\tau \to \ell\eta$	$< 6.5 \times 10^{-8}$ [245]	$C_S \sim \lambda^{4.5}$
$\tau \to \ell\rho$	$< 1.2 \times 10^{-8}$ [247]	$C_V \sim \lambda^{4.5}$
$B^0_d \to e\tau$	$< 2.8 \times 10^{-5}$ [47]	$C_P \sim \lambda^{5}$
		$C_A \sim \lambda^{4.5}$

Table 5.3: Some current and upcoming experimental bounds on LFV Branching Ratios ($\tau \leftrightarrow \mu$ results are similar to $\tau \leftrightarrow e$). The third column gives the order of magnitude of dimension six operator coefficients that reproduce the experimental numbers, in powers of $\lambda \simeq 1/5$. The listed coefficients C_{Lor} contribute to the process at tree level, are labelled by the operator's Lorentz structure, and are normalised to a scale $\Lambda = v = 174$ GeV in eqn (5.1). The meson decay bounds are from [47], the coefficient sensitivities from [322,329].

The dipole is a special case, because the operators contain not only fields, but also a built-in parametric suppression factor m_μ. This is the usual operator definition, and makes sense because in SMEFT the operator has a Higgs leg which frequently attaches to the muon line. However, in some loop diagrams (for instance Barr-Zee) the Higgs is attached to a heavier particle in a loop, so such diagrams would gain a factor $1/(2\lambda^5)$ in our power-counting scheme. For a different normalisation of the dipole operator, the power-counting sensitivity would change. For instance,

$$\delta\mathcal{L} = 2\sqrt{2}G_F(C_{D,L}v\bar{e}\sigma \cdot FP_L\mu + C_{D,R}v\bar{e}\sigma \cdot FP_R\mu) \tag{5.14}$$

gives $|C_{D,R}|, |C_{D,L}| \lesssim \lambda^{16}$.

The sensitivity of $\mu \to e\gamma$ to other operators can be estimated in our power-counting scheme by drawing diagrams. For instance, tensor operators mix to the dipole via the left diagram of Fig. 5.1. Below the electroweak scale and normalizing as in eq. (5.11), the contribution to the dipole

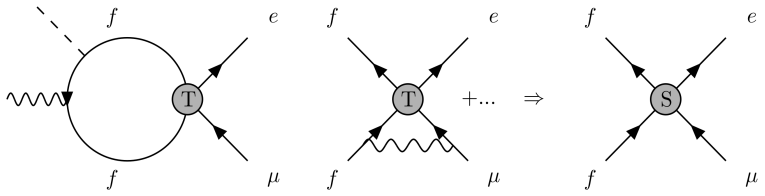

Figure 5.1: On the left, a diagram mixing the tensor operator to the dipole (the Higgs leg is replaced by a mass insertion in the EFT below m_W). On the right, one of the diagrams mixing tensor operators to scalars (the gauge boson can attach to any two legs not belonging to the same bilinear).

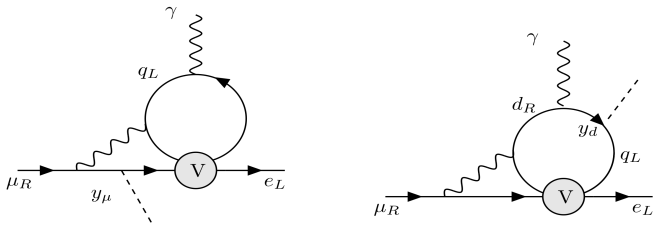

Figure 5.2: Representative diagrams allowing two-loop mixing of vector operators to the dipole.

coefficient is of order

$$\Delta C_D \frac{m_\mu}{v^2} \sim e \frac{\log}{16\pi^2} C_T^{ff} \frac{m_f}{\Lambda_{\rm NP}^2} \Rightarrow \Delta C_D \sim e\lambda^2 C_T^{ff} \frac{y_f}{y_\mu} \frac{v^2}{\Lambda_{\rm NP}^2} \tag{5.15}$$

where $f = u, d, s, c, b, e, \mu, \tau$, and the estimate in our power-counting scheme can be obtained using table 5.2.

Scalar and vector operators can contribute to the dipole via two-loop diagrams, that arise either as one-loop mixing into the tensor, or direct mixing to the dipole at two-loop. Below the weak scale, the scalar to tensor mixing is via diagrams like the right figure 5.1, where the gauge boson is a photon, which gives

$$\Delta C_D \sim e^3 \frac{\log^2}{(16\pi^2)^2} C_S^{ff} \frac{y_f}{y_\mu} \frac{v^2}{\Lambda_{\rm NP}^2} \tag{5.16}$$

where now $f = u, d, s, c, b, \tau$. The vector to dipole mixing is via diagrams such as figure 5.2. We estimate the diagrams on the left and right as

$$\Delta C_D \sim e^3 \frac{\log}{(16\pi^2)^2} C_V \left(\frac{v}{\Lambda_{\rm NP}}\right)^2 \times \begin{cases} 1 \\ \frac{y_d}{y_\mu} \end{cases} \tag{5.17}$$

so there is sensitivity to vector coefficients for scales below 10 $T\!e$V (which is consistent with the bound in [322, 323]).

Approximating physical predictions in terms of powers of some parameter is always somewhat arbitrary and erroneous (Indeed, although we count in λ, we allow for $\sqrt{\lambda}$ in table 5.3). In order to

f	Power Counting	Running
e	~ 20 TeV	~ 13 TeV
μ	~ 300 TeV	~ 190 TeV
τ	$\sim 10^3$ TeV	$\sim 1.1 \times 10^3$ TeV
u	~ 50 TeV	~ 71 TeV
d	~ 50 TeV	~ 73 TeV
s	~ 200 TeV	~ 330 TeV
c	$\sim 10^3$ TeV	$\sim 1.7 \times 10^3$ TeV
b	$\sim 2 \times 10^3$ TeV	$\sim 2 \times 10^3$ TeV

Table 5.4: Powercounting estimates of the mixing from tensor to dipole operators below m_W, compared to the solutions of the RGEs [322,323].

test our recipe, in table 5.4 we compare our power-counting estimates to the solutions of the RGEs; this estimate is obtained in the EFT below m_W, for which the solution of the "leading order" RGEs is given in [322,323]. The table shows that our estimate of the scale $\Lambda_{\rm NP}$ where C_T^{ff} would be ~ 1, (obtained by combining eqn (5.15) with column three of table 5.3), differs by at most $\sqrt{3}$ from the solution of the RGEs (this corresponds to a factor ≤ 3 for C, so less than an order of magnitude in the rate). For the second-order/two-loop mixing of eqns (5.16,5.17) we find that the powercounting can mis-estimate $\Lambda_{\rm NP}$ by a factor 2-3.

5.3 Questions

This section uses the power-counting proposal of the previous section to study what physics should be included at "leading order", in the SMEFT RGEs for LFV operators. In the first sections, the focus is on $\mu \leftrightarrow e$ flavour change, due to the sensitivity of current and upcoming experiments; the importance of dimension eight operators and two-loop anomalous dimensions for τ-LFV is briefly discussed in section 5.3.5.

5.3.1 Dimension eight operators

This section explores when which dimension eight operators are required, and whether their RGEs are required.

We suppose that the New Physics responsable for LFV is beyond the reach of the LHC, so $\Lambda_{\rm NP} \gtrsim 4$ TeV. In the normalisation convention of table 5.3, this implies that coefficients of dimension eight operators at are suppressed by $\sim \lambda^8$:

$$\frac{f(g_{NP},...)}{(4\text{ TeV})^4}\mathcal{O}^{(8)} = \frac{{}^{(8)}C}{v^4}\mathcal{O}^{(8)} \Rightarrow {}^{(8)}C \lesssim \frac{v^4}{(4\text{ TeV})^4} \simeq \lambda^8 \tag{5.18}$$

Comparing to the tree-level sensitivities given in table 5.3, one sees that kaon and muon decays are generically sensitive to dimension eight operators induced by new particles in the interesting mass range just beyond the reach of the LHC. Pushing the New Physics scale above 20 TeV would give ${}^{(8)}C \lesssim \lambda^{12}$, making most dimension eight operators irrelevant.

There are thousands of LFV dimension eight operators [308, 309], so it would be attractive to include only some of them in a first approximation. Indeed, in a bottom-up perspective, only the dimension eight operators to which observables are sensitive are required. So we reject derivative operators such as

$$D^\alpha(\bar{e}\gamma_\beta\mu)D_\alpha(\bar{f}\gamma^\beta f)$$

because their contribution to low-energy S-matrix elements should be suppressed by $\{s,t,u\}/v^2$, suggesting that K and μ processes have no sensitivity to dimension eight derivative operators. We also neglect operators with more than four legs after electroweak symmetry-breaking, on the assumption that they do not contribute (at tree level) to our low-energy observables.

There remain about four dozen $\mu \leftrightarrow e$ operators (given in Appendix C in the notation of [308]):

1. four-particle operators which are forbidden at dimension 6 due to gauge invariance.

2. dimension six SMEFT operators with an additional H and $H^\dagger$, such as $(HH^\dagger)\bar{\ell}H\sigma^{\alpha\beta}eF_{\alpha\beta}$ or $(\bar{\ell}_e H\sigma^{\alpha\beta}\mu)(\bar{q}_i\tilde{H}\sigma_{\alpha\beta}u_j)$. It may seem unlikely that the dimension eight contribution could be relevant given the possibility of a dimension six term[4]; however, being agnostic could be appropriate in EFT, and dimension eight operators are considered, for instance, in studies of Non-Standard neutrino Interactions [343].

These operators are schematically listed in tables 5.5 and 5.6, along with the scale below they could contribute to observables with a coefficient $C \lesssim 1$. So they should be considered in the EFT parametrisation of any model constructed below this scale.

The effects of these operators can be partially accounted for by matching the model onto them at $\Lambda_{\rm NP}$, and then including them in the matching at the weak scale onto the low energy EFT. These matching conditions for LFV operators are given in appendix C.2 (at tree level).

Many of these operators contribute to observables via loops, so including them in RGEs is relevant. Since they match at m_W onto low-energy four-particle interactions, the Renormalisation Group running below m_W is known and will occur automatically once they are included in the matching.

The RG running in SMEFT is missing. Above m_W , the Higgs and W bosons can mix operators differently from the gluon and photon, for instance by modifying the SU(2) contractions (see eg the RGEs for a subset of dimension eight operators in [318]). Dimension eight four-fermion operators involving two tops pose a particular problem, because their leading contribution to low energy LFV is likely to arise from the unknown RG running in SMEFT. Fortunately, many of these top operators are dimension six operators with an extra $H^\dagger$ and H (only the operator $\sim(\bar{e}P_R\mu)(\bar{t}P_L t)$ arises first at dimension eight), so one could hope that models dominantly generate dimension six operators. Alternatively, one could envisage to add the coefficients of dimension eight top operators to the dimension six coefficients at $\Lambda_{\rm NP}$, and evolve them with the SMEFT RGEs at dimenson six, which will include a subset of the loops. We leave calculating the anomalous dimensions for a later project.

[4]The dimension six coefficient could perhaps be suppressed by additional loops or small couplings with respect to dimension eight.

operator	$\Lambda_{\rm NP}$ (in TeV)	process
$(\bar{\ell}_e H e_\mu)(\bar{q}_d H d_d)$	55	$\mu A \to eA$
$(\bar{\ell}_e H e_\mu)(\bar{u}_u \tilde{H}^\dagger q_u)$	55	$\mu A \to eA$
$(\bar{\ell}_e H e_\mu)(\bar{q}_s H d_s)$	26	$\mu A \to eA$
$(\bar{\ell}_e H \sigma e_\mu)(\bar{q}_d H \sigma d_d)$	25	$\mu A \to eA$
$(\bar{\ell}_e H \sigma e_\mu)(\bar{q}_b H \sigma d_b)$	25	$\mu A \to eA$
$(\bar{\ell}_e H e_\mu) GG$	20	$\mu A \to eA$
$(\bar{\ell}_e H \sigma e_\mu)(\bar{\ell}_\tau H \sigma e_\tau)$	20	$\mu \to e\gamma$
$(\bar{\ell}_e H e_\mu)(\bar{\ell}_e H e_e)$	15	$\mu \to e\bar{e}e$
$(\bar{\ell}_e H e_\mu)(\bar{u}_c \tilde{H}^\dagger q_c)$	15	$\mu A \to eA$
$(\bar{\ell}_e H \sigma e_\mu)(\bar{q}_s H \sigma d_s)$	15	$\mu A \to eA$
$(\bar{\ell}_e H e_\mu)(\bar{u}_t \tilde{H}^\dagger q_t)$	10	$\mu \to e\gamma$
$(\bar{\ell}_e H e_\mu)(\bar{q}_b H d_b)$	10	$\mu A \to eA$
$(\bar{\ell}_e H e_\mu)(\bar{\ell}_\mu H e_\mu)$	8	$\mu \to e\gamma$
$(\bar{\ell}_e H e_\mu) FF$	3	$\mu A \to eA$

Table 5.5: Dimension eight operators which induce at low energy four-particle contact interactions that do not arise at dimension six. The operators are represented schematically in the first column, and the second column gives the scale $\Lambda_{\rm NP}$ up to which the process of the third column (with upcoming sensitivity) could probe coefficients $\lesssim 1$. (The estimate for $(\bar{\ell}_e H e_\mu) FF$ is from [326].) .

5.3.2 2-loop anomalous dimensions?

This section aims to identify relevant mixing that could arise from the two-loop RGEs of SMEFT, so we are looking for two-loop diagrams that would *not* be generated at second order in the one-loop RGEs.

One can see why these could be interesting, by considering the QED×QCD-invariant EFT below m_W, where at one-loop, vector operators mix among themselves, and the dipoles+scalars+tensors mix among themselves, but there are no divergent one-loop diagrams mixing vectors and non-vectors. Therefore, to all orders in the one-loop RGEs, the vectors evolve separately from the others. However, vector to dipole mixing occurs at two-loop, and is encoded in the the two-loop RGEs [344]; a few diagrams are given in figure 5.2. So we are looking for two-loop diagrams that allow operator $\mathcal{O}$ to mediate process $\mathcal{P}$, when $\mathcal{O}$ cannot mediate $\mathcal{P}$ via the one-loop RGEs.

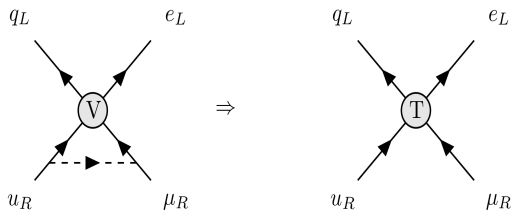

Figure 5.3: Vector mixing to the tensor via Higgs exchange.

operator	$\Lambda_{\rm NP}$ (in TeV)	process
$(H^\dagger H)(\bar{\ell}_e \sigma e_\mu)(\bar{q}_t \sigma u_t)$	100	$\mu \to e\gamma$
$(HH^\dagger)(\bar{\ell}_e e_\mu)(\bar{d}_d q_d)$	55	$\mu A \to eA$
$(HH^\dagger)(\bar{\ell}_e e_\mu)\varepsilon(\bar{q}_u u_u)$	55	$\mu A \to eA$
$(HH^\dagger)(\bar{\ell}_e e_\mu)(\bar{d}_s q_s)$	25	$\mu A \to eA$
$(HH^\dagger)(\bar{\ell}_e \gamma^\alpha \ell_\mu)(\bar{q}_u \gamma_\alpha q_u)$	22	$\mu A \to eA$
$(HH^\dagger)(\bar{\ell}_e \gamma^\alpha \ell_\mu)(\bar{u}_u \gamma_\alpha u_u)$	22	$\mu A \to eA$
$(HH^\dagger)(\bar{\ell}_e \gamma^\alpha \ell_\mu)(\bar{q}_d \gamma_\alpha q_d)$	22	$\mu A \to eA$
$(HH^\dagger)(\bar{\ell}_e \gamma^\alpha \ell_\mu)(\bar{d}_d \gamma_\alpha d_d)$	22	$\mu A \to eA$
$(HH^\dagger)\bar{\ell}_e H \sigma^{\alpha\beta} e_\mu F_{\alpha\beta}$	20	$\mu \to e\gamma$
$(HH^\dagger)(\bar{\ell}_e \gamma^\alpha \ell_\mu)(\bar{\ell}_e \gamma_\alpha \ell_e)$	18	$\mu \to e\bar{e}e$
$(HH^\dagger)(\bar{\ell}_e \gamma^\alpha \ell_\mu)(\bar{e}_e \gamma_\alpha e_e)$	18	$\mu \to e\bar{e}e$
$(HH^\dagger)(\bar{e}_e \gamma^\alpha e_\mu)(\bar{e}_e \gamma_\alpha e_e)$	18	$\mu \to e\bar{e}e$
$(HH^\dagger)(\bar{\ell}_e e_\mu)\varepsilon(\bar{q}_c u_c)$	15	$\mu A \to eA$
$(HH^\dagger)(\bar{\ell}_e e_\mu)(\bar{d}_b q_b)$	10	$\mu A \to eA$

Table 5.6: Dimension eight operators which induce low energy contact interactions that *do* arise at dimension six. In the first column the operators are represented schematically(other distributions of the Higgses, or triplet constractions, could be possible), and the second column gives the scale $\Lambda_{\rm NP}$ up to which the process of the third column (with upcoming sensitivity) could probe coefficients $\lesssim 1$. .

In SMEFT, there can be 1-loop vector to tensor mixing by exchanging an Higgs, as illustrated in Fig.5.3. Closing the quark legs gives a contribution to the dipole. For instance, considering the vector $\mathcal{O}_{\ell q}^{(1)}$ we find

$$\Delta C_D \sim e \left(\frac{\log}{16\pi^2}\right)^2 C_{\ell q}^{(1)e\mu nm} [Y_u Y_u^\dagger]_{nm} \frac{v^2}{\Lambda_{\rm NP}^2} \sim e\lambda^4 C_{\ell q}^{(1)e\mu nm} [Y_u Y_u^\dagger]_{nm} \frac{v^2}{\Lambda_{\rm NP}^2} \tag{5.19}$$

which results in a sensitivity to $C_{\ell q}^{(1)e\mu tt}$ up to $\Lambda_{\rm NP} \sim 50$ TeV. Estimates similar to eqn (5.19) hold for all vector operators which can mix to the u-type tensor.

Vector operators also can mix directly to the dipole in the 2-loop RGEs through gauge interactions, as illustrated by the diagram on the left of figure 5.2. The powercounting estimate for these diagrams

$$\Delta C_D \sim e^3 \frac{\log}{(16\pi^2)^2} C_V \frac{v^2}{\Lambda_{\rm NP}^2} \tag{5.20}$$

suggests that there is sensitivity to vector coefficients for scales below 10 TeV —which is larger than the vector→tensor→ dipole contribution for all operators not involving a top quark, see table 5.7.

There could also be two-loop mixing of the $\mathcal{O}_{LEDQ}$ scalar to the dipoles. For comparaison, at one loop the u quark scalar operator $\mathcal{O}_{LEQU}$ mixes to the tensor, which mixes to the dipole, and due to Yukawa enhancement and large anomalous dimensions, this second-order process in the one-loop RGEs is important. In the d-quark sector, there is no dimension six tensor, so no equivalent process

occurs; however the diagrams are there, and $\mathcal{O}_{LEDQ}$ can be Fierzed to the vector $-\frac{1}{2}(\bar{\ell}\gamma_\alpha q)(\bar{d}\gamma_\alpha e)$ which mixes at two-loop to the dipole [344]. The powercounting estimate is

$$\Delta C_D \sim e g^2 \lambda^5 C^{ij}_{\ell edq} [Y_d]_{ij} \frac{v^2}{\Lambda^2_{\rm NP}} \tag{5.21}$$

which suggests that $\mu \to e\gamma$ could be sensitive to coefficients $\lesssim 1$ up to the scales given in table 5.7.

operator	2loop V→ D($\Lambda_{\rm NP}$ in TeV)	V→T→D($\Lambda_{\rm NP}$ in TeV)
$\mathcal{O}^{(1)e\mu tt}_{\ell q}$	10	50
$\mathcal{O}^{e\mu ff}_{V}$	10	
$\mathcal{O}^{e\mu dd}_{\ell edq}$	5	—
$\mathcal{O}^{e\mu ss}_{\ell edq}$	20	—
$\mathcal{O}^{e\mu bb}_{\ell edq}$	100	—

Table 5.7: Operators which contribute to $\mu \to e\gamma$ via two-loop mixing in the RGEs, and in the second column, our powercounting estimate for the scale $\Lambda_{\rm NP}$ up to which coefficients $\lesssim 1$ could be probed. The third column gives the estimated sensitivity obtainable via the one-loop RGEs. $\mathcal{O}^{e\mu ff}_{V}$ schematically refers to all the dimension six vector four-fermion operators with $f \neq t$. .

These results show that the two-loop vector to dipole mixing can be relevant, and often dominates over the mixing involving a Higgs loop, which occurs at second-order in the one-loop RGEs. It would be desirable to include these two-loop anomalous dimensions. However, although they are known in QCD and QED [323,344,345], a complete computation in SMEFT is currently missing in the literature [346].

5.3.3 CKM

CKM mixing angles can appear in various places in SMEFT: in matching of the higher scale theory onto SMEFT, in the RG running of operator coefficients and of SM couplings, and in matching the SMEFT operators at m_W onto the QED×QCD-invariant low energy theory. Including CKM in matching at m_W is straightforward, but it could be conceptually simpler to set $V_{CKM} = 1$ in the RGEs for the operator coefficients. This section explores the errors that could arise from this approximation, by allowing one non-zero operator at a time at $\Lambda_{\rm NP}$, and estimating the magnitude of low-energy coefficients that it generates at one-loop $\propto [V_{\rm CKM}]_{ij}, i \neq j$. If no experiment has sensitivity to the contributions proportional to CKM mixing angles, then one can conclude that $V_{\rm CKM} = 1$ is an acceptable approximation in the RGEs.

The CKM matrix also appears in the RGEs of the renormalisable SM couplings, where it causes the eigenbases of $Y_d Y_d^\dagger$ and $Y_u Y_u^\dagger$ to rotate with scale. This is due to wavefunction corrections. Since wavefunction diagrams also decorate the operators, we assume this is a "universal" effect, automatically included by working in the rotating $Y_u Y_u^\dagger$ eigenbasis, and do not powercount the associated diagrams [5].

[5] For instance, an off-diagonal $[Y_u]^{ct} \sim 3\log/(32\pi^2) V_{cb} y_b^2 V_{tb} y_t$ is generated by a Higgs loop on the q_L line. Inside the loop mixing $\mathcal{O}_{LEQU,3} \to \mathcal{O}_D$, this could give sensitivity to $\mathcal{O}^{e\mu ct}_{LEQU,3}$, in an unrotating basis for q_L.

Recall that we work in the Y_d eigenbasis for the $\{d_R\}$, and the Y_u eigenbasis for the $\{u_R\}$ and $\{q_L\}$. So V_{CKM} only appears in Higgs loops, at vertices $\propto Y_d = V_{\rm CKM} D_d$. It therefore enters the one-loop RGEs of $\mathcal{O}_{LQ1}$,$\mathcal{O}_{LQ3}$, $\mathcal{O}_{LD}$, $\mathcal{O}_{ED}$ $\mathcal{O}_{EQ}$ and $\mathcal{O}_{LEDQ}$.

Consider first operators at $\Lambda_{\rm NP}$ with a doublet quark bilinear $(\overline{q}_i\gamma_\alpha q_j)$, where $i,j \in \{u,c,t\}$. Higgs exchange between the quark legs can dress this quark bilinear to generate

$$(\overline{q}_i\gamma_\alpha q_j) \to V^{ip}_{CKM} y_{d_p} V^{jr}_{CKM} y_{d_r} \frac{\log}{16\pi^2} (\overline{d}_p \gamma_\alpha d_r) \tag{5.22}$$

where the approximate magnitude of $V^{ip}_{CKM} y_{d_p} V^{jr}_{CKM} y_{d_r}$, for all possible flavours of the doublet and singlet lines, is given in table 5.8. If the CKM matrix is approximated as the identity, then only the diagonal components of the table would remain.

$ij\backslash pr$	bb	bs	bd	ss	sd	dd
tt	λ^5	$\lambda^{9.5}$	λ^{13}	λ^{14}	$\lambda^{17.5}$	λ^{21}
tc	λ^7	$\lambda^{7.5}$	$\lambda^{10.5}$	λ^{12}	λ^{15}	$\lambda^{18.5}$
tu	$\lambda^{8.5}$	$\lambda^{8.5}$	$\lambda^{9.5}$	λ^{13}	λ^{14}	$\lambda^{17.5}$
cc	λ^9	$\lambda^{9.5}$	$\lambda^{12.5}$	λ^{10}	λ^{13}	λ^{16}
cu	$\lambda^{10.5}$	$\lambda^{10.5}$	$\lambda^{11.5}$	λ^{11}	λ^{12}	λ^{15}
uu	λ^{12}	λ^{12}	λ^{13}	λ^{12}	λ^{13}	λ^{14}

Table 5.8: Estimates for the Yukawa and CKM suppression ($\simeq V^{ip}_{CKM} y_{d_p} V^{jr}_{CKM} y_{d_r}$) of the mixing between operators containing $(\overline{q}_i\gamma_\alpha q_j)$ into operators containing $(\overline{d}_p\gamma_\alpha d_r)$. The indices ij are given in the left column, and pr in the top line.

From the table 5.8, one sees that mixing induced by non-vanishing CKM angles is suppressed by $< \lambda^{7+2} v^2/\Lambda^2_{\rm NP}$ (where the additional λ^2 is for the $\log/16\pi^2$ loop suppression). Such contributions are clearly negligeable in the RGEs for $\tau \to \ell$ operators; to determine whether they should be included in the RGEs for $\mu \leftrightarrow e$ operators, we compare to the sensitivity of upcoming experiments. In the case of $p = r$ but $i \neq j$, the best sensitivity is from $\mu \to e$ conversion. We estimate that $\mu A \to eA$ could be sensitive to the mixing from $(\overline{q}_t\gamma_\alpha q_c) \to (\overline{b}\gamma_\alpha P_R b)$ for an experimental reach $\text{BR}(\mu A \to eA) \lesssim 10^{-16} \frac{v^4}{\Lambda^4_{\rm NP}}$, and to the $cu \to ss, dd$ mixing for $\text{BR}(\mu A \to eA) \lesssim 10^{-20} \frac{v^4}{\Lambda^4_{\rm NP}}$. This suggests that the RGE-mixing of operators involving $(\overline{q}_i\gamma_\alpha q_j)$, into operators involving $(\overline{d}_p\gamma_\alpha d_p)$, for $i \neq j$ and $p = q$, is negligeable in the forseeable future. In the converse case, of RGE-mixing of flavour-diagonal operators $(\overline{q}_i\gamma_\alpha q_i)$, into quark flavour non-diagonal operators $(\overline{d}_p\gamma_\alpha d_r)$, table 5.8 indicates that the least suppressed mixings are $tt, cc \to bs \propto \lambda^{9.5} \frac{v^2}{\Lambda^2_{\rm NP}}$, and $cc, uu \to sd \propto \lambda^{13} \frac{v^2}{\Lambda^2_{\rm NP}}$, which is beyond the sensitivity of the meson decay searches listed in table 5.3.

The CKM angles can also enter in the mixing of the singlet quark current $(\overline{d}_p\gamma_\alpha d_p)$ into doublets $(\overline{q}_i\gamma_\alpha q_j)$. Similarly to the doublet to singlet mixing discussed above, the effects of CKM are beyond upcoming experimental sensitivities. A novel feature in this case is that approximating the CKM angles to vanish can generate flavour change when there is none. For example, the s_R leg of an operator could transform under RG running into a left-handed doublet quark (due to Higgs exchange), which in the SM would be in the s_L direction. But in our approximation where $Y_d Y_d^\dagger$ is diagonal in the $Y_u Y_u^\dagger$ eigenbasis, it is in the c_L direction, so matches at m_W onto $\sum_p V^{cp}_{CKM} d_{Lp}$.

Finally, there are diagrams with one Higgs vertex on the quark line and one on a lepton line, which *eg* mix vector and scalar operators. The mixing from scalar into vector operators, such as $\mathcal{O}_{LEDQ} \to \{\mathcal{O}_{LQ}^{(1)}, \mathcal{O}_{EQ}\}$ can be neglected because the lepton Yukawas are smaller than that of the b, so any quark-flavour-changing contribution is more suppressed than the $(\overline{d}_p\gamma_\alpha d_p) \leftrightarrow (\overline{q}_i\gamma_\alpha q_j)$ mixing discussed above. It is also the case that quark-flavour-changing mixing from vectors to scalars is below the sensitivity of upcoming experiments, despite that the experimental sensitivity to scalar operators can be better than to vectors (see table 5.3). In the case of $\mu \leftrightarrow e$ searches, this is because the mixing is suppressed by $y_\mu \sim \lambda^5$, and for $\tau \leftrightarrow \ell$ searches, the experiments are less sensitive.

So we conclude that CKM angles can be neglected in the SMEFT RGEs for LFV operators, provided that one runs in the $Y_u Y_u^\dagger$ eigenbasis for the $\{q_L\}$, and that CKM mixing is retained in matching at m_W.

5.3.4 LFV Yukawa couplings

In the SM, the Yukawa matrix of the charged leptons is the only basis-choosing interaction in the leptonic sector — the gauge interactions are "universal", that is, proportional to the identity matrix in generation space, so the eigenvectors do not choose directions. In the real world (not described by the SM), the neutrino mass matrix provides another eigenbasis, but the magnitude of neutrino masses is so small that their direct GIM-suppressed contribution to LFV is irrelevant (instead, they provide motivation to search for LFV).

LFV operators that are added to the Lagrangian below the weak scale are inevitably written in the mass eigenstate basis of the charged leptons. Above the weak scale in SMEFT, there are two possibilities: the mass eigenstate basis, or the Yukawa eigenstate basis — which may be different in the presence of the operator $\mathcal{O}_{eH}$. The physics, of course, cannot depend on a basis choice, but the calculation may be more intuitive and simple in somes bases than in others. So which is the best choice?

Suppose one thinks top-down; then at $\Lambda_{\rm NP}$, the New Physics model is matched to the SM +operators. The obvious basis in this case for SMEFT is the D_e-basis where the lepton Yukawa matrix is diagonal : $Y_e = D_e = \text{diag}\{y_e, y_\mu, y_\tau\}$. This choice is motivated by LFV being a NP effect, and ensures that the SMEFT RGEs, which describe SM dynamics, cannot change the flavours of lepton legs.

However, when the Higgs gets a vev in the presence of the $\mathcal{O}_{eH}$ operator, the D_e basis may no longer be the mass eigenstate basis, due to additional off-diagonal contributions of $\mathcal{O}_{eH}$ to the mass matrix. So a basis rotation during the matching at m_W would be required, from the D_e basis to the mass eigenstate basis in which the restrictive low-energy constraints are expressed. Current constraints/sensitivities on the off-diagonal elements of $\mathcal{O}_{eH}$ imply that the angles of this rotation are small: estimating $\theta_{ij} \sim C_{eH}^{ij} v^3/(\Lambda_{\rm NP}^2 \max\{m_i, m_j\})$ for $i \neq j$ gives

$$\theta_{\ell\tau},\ \theta_{\tau\ell} \lesssim \lambda \quad , \quad \theta_{e\mu},\ \theta_{\mu e} \lesssim \lambda^4 \tag{5.23}$$

where $\ell \in \{e, \mu\}$.

If the New Physics scale is sufficiently high that only dimension six operators are relevant, one might hope to neglect this rotation in matching, because the angles are $\propto Cv^2/\Lambda_{\rm NP}^2$, so any effect on a NP operator would be $\mathcal{O}(1/\Lambda_{\rm NP}^4)$. (Below m_W, there are also contact interactions induced by

the W, Z, h, which could becomes flavour-changing under a basis rotation. However, the W and Z interactions are "universal", so unconcerned by basis rotations, and the higgs-mediated operators are suppressed by SM Yukawas, so the dimension six flavour-changing operators induced by the rotation are unobservable.) However, as previously discussed, LFV data can have sensitivity to operators suppressed by $\mathcal{O}(1/\Lambda_{\rm NP}^4)$, and the mixing angles of eqn (5.23) are also enhanced by inverse Yukawas. The power-counting rules suggest that flavour-diagonal coefficients at $\Lambda_{\rm NP} \sim 4$ TeV could be rotated into $\tau \leftrightarrow \ell$ operators suppressed by λ^5, and into $\mu \leftrightarrow e$ suppressed by λ^8. This is within current experimental sensitivities.

We advocate *not* making the transformation from the mass to Yukawa eigenstate basis at m_W. This is because the rotation is unknown, and the angles are insufficiently suppressed (see Eq. 5.23). Instead, we remain in the mass eigenstate basis above the weak scale; this is consistent with our bottom-up perspective, because it is the basis where the constraints apply. The lepton Yukawa matrix can be off-diagonal in this basis(see eqn 5.9), but the off-diagonals $\sim \theta_{ij} y_j$ are much smaller than the θ_{ij}s of eqn (5.23) because they are suppressed also by small lepton Yukawas. The power-counting suggests that they can be neglected in the RGEs, for instance

$$[Y_e]_{\mu e} \frac{\log}{16\pi^2} \frac{v^2}{\Lambda_{\rm NP}^2} \lesssim \lambda^{15} \quad .$$

So in practise, we work in the mass eigenstate basis at all scales, but treat the lepton Yukawa matrix as diagonal in the RGEs of SMEFT. The inconvenience of this choice is that in matching a model onto the operators, one must identify the mass eigenstate basis in the model, and obtain operator coefficients in that basis.

5.3.5 LFV with τs

This section briefly discusses the ingredients required for a "leading order" SMEFT study of LFV involving τs.

For the majority of τ LFV processes listed in Table 5.3 there is sensitivity to Wilson coefficients that are $\gtrsim \lambda^5$. Since a loop costs a factor λ^2, loop effects in the τ sector could be relevant for $(v^2/\Lambda_{\rm NP}^2) \geq \lambda^3$, but this implies a New Physics scale within the LHC reach.

In the case of the more sensitive $\tau \to e(\mu)\gamma$ searches, the corresponding diagrams can be power counted as for $\mu \to e\gamma$, replacing the muon leg with a tau leg. Since the constraints concern dipole coefficients defined with a built-in yukawa of the heavier lepton, we encounter two possibilities in the diagrams:

- either one Higgs leg is attached to the decaying lepton line and the power counting estimate is the same,
- or no Higgs-heavy lepton vertex is present and the diagrams are suppressed by a factor $y_\mu/y_\tau = 2\lambda^2$ with respect to the corresponding $\mu \to e\gamma$ one.

In both cases, given the lesser sensitivity in the τ sector, we can conclude that any approximation that we justify through power counting for μ-s is also valid for τ LFV processes.

As a result, two-loop anomalous dimensions should be irrelevant in $\tau \leftrightarrow \ell$ processes, due to the estimated suppression $\sim \lambda^5$ of two-loop diagrams. This should remain true even in the case of $\tau \to e(\mu)\gamma$.

Furthermore, the requirement of eq. (5.18) on 8-dimensional operator coefficients for $\Lambda_{\rm NP} \gtrsim 4$ TeV

$$^{(8)}C \lesssim \lambda^8$$

is sufficient to argue that any τ LFV observable is not sensitive to dimension eight operators.

5.4 Summary

Effective Field Theory can be envisaged from a bottom-up or top-down perspective. In bottom-up EFT for lepton flavour change, the aim is to map experimental constraints onto the correct sum of operator coefficients at the New Physics scale $\Lambda_{\rm NP}$, in order to identify the area in coefficient space where BSM models must sit. From a top-down perspective, one can map a LFV model onto operator coefficients at $\Lambda_{\rm NP}$, calculate observables using EFT, and this should correctly reproduce model predictions to within a calculable uncertainty. In both perspectives, the EFT calculation must include correctly every operator coefficient that could contribute to an observable, irrespective of its dimension or of the order in the loop or coupling expansions.

To ensure that we use SMEFT correctly for describing LFV, we introduced a power-counting scheme, that allows to organise all the SMEFT perturbative expansions — in loops, couplings, mixing angles and the ratio of the weak scale to the New Physics $v/\Lambda_{\rm NP}$ —in terms of a small "Cabibbo-Wolfenstein-like" parameter $\lambda \approx 0.2$. This power-counting scheme is described in section 5.2.2, and summarised in table 5.2. The future reach of various experiments can be expressed in powers of λ (see table 5.3) — so for instance, the upcoming MEGII experiment searching for $\mu \to e\gamma$ could probe dipole coefficients up to $\mathcal{O}(\lambda^{12})$. Then one can draw diagrams, arising at various orders in the different perturbative expansions, and do two things; first, compare different contributions of an operator to an observable, to identify the leading one, (see eg section 5.2.3 and 5.3.2). And secondly, one can determine which operators can affect which observables by comparing the power-counting estimates to the future experimental sensitivity. Some examples are given in Section 5.2.3.

For LFV operators, the SMEFT expansion in operator dimension can be written as an expansion in $v^2/\Lambda^2_{\rm NP}$, where the New Physics scale $\Lambda_{\rm NP}$ plays two roles in our manuscript. On one hand, it is the unknown mass of the lightest lepton flavour changing new particle (see the Lagrangian of eqn (5.1)), which we take "beyond the reach of the LHC": $\Lambda_{\rm NP} \gtrsim 4$ TeV (so $v^2/\Lambda^2_{\rm NP} \lesssim \mathcal{O}(\lambda^4)$ in the powercounting scheme). However, since $\Lambda_{\rm NP}$ is unknown, we simultaneously count the order of an operators contribution by the scale it could probe with a coefficient of $\mathcal{O}(1/\Lambda^{2n}_{\rm NP})$.

In the SMEFT, there are already many operators at dimension six, and their RGEs are only known at one-loop. So in section 5.3, we use the powercounting scheme to explore whether dimension six operators and one-loop RGEs are sufficient to describe LFV at the sensitivity of experiments under construction. Section 5.3.2 suggests that some two-loop anomalous dimensions are required for $\mu \leftrightarrow e$ flavour change, when $\Lambda_{\rm NP} \lesssim 20$ TeV. The calculation of these anomalous dimensions is in progress [346].

Section 5.3.1 finds that upcoming $\mu \leftrightarrow e$ data can be sensitive to dimension eight SMEFT operators, about four dozen of them for $\Lambda_{\rm NP} \gtrsim 4$ TeV, but none at scales $\Lambda_{\rm NP} \gtrsim 100$ TeV. The relevant dimension eight operators match onto three-or four-point interactions below the weak scale, and can be divided into two sets: those which are the lowest-dimension SMEFT operator inducing a

given contact interaction below m_W, and a second set that induces low-energy contact interactions already present at dimension six. The scale $\Lambda_{\rm NP}$ up to which the operators can be relevant is given in tables 5.5 and 5.6. These dimension eight operators are listed in Appendix C, and are included in the matching onto operators below m_W in Appendix C.2.

The power counting scheme can also be used to simplify and streamline calculations with the existing SMEFT operators and RGEs, for instance by neglecting flavour-changing SM interactions. We perform two such exercises; section 5.3.3 checks that CKM mixing can be neglected in the RGEs for LFV operators, provided that it is included in matching, and that the SMEFT RGEs run in the $Y_u Y_u^\dagger$ eigenbasis for the $\{q_L\}$. Section 5.3.4 explores the case where operators of the form $C^{ij}(H^\dagger H)^n \bar{\ell}_i H e_j$, with $i \neq j$, are allowed to contribute to the charged lepton mass matrix. This implies that in the charged lepton mass eigenstate basis (where all experimental constraints are given), the charged lepton Yukawa Y_e has unknown off-diagonal elements. The power-counting suggests that if these flavour-changing Yukawas are below current experimental sensitivities, they can be neglected in the SMEFT RGEs.

In this chapter, we estimated lower bounds on the scale Λ_{NP}, such that the predictions of lepton flavour changing New Physics models from beyond Λ_{NP} can be obtained with the dimension six operators of SMEFT and their one-loop RGEs. These results could be used to motivate, or justify, SMEFT studies of LFV.

Chapter 6

The sensitivity of $\mu \to e$ to τ flavour change

6.1 Introduction

Process	Current bound on BR	Future Sensitivity
$\mu \to e\gamma$	$< 4.2 \times 10^{-13}$ [223]	10^{-14} [224]
$\mu \to \bar{e}ee$	$< 1.0 \times 10^{-12}$ [239]	10^{-16} [231]
$\mu A \to eA$	$< 7 \times 10^{-13}$ [339]	10^{-16} [275,340]
$\tau \to l\gamma$	$< 3.3 \times 10^{-8}$ [243]	$3 \times 10^{-9}(e), 10^{-9}(\mu)$
$\tau \to e\bar{e}e$	$< 2.7 \times 10^{-8}$ [244]	5×10^{-9} [341]
$\tau \to \mu\bar{\mu}\mu$	$< 2.1 \times 10^{-8}$ [244]	4×10^{-9} [341]
$\tau \to \mu\bar{e}e, e\bar{\mu}\mu$	$< 1.8, 2.7 \times 10^{-8}$ [244]	$3,5 \times 10^{-9}$ [341]
...	...	...
$\tau \to \ell\pi^0$	$< 8.0 \times 10^{-8}$ [245]	4×10^{-9} [341]
$\tau \to \ell\eta$	$< 6.5 \times 10^{-8}$ [245]	7×10^{-9} [341]
$\tau \to \ell\rho$	$< 1.2 \times 10^{-8}$ [247]	10^{-9} [341]
$h \to e^{\pm}\mu^{\mp}$	$< 6.1 \times 10^{-5}$ [190]	2.1×10^{-5} [347]
$h \to e^{\pm}\tau^{\mp}$	$< 2.2 \times 10^{-3}$ [191]	2.4×10^{-4} [347]
$h \to \tau^{\pm}\mu^{\mp}$	$< 1.5 \times 10^{-3}$ [191]	2.3×10^{-4} [347]

Table 6.1: Some $\mu \leftrightarrow e$ and $\tau \leftrightarrow l$ processes ($l \in \{e, \mu\}$), with the current experimental bound on the branching ratios. The last column lists the future sensitivities used in our projections, which correspond to the expected reach of upcoming or planned experiments (except for $\mu \to e\gamma$, where the MEGII experiment at PSI, which starts taking data in 2022, aims to reach $BR \sim 6 \times 10^{-14}$). Additional $\tau \leftrightarrow l$ processes involving b quarks are listed in table D.1.

As discussed in Chapter 3, the current limits on $\mu \to e$ flavour change are more retrictive than those on $\tau \to l$, where $l \in \{e, \mu\}$, due to the possibility of making intense muon beams. A significant gain in sensitivity is expected at upcoming $\mu \to e$ experiments (see table 6.1), sometimes allowing:

$$Br(\mu \to e \dots) \lesssim Br(\tau \to e \dots) Br(\tau \to \mu \dots) \tag{6.1}$$

Improving the sensitivity to $\tau \leftrightarrow l$ processes by producing the τ in the final state has been explored at the future Electron Ion Collider [348] and electron-positron machines [349]. Instead, we focus

on the relation among the three $\Delta F = 1$ lepton flavour changes:

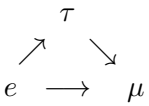

If two lepton flavours are unconserved, then no symmetry forbids the third to happen, so it could be generated from the first two at some order in the perturbative expansion. Eq. (6.1) tells us that $\mu \to e$ searches are potentially sensitive to the product of $\mu \to \tau$ and $\tau \to e$ interactions respecting τ LFV constraints. So the aim of this chapter, is to explore what can be learned about $\tau \leftrightarrow l$ interactions, using $\mu \to e$ observables. We are interested in the model-independent aspects of this question, so we assume that the NP responsable for LFV is heavy, and use EFTs to parametrise low energy LFV.

We will suppose a New Physics scale $\Lambda_{\rm NP} \geq 4$ TeV ("beyond the LHC"), describe $\tau \to l$ interactions via dimension six operators, and calculate the log-enhanced contributions to dimension eight $\mu \to e$ operator coefficients, which appear in their Renormalization Group evolution between $\Lambda_{\rm NP}$ and m_W. These contributions arise from the insertion in loop diagrams of both a $\mu \to \tau$ and a $\tau \to e$ operator, and can be reliably computed in EFT — although they may not be the dominant contributions to $\mu \to e$ processes coming from $\tau \leftrightarrow l$ interactions (see section 6.2.1). We will find that upcoming $\mu \leftrightarrow e$ searches could be sensitive to $\tau \leftrightarrow \ell$ interactions beyond the reach of upcoming τ experiments.

The chapter is organized as follows. In Section 6.2 we introduce the formalism for the EFT calculation (notation and operators), and we make several estimates to focus the calculations on contributions within future $\mu \to e$ experimental sensitivity. Our results are illustrated in Section 6.3, where the Renormalization Group Equations (RGEs) for dimension eight operators are reviewed, we discuss examples of anomalous dimensions calculated from double insertions of dimension six operators, and give the weak scale matching of $\mu \to \tau \times \tau \to e$ onto low energy $\mu \to e$ operators. The complete results for (dimension 6)$^2 \to$ dimension 8 mixing can be found in appendix D.2. In Section 6.4 we discuss some phenomenological implications : $\mu \to e$ observables are sensitive to products of $\tau \leftrightarrow l$ operator coefficients and we compare this sensitivity to the limits coming from searches for $\tau \leftrightarrow l$ processes.

6.2 EFT, operators and notation

In this section, we start by comparing our calculation to the expectations of a few models in subsection 6.2.1, then review the EFT framework in sections 6.2.2 to 6.2.4. Finally in subsection 6.2.5, we estimate which $(\mu \to \tau) \times (\tau \to e)$ loop diagrams could be accessible to future $\mu \to e$ experiments, making them interesting to calculate.

6.2.1 A few models

In this subsection, we discuss two models—one being the SM— in order to illustrate the relationships between $\tau \leftrightarrow l$ and $\mu \leftrightarrow e$ observables, and to compare our EFT calculation with the expectations of UV complete models.

(a) (b)

Figure 6.1: The GIM mechanism in $K - \bar{K}$ mixing: in the SM box calculation of figure (a), the mass-independent dimension six contribution cancels in the flavour sum because of CKM unitarity. Then at $\mathcal{O}(G_F^2)$, the top contribution is not dominant due to small mixing with the down quark, whereas the dimension eight term $\sim G_F^2 m_c^2$ is relevant. It can be calculated in the low-energy EFT (Fermi theory) as the loop contribution with two dimension six operators inserted, as illustrated in (b)

First, consider a model where two heavy bosons, $M \gg m_W$, are added to the SM, with flavour diagonal, and respectively $\tau \leftrightarrow \mu$ and $\tau \leftrightarrow e$ renormalizable interactions. A first source of $\mu \leftrightarrow e$ flavour change could be additional renormalizable $\mu \leftrightarrow e$ interactions of the heavy bosons — not forbidden by symmetry — but these do not interest us, because their magnitude depends on the model and is independent of the $\tau \leftrightarrow l$ interactions. We are interested in $\mu \to e$ processes which occur due to diagrams involving both the $\mu \to \tau$ and $\tau \to e$ interactions. The part of these amplitudes which is reproduced by our EFT calculation, can be identified by matching the model onto EFT at the heavy boson mass scale M. The model generates $\tau \leftrightarrow l$ four-fermion amplitudes at tree level, and could induce $\mu \leftrightarrow e$ amplitudes at one loop. These all are expected to match onto dimension six operators in the EFT, with coefficients of $\mathcal{O}(\lambda_{\tau l}/M^2)$ and $\mathcal{O}(\frac{\lambda^*_{\mu\tau}\lambda_{\tau e}}{16\pi^2 M^2})$. Our EFT calculation cannot reproduce these model dependent coefficients. Instead, the EFT below the heavy boson scale allows to combine the dimension six $\tau \leftrightarrow e$ and $\tau \leftrightarrow \mu$ operators into a dimension eight $\mu \leftrightarrow e$ operator, giving a contribution to the $\mu \leftrightarrow e$ amplitude $\lesssim \mathcal{O}(\frac{\lambda^*_{\mu\tau}\lambda_{\tau e} v^2}{16\pi^2 M^4})$ (v is the vacuum expectation value of the SM Higgs). By power-counting, this is subdominant compared to the model-dependent matching contribution discussed above. So this model illustrates that $\tau \leftrightarrow e$ and $\tau \leftrightarrow \mu$ interactions could generically combine into larger $\mu \leftrightarrow e$ rates than the EFT allows to compute.

As a second example, consider $K - \bar{K}$ mixing in the SM, where the dominant contribution is computable in the EFT (Fermi theory). The box diagram in the full SM is illustrated in figure 6.1 (a); evaluated with only massless u quarks in the loop, it gives an amplitude $\propto (V_{us}^* V_{ud})^2/(16\pi^2 m_W^2)$, where V is the CKM matrix. This would match at m_W onto a dimension six $\Delta F = 2$ operator in the low-energy theory Fermi theory. However, due to CKM unitarity, this $\mathcal{O}(\frac{1}{16\pi^2 m_W^2})$ amplitude vanishes when summing over all up-type quark flavours and neglecting their masses. Instead, the amplitude in the full SM has a GIM dependence on the quark masses $\propto (V_{cs}^* V_{cd})^2 m_c^2/16\pi^2 m_W^4 + (V_{ts}^* V_{td})^2 m_t^2/16\pi^2 m_W^4$. In matching this to the low-energy EFT, the $m_t^2/16\pi^2 m_W^4$ piece would match onto a dimension six operator, but is negligeable due to the small mixing between the third and first generation. And the log-enhanced part of the amplitude $\propto m_c^2$ is reproduced in the EFT by calculating the diagram with two insertions of dimension six operators,

illustrated in Figure 6.1 (b). So in the Standard Model, our calculation can sometimes reproduce the observed flavour changing rates.

6.2.2 EFT for LFV

We parametrise the lepton flavour changing interaction in the EFT (see section 4.3.2). Above the weak scale, we use the Lagrangian of the SMEFT, and since we are interested in LFV operators of dimension 6 or 8, we write

$$\mathcal{L}_{\text{SMEFT}} = \mathcal{L}_{\text{SM}} + \left(\sum_{A,\zeta} \frac{C_A^{[6]\zeta} \mathcal{O}_A^{[6]\zeta}}{v^2} + \sum_{B,\xi} \frac{C_B^{[8]\xi} \mathcal{O}_B^{[8]\xi}}{v^4} + \text{h.c} \right) \tag{6.2}$$

where $v = 174$ GeV, the operator subscripts indicate the gauge structure and particle content, and the superscripts contain the operator dimension in brackets [suppressed when unneccessary], additional information about the operator structure in parentheses (see section 6.2.3 for examples), and the flavour indices. The LFV operators of interest here are listed in section 6.2.3. In the flavour sums of Eq. (6.2), each index runs over all three generations. The doublet and singlet lepton generations are the charged lepton mass eigenstates $\{e, \mu, \tau\}$, the singlet quarks are also labelled by their flavour, and the quark doublets are in the u-type mass basis, with generation indices that run $1 \to 3$.

The SM Lagrangian is in the notation of Chapter 2. At all scales, the doublet and singlet leptons are in the low energy mass eigenstate basis, so the lepton Yukawa matrix $[y_e]$ can have off-diagonal entries, in the presence of the operator $\mathcal{O}_{eH}$ (see equations 6.17 and 6.87). We follow the results of Chapter 5 in choosing this basis, because it defines lepton flavour in the presence of LFV, so it simplifies our calculations(as mentioned at the end of section 6.2.4). The Yukawa matrix eigenvalue of fermion f is written y_f.

The dimension six operators in Eq. (6.2) are in the "on-shell" basis of [304] as pruned in [305], where "on-shell" means that the equations of motion were used to reduce the basis. Complete bases of on-shell dimension eight operators have appeared recently [308, 309], and our dimension eight operators are in these lists. However in reality, we are only interested in the subset of dimension eight $\mu \leftrightarrow e$ operators to which experiments could be sensitive, which was given in Chapter 5. Finally, some operators in Eq. (6.2) are hermitian in flavour space (*ie* $[\mathcal{O}_A^{\bar{i}j\bar{k}l}]^\dagger = \mathcal{O}_A^{\bar{j}i\bar{l}k}$); we include these operators multiplied by an extra 1/2, as the Hermitian conjugate is included in (6.2) and summing over flavour indices would otherwise lead to double counting with respect to the conventions of [315].

We assume LFV heavy particles are beyond the reach of the LHC in the next decade, because we are interested in combining observables from upcoming experiments at low-energy. Concretely, this means that the operator coefficients, or Wilson coefficients (WCs), satisfy

$$C_A^{[n]\zeta} \leq \left(\frac{v}{\Lambda_{\text{NP}}} \right)^{n-4} \quad , \quad \Lambda_{\text{NP}} = 4 \text{ TeV} \quad , (v = 174 \text{ GeV})$$

and that we calculate Renormalisation Group running of LFV operators in SMEFT from $\Lambda_{\text{NP}} \to m_W$. Should new particles with LFV interactions and masses $m_W < M_{NP} < 4$ TeV induce larger coefficients, our results would still apply, but might be incomplete because additional operators and diagrams could contribute.

The WCs $\{C_A^{[n]\zeta}\}$ function as coupling constants for LFV interactions. Their numerical value can be obtained by matching the EFT onto a model, for instance by equating the Greens functions of the model and the EFT at the new particle mass scale $\sim \Lambda_{\rm NP}$. The Renormalisation the Group Equations (RGEs) govern the scale dependence of the WCs below $\Lambda_{\rm NP}$. The solution of these equations resums the logarithms that are generated by the light particle, which propagate as dynamical particles in the EFT. So in SMEFT, the one-loop RGEs of dimension six SMEFT operators arise from decorating a dimension six operator with a loop involving renormalisable interactions [315–317], and from loops involving two dimension 5 operators [314]. The mixing of a product of dimension five and six operators into dimension seven has also been calculated in SMEFT [350], as have some anomalous dimensions for some operators of dimension eight [318–320].

Upon reaching a particle mass scale, the high scale EFT can be matched onto another EFT, where the now-heavy particles are removed. For instance, in crossing the electroweak scale, SMEFT Greens functions are calculated in the broken SM, with the Higgs doublet written

$$H = \begin{pmatrix} G^+ \\ v + \frac{1}{\sqrt{2}}(h + iG^0) \end{pmatrix} \tag{6.3}$$

where the Gs are the Goldstones and h is the SM Higgs boson. These Greens functions are then matched to those of a QED and QCD invariant EFT (we refer to it as low energy EFT) in which the non-renormalisable operators are built out of SM fields lighter than the W boson [311].

The running and matching continues from the weak scale down to the experimental scale, where rates can be calculated in terms of the WCs and matrix elements of the operators. For three or four-legged $\mu \to e$ processes which are otherwise flavour diagonal (*ie* $\mu \to e\gamma$ and $\mu \to e\gamma\gamma$, but not including $K \to \mu^\pm e^\mp$), the "leading" evolution between the experimental scale and the weak scale has been obtained [323]. This includes the one-loop RGEs for dimension five and six operators, and some large two-loop anomalous dimensions where the one loop mixing vanishes [344]. Several branching ratio calculations in the low energy EFT are given in the $\mu \to e$ review [142], and $\mu A \to eA$ conversion rates can be calculated from [351]. These results can be combined to calculate the current and upcoming sensitivity of $\mu \leftrightarrow e$ experiments to WCs at the weak scale, and also extrapolated to give the sensitivities to the $\tau \leftrightarrow l$ WCs considered in this manuscript [352].

The aim of this chapter is to calculate the contributions to $\mu \to e$ observables that arise from combining $\tau \to e$ and $\mu \to \tau$ operators. This could occur in SMEFT running, in matching at the weak scale, and in running below the weak scale. In SMEFT, loop diagrams containing pairs of dimension six operators renormalize the Wilson coefficients of dimension eight operators, such that the RGEs for the latter take the schematic form [333]

$$(16\pi^2)\frac{d\vec{C}_A^{[8]}}{d\log M} = \vec{C}_B^{[8]}\gamma_{BA} + \vec{C}_X^{[6]}\hat{\gamma}_{XY,A}\vec{C}_Y^{[6]}, \tag{6.4}$$

having aligned the operator coefficients in the row vectors $\vec{C}^{[8]}$, $\vec{C}^{[6]}$, and where γ is the anomalous dimension matrix of dimension eight coefficients while $\hat{\gamma}$ mixes pairs of dimension six into dimension eight. The RGEs of dimension eight operators are currently unknown and only partial calculations have been performed [318, 320]. This work fits into this ongoing effort. We calculate at leading-log, i.e we compute the one-loop RGEs and match at tree-level onto the low energy EFT. This

consistency between the running and matching orders frees the calculation from scheme-dependent contributions.

We define the anomalous dimensions with a $1/(16\pi^2)$ prefactor, while we unconventionally do not factor out SM couplings. Two insertion of dimension six operators renormalize the dimension eight coefficients as

$$\Delta\vec{C}_A^{[8]} = \vec{C}_X^{[6]}\hat{Z}_{XY,A}\vec{C}_Y^{[6]}, \tag{6.5}$$

where $\hat{Z}$ is the divergent renormalization factor and may contain renormalizable couplings. In dimensional regularization, the independence of bare Wilson coefficients from the arbitrary renormalization scale gives the anomalous dimension matrix of Eq. (6.4), which at one-loop and with our conventions takes the following form

$$\hat{\gamma} \propto 16\pi^2\varepsilon\hat{Z}. \tag{6.6}$$

Note that $\hat{Z} \propto 1/\varepsilon$ and the product above is finite as expected. A more detailed derivation of $\hat{\gamma}$ can be found in section 6.3.1.

Pairs of $\tau \leftrightarrow l$ operators also contribute to $\mu \to e$ amplitudes in matching SMEFT onto the low energy EFT at m_W. In "integrating out" the heavy bosons h, Z and replacing the Higgs doublet with its vacuum expectation value, it is possible to draw diagrams built out of $\tau \leftrightarrow l$ operators that match onto three or four-legged $\mu \to e$ operators in the low energy EFT. We calculate these matching conditions, which are meant to complete the tree-level $\mathcal{O}\big(v^4/\Lambda_{\rm NP}^4\big)$ matching performed in the Appendix of Chapter 5.

Finally, combining two $\tau \leftrightarrow l$ operators contributes to the RGEs of Wilson coefficients in the EFT below m_W. We neglect these running contributions because they carry a suppression factor with respect to dimension six anomalous dimensions which is $\lesssim m_b^2/\Lambda_{\rm NP}^2$, given that the bottom quark is the heaviest dynamical particle in the EFT. Such suppression is absent in SMEFT, where the top quark, the Higgs and gauge bosons are present, allowing Higgs legs to be attached with order one couplings to heavier particles running in loops. SMEFT has also the advantage of having two-fermion "penguin" operators that are efficiently generated in mixing and which match onto vector operators in the low energy EFT. For the above reasons we focus on SMEFT RGEs and matching, while we neglect the running below m_W.

Equation (6.4) has a straightforward solution if the anomalous dimension matrices are constant, which occurs when the running of all-but-one of the SM renormalisable couplings can be neglected. We take all SM couplings constant between $m_W \to \Lambda_{\rm NP} = 4$ TeV, in solving Eq. (6.4). It is augmented by the RGEs of dimension six coefficients:

$$\frac{d\vec{C}^{[6]}}{dt} = -\vec{C}^{[6]}\tilde{\gamma} \tag{6.7}$$

where $t = \log(\Lambda_{\rm NP}/M)/(16\pi^2)$ and M is the sliding renormalization scale. The solution is

$$\vec{C}^{[6]}(t) = \vec{C}^{[6]}(0)\exp(-\tilde{\gamma}t) \tag{6.8}$$

$$\begin{aligned}\vec{C}^{[8]}(t) = \Bigg[\vec{C}^{[8]}(0) - \int_0^t d\tau\vec{C}^{[6]}(0)\exp(-\tilde{\gamma}\tau)\hat{\gamma}\times \\ \times\exp\big(-\tilde{\gamma}^T\tau\big)\vec{C}^{[6]}(0)\exp(\gamma\tau)\Bigg]\exp(-\gamma t).\end{aligned} \tag{6.9}$$

Expanding the exponential at leading log, the dimension eight coefficients at the electroweak scale take the following form

$$\vec{C}^{[8]}(m_W) = \vec{C}^{[8]}(\Lambda_{\rm NP})\Big(1 - \frac{\gamma}{16\pi^2}\log\Big(\frac{\Lambda_{\rm NP}}{m_W}\Big)\Big)$$
$$-\vec{C}^{[6]}(\Lambda_{\rm NP})\frac{\hat{\gamma}}{16\pi^2}\vec{C}^{[6]}(\Lambda_{\rm NP})\log\Big(\frac{\Lambda_{\rm NP}}{m_W}\Big) + \dots \ . \tag{6.10}$$

6.2.3 Operators

This subsection lists the operators included in the SMEFT Lagrangian of Eq. (6.2). They are classified into subgroups ($D_6, 4f_6 \dots$), in order to facilitate the estimates of section 6.2.5.

The SMEFT dimension six operators that are $\tau \to e$ or $\mu \to \tau$ flavour changing are the following, where the indices ij take the values $e\tau$ or $\tau\mu$ (except for the $4l_6$ operators).

- Dipole operators $\equiv D_6$:

$$\mathcal{O}^{ij}_{eB} = y_\tau(\bar{\ell}_i H\sigma^{\alpha\beta}e_j)B_{\alpha\beta}$$
$$\mathcal{O}^{ij}_{eW} = y_\tau(\bar{\ell}_i\tau^a H\sigma^{\alpha\beta}e_j)W^a_{\alpha\beta} \tag{6.11}$$

  The Hermitian conjugates with exchanged $i \leftrightarrow j$ match onto the dipole operator with opposite chirality.

- Penguin operators $\equiv P_6$:

$$\mathcal{O}^{ij}_{He} = i(\bar{e}_i\gamma^\alpha e_j)(H^\dagger \overset{\leftrightarrow}{D}_\alpha H) \tag{6.12}$$
$$\mathcal{O}^{ij}_{H\ell(1)} = i(\bar{\ell}_i\gamma^\alpha \ell_j)(H^\dagger \overset{\leftrightarrow}{D}_\alpha H) \tag{6.13}$$
$$\mathcal{O}^{ij}_{H\ell(3)} = i(\bar{\ell}_i\tau^a\gamma^\alpha \ell_j)(H^\dagger \overset{\leftrightarrow}{D}^a_\alpha H) \tag{6.14}$$

  where we have defined

$$iH^\dagger \overset{\leftrightarrow}{D}_\mu H \equiv iH^\dagger(D_\mu H) - i(D_\mu H^\dagger)H \tag{6.15}$$
$$iH^\dagger \overset{\leftrightarrow}{D}^a_\mu H \equiv iH^\dagger\tau^a(D_\mu H) - i(D_\mu H^\dagger)\tau^a H. \tag{6.16}$$

- Yukawa operators $\equiv Y_6$:

$$\mathcal{O}^{ij}_{eH} = (\bar{\ell}_i H e_j)(H^\dagger H) \tag{6.17}$$

  and their Hermitian conjugates.

- Four lepton operators $\equiv 4l_6$:

$$\mathcal{O}^{ijkl}_{ee} = (\bar{e}_i\gamma^\alpha e_j)(\bar{e}_k\gamma_\alpha e_l) \tag{6.18}$$
$$\mathcal{O}^{ijkl}_{\ell e} = (\bar{\ell}_i\gamma^\alpha \ell_j)(\bar{e}_k\gamma_\alpha e_l) \tag{6.19}$$
$$\mathcal{O}^{ijkl}_{\ell\ell} = (\bar{\ell}_i\gamma^\alpha \ell_j)(\bar{\ell}_k\gamma_\alpha \ell_l) \tag{6.20}$$

  where the pairs ij, kl, kj, il can be $e\tau$ or $\tau\mu$, while the remaining pair is diagonal and can be $\{e, \mu, \tau\}$.

- Two-lepton two-quark operators $\equiv 4f_6$:

$$\mathcal{O}_{\ell q}^{(1)ijnm} = (\bar{\ell}_i \gamma^\alpha \ell_j)(\bar{q}_n \gamma_\alpha q_m) \tag{6.21}$$
$$\mathcal{O}_{lq}^{(3)ijnm} = (\bar{\ell}_i \tau^a \gamma^\alpha \ell_j)(\bar{q}_n \tau^a \gamma_\alpha q_m) \tag{6.22}$$
$$\mathcal{O}_{\ell u}^{ijnm} = (\bar{\ell}_i \gamma^\alpha \ell_j)(\bar{u}_n \gamma_\mu u_m) \tag{6.23}$$
$$\mathcal{O}_{\ell d}^{ijnm} = (\bar{\ell}_i \gamma^\alpha \ell_j)(\bar{d}_n \gamma_\alpha d_m) \tag{6.24}$$
$$\mathcal{O}_{eq}^{ijnm} = (\bar{e}_i \gamma^\alpha e_j)(\bar{q}_n \gamma_\alpha q_m) \tag{6.25}$$
$$\mathcal{O}_{eu}^{ijnm} = (\bar{e}_i \gamma^\alpha e_j)(\bar{u}_n \gamma_\alpha u_m) \tag{6.26}$$
$$\mathcal{O}_{ed}^{ijnm} = (\bar{e}_i \gamma^\alpha e_j)(\bar{d}_n \gamma_\alpha d_m) \tag{6.27}$$
$$\mathcal{O}_{\ell edq}^{ijnm} = (\bar{\ell}_i e_j)(\bar{d}_n q_m) \tag{6.28}$$
$$\mathcal{O}_{\ell equ}^{ijnm} = (\bar{\ell}_i e_j)\varepsilon(\bar{q}_n u_m) \tag{6.29}$$

  with $n, m \in \{1, 2, 3\}$ running over the three quark families.

At dimension eight, there are thousands of operators, but here are listed only the subset relevant for our calculations, where relevant means that their contribution could be detectable in the upcoming $\mu \to e$ experimental searches, assuming a NP scale $\Lambda_{\rm NP} \gtrsim 4$ TeV. A list of such operators was identified in Chapter 5, and is given below.

These include dipole operators $\equiv D_8$

$$\begin{aligned}
\mathcal{O}_{\ell eWH^3}^{(1)e\mu} &= y_\mu (\bar{\ell}_e \tau^a H \sigma^{\alpha\beta} e_\mu) W^a_{\alpha\beta} (H^\dagger H) \\
\mathcal{O}_{\ell eWH^3}^{(2)e\mu} &= y_\mu (\bar{\ell}_e H \sigma^{\alpha\beta} e_\mu) W^a_{\alpha\beta} (H^\dagger \tau^a H) \\
\mathcal{O}_{\ell eBH^3}^{e\mu} &= y_\mu (\bar{\ell}_e H \sigma^{\alpha\beta} e_\mu) B_{\alpha\beta} (H^\dagger H)
\end{aligned} \tag{6.30}$$

and their Hermitian conjugates with the lepton indices exchanged. Two-lepton two-quark vector $\equiv 4f_8$

$$\mathcal{O}_{\ell^2 q^2 H^2}^{(1)e\mu nn} = (\bar{\ell}_e \gamma^\alpha \ell_\mu)(\bar{q}_n \gamma_\alpha q_n)(H^\dagger H) \tag{6.31}$$
$$\mathcal{O}_{\ell^2 q^2 H^2}^{(2)e\mu nn} = (\bar{\ell}_e \tau^a \gamma^\alpha \ell_\mu)(\bar{q}_n \gamma_\alpha q_n)(H^\dagger \tau^a H) \tag{6.32}$$
$$\mathcal{O}_{\ell^2 q^2 H^2}^{(3)e\mu nn} = (\bar{\ell}_e \tau^a \gamma^\alpha \ell_\mu)(\bar{q}_n \tau^a \gamma_\alpha q_n)(H^\dagger H) \tag{6.33}$$
$$\mathcal{O}_{\ell^2 q^2 H^2}^{(4)e\mu nn} = (\bar{\ell}_e \gamma^\mu \ell_\mu)(\bar{q}_n \tau^a \gamma_\mu q_n)(H^\dagger \tau^a H) \tag{6.34}$$
$$\mathcal{O}_{\ell^2 u^2 H^2}^{(1)e\mu nn} = (\bar{\ell}_e \gamma^\alpha \ell_\mu)(\bar{u}_n \gamma_\mu u_n)(H^\dagger H) \tag{6.35}$$
$$\mathcal{O}_{\ell^2 u^2 H^2}^{(2)e\mu nn} = (\bar{\ell}_e \tau^a \gamma^\alpha \ell_\mu)(\bar{u}_n \gamma_\alpha u_n)(H^\dagger \tau^a H) \tag{6.36}$$
$$\mathcal{O}_{\ell^2 d^2 H^2}^{(1)e\mu nn} = (\bar{\ell}_e \gamma^\alpha \ell_\mu)(\bar{d}_n \gamma_\alpha d_n)(H^\dagger H) \tag{6.37}$$
$$\mathcal{O}_{\ell^2 d^2 H^2}^{(2)e\mu nn} = (\bar{\ell}_e \tau^a \gamma^\alpha \ell_\mu)(\bar{d}_n \gamma_\alpha d_n)(H^\dagger \tau^a H) \tag{6.38}$$
$$\mathcal{O}_{e^2 q^2 H^2}^{(1)e\mu nn} = (\bar{e}_e \gamma^\alpha e_\mu)(\bar{q}_n \gamma_\alpha q_n)(H^\dagger H) \tag{6.39}$$
$$\mathcal{O}_{e^2 q^2 H^2}^{(2)e\mu nn} = (\bar{e}_e \gamma^\alpha e_\mu)(\bar{q}_n \tau^a \gamma_\alpha q_n)(H^\dagger \tau^a H) \tag{6.40}$$
$$\mathcal{O}_{e^2 u^2 H^2}^{e\mu nn} = (\bar{e}_e \gamma^\alpha e_\mu)(\bar{u}_n \gamma_\alpha u_n)(H^\dagger H) \tag{6.41}$$
$$\mathcal{O}_{e^2 d^2 H^2}^{e\mu nn} = (\bar{e}_e \gamma^\alpha e_\mu)(\bar{d}_n \gamma_\alpha d_n)(H^\dagger H) \tag{6.42}$$

with in most cases $n = u, d$ belonging to the first generation quarks. There are also penguin operators $\equiv P_8$

$$\begin{aligned}
\mathcal{O}^{(1)e\mu}_{\ell^2H^4D} &= i(\bar{\ell}_e\gamma^\alpha\ell_\mu)(H^\dagger\overset{\leftrightarrow}{D}_\alpha H)(H^\dagger H)\\
\mathcal{O}^{(2)e\mu}_{\ell^2H^4D} &= i(\bar{\ell}_e\tau^a\gamma^\alpha\ell_\mu)[(H^\dagger\overset{\leftrightarrow}{D}^a_\alpha H)(H^\dagger H) + (H^\dagger\overset{\leftrightarrow}{D}_\alpha H)(H^\dagger\tau^a H)]\\
\mathcal{O}^{e\mu}_{e^2H^4D} &= i(\bar{e}_e\gamma^\alpha e_\mu)(H^\dagger\overset{\leftrightarrow}{D}_\alpha H)(H^\dagger H).
\end{aligned} \tag{6.43}$$

Furthermore, the following two-fermion two-lepton scalar and tensor operators are also relevant

$$\mathcal{O}^{(1)e\mu nn}_{\ell edqH^2} = (\bar{\ell}_e e_\mu)(\bar{d}_n q_n)(H^\dagger H) \tag{6.44}$$
$$\mathcal{O}^{(2)e\mu nn}_{\ell edqH^2} = (\bar{\ell}_e e_\mu)\tau^a(\bar{d}_n q_n)(H^\dagger\tau^a H) \tag{6.45}$$
$$\mathcal{O}^{(1)e\mu nn}_{\ell equH^2} = (\bar{\ell}_e e_\mu)\varepsilon(\bar{q}_n u_n)(H^\dagger H) \tag{6.46}$$
$$\mathcal{O}^{(2)e\mu nn}_{\ell equH^2} = (\bar{\ell}_e e_\mu)\tau^a\varepsilon(\bar{q}_n u_n)(H^\dagger\tau^a H) \tag{6.47}$$
$$\mathcal{O}^{(3)e\mu nn}_{\ell equH^2} = (\bar{\ell}_e\sigma^{\alpha\beta} e_\mu)\varepsilon(\bar{q}_n\sigma_{\alpha\beta} u_n)(H^\dagger H) \tag{6.48}$$
$$\mathcal{O}^{(4)e\mu nn}_{\ell equH^2} = (\bar{\ell}_e\sigma^{\alpha\beta} e_j)\tau^a\varepsilon(\bar{q}_n\sigma_{\alpha\beta} u_n)(H^\dagger\tau^a H) \tag{6.49}$$
$$\mathcal{O}^{(3)e\mu nn}_{\ell edqH^2} = (\bar{\ell}_e H e_\mu)(\bar{q}_n H d_n) \tag{6.50}$$
$$\mathcal{O}^{(4)e\mu nn}_{\ell edqH^2} = (\bar{\ell}_e\sigma^{\alpha\beta} H e_\mu)(\bar{q}_n\sigma_{\alpha\beta} H d_n) \tag{6.51}$$
$$\mathcal{O}^{(5)e\mu nn}_{\ell equH^2} = (\bar{\ell}_e H e_\mu)(\bar{u}_n\tilde{H}^\dagger q_n), \tag{6.52}$$

with $n = u, c, t, d, s, b$ running over all quark flavours. Finally the four-lepton operators $\equiv 4l_8$ read

$$\mathcal{O}^{(4)e\mu\tau\tau}_{\ell^2e^2H^2} = (\bar{\ell}_e H\sigma^{\alpha\beta} e_\mu)(\bar{\ell}_\tau H\sigma_{\alpha\beta} e_\tau) \tag{6.53}$$
$$\mathcal{O}^{(3)e\mu ee}_{\ell^2e^2H^2} = (\bar{\ell}_e H e_\mu)(\bar{\ell}_e H e_e) \tag{6.54}$$
$$\mathcal{O}^{(1)e\mu ee}_{\ell^4H^2} = (\bar{\ell}_e\gamma^\alpha\ell_\mu)(\bar{\ell}_e\gamma_\alpha\ell_e)(H^\dagger H) \tag{6.55}$$
$$\mathcal{O}^{(2)e\mu ee}_{\ell^4H^2} = (\bar{\ell}_e\gamma^\alpha\ell_\mu)(\bar{\ell}_e\tau^a\gamma_\alpha\ell_e)(H^\dagger\tau^a H) \tag{6.56}$$
$$\mathcal{O}^{(1)e\mu ee}_{\ell^2e^2H^2} = (\bar{\ell}_e\gamma^\alpha\ell_\mu)(\bar{e}_e\gamma_\alpha e_e)(H^\dagger H) \tag{6.57}$$
$$\mathcal{O}^{(2)e\mu ee}_{\ell^2e^2H^2} = (\bar{\ell}_e\tau^a\gamma^\alpha\ell_\mu)(\bar{e}_e\gamma_\alpha e_e)(H^\dagger\tau^a H) \tag{6.58}$$
$$\mathcal{O}^{e\mu ee}_{e^4H^2} = (\bar{e}_e\gamma^\alpha e_\mu)(\bar{e}_e\gamma_\alpha e_e)(H^\dagger H). \tag{6.59}$$

Note that in the Lagrangian of Eq. (6.2) we sum over all possible generation indices, and more flavour structures are relevant for low energy LFV interactions. For instance, $\mathcal{O}^{e\mu ee}_{\ell^4H^2}, \mathcal{O}^{eee\mu}_{\ell^4H^2}$ match onto the same vector operator in the EFT below m_W. Similarly, in the case of $e\mu\tau\tau$ tensor operator, the permutations $\tau\tau e\mu, \tau\mu e\tau, e\tau\tau\mu$ must be considered.

6.2.4 Equations of Motion

In this section, we discuss some of the technical subtleties that occur when two dimension six operators mix into dimension eight operators. In our calculations of anomalous dimensions we

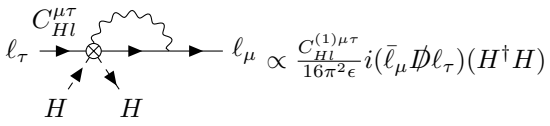

(a)

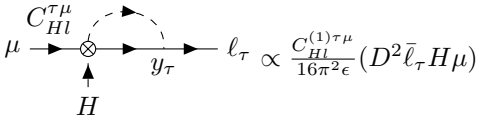

(b)

Figure 6.2: One-loop diagrams with the penguin operators of Eq. (6.12). Matching the divergences off-shell, the redundant operators $i(\bar{\ell}_\mu \not{D} \ell_\tau)(H^\dagger H)$, $(D^2 \bar{\ell}_\tau H \mu)$ are generated.

consider two different approaches: we can systematically apply the equations of motions onto the amplitudes of our loop calculations in order to arrive at expressions that are proportional to tree-level amplitudes of the on-shell, or "physical" operators. Alternatively, we could use a complete set of off-shell operators and project our loop amplitudes onto the on-shell operator basis. The situation is slightly complicated by the facts that the dimension six operators will contribute themselves to the equations of motion, and that there are a huge number of dimension eight operators. In the following we will show how both approaches are equivalent in our calculation, where we determine the mixing into the subset of dimension eight operators that contribute to LFV at low energy experiments.

Working with a on-shell (or physical) operator basis implies the choice of a set of operators that vanish when the Equation of Motions (EOM) are satisfied. Take two operators $\mathcal{O}_1, \mathcal{O}_2$ which differ by an operator $\mathcal{O}_{EOM}$ that is EOM vanishing, i.e

$$\mathcal{O}_1 - \mathcal{O}_2 = \mathcal{O}_{EOM} \propto \frac{\delta S}{\delta \phi} \tag{6.60}$$

where S is the action and ϕ labels a generic field. $\mathcal{O}_{EOM}$ can be dropped in physical processes because it leads to vanishing $S-$matrix elements, so that the operators $\mathcal{O}_1$, $\mathcal{O}_2$ are physically equivalent and only one of them is retained in the basis (see section 4.2.1.1 of Chapter 4)

For instance, at dimension six, the operators

$$i(\bar{\ell}_\mu \not{D} \ell_\tau)(H^\dagger H) \ , \ (D^2 \bar{\ell}_\tau H \mu) \tag{6.61}$$

can be generated at one-loop from a penguin operator (see Figure 6.2). The first is relevant here, because it is on-shell equivalent to $(\bar{\ell}_\mu H e_\tau)(H^\dagger H)$ by means of the dimension four EOM of the lepton field $i(\not{D} \ell_\tau) = y_\tau H e_\tau$. (The second operator will be relevant for the $C_{Hl} \times C_{He}$ mixing into dipoles, which is discussed in section 6.3.1.1.)

Therefore, we can project an amplitude that is proportional to the left hand side of the previous equation of motion

$$\begin{aligned} i(\bar{\ell}_\mu \not{D} \ell_\tau)(H^\dagger H) \to & [i(\bar{\ell}_\mu \not{D} \ell_\tau)(H^\dagger H) - y_\tau (\bar{\ell}_\mu H e_\tau)(H^\dagger H)] \\ & + y_\tau (\bar{\ell}_\mu H e_\tau)(H^\dagger H) \end{aligned} \tag{6.62}$$

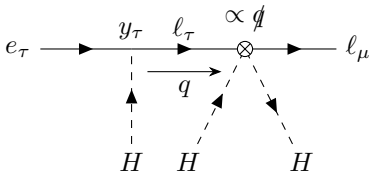

Figure 6.3: The diagram shows that the operator $i(\bar{\ell}_\mu \not{D} \ell_\tau)(H^\dagger H)$ leads to the same $S-$matrix elements as $y_\tau(\bar{\ell}_\mu H e_e)(H^\dagger H)$. The non-local momentum dependence of the internal line propagator cancels with the inverse propagator present in the Equation of Motion.

onto physical and EOM vanishing – in brackets – operators. In Figure 6.3 we show how the equivalence can be understood diagrammatically: the $\not{D}$ operator Feynman rule is proportional to the $\not{q}$ momentum of the virtual ℓ_τ line coming out of a renormalizable Yukawa coupling; the momentum dependence cancels with the ℓ_τ propagator, yielding an $S-$matrix element reproduced by the local operator $y_\tau(\bar{\ell}_\mu H e_\tau)(H^\dagger H)$.

Once a reduced physical basis is identified, the theory can be consistently renormalized among on-shell operators, as redundant counterterms $A\mathcal{O}_2/\varepsilon$ are equivalent to $A(\mathcal{O}_1 - \mathcal{O}_{EOM})/\varepsilon$ and EOM vanishing operators mix exclusively among themselves in the RGEs [353][1].

However, in order to consistently renormalize an EFT in a given basis up to dimension eight $(1/\Lambda_{\rm NP}^4)$, the dimension six $(1/\Lambda_{\rm NP}^2)$ terms in the EOM must be included when removing redundant operators. Concretely, if a divergent contribution to a redundant dimension six operator, $\mathcal{O}_2^{[6]}/(\Lambda_{\rm NP}^2\varepsilon)$ is generated via loops, then it can be rewritten

$$\frac{A}{\Lambda_{\rm NP}^2\varepsilon}\left(\mathcal{O}_1^{[6]} + \frac{\mathcal{O}^{[8]}}{\Lambda_{\rm NP}^2} - \mathcal{O}_{EOM}\right) \tag{6.63}$$

where $O_1^{[6]}$ is equivalent to $O_2^{[6]}$ via the renormalizable EOM $\delta S^{d=4}/\delta\phi = 0$ of Eq. (6.60), and the dimension eight $\mathcal{O}^{[8]}$ is generated by the dimension six corrections $\delta S^{d=6}/\delta\phi$. The dimension eight contribution is proportional to the product of two dimension six operator coefficients, which is the kind of contribution that we are interested in.

As an example of the impact of dimension six terms in the EOM, suppose that the only $\tau \leftrightarrow e$ operator at dimension six is $\mathcal{O}_{\ell edq}^{e\tau nm} = (\bar{\ell}_\tau e_e)(\bar{d}_n q_m)$, and that the operator $i(\bar{\ell}_\mu \not{D} \ell_\tau)(H^\dagger H)$ is generated via loop corrections. Then Eq. (6.62), up to dimension 8, becomes

$$\begin{aligned} i(\bar{\ell}_\mu \not{D} \ell_\tau)(H^\dagger H) \to \Bigg[& i(\bar{\ell}_\mu \not{D} \ell_\tau)(H^\dagger H) - y_\tau(\bar{\ell}_\mu H e_\tau)(H^\dagger H) + \\ & + \frac{C_{\ell edq}^{\tau enm}}{\Lambda_{\rm NP}^2}(\bar{\ell}_\mu e_e)(\bar{d}_n q_m)(H^\dagger H)\Bigg] \\ & + y_\tau(\bar{\ell}_\mu H e_\tau)(H^\dagger H) - \frac{C_{\ell edq}^{\tau enm}}{\Lambda_{\rm NP}^2}(\bar{\ell}_\mu e_e)(\bar{d}_n q_m)(H^\dagger H) \end{aligned} \tag{6.64}$$

where the EOM vanishing operator in square brackets now contains the dimension eight $\mathcal{O}_{\ell edqH^2}^{(1)iknm} = (\bar{\ell}_\mu e_e)(\bar{d}_n q_m)(H^\dagger H)$. Similarly to the renormalizable case, the on-shell equivalence is apparent

[1] Gauge fixing and ghost terms that appear in the EOM are found to have no physical effects in operator mixing and $S-$matrix elements [353].

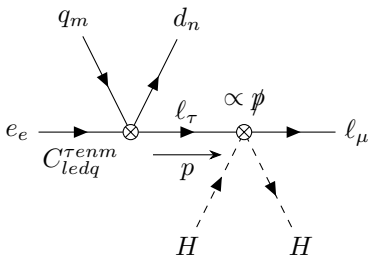

Figure 6.4: Correction to the Equation of Motion due to dimension six operators. At $1/\Lambda^4_{\rm NP}$ order, the operator $i(\bar{\ell}_\mu \not{D} \ell_\tau)(H^\dagger H)$ is on-shell equivalent to a combination of dimension six and dimension eight operators. The dimension eight contribution can be understood by attaching dimension six interactions to the operator, where the internal line propagator cancels against the vertex Feynman rule. The diagram shows an example with the insertion $\mathcal{O}^{\tau enm}_{ledq} = (\bar{\ell}_\tau e_e)(\bar{d}_n q_m)$, which reproduces the EOM reduction of Eq. (6.64).

diagrammatically, by dressing the redundant operator with dimension six contact interactions as shown in Figure 6.4. Once again the inverse propagator that is present in the EOM, and appears in the operator Feynman rule, cancels the momentum dependence of the internal line, such that the amplitude is local and equivalent to a dimension eight operator. Its coefficient will be proportional to the product of two dimension six WC.

For instance, $i(\bar{\ell}_\mu \not{D} \ell_\tau)(H^\dagger H)$ is generated in matching off-shell the divergence of the one-loop diagram of Figure 6.2 that involves the penguin operators of eq (6.12). Eq. (6.64) allows to project the divergence onto the on-shell basis, giving a contribution to the renormalisation of the dimension eight $\mu \leftrightarrow e$ operator $\mathcal{O}^{(1)\mu enm}_{\ell edqH^2} = (\bar{\ell}_\mu e_e)(\bar{d}_n q_m)(H^\dagger H)$ from the product $\mathcal{O}^{(1)}_{H\ell} \times \mathcal{O}_{\ell edq}$. This contribution from the EOM projection must be included in calculating the mixing from (dimension 6)$^2 \to$ dimension 8, together with one particle irreducible (1PI) diagrams $\propto C^{(1)}_{H\ell} \times C_{\ell edq}$. (Indeed, the anomalous dimension is only gauge invariant if one includes both the IP1 vertex and the non-1PI "wavefunction" contributions.)

The EOM contribution can be reproduced by calculating non-1PI divergent diagrams, as shown in figure 6.4. In working with a subspace of dimension eight operators (as we do here), proceeding diagrammatically can be particularly convenient. Our subspace is phenomenologically selected to contribute to the low energy $\mu \to e$ processes. When using the EOM to project the off-shell divergences, the redundant terms must be written in terms of operators in the full basis (which can include operators outside the subspace) and the EOM vanishing operators that the basis choice implies. In the end, only the interesting operators in the subspace are retained but it required working with the full basis as an intermediate step. On the other hand, in the approach of calculating one-particle -reducible diagrams, it is often easier to restrict to diagrams that directly give dimension eight operators of the subspace. In this manuscript, we calculate the one-particle-reducible diagrams that generate the relevant dimension eight operators. We cross-checked our diagrammatic results by calculating the dimension eight LFV operators obtained from the list of EOM-vanishing operators in [305], by using Equations of Motion up to dimension six.

Finally, recall that we work in the low-energy mass eigenstate basis of the leptons, where the

lepton mass matrix is:

$$m_{e_i}\delta_{ij} = v\left([y_e]_{ij} - C_{eH}^{ij}\right) \quad . \tag{6.65}$$

So in the above diagrammatic and EOM-based arguments, the Yukawa matrix element y_τ is replaced by the matrix element of the parenthese on the right side of (6.65), which is also flavour-diagonal[2]. Therefore we do not include non-1PI diagrams involving a loop on the external leg of $\mathcal{O}_{eH}^{ij}$.

6.2.5 Estimates

The goal of this section is to better identify the dimension eight contributions that are interesting to calculate in the context of $\mu \to e$ LFV, that is, those that will be within the reach of future experiments. The Wilson coefficients of the dimension eight operators presented in the previous section were estimated in Chapter 5 to be within upcoming experimental sensitivity if they have values $\gtrsim v^4/\Lambda^4$, for $\Lambda \gtrsim 4$ TeV. We estimate in this section the additional loop and small couplings suppression that could be encountered in generating these coefficients in running and matching. This will allow to narrow-down the list of diagrams that should be calculated.

In estimating diagrams built out of $\mu \to \tau \times \tau \to e$ operators, we take into account the constraints on $\tau \leftrightarrow l$ processes coming from the bounds reported in the lower part of Table 6.1. Employing the acronyms introduced in the previous section for sets of τ LFV operators, current and upcoming one-at-a-time-limits on their coefficients are written in Table 6.2. These estimates assume that the Branching Ratio sensitivities on τ decays will improve of an order of magnitude at BelleII [341], and use the future sensitivities to $h \to \tau^\pm l^\mp$ decays at the ILC [347]. In the case where the operators are not (or are only loosely) bounded, we assume

$$C^{[6]l\tau\ldots} \lesssim (v/4\text{ TeV})^2 \sim 2\times 10^{-3} \tag{6.66}$$

corresponding to an $\mathcal{O}(1)$ coefficient at a New Physics scale of 4 TeV.

Operator coefficient	Current sensitivity	Future sensitivity	Process
$C_{D_6}^{l\tau}$	$\lesssim 7\times 10^{-6}$	$\lesssim 2\times 10^{-6}$	$\tau \to l\gamma$
$C_{Y_6}^{l\tau}$	$\lesssim 10^{-3}$	$\lesssim 3\times 10^{-4}$	$h \to l\tau$
$C_{P_6}^{l\tau}$	$\lesssim 4\times 10^{-4}$	$\lesssim 10^{-4}$	$\tau \to \bar{l}ll$
$C_{4l_6}^{l\tau ll}$	$\lesssim 3\times 10^{-4}$	$\lesssim 10^{-4}$	$\tau \to \bar{l}ll$
$C_{4f_6}^{l\tau qq}$	$\lesssim 3\times 10^{-4}$	$\lesssim 10^{-4}$	$\tau \to l\pi(\eta)$

Table 6.2: Sensitivities to $\tau \leftrightarrow l$ dimension six operator coefficients, normalized as in Eq. (6.2). Current limits come from the Branching ratio bounds of Table 6.1, while the third column assumes that the experimental sensitivity to $\tau \leftrightarrow l$ decays will improve by an order of magnitude.

Diagrams that can generate the dimension eight $\mu \leftrightarrow e$ operators of section 6.2.3, in matching or in running, are drawn with a pair of $\tau \leftrightarrow l$ operators. The contribution to the coefficients are estimated as

$$\Delta C^{[8]e\mu} \simeq C_1^{[6]e\tau} C_2^{[6]\tau\mu} \left(\frac{1}{16\pi^2}\right)^n \times \left\{y^k\ g^l\ \lambda^m \ldots\right\} \times \log \tag{6.67}$$

[2]However, in this basis, the h retains LFV interactions — see Eq. (6.88).

Operator coefficient	Current sensitivity	Future sensitivity	Process
$C_{D_8}^{e\mu}$	$\lesssim 10^{-8}$	$\lesssim 1.5 \times 10^{-9}$	$\mu \to e\gamma$
$C_{4f_8,T}^{e\mu tt}$	$\lesssim 3 \times 10^{-11}$	$\lesssim 5 \times 10^{-12}$	$\mu \to e\gamma$
$C_{4l_8,T}^{e\mu\tau\tau}, C_{4f_8,T}^{e\mu cc}$	$\lesssim 10^{-8}$	$\lesssim 1.5 \times 10^{-9}$	$\mu \to e\gamma$
$C_{4f_8,T}^{e\mu bb}$	$\lesssim 8 \times 10^{-9}$	$\lesssim 10^{-9}$	$\mu \to e\gamma$
$C_{P_8}^{e\mu}$	$\lesssim 10^{-7}$	$\lesssim 10^{-9}$	$\mu A \to eA$
$C_{4l_8}^{e\mu ee}$	$\lesssim 8 \times 10^{-7}$	$\lesssim 8 \times 10^{-9}$	$\mu \to \bar{e}ee$
$C_{4f_8,S}^{e\mu uu, e\mu dd}$	$\lesssim 10^{-8}$	$\lesssim 10^{-10}$	$\mu A \to eA$

Table 6.3: Sensitivities to $\mu \to e$ dimension eight operator coefficients, normalized as in Eq. (6.2). Current and future limits correspond to the experimental sensitivities of Table 6.1. T, S label the Lorentz structure of the operator for tensor and scalar respectively. For instance, $C_{4f_8,T}^{e\mu tt}$ is the coefficient of the dimension eight tensor in Eq. (6.49) with top quarks.

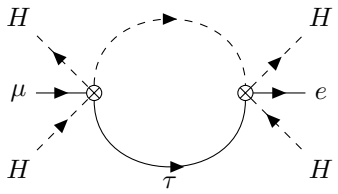

Figure 6.5: Mixing to the dimension eight $\mu \to e$ penguin operator from double insertion of dimension six Yukawas $Y_6 \times Y_6 \to P_8$.

where n is the number of loops, SM couplings are factored out into the curly brackets, and the $\log(4\ \text{TeV}/m_W)$ factor is present in running, while absent in matching. In running, we restrict the number of loops to $n = 1$, while up to two loop diagrams contribute in "tree-level"(in the low-energy EFT) matching.

An example of a diagram contributing to the RGEs is shown in the diagram of Figure 6.5, where two Yukawa operators $\mathcal{O}_{eH}^{e\tau} \times \mathcal{O}_{eH}^{\tau\mu} \sim Y_6 \times Y_6$ mix into dimension eight $\mu \to e$ penguin operators $\mathcal{O}_{e^2H^2D}^{e\mu}, O_{l^2H^2D}^{e\mu} \sim P_8$ by exchanging the τ and closing the loop with a Higgs line. The estimated contribution to the penguin coefficients is then

$$\Delta C_{P_8} \sim (C_{Y_6})^2 \frac{\log(4\ \text{TeV}/m_W)}{16\pi^2} \sim 3 \times 10^{-9}. \tag{6.68}$$

Future $\mu A \to eA$ experiments will be sensitive to penguin coefficients larger than $\sim 10^{-9}$, hence our estimate lies within experimental reach and $Y_6 \times Y_6 \to P_8$ mixing is calculated in section 6.3.

As another example, $\tau \leftrightarrow l$ dipoles D_6 are defined with a built-in τ Yukawa suppression — see Eq. (6.11)— so $y_\tau \sim 10^{-2}$ multiplies any dipole insertion. For instance, if $D_6 \times \mathcal{O}_6$ mix into a dimension eight operator $\mathcal{O}_8$, its coefficient is estimated to be

$$\Delta C_8 \sim y_\tau C_{D_6} C_6 \frac{\log(4\ \text{TeV}/m_W)}{16\pi^2} \lesssim 10^{-12}, \tag{6.69}$$

where we took $C_6 \lesssim v^2/\Lambda^2$, for $\Lambda \sim 4$ TeV. Equation (6.69) is smaller than any future $\mu \to e$ sensitivity to operator coefficients, so we disregard mixing that involves τ dipoles in our calculations.

The results of our estimates are summarized in Tables 6.4 and 6.5, referring respectively to RGEs and matching contributions. There, we report the potentially detectable dimension eight operators generated by a given pair of dimension six operators.

	P_6	Y_6	$4l_6$	$4f_6$
P_6	$D_8 \equiv 0$	$D_8 \equiv 0$	$\times$	$4f_8$
Y_6	$D_8 \equiv 0$	P_8	$\times$	$\times$
$4l_6$	$\times$	$\times$	$\times$	$\times$
$4f_6$	$4f_8$	$\times$	$\times$	$4f_8$

Table 6.4: We present the dimension eight operators that we estimate to be generated within experimental sensitivity through (dimension six)^2 mixing in the RGEs. The $\times$ means that the contributions is too small or that there is no one-loop diagram that can generate the desired dimension eight operators with the given pair. $P_6 \times P_6 \to D_8$, $Y_6 \times P_6 \to D_8$ mixing diagrams exist and appear to be interesting, however we find that the anomalous dimension vanishes (see section 6.3.1.1).

	P_6	Y_6	$4l_6$	$4f_6$
P_6	$\times$	D_8	$\times$	$\times$
Y_6	$\times$	$D_8, 4l_8$	$\times$	$\times$
$4l_6$	$\times$	$\times$	$\times$	$\times$
$4f_6$	$\times$	$\times$	$\times$	$\times$

Table 6.5: We present the dimension eight operators that we estimate to be generated within experimental sensitivity through (dimension six)^2 in matching. The $\times$ means that the contributions is too small or that there is no tree-level matching that can generate the desired dimension eight operators with the given pair.

6.3 Calculation

The contributions that were estimated in the previous section to be within experimental sensitivity are calculated here. Section 6.3.1 determines the divergences of the relevant one-loop diagrams and relates them to the anomalous dimensions of the dimension eight Wilson coefficients in SMEFT, and in Section 6.3.2, pairs of $\tau \leftrightarrow l$ dimension six operators are tree-level-matched at m_W onto the low energy $\mu \to e$ EFT.

6.3.1 SMEFT Running

In this section, we outline the calculation of the anomalous dimension matrix $\hat{\gamma}_{XY,A}$, that mixes the dimension six $\tau \leftrightarrow l$ operators $\mathcal{O}_X^{[6]}, \mathcal{O}_Y^{[6]}$ into the $\mu \to e$ dimension eight $\mathcal{O}_A^{[8]}$. We work in

dimensional regularization in $4-2\varepsilon$ dimensions and renormalize in the $\overline{\text{MS}}$ scheme, where we label the renormalization scale with M (rather than the usual μ). Double insertions of dimension six operators renormalize dimension eight coefficients as

$$\Delta\vec{C}_A^{[8]} = \vec{C}_X^{[6]}\hat{Z}_{XY,A}\vec{C}_Y^{[6]}, \tag{6.70}$$

where the Wilson coefficients of dimension eight and six are respectively aligned in the row vectors $\vec{C}^{[8]}$, $\vec{C}^{[6]}$, dimension eight and six operator labels are respectively capitals from the beginning and end of the alphabet, and flavour indices are suppressed. The bare dimension eight coefficients can be written as

$$\vec{C}_{A,bare}^{[8]} = M^{a_A\varepsilon}(\vec{C}_B^{[8]}Z_{BA} + \vec{C}_X^{[6]}\hat{Z}_{XY,A}\vec{C}_Y^{[6]}) \tag{6.71}$$

where we have factored out the sliding scale power $M^{a_A\varepsilon}$ to assure that the renormalized WC stay dimensionless in $d = 4-2\varepsilon$ space-time dimensions. The RGEs can be obtained from the independence of the bare Lagrangian from the arbitrary renormalization scale M

$$(16\pi^2)\frac{d\vec{C}_{A,bare}^{[8]}}{d\log M} = 0, \tag{6.72}$$

which implies the following differential equation for the renormalized Wilson coefficients

$$\begin{aligned}(16\pi^2)\frac{d\vec{C}_A^{[8]}}{d\log M} = (16\pi^2)\Big[&- a_A\varepsilon(\vec{C}_A^{[8]} + \vec{C}_X^{[6]}\vec{C}_Y^{[6]}\hat{Z}_{XY,B}Z_{BA}^{-1}) \\ &-\vec{C}_B^{[8]}\frac{dZ_{BC}}{d\log M}Z_{CA}^{-1} + -\frac{d\vec{C}_X^{[6]}}{d\log M}\hat{Z}_{XY,B}\vec{C}_Y^{[6]}Z_{BA}^{-1} + \\ &-\vec{C}_X^{[6]}\hat{Z}_{XY,B}\frac{d\vec{C}_Y^{[6]}}{d\log M}Z_{BA}^{-1} - \vec{C}_X^{[6]}\frac{d\hat{Z}_{XY,B}}{d\log M}\vec{C}_Y^{[6]}Z_{BA}^{-1}\Big].\end{aligned} \tag{6.73}$$

The RGEs of dimension six Wilson coefficients are the following

$$(16\pi^2)\frac{d\vec{C}_X^{[6]}}{d\log M} = -(16\pi^2)a_X\varepsilon\vec{C}_X^{[6]} + \vec{C}_Y^{[6]}\tilde{\gamma}_{YX} + \dots \tag{6.74}$$

where $a_X\varepsilon$ is the mass dimension of the bare coefficient of $\mathcal{O}_X$ and $\tilde{\gamma}$ is the anomalous dimension matrix for dimension six operators. In the limit $\varepsilon \to 0$, the term proportional to ε is irrelevant for the dimension six renormalization, while it plays a crucial role in $(\text{dimension6})^2$ to dimension eight mixing. Upon substitution, Eq. (6.73) becomes

$$\begin{aligned}(16\pi^2)\frac{d\vec{C}_A^{[8]}}{d\log M} = (16\pi^2)\Big[&- a_A\varepsilon\vec{C}_A^{[8]} + \vec{C}_B^{[8]}\gamma_{BA} \\ &-(a_A - a_X - a_Y)\varepsilon(\vec{C}_X^{[6]}\vec{C}_Y^{[6]}\hat{Z}_{XY,B}Z_{BA}^{-1}) \\ &-\vec{C}_X^{[6]}\frac{d\hat{Z}_{XY,B}}{d\log M}\vec{C}_Y^{[6]}Z_{BA}^{-1}\Big] \\ -\vec{C}_W^{[6]}\tilde{\gamma}_{WX}\hat{Z}_{XY,B}\vec{C}_Y^{[6]}Z_{BA}^{-1} &- \vec{C}_X^{[6]}\hat{Z}_{XY,B}\vec{C}_W^{[6]}\tilde{\gamma}_{WY}Z_{BA}^{-1}\end{aligned}$$

having defined $\gamma_{BA} \equiv -(16\pi^2)\frac{dZ_{BC}}{d\log M} Z^{-1}_{CA}$, which is the anomalous dimension matrix of dimension eight operators. At one-loop we can replace Z with the identity and neglect the second line of the above equation, since $\tilde{\gamma}$ and $\hat{Z}$ both appear at one loop at leading order. The product $\varepsilon\hat{Z}$ is finite, and the RGEs in $d = 4$ dimensions read

$$\begin{aligned}(16\pi^2)\frac{d\vec{C}^{[8]}_A}{d\log M} &= \vec{C}^{[8]}_B\gamma_{BA} \\ -(16\pi^2)(a_A - a_X - a_Y)\vec{C}^{[6]}_X\vec{C}^{[6]}_Y\varepsilon\hat{Z}_{XY,A} &\\ - (16\pi^2)\vec{C}^{[6]}_X\frac{d\hat{Z}_{XY,A}}{d\log M}\vec{C}^{[6]}_Y &\\ \equiv \vec{C}^{[8]}_B\gamma_{BA} + \vec{C}^{[6]}_X\hat{\gamma}_{XY,A}\vec{C}^{[6]}_Y &\end{aligned} \tag{6.75}$$

The one-loop $\hat{\gamma}$ anomalous dimension matrix that mixes two dimension six operators into dimension eight is finally

$$\hat{\gamma}_{XY,A} = (16\pi^2)\left[(a_X + a_Y - a_A)\varepsilon\hat{Z}_{XY,A} - \frac{d\hat{Z}_{XY,A}}{d\log M}\right]. \tag{6.76}$$

The second term contribute to the mixing when renormalizable couplings appear in $\hat{Z}$, which carry an implicit dependence on the renormalization scale M. The beta functions of renormalized SM couplings for $\varepsilon > 0$ take the form $\beta_\varepsilon(\{g, g', y\}) = -\varepsilon\{g, g', y\} + \beta(\{g, g', y\})$ and at one-loop

$$\begin{aligned}-\frac{d\hat{Z}_{XY,A}}{d\log M} &= -\frac{d\hat{Z}_{XY,A}}{d\{g, g', y\}}\beta_\varepsilon(\{g, g', y\}) \\ &= \varepsilon\frac{d\hat{Z}_{XY,A}}{d\{g, g', y\}} \times \{g, g', y\} + \text{higher loops.}\end{aligned} \tag{6.77}$$

6.3.1.1 $\mu \to \tau \times \tau \to e$ in SMEFT

We calculate the divergent part of one-loop diagrams with the product of $\mu \to \tau \times \tau \to e$ operator insertions, which, according to the estimates summarized in Table 6.4, give potentially detectable contributions to $\mu \to e$ observables in the dimension eight running. We work in SMEFT and unbroken SU(2), where all SM particles are taken massless, including the Higgs doublet. The diagrams have been drawn by hand and were also generated with a code based on FeynArts [354] and FeynRules [355]. In most cases[3], the dimension eight operators to which $\mu \to e$ observables are sensitive do not contain τ external legs, so we here consider diagrams with a virtual τ line connecting two dimension six SMEFT operators. We are interested in one-particle-irreducible divergent diagrams (which restrict the number of internal propagators) that can generate the dimension eight operators of section 6.2.2 (which constrain the external legs), and also in some one-particle-reducible divergent diagrams that reproduce the contribution of the dimension six correction in the EOM, as discussed in section 6.2.4. Yukawa couplings smaller than $y_\tau \sim 10^{-2}$ are neglected, because they lead to $\mu \to e$ coefficients below experimental sensitivity, assuming dimension six WC $C^{[6]} \lesssim v^2/\Lambda^2_{\rm NP}$ and $\Lambda_{\rm NP} = 4\,\mathrm{TeV}$. However, the estimates of section 6.2.5 select diagrams that only involve top Yukawas y_t and single insertions of y_τ, while the bottom and charm Yukawas y_b,y_c do not appear.

[3]The exception is the $\mu e\tau\tau$ tensors, but the leading contribution to these is from tree-level matching onto the low energy EFT, which is discussed the next section.

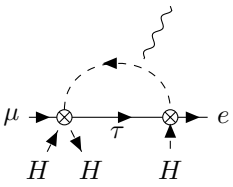

(a) $Y_6 \times P_6 \to D_8$

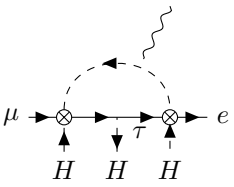

(b) $P_6 \times P_6 \to D_8$

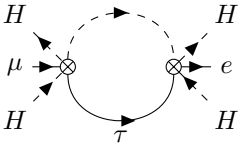

(c) $Y_6 \times Y_6 \to P_8$

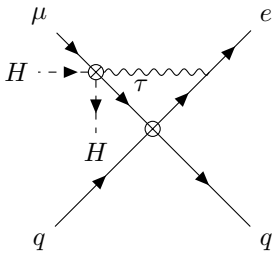

(d) $P_6 \times 4f_6 \to 4f_8$

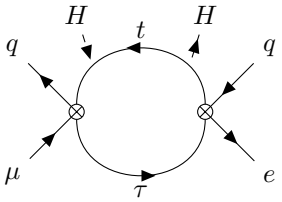

(e) $4f_6 \times 4f_6 \to 4f_8$

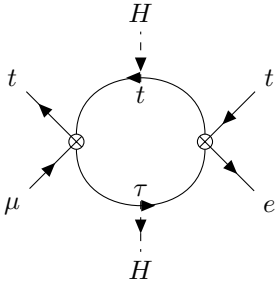

(f) $4f_6 \times 4f_6 \to 4f_8$

Figure 6.6: Classes of divergent diagrams that give observable contributions to $\mu \to e$ processes, as identified in Table 6.4.

In Figure 6.6 we show the "classes" of diagrams listed in Table 6.4, that were estimated to be within $\mu \to e$ experimental sensitivity. Each class is described below. The divergences were calculated both by hand and with an in-house developed Mathematica program, making use of the Feynman Rules listed in Appendix D.1.

- **Figure 6.6a:** $Y_6 \times P_6 \to D_8$
  The penguin operators of Eq.s (6.12)-(6.14) can be combined with the Yukawa operators of Eq. (6.17). The chirality flips on the lepton line, so attaching a gauge boson potentially generates the $\mu \to e$ dipoles of Eq. (6.30). The gauge bosons can be inserted on the internal Higgs and lepton lines or can come out of penguin operators, while the three external Higgs can be permuted in several ways among the dimension six vertices. Also, in the diagram

depicted, the Yukawa operator is $\mu \to \tau$ and the penguin is $\tau \to e$, but the two vertices can be exchanged: for instance, in the case of external left-handed electrons, the possible operator combinations are: $\mathcal{O}_{He}^{\tau\mu} \times \mathcal{O}_{eH}^{e\tau}$, $\mathcal{O}_{eH}^{\tau\mu} \times \mathcal{O}_{Hl}^{(1)e\tau}$, $\mathcal{O}_{eH}^{\tau\mu} \times \mathcal{O}_{Hl}^{(3)e\tau}$. We find that these anomalous dimensions vanish. This is consistent with the dimension six version of this calculation, where neither penguin operators dressed with renormalizable Yukawa couplings, nor $\mathcal{O}_{eH}$ dressed with a gauge loop, mix into the dimension six dipoles [356]. Note that in broken SU(2) and unitary gauge, dimension six penguins and Yukawas give Feynman rules that look like SM renormalisable interactions. By analogy with the SM, we expect them to not generate divergent non-renormalisable dipoles. The same argument applies to the $P_6 \times P_6 \to D_8$ mixing discussed in the next paragraph

- **Figure 6.6b:** $P_6 \times P_6 \to D_8$

  The diagrams feature double insertions of penguin operators - see Eq.s (6.12)-(6.14). The two vertices couple to vector currents of leptons, so to mix into the $\mu \to e$ dipoles, the chirality flip is achieved by attaching a Higgs to the τ virtual line. The contribution is estimated to lie within experimental sensitivity, because the generated $\mu \to e$ dipole coefficient is enhanced by the ratio y_τ/y_μ due to the Yukawa couplings in the dipole operator definitions in Eq. (6.30). The gauge bosons can be attached to the Higgs and τ in the loop, or can belong to one of the penguin vertices. Furthermore, all possible permutations of the external Higgses are taken into account. The operator pairs are $\mathcal{O}_{He} \times \mathcal{O}_{H\ell}^{(1),(3)}$, where the $\tau \to e$ LFV can be mediated by either right-handed or left-handed penguins, depending on the chirality of the external legs. As the previous case, the mixing into the $\mu \to e$ dipole is found to vanish.

  In addition to the 1PI diagrams of Figure 6.6b, dimension six terms in the EOM contribute to the mixing. Loop diagrams where the Higgs leg of a penguin operator closes into the τ line via a Yukawa interaction renormalize the redundant operator $(D^2\bar{\ell}_\tau)He_i$ (see Figure 6.2b). When the divergence is projected onto the on-shell basis, the penguin correction to the EOM gives additional $P_6 \times P_6 \to D_8$ mixing. However, the combination of SMEFT $\mu \to e$ dipoles that is generated is orthogonal to the γ dipole and does not contribute to low energy $\mu \to e$ observables. This is also apparent in considering non-1PI diagrams (see section 6.2.4) where a penguin operator is inserted in the τ line of $D^2\bar{\ell}_\tau He_i$; the amplitude is local and reproduces the EOM result when the external gauge boson belongs to the penguin vertex. In broken SU(2), penguins give flavour changing (and correct the flavour diagonal) couplings with the Z, but leave QED interactions untarnished.

- **Figure 6.6c:** $Y_6 \times Y_6 \to P_8$

  In this class of diagrams the loop is closed with Higgs exchange between two Yukawa operators. The superficial degree of divergence is 1, and the divergence is linear in momentum. With four external Higgses, it mixes into the dimension eight $\mu \to e$ penguin operators of Eq. (6.43). For right-handed leptons the inserted operators are $\mathcal{O}_{eH}^{\tau\mu} \times \mathcal{O}_{eH}^{*\tau e}$, while $\mathcal{O}_{eH}^{*\mu\tau} \times \mathcal{O}_{eH}^{e\tau}$ gives mixing into left-handed penguins.

- **Figure 6.6d:** $4f_6 \times P_6 \to 4f_8$

  Two-lepton two-quark $\tau \to l$ operators can mix into $\mu \to e$ dimension eight four fermion operators by inserting a penguin in the tau line and closing the loop with a gauge boson. Only

two-lepton two quark operators are considered because they contribute to $\mu \to e$ conversion (while tensors with heavy quarks contribute to $\mu \to e\gamma$), which is the process with the best upcoming sensitivity to operator coefficients. The gauge boson is attached to the other fermion lines in every possible way, and the diagram shows just one example. As discussed in section 6.2.4, we also include dimension six corrections to the EOM or, equivalently, non-1PI diagrams where the loop of Figure 6.2 dresses one of the lepton lines. These diagrams are analogous to fermion wave function renormalization and are pure-gauge, i.e $\propto \xi$ in the R_ξ gauge; to avoid calculating wave function-like diagrams, the calculation is done for $\xi = 0$, commonly known as Landau gauge. In Table 6.7 we summarize the $\mu \to e$ dimension eight operators generated by the product of $\tau \to l$ penguins with four fermion operators.

- **Figure 6.6e-6.6f:** $4f_6 \times 4f_6 \to 4f_8$ In the last two diagrams, pairs of two-lepton two-quark dimension six operators are connected through a fermion loop, where two Higgs legs are inserted. With the exception of dimension eight tensor with tops, $\mu \to e$ observables are sensitive to the resulting dimension eight coefficients only if the Higgs are attached to a top internal line. In the case of tensors with tops, the better sensitivity allows for the topology of Figure 6.6f, where a τ Yukawa is present. In Table 6.6 we list the dimension eight operators that are generated for every pair of dimension six four fermion operators.

The complete anomalous dimensions for the above classes of diagrams can be found in Appendix D.2.

We discuss the example of a pair of dimension six $\tau \leftrightarrow l$ Yukawa operators mixing into the $\mu \to e$ dimension eight penguins, depicted in the representative diagram of Figure 6.6c. The counterterms that renormalize the divergences are the following

$$\begin{aligned}
\left(C_{eH}^{\tau\mu}\hat{Z}C_{eH}^{*\tau e}\right)^{e\mu}_{e^2H^4D} &= -\frac{C_{eH}^{\tau\mu}C_{eH}^{*\tau e}}{32\pi^2\varepsilon} \\
\left(C_{eH}^{\tau\mu}\hat{Z}C_{eH}^{*\tau e}\right)^{e\mu}_{ve^2H^4D} &= -\frac{3C_{eH}^{\tau\mu}C_{eH}^{*\tau e}}{32\pi^2\varepsilon} \\
\left(C_{eH}^{*\mu\tau}\hat{Z}C_{eH}^{e\tau}\right)^{(1)e\mu}_{\ell^2H^4D} &= \frac{C_{eH}^{*\mu\tau}C_{eH}^{e\tau}}{64\pi^2\varepsilon} \\
\left(C_{eH}^{*\mu\tau}\hat{Z}C_{eH}^{e\tau}\right)^{(1)e\mu}_{v\ell^2H^4D} &= -\frac{C_{eH}^{*\mu\tau}C_{eH}^{e\tau}}{64\pi^2\varepsilon} \\
\left(C_{eH}^{*\mu\tau}\hat{Z}C_{eH}^{e\tau}\right)^{(2)e\mu}_{\ell^2H^4D} &= \frac{C_{eH}^{*\mu\tau}C_{eH}^{e\tau}}{128\pi^2\varepsilon} \\
\left(C_{eH}^{*\mu\tau}\hat{Z}C_{eH}^{e\tau}\right)^{(2)e\mu}_{v\ell^2H^4D} &= -\frac{C_{eH}^{*\mu\tau}C_{eH}^{e\tau}}{16\pi^2\varepsilon} \\
\left(C_{eH}^{*\mu\tau}\hat{Z}C_{eH}^{e\tau}\right)^{(4)e\mu}_{\ell^2H^4D} &= \frac{C_{eH}^{*\mu\tau}C_{eH}^{e\tau}}{128\pi^2\varepsilon}
\end{aligned} \tag{6.78}$$

where the subscript of the parentheses label the corresponding dimension eight operators. The operator
$\mathcal{O}^{(4)e\mu}_{\ell^2H^4D} = \varepsilon^{IJK}(\bar{\ell}_e\tau^I\gamma^\alpha\ell_\mu)(H^\dagger\tau^J H)D_\alpha(H^\dagger\tau^K H)$ is not in the list of section 6.2.2 because it does not contribute to low energy $\mu \to e$ observables, although it appears as a counterterm. Furthermore,

	$C_{\ell q}^{(1)}$	$C_{\ell q}^{(3)}$	$C_{\ell u}$	C_{eq}	C_{eu}	$C_{\ell edq}, C_{\ell edq}^{*}$	$C_{\ell equ}^{(1)}, C_{\ell equ}^{*(1)}$	$C_{\ell equ}^{(3)}, C_{\ell equ}^{*(3)}$
$C_{\ell q}^{(1)}$	$C_{\ell^2 q^2 H^2}^{(1),(4)}$	$C_{\ell^2 q^2 H^2}^{(2),(3),(5)}$	$\times$	$\times$	$C_{\ell equ H^2}^{(3),(4)}$	$C_{\ell edq H^2}^{(1),(2)}$ $C_{\ell edq H^2}^{*(1),(2)}$	$C_{\ell equ H^2}^{(1),(2),(3),(4)}$ $C_{\ell equ H^2}^{*(1),(2),(3),(4)}$	$C_{\ell equ H^2}^{(1),(2),(3),(4)}$ $C_{\ell equ H^2}^{*(1),(2),(3),(4)}$
$C_{\ell q}^{(3)}$		$C_{\ell^2 q^2 H^2}^{(1),(2)}$	$\times$	$\times$	$C_{\ell equ H^2}^{(3),(4)}$	$C_{\ell edq H^2}^{(1),(2)}$ $C_{\ell edq H^2}^{*(1),(2)}$	$C_{\ell equ H^2}^{(1),(2),(3),(4)}$ $C_{\ell equ H^2}^{*(1),(2),(3),(4)}$	$C_{\ell equ H^2}^{(1),(2),(3),(4)}$ $C_{\ell equ H^2}^{*(1),(2),(3),(4)}$
$C_{\ell u}$			$C_{\ell^2 u^2 H^2}^{(1)}$	$C_{\ell equ H^2}^{(3),(4)}$	$\times$	$\times$	$C_{\ell equ H^2}^{(1),(3)}$ $C_{\ell equ H^2}^{*(1),(3)}$	$C_{\ell equ H^2}^{(1),(3)}$ $C_{\ell equ H^2}^{*(1),(3)}$
C_{eq}				$C_{e^2 q^2 H^2}^{(1),(2)}$	$\times$	$C_{\ell edq H^2}^{(1),(2)}$ $C_{\ell edq H^2}^{*(1),(2)}$	$C_{\ell equ H^2}^{(1),(2),(3),(4)}$ $C_{\ell equ H^2}^{*(1),(2),(3),(4)}$	$C_{\ell equ H^2}^{(1),(2),(3),(4)}$ $C_{\ell equ H^2}^{*(1),(2),(3),(4)}$
C_{eu}					$C_{e^2 u^2 H^2}$	$\times$	$C_{\ell equ H^2}^{(1),(3)}$ $C_{\ell equ H^2}^{*(1),(3)}$	$C_{\ell equ H^2}^{(1),(3)}$ $C_{\ell equ H^2}^{*(1),(3)}$
$C_{\ell edq}, C_{\ell edq}^{*}$						$C_{e^2 d^2 H^2}$ $C_{\ell^2 d^2 H^2}^{(1),(2)}$	$\times$	$\times$
$C_{\ell equ}^{(1)}, C_{\ell equ}^{*(1)}$							$C_{e^2 u^2 H^2}$ $C_{e^2 q^2 H^2}^{(1)}$ $C_{\ell^2 u^2 H^2}^{(1),(2)}$ $C_{\ell^2 q^2 H^2}^{(1),(3)}$	$C_{e^2 u^2 H^2}$ $C_{e^2 q^2 H^2}^{(1)}$ $C_{\ell^2 u^2 H^2}^{(1),(2)}$ $C_{\ell^2 q^2 H^2}^{(1),(3)}$
$C_{\ell equ}^{(3)}, C_{\ell equ}^{*(3)}$								$C_{e^2 u^2 H^2}$ $C_{e^2 q^2 H^2}^{(1)}$ $C_{\ell^2 u^2 H^2}^{(1),(2)}$ $C_{\ell^2 q^2 H^2}^{(1),(3)}$

Table 6.6: Dimension eight operators generated through the diagrams of Figure 6.6e and 6.6f with pairs of two-lepton two-quark operators, $4f_6 \times 4f_6$. Most of dimension eight coefficients are proportional to y_t^2, with the exception of $\mathcal{O}_{\ell u} \times \mathcal{O}_{eq}$, $\mathcal{O}_{\ell q} \times \mathcal{O}_{eu}$ mixing into the tensors $\mathcal{O}_{\ell equ H^2}^{(3),(4)}$, where the Yukawa couplings $y_\tau y_t$ multiply the coefficient.

the following redundant operators are radiatively generated in our off-shell calculation

$$\begin{aligned}\mathcal{O}_{ve^2H^4D}^{e\mu} &= i(\bar{e}\overleftrightarrow{\not{D}}\mu)(H^\dagger H)^2 \\ &\equiv i(\bar{e}\not{D}\mu)(H^\dagger H)^2 - i(\not{D}\bar{e}\mu)(H^\dagger H)^2\end{aligned} \tag{6.79}$$

$$\mathcal{O}_{v\ell^2H^4D}^{(1)e\mu} = i(\bar{\ell}_e\overleftrightarrow{\not{D}}\ell_\mu)(H^\dagger H)^2 \tag{6.80}$$

$$\mathcal{O}_{v\ell^2H^4D}^{(2)e\mu} = i(\bar{\ell}_{eI}\overleftrightarrow{\not{D}}\ell_{\mu J})(H_I H_J^\dagger)(H^\dagger H). \tag{6.81}$$

These are related to the physical/on-shell basis as follows

$$\mathcal{O}_{ve^2H^4D}^{e\mu} = \mathcal{O}_v^{e\mu} + [y_e^*]_{i\mu}\mathcal{O}_{leH^5}^{*ie} + [y_e]_{ie}\mathcal{O}_{leH^5}^{i\mu} \tag{6.82}$$

$$\mathcal{O}_{v\ell^2H^4D}^{(1)e\mu} = \mathcal{O}_v^{(1)e\mu} + [y_e]_{\mu i}\mathcal{O}_{leH^5}^{ei} + [y_e^*]_{ei}\mathcal{O}_{leH^5}^{*\mu i} \tag{6.83}$$

$$\mathcal{O}_{v\ell^2H^4D}^{(2)e\mu} = \mathcal{O}_v^{(2)e\mu} + [y_e]_{\mu i}\mathcal{O}_{leH^5}^{ei} + [y_e^*]_{ei}\mathcal{O}_{leH^5}^{*\mu i} \tag{6.84}$$

	$C^{(1)}_{\ell q}$	$C^{(3)}_{\ell q}$	$C_{\ell u}$	$C_{\ell d}$	$C_{\ell edq}, C^*_{\ell edq}$	$C^{(1)}_{\ell equ}, C^{*(1)}_{\ell equ}$	$C^{(3)}_{\ell equ}, C^{*(3)}_{\ell equ}$
$C_{H\ell(1)}$	$C^{(1),(4)}_{\ell^2 q^2 H^2}$	$C^{(2),(3),(5)}_{\ell^2 q^2 H^2}$	$C^{(1)}_{\ell^2 u^2 H^2}$	$C^{(1)}_{\ell^2 d^2 H^2}$	$C^{(1)}_{\ell edq H^2}$ $C^{*(1)}_{\ell edq H^2}$	$C^{(1),(3),(4)}_{\ell equ H^2}$ $C^{*(1),(3),(4)}_{\ell equ H^2}$	$C^{(1),(2),(3),(4)}_{\ell equ H^2}$ $C^{*(1),(2),(3),(4)}_{\ell equ H^2}$
$C_{H\ell(3)}$	$C^{(2),(3)}_{\ell^2 q^2 H^2}$	$C^{(1),(4),(5)}_{\ell^2 q^2 H^2}$	$C^{(2)}_{\ell^2 u^2 H^2}$	$C^{(2)}_{\ell^2 d^2 H^2}$	$C^{(2)}_{\ell edq H^2}$ $C^{*(2)}_{\ell edq H^2}$	$C^{(2),(3),(4)}_{\ell equ H^2}$ $C^{*(2),(3),(4)}_{\ell equ H^2}$	$C^{(1),(2),(3),(4)}_{\ell equ H^2}$ $C^{*(1),(2),(3),(4)}_{\ell equ H^2}$

	C_{eq}	C_{eu}	C_{ed}	$C_{\ell edq}, C^*_{\ell edq}$	$C^{(1)}_{\ell equ}, C^{*(1)}_{\ell equ}$	$C^{(3)}_{\ell equ}, C^{*(3)}_{\ell equ}$
C_{He}	$C^{(1),(2)}_{e^2 q^2 H^2}$	$C_{e^2 u^2 H^2}$	$C_{e^2 d^2 H^2}$	$C^{(1),(2)}_{\ell edq H^2}$ $C^{*(1),(2)}_{\ell edq H^2}$	$C^{(1),(2),(3),(4)}_{\ell equ H^2}$ $C^{*(1),(2),(3),(4)}_{\ell equ H^2}$	$C^{(1),(2),(3),(4)}_{\ell equ H^2}$ $C^{*(1),(2),(3),(4)}_{\ell equ H^2}$

Table 6.7: Dimension eight operators generated via the diagrams of Figure 6.6d with pairs of two-lepton two-quark $4f_6$ and penguins P_6

where $\mathcal{O}^{ij}_{\ell e H^5} = (\bar{\ell}_i H e_j)(H^\dagger H)^2$, and each of $\mathcal{O}^{e\mu}_v$, $\mathcal{O}^{(1)e\mu}_v$, $\mathcal{O}^{(2)e\mu}_v$ vanishes, when the renormalizable EOM on singlet and doublet leptons $i(\not{D}\mu) - [y^*_e]_{i\mu}(H^\dagger \ell_i) = 0$, $i(\not{D}\ell_\mu) - [y_e]_{\mu i}(H e_i) = 0$ are satisfied. The off-shell counterterms are on-shell equivalent to $[y^*_e]_{i\mu}\mathcal{O}^{*ie}_{\ell e H^5} + [y_e]_{ie}\mathcal{O}^{i\mu}_{\ell e H^5}$, which is beyond $\mu \to e$ experimental reach. The resulting RGEs are obtained from Eq. (6.78) and (6.75), and read

$$16\pi^2 \dot{C}^{e\mu}_{e^2 H^4 D} = -C^{\tau\mu}_{eH} C^{*\tau e}_{eH} \tag{6.85}$$

$$16\pi^2 \dot{C}^{(1)e\mu}_{\ell^2 H^4 D} = \frac{1}{2} C^{*\mu\tau}_{eH} C^{e\tau}_{eH} \qquad 16\pi^2 \dot{C}^{(2)e\mu}_{\ell^2 H^4 D} = \frac{1}{4} C^{*\mu\tau}_{eH} C^{e\tau}_{eH} \tag{6.86}$$

where the dot on the dimension eight coefficients corresponds to $d/d\log M$.

6.3.2 Matching SMEFT onto the low energy EFT

In Table 6.5 of Section 6.2.3, we identified the relevant matching contributions to low energy $\mu \leftrightarrow e$ interactions from the double insertion of $\mu \to \tau \times \tau \to e$ dimension six SMEFT operators. At the matching scale m_W, the electroweak symmetry is spontaneously broken by the Higgs VEV, and the h, Z, W and t are removed from the low energy EFT. The matching is performed by identifying the matrix elements of a $\mu \to e$ process calculated in the theories above and below the matching scale, with the electroweak symmetry broken in both theories. As a result, products of $\tau \leftrightarrow l$ SMEFT operators can match onto $\mu \to e$ three and four point functions. The interesting diagrams are illustrated in Figure 6.7. When the Higgs doublet acquires a VEV, Yukawa operators contribute to the mass matrix

$$m_{e_i}\delta_{ij} = v\left([y_e]_{ij} - C^{ij}_{eH}\right) \tag{6.87}$$

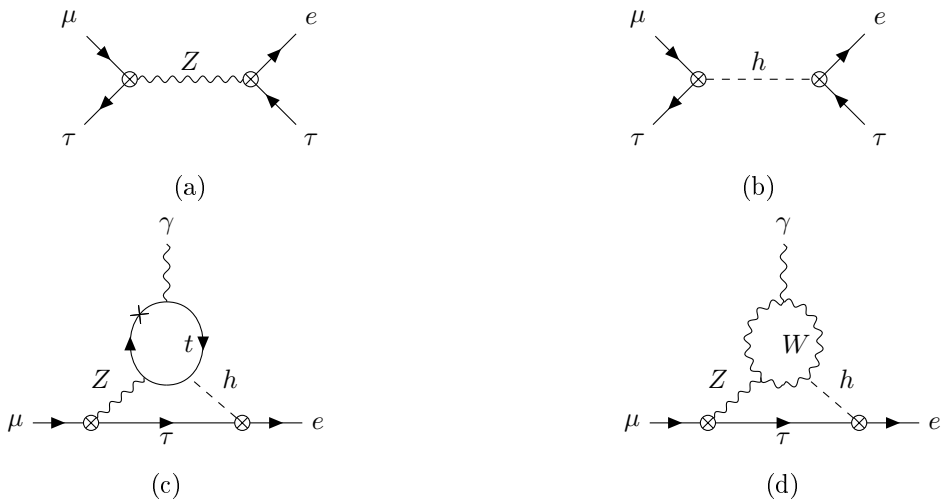

Figure 6.7: Diagrams matching pairs of dimension six $\tau \to l$ SMEFT operators onto low energy $\mu \to e$ operators.

and the h couplings

$$\begin{aligned} &-\frac{h}{\sqrt{2}}\bar{e}_i P_R e_j \left([y_e]_{ij} - 3C_{eH}^{ij}\right) + \text{h.c} = \\ &= -\frac{h}{\sqrt{2}}\bar{e}_i P_R e_j \left(\frac{m_{e_i}\delta_{ij}}{v} - 2C_{eH}^{ij}\right) + \text{h.c} \end{aligned} \tag{6.88}$$

of charged leptons with a different prefactor, such that h acquires LFV couplings in the lepton mass eigenstate basis.

The two-loop Barr-Zee diagrams (Figure 6.7c-6.7d) match to the dipole at tree level in the low energy EFT and correspond to a dimension 10 dipole in SMEFT. Therefore, the matching contribution should be independent of the renormalisation scheme in both EFTs, because $(\text{dim6})^2$ terms in the RGEs cannot generate a dimension 10 operator, and tree-level is scheme-independent. The lepton line is connected via Z and h exchange to a top or W loop, where the Z and h respectively couple to the lepton line via a penguin and an off-diagonal Yukawa operator. Such diagrams can be significant [357] (despite the two-loop suppression), because they are not suppressed by small Yukawa couplings. We estimate these diagrams from the results of [195], who calculated the Barr-Zee diagrams in the two Higgs Doublet Model (2HDM) with LFV couplings, where they provide the leading contribution to $\mu \to e\gamma$ (because the diagrams are not suppressed by y_μ). In the 2HDM results of [195], the Z-diagrams are suppressed (relative to γ diagrams) because the C-even dipole moment only couples the Z to the vector current of leptons, so there is a suppression of $(1 - 4\sin^2\theta_W) \lesssim 0.03$. However in our case, the Z-lepton vertex is a penguin operator with a flavour-changing coefficient that we wish to constrain, and so does not suffer from such SM factors.

The estimated contributions to the dipole coefficients are [358] :

$$C_{D,R} \simeq \frac{9e\alpha_e}{64\pi^3}\frac{v}{m_\mu}\left[C_{He}^{\tau\mu}C_{eH}^{e\tau} + \left(C_{H\ell}^{(1)e\tau} + C_{H\ell}^{(3)e\tau}\right)C_{eH}^{\tau\mu}\right]$$
$$C_{D,L} \simeq \frac{9e\alpha_e}{64\pi^3}\frac{v}{m_\mu}\left[C_{eH}^{*\tau e}\left(C_{H\ell}^{(1)\tau\mu} + C_{H\ell}^{(3)\tau\mu}\right) + C_{eH}^{*\mu\tau}C_{He}^{e\tau}\right] \tag{6.89}$$

A dipole is also generated at one-loop with a pair of penguin operators, which look like the flavor changing version of the electroweak correction to $(g-2)_\mu$ with a Z exchange. However, assuming the future limits on penguin coefficients shown in Table 6.2, the contribution is below $\mu \to e\gamma$ upcoming experimental sensitivity.

Four lepton $e\mu\tau\tau$ operators get matching contribution from tree-level diagrams with a Z, h exchange between penguin vertices or LFV Higgs boson couplings, as illustrated in the diagrams of Figure 6.7a and 6.7b. SMEFT $\tau-$LFV penguins and Yukawa corrections are matched at m_W onto low energy four lepton operator coefficients as follows

$$C_{T,RR}^{e\mu\tau\tau} = -\frac{1}{4}C_{eH}^{e\tau}C_{eH}^{\tau\mu}\frac{v^2}{m_h^2} \tag{6.90}$$
$$C_{T,LL}^{e\mu\tau\tau} = -\frac{1}{4}C_{eH}^{*\tau e}C_{eH}^{*\mu\tau}\frac{v^2}{m_h^2} \tag{6.91}$$
$$C_{S,RR}^{e\mu\tau\tau} = -C_{eH}^{e\tau}C_{eH}^{\tau\mu}\frac{v^2}{m_h^2} \tag{6.92}$$
$$C_{S,LL}^{e\mu\tau\tau} = -C_{eH}^{*\tau e}C_{eH}^{*\mu\tau}\frac{v^2}{m_h^2} \tag{6.93}$$
$$C_{S,RL}^{e\mu\tau\tau} = \frac{2g^2}{\cos^2\theta_W}\left(C_{He}^{\tau\mu}C_{H\ell}^{(1)e\tau} + C_{He}^{\tau\mu}C_{H\ell}^{(3)e\tau}\right)\frac{v^2}{M_Z^2} \tag{6.94}$$
$$C_{S,LR}^{e\mu\tau\tau} = \frac{2g^2}{\cos^2\theta_W}\left(C_{He}^{e\tau}C_{Hl}^{(1)\tau\mu} + C_{He}^{e\tau}C_{H\ell}^{(3)\tau\mu}\right)\frac{v^2}{M_Z^2} \tag{6.95}$$
$$C_{V,LL}^{e\mu\tau\tau} = -\frac{g^2}{\cos^2\theta_W}\Big(C_{H\ell}^{(1)e\tau}C_{H\ell}^{(1)\tau\mu} + C_{H\ell}^{(3)e\tau}C_{H\ell}^{(3)\tau\mu} + \\ + C_{H\ell}^{(1)e\tau}C_{H\ell}^{(3)\tau\mu} + C_{H\ell}^{(1)\tau\mu}C_{H\ell}^{(3)e\tau}\Big)\frac{v^2}{M_Z^2} \tag{6.96}$$
$$C_{V,RR}^{e\mu\tau\tau} = -\frac{g^2}{\cos^2\theta_W}C_{He}^{e\tau}C_{He}^{\tau\mu}\frac{v^2}{M_Z^2} \tag{6.97}$$

where the low energy EFT basis is in the notation of [322] (see section 4.3.2 of Chapter 4). We report for completeness the matching conditions for $e\mu\tau\tau$ vector coefficients, although $\mu \to e$ observables are not sensitive to them.

6.4 Phenomenological implications

This section gives limits on pairs of $\tau \leftrightarrow l$ coefficients from their contribution to $\mu \to e$ processes, and we discuss some examples where the upcoming sensitivity of $\mu \to e$ observables is complementary to the future direct limits from $\tau \to l$ processes. Section 6.4.1 considers $\mu \leftrightarrow e$ amplitudes generated

by the fish diagrams of Figure 6.6e-6.6f, and compares with the limits arising from $B \to \tau$ LFV decays (summarised in Appendix D.3). An example of $\mu \leftrightarrow e$ from matching out the Higgs is given in Section 6.4.2, where we compare the sensitivity of $\mu \to e$ processes to $h \to \tau^{\pm} l^{\mp}$ decays. Appendix D.4 gives results for the cases where the $\mu \leftrightarrow e$ sensitivity is marginal or uninteresting.

The limits we quote apply to pairs of $\tau \leftrightarrow l$ coefficients at a New Physics scale $\Lambda_{\rm NP} = 4$ TeV. The NP scale is relevant because it appears in the logarithms of the RG running. We assume that dimension six $\tau \leftrightarrow l$ operators are generated at $\Lambda_{\rm NP} = 4$ TeV and contribute to $\mu \to e$ observables in two ways: first, as discussed in section 6.3.1, via Renormalisation Group mixing into dimension eight $\mu \to e$ operators in SMEFT between $\Lambda_{\rm NP}$ and m_W, and second via the matching at m_W of combined dimension six $\tau \leftrightarrow l$ operators onto $\mu \to e$ operators as calculated in section 6.3.2. The running is described with the solution of the RGEs given in Eq. (6.10), then the dimension eight $\mu \to e$ operators are matched onto the low energy EFT as given in Appendix C.2. The sensitivity of current $\mu \leftrightarrow e$ experiments to coefficients at m_W is tabulated in [322]; we extrapolate these limits to the future experimental reaches given in table 6.1, in order to determine the experimental sensitivities of $\mu \to e$ processes to the product of $\tau \to l$ operator coefficients. In most cases, we just rescale the sensitivities of [322]. But for the limits from $\mu A \to eA$ on vector operators with quarks, we recalculate the sensitivities on an Aluminium target, as will be used by upcoming experiments. The current bounds are from Gold targets, which have more neutrons than protons, whereas Aluminium contains equal numbers of protons and neutrons (u and d quarks). So Gold has comparable sensitivity to $(\bar{e}\gamma\mu)(\bar{u}\gamma u + \bar{d}\gamma d)$ and $(\bar{e}\gamma\mu)(\bar{u}\gamma u - \bar{d}\gamma d)$, whereas the sensitivity of Aluminium to $(\bar{e}\gamma\mu)(\bar{u}\gamma u - \bar{d}\gamma d)$ is suppressed by a loop.

Note that we distinguish *sensitivities* from *constraints* or *bounds*. But we use *limits* to mean either. A constraint identifies the region of parameter space where the coefficients must sit, while a sensitivity represents the smallest absolute value that can be experimentally detected. The notion of sensitivity is particularly useful when the number of parameters is larger than the number of observables, so that exclusion bounds on single coefficients cannot be inferred. A coefficient smaller than the sensitivity escapes experimental detection but larger values can also escape detection if accidental cancellations occur. In practise, in this manuscript we obtain sensitivities, because we consider one non-zero pair of $\tau \leftrightarrow l$ operators at a time and compute the contribution to $\mu \to e$ observables.

Our results are interesting, because they show that upcoming $\mu \leftrightarrow e$ experiments could be sensitive to $\tau \leftrightarrow l$ coefficients beyond the reach of $\tau \leftrightarrow l$ searches. We obtain experimental sensitivities $B_{\mu\leftrightarrow e}$ to the product of coefficients

$$\left| C^{[6]\tau\mu} C^{[6]e\tau} \right| \lesssim B_{\mu\leftrightarrow e}. \tag{6.98}$$

The same coefficients $C^{[6]\tau\mu}$, $C^{[6]e\tau}$ might contribute to constrained $\tau \leftrightarrow l$ processes and be respectively subjected to the sensitivity "limits" $B_{\tau\to\mu}$, $B_{\tau\to e}$ imposed by direct τLFV searches. In the $C^{[6]\tau\mu} - C^{[6]e\tau}$ plane, this identifies an ellipse

$$\frac{\left|C^{[6]\tau\mu}\right|^2}{B^2_{\tau\leftrightarrow\mu}} + \frac{\left|C^{[6]e\tau}\right|^2}{B^2_{\tau\leftrightarrow e}} \lesssim 1 \tag{6.99}$$

that encloses the coefficient space to which $\tau \leftrightarrow l$ observables are not sensitive. On the other hand, $\mu \to e$ searches can detect coefficients in the region bounded by the hyperbola in Eq. (6.98). If the

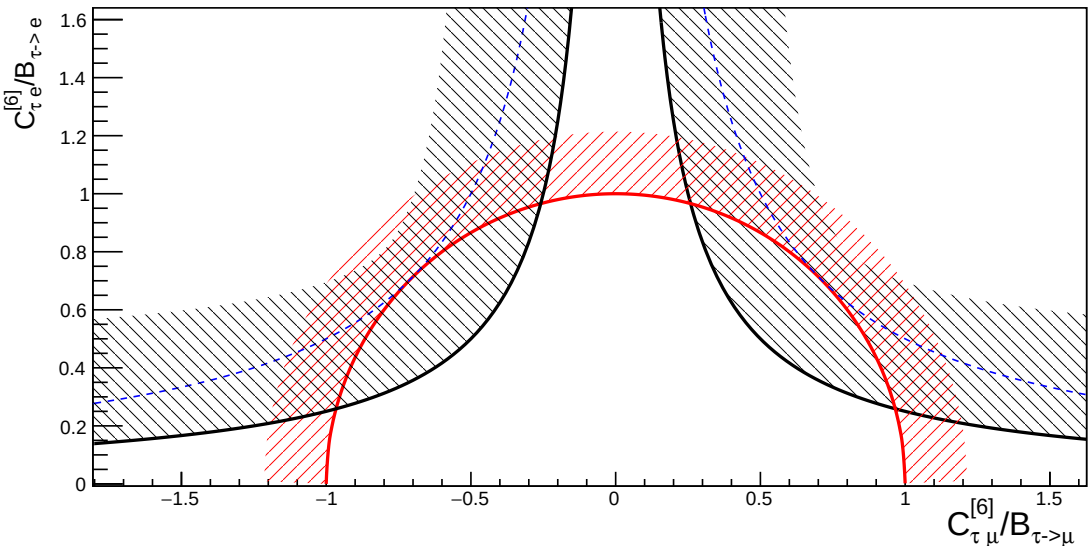

Figure 6.8: The plot shows the parameter space probed by direct $\tau \leftrightarrow l$ searches and by $\mu \to e$ observables, in the $C_{\tau\mu} - C_{\tau e}$ plane. The direct searches can probe the region outside the ellipse of Eq. (6.99) (which correspond to the red circle when the Wilson coefficients are normalized by the sensitivities $B_{\tau\leftrightarrow l}$ of the $\tau \leftrightarrow l$ processes), while $\mu \to e$ is sensitive to the area above the hyperbolae, as defined in Eq. (6.98). The blue dashed hyperbolae correspond to the boundary condition $B_{\mu\leftrightarrow e}/(B_{\tau\leftrightarrow e}B_{\tau\leftrightarrow\mu}) = 1/2$, while the black ones satisfies $B_{\mu\leftrightarrow e}/(B_{\tau\leftrightarrow e}B_{\tau\leftrightarrow\mu}) < 1/2$. In this second case $\mu \to e$ searches are able to probe parameter space missed by $\tau \leftrightarrow l$ observables.

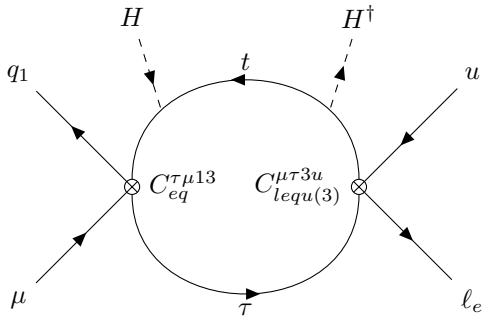

Figure 6.9: The operators $C_{eq}^{e\tau 31}, C_{\ell equ}^{(3)e\tau 31}$ are inserted in the left diagram and mix into the dimension eight $\mu \to e$ scalar/tensor operators $\mathcal{O}_{\ell equH^2}^{(1),(2),(3),(4)}$ of Eq.s (6.47)-(6.49).

following inequality is satisfied

$$B_{\mu\leftrightarrow e} < \frac{B_{\tau\leftrightarrow e} B_{\tau\leftrightarrow\mu}}{2} \tag{6.100}$$

the hyperbola enters the ellipse and $\mu \to e$ processes are able to probe a region of parameter space that eludes the direct $\tau \leftrightarrow l$ searches. This is illustrated in Figure 6.8. In the subsequent sections we discuss examples where Eq. (6.100) is satisfied considering the upcoming experimental sensitivities on $\mu \to e$ and $\tau \to l$ processes.

6.4.1 Fish diagrams with internal top quarks

In this section, we discuss some examples where the sensitivity of $\mu \to e$ conversion to some $\tau \leftrightarrow l$ coefficients is complementary to B decays. The "fish" diagrams that mix four fermion $\tau \leftrightarrow l$ interactions into dimension eight $\mu \to e$ operators are illustrated in Figure 6.6e-6.6f of section 6.3.1. In these diagrams, one or two Higgs are attached to a heavy top internal line, so the $\tau \leftrightarrow l$ operators that our calculation can probe contain one quark doublet or up-type singlet in the third generation. In the former case, the operator can contribute to the LFV decays of the B mesons with a τ (ν_τ) in the final state. Recall that the quark doublets are in the $u-$basis, so these operators also match via CKM mixing onto low energy contact interactions with $d-$type quarks of the first and second generations. For the operators considered here, we checked that the limits on their coefficients arising from CKM-suppressed contributions to τ LFV processes with d and s quarks, such as $K^\pm \to l^\pm \nu$ and τ hadron decays, are not competitive with the limits inferred from B decays.

The following subsections are organized by the different $\mu \to e$ interactions that the $\tau \leftrightarrow l$ operators mix into.

6.4.1.1 $\mu \to e$ scalars

Consider, for example, the operators $\mathcal{O}_{eq}^{\tau\mu 13} = (\bar{\tau}\gamma\mu)(\bar{q}_1\gamma q_3)$ and $\mathcal{O}_{\ell equ}^{(3)e\tau 31} = (\bar{\ell}_e\sigma\tau)(\bar{q}_3\sigma u)$, which mix into the $\mu \to e$ scalar and tensor dimension eight operators $\mathcal{O}_{\ell equH^2}^{(1),(2),(3),(4)}$ of Eq.s (6.47)-(6.49) (with up quarks) via the diagram of Figure 6.9. These match at m_W onto scalar and tensor

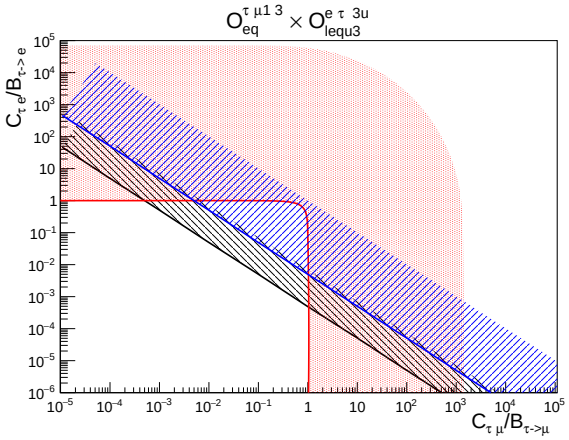

(a) Parameter space probed by $\mu \to e$ conversion (straight lines) and LFV B decays (box), in the $C_{eq}^{\tau\mu 13} - C_{\ell equ}^{(3)e\tau 3u}$ plane. The blue line correspond to the current experimental reach, while in the black one we assume $Br(\mu Al \to eAl) \sim 10^{-16}$. In both cases, the $\mu \to e$ hyperbole enter the ellipse beyond the reach of B decays.

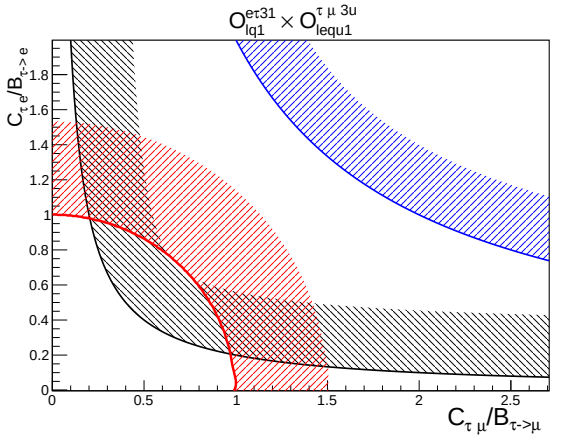

(b) Similar to Figure 6.10a, in the $C_{\ell q}^{(1)e\tau 13} - C_{\ell equ}^{(1)\tau\mu 3u}$ plane. For this pair of operators, $\mu \to e$ will have a better sensitivity to the coefficient product than B decays with the upcoming experimental improvement.

Figure 6.10

operators in the low energy EFT, with the following coefficients[4]

$$C_{S,RR}^{uu}(m_W) = \frac{3}{2\pi^2}\frac{m_t^2}{v^2} C_{eq}^{\tau\mu 13} C_{\ell equ}^{(3)e\tau 3u} \log\left(\frac{m_W}{\Lambda_{\rm NP}}\right) \tag{6.101}$$

$$C_{T,RR}^{uu}(m_W) = \frac{3}{8\pi^2}\frac{m_t^2}{v^2} C_{eq}^{\tau\mu 13} C_{\ell equ}^{(3)e\tau 3u} \log\left(\frac{m_W}{\Lambda_{\rm NP}}\right) \tag{6.102}$$

where $m_t \sim v$ is the top quark mass and the SMEFT operator coefficients are at $\Lambda_{\rm NP}$.

[4] This simple solution does not include the QCD running of tensors and scalars from $\Lambda_{\rm NP} \to m_W$. Since QCD does not renormalize vector coefficients, this QCD running is analogous to the rescaling of QED tensor↔scalar mixing below m_W [322],and can be estimated to be a $\lesssim 10\%$ effect. It is therefore neglected.

Scalar operators with up quarks contribute at tree-level to $\mu \to e$ conversion in nuclei (see eg [351]), where a muon is stopped in a target, captured by a nucleus, and converts into an electron in the presence of LFV interaction with nucleons. Scalar interactions of first generation quarks match onto nucleon operators with large matching coefficients, and the rate for spin-independent conversion is enhanced by the atomic number of the target, giving a good current sensitivity to scalar coefficients $C_S^{uu} \lesssim 10^{-8}$ [322]. Including the impressive improvement in sensitivity promised by upcoming experiments, $Br(\mu Au \to eAu) \lesssim 10^{-12} \to Br(\mu Al \to eAl) \sim 10^{-16}$, $\mu \to e$ conversion will be able to probe scalar coefficients as small as $C_S^{uu} \sim 10^{-10}$.

Tensors with light-quarks contribute to the spin-independent rate via their QED mixing into scalars, which introduces a $\sim 1/10$ suppression. For this reason, the tensor of Eq. (6.102) contribute to the $\mu \to e$ conversion rate as $C_T \sim C_S/40$ and is therefore neglected. So the upcoming $\mu \to e$ conversion experiments can set the following limit (sensitivity) on the product of the coefficients at $\Lambda_{\rm NP} = 4$ TeV

$$C_{eq}^{\tau\mu 13} \times C_{\ell equ}^{(3)e\tau 31} \lesssim 1.5 \times 10^{-10} \tag{6.103}$$

The two $\tau \leftrightarrow l$ operators could also induce the leptonic decays of B mesons $B_d^0 \to \mu^\pm \tau^\mp$ and $B^+ \to \overline{\tau}\nu$. The current 95%C.L. experimental constraints on these processes lead to the following limits on the coefficients

$$\begin{aligned} Br(B_d^0 \to \mu^\pm \tau^\mp) < 1.4 \times 10^{-5} \;\; &\to \;\; C_{eq}^{\tau\mu 13} \lesssim 1.4 \times 10^{-3} \\ Br(B^+ \to \overline{\tau}\nu) = 1.6 \times 10^{-4} \;\; &\to \;\; C_{lequ}^{(3)e\tau 31} \lesssim 2.2 \times 10^{-3}. \end{aligned} \tag{6.104}$$

These limits were obtained with the public code Flavio [360] and analytically, and are discussed in more detail in Appendix D.3, which reviews the sensitivity of B decays to interesting operator coefficients.

In order to compare future B decay sensitivities to the future reach of $\mu \to e$ conversion, we suppose that Belle II could improve the sensitivities to B decays by an order of magnitude, so the limits of Eq. (6.104) on the Wilson coefficients will get $\sim \sqrt{10}$ better. Comparing the product of the upcoming B sensitivities with the limit in Eq. (6.103) that arise from future $\mu \to e$ conversion gives (the (f) superscript stands for "future")

$$B_{\mu\leftrightarrow e}^{(f)} = (B_{\tau\leftrightarrow e}^{(f)} B_{\tau\leftrightarrow\mu}^{(f)}) \times (5 \times 10^{-4}) \tag{6.105}$$

which satisfies the condition of Eq. (6.100). We fall in the scenario depicted in Figure 6.10a, where $\mu \to e$ probes a region inside the ellipse, beyond the reach of $B \to \tau$ direct searches. Notice that the hyperbola of the current $\mu \to e$ conversion results already enters the ellipse of the $B \to \tau$ LFV decays (with the current sensitivities $B_{\mu\leftrightarrow e}^{(c)}/(B_{\tau\leftrightarrow e}^{(c)} B_{\tau\leftrightarrow\mu}^{(c)}) \sim 5 \times 10^{-3}$). This is because tensors contribute to the B decays rate via the one-loop QED mixing to scalars, while the (dimension six)$^2 \to$ (dimension eight) mixing benefits from a large anomalous dimension.

The pair of $\tau \leftrightarrow l$ dimension six operators $C_{\ell q}^{(1)e\tau 13} C_{\ell equ}^{(1)\tau\mu 3u}$ similarly mixes into the dimension eight $\mu \to e$ scalars with a singlet u. In this case, B decays are currently more sensitive than $\mu \to e$ processes to the product of the coefficients ($B_{\mu\leftrightarrow e}^{(c)}/(B_{\tau\leftrightarrow e}^{(c)} B_{\tau\leftrightarrow\mu}^{(c)}) \sim 2$). However, in the next generation of experiments, the sensitivity ratio will be reduced by one order of magnitude to $B_{\mu\leftrightarrow e}^{(f)}/(B_{\tau\leftrightarrow e}^{(f)} B_{\tau\leftrightarrow\mu}^{(f)}) \sim 0.2$, allowing the $\mu \to e$ conversion hyperbola to enter the ellipse of the direct $\tau \leftrightarrow l$ searches (see Figure 6.10b).

In Tables 6.8 and 6.9, we compare the sensitivities of $\tau \leftrightarrow l$ and $\mu \to e$ processes to the product of several operators that mix into scalars with first generation quarks, via diagrams similar to Figure 6.9. Note that the pairs in the table feature an electron doublet and a singlet muon, but opposite chiralities are also possible. For instance, $C_{eq}^{\tau\mu 13} C_{\ell equ}^{(1)e\tau 3u}$ mix into $C_{\ell equH^2}^{(1),(2)e\mu 1u}$ while $C_{eq}^{e\tau 31} C_{\ell equ}^{*(1)\mu\tau 3u}$ contributes to the RGEs of $C_{\ell equH^2}^{*(1),(2)\mu e 1u}$. Although the anomalous dimensions are the same (and so are the $\mu \to e$ sensitivities), the dimension six operator that was $\tau \leftrightarrow e$ is now $\tau \leftrightarrow \mu$ and vice-versa, which might lead to slightly different direct limits on the $\tau \leftrightarrow l$ interactions. In the above-example, the branching ratios sensitivities of the B_d^0 decay into $\tau e, \tau\mu$ differ by a factor ~ 3, and as a result the limits on the vector coefficients $C_{eq}^{e\tau 13}, C_{eq}^{\tau\mu 31}$ is $\sim \sqrt{3}$ different. We do not present the tables for the pairs with exchanged $\mu \leftrightarrow e$, as the marginally different numbers do not modify our conclusions.

coefficients	$B_{\tau\leftrightarrow e}^{(c)} B_{\tau\leftrightarrow\mu}^{(c)}$	$B_{\mu\to e}^{(f)}$
$C_{\ell u}^{e\tau tu} C_{\ell equ}^{(1)\tau\mu 1t}$	—×—	2×10^{-9}
$C_{\ell u}^{e\tau tu} C_{\ell equ}^{(3)\tau\mu 1t}$	—×—	1.5×10^{-10}
$C_{eq}^{\tau\mu 13} C_{\ell equ}^{(1)e\tau 3u}$	$1.5 \times 10^{-3}(c) \times 4.3 \times 10^{-4}(c)$	2×10^{-9}
$C_{eq}^{\tau\mu 13} C_{\ell equ}^{(3)e\tau 3u}$	$1.5 \times 10^{-3}(c) \times 2.4 \times 10^{-3}(c)$	1.5×10^{-10}
$C_{eu}^{\tau\mu tu} C_{\ell equ}^{(1)e\tau 1t}$	—× —	2×10^{-9}
$C_{eu}^{\tau\mu tu} C_{\ell equ}^{(3)e\tau 1t}$	—× —	1.5×10^{-10}
$C_{\ell q}^{(1)e\tau 13} C_{\ell equ}^{(1)\tau\mu 3u}$	$2.3 \times 10^{-3}(c) \times 4.3 \times 10^{-5}(c)$	2×10^{-9}
$C_{\ell q}^{(3)e\tau 13} C_{\ell equ}^{(1)\tau\mu 3u}$	$2.3 \times 10^{-3}(c) \times 4.3 \times 10^{-5}(c)$	2×10^{-9}
$C_{\ell q}^{(1)e\tau 13} C_{\ell equ}^{(3)\tau\mu 3u}$	$2.3 \times 10^{-3}(c) \times 1.8 \times 10^{-4}(c)$	1.5×10^{-10}
$C_{\ell q}^{(3)e\tau 13} C_{\ell equ}^{(3)\tau\mu 3u}$	$2.3 \times 10^{-3}(c) \times 1.8 \times 10^{-4}(c)$	1.5×10^{-10}

Table 6.8: The product of current (c) direct limits $B_{\tau\leftrightarrow e}^{(c)} B_{\tau\leftrightarrow\mu}^{(c)}$ on pairs of coefficients that mix to a $\mu \to e$ dimension eight scalar operator with a singlet u quark (see Eq. (6.47)), upon which applies the limit $B_{\mu\to e}^{(f)}$ arising from future $\mu \to e$ conversion ($Br(\mu Al \to eAl) \sim 10^{-16}$). The "limits" are on coefficients at $\Lambda_{\rm NP} \sim 4$ TeV. Details on the limits that apply to operators with permuted indices are given in the text below Eq. (6.105). To compare $B_{\mu\to e}^{(f)}$ with the future sensitivity of direct $\tau \leftrightarrow l$ searches, the product $B_{\tau\leftrightarrow e}^{(c)} B_{\tau\leftrightarrow\mu}^{(c)}$ should be divided by 10: $B_{\tau\leftrightarrow e}^{(f)} B_{\tau\leftrightarrow\mu}^{(f)} \sim B_{\tau\leftrightarrow e}^{(c)} B_{\tau\leftrightarrow\mu}^{(c)}/10$.

coefficients	$B_{\tau\leftrightarrow e}^{(c)} B_{\tau\leftrightarrow\mu}^{(c)}$	$B_{\mu\to e}^{(f)}$
$C_{\ell q}^{(3)e\tau 31} C_{\ell edq}^{\tau\mu d3}$	$2.3 \times 10^{-3}(c) \times 2.2 \times 10^{-4}(c)$	1×10^{-9}
$C_{\ell q}^{(3)\tau\mu 13} (C_{\ell edq}^{\tau e d3})^*$	$1.5 \times 10^{-3}(c) \times 3.4 \times 10^{-4}(c)$	1×10^{-9}

Table 6.9: Similar to table 6.8, for dimension eight scalar $\mu \to e$ operators involving a singlet d quark (see Eq. (6.45)). The limit $B_{\mu\to e}^{(f)}$ arises from $\mu \to e$ conversion ($Br(\mu Al \to eAl) \sim 10^{-16}$).

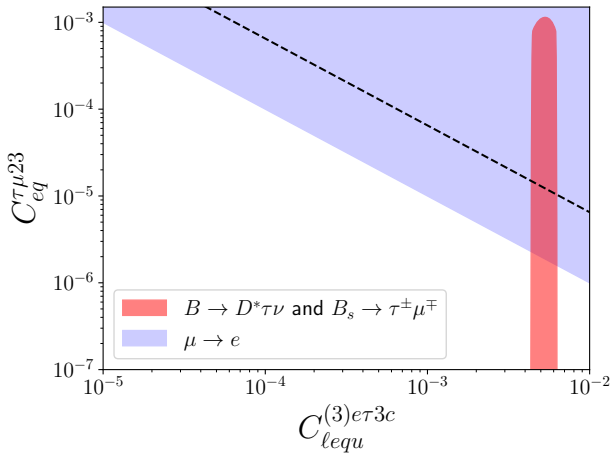

Figure 6.11: The plot shows the parameter space probed by B LFV decays and by future $\mu \to e\gamma$, in the $C_{\ell equ}^{(3)e\tau 3c} - C_{eq}^{\tau\mu 23}$ plane. The ellipse is centered to the best-fit value of $C_{\ell equ}^{(3)e\tau 3c}$ that can explain the R_{D^*} anomaly (see text for details). Non-observation of $\mu \to e\gamma$ can give a limit on $C_{eq}^{\tau\mu 23}$ (assuming only this pair to be non-zero). The dashed line correspond to the current MEG upper bound $Br(\mu \to e\gamma) < 4 \times 10^{-13}$.

6.4.1.2 $\mu \to e$ tensors with heavy quarks

The fish diagrams that generated scalar and tensor $\mu \to e$ operators on u quarks, arise also with external c quarks. Although the sensitivity of $\mu \to e$ conversion to charm scalars is insufficient for our purposes, $\mu \to e\gamma$ has interesting sensitivity to the charm tensors, because their mixing to the dipole is enhanced $\propto m_c/m_\mu$. The pairs of $\tau \leftrightarrow l$ operators that mix to $\mu \leftrightarrow e$ tensors with external charms, and the sensitivities of B decays and $Br(\mu \to e\gamma) < 10^{-14}$ are summarized in Table 6.10.

Leptonic and semi-leptonic B decays have recently attracted attention due to several anomalies with respect to SM expectations, see e.g. Ref. [361]. Our LFV operators could potentially address the anomalies in "charged current" b transitions (such as $B^+ \to \tau^+\nu$), when the discrepancy require a enhanced rates (because LFV operator cannot interfere destructively with the SM). An example is the SM expectation for $R^{\rm SM}_{D^*\tau/l} \equiv Br(B \to D^*\tau\bar{\nu})/Br(B \to D^* l\bar{\nu}) \sim 0.24$ [360] which is smaller than the observed value $R^{exp}_{D^*\tau/l} \sim 0.3$ [362]. We can fit the difference by enhancing the branching fraction in the numerator with the tensor operator $C_{\ell equ}^{(3)l\tau 3c}$. The latter can be paired with the vector $C_{eq}^{\tau\mu 23}$ to mix into a dimension eight tensor with external charms, to which $Br(\mu \to e\gamma) \sim 10^{-14}$ has the sensitivity $B_{\mu\to e}$ reported in Table 6.10. In the $C_{\ell equ}^{(3)e\tau 3c} - C_{eq}^{\tau\mu 23}$ plane, the ellipse is now shifted to the right and centered on the best-fit value of $C_{\ell equ}^{(3)e\tau 3c}$ (see Figure 6.11). In the simplified scenario where the discrepancy $\left|R^{\rm SM}_{D^*\tau/e} - R^{\rm exp}_{D^*\tau/e}\right|$ is fully explained by the presence of the $\tau \leftrightarrow e$ tensor, non-observation $\mu \to e\gamma$ signal in future experiments would make it unlikely for the coefficients to occupy the portion of the red ellipse overlaping the blue region.

Table 6.11 summarises the case of $\mu \leftrightarrow e$ operator with external top quarks. The mixing of tensors with a top bilinear into the dipole is enhanced by the ratio m_t/m_μ, so the upcoming $\mu \to e\gamma$ experiments can probe dimension 6 coefficients $C_T^{[6]e\mu tt} \gtrsim 5 \times 10^{-12}$. We suppose that the SMEFT

mixing of dimension eight tensors into the dimension eight dipoles is comparable to the dimension six mixing [356]. This impressive sensitivity explains why the diagrams of Figure 6.6f with external top legs are interesting regardless of the y_τ Yukawa suppression.

The SMEFT $\tau \leftrightarrow l$ operators that are inserted in those diagrams contain a flavour diagonal quark pair in the third generation. Vectors with tops contribute to the rate of $\tau \to 3l$ via one-loop penguin diagrams, while the dimension six tensors contribute to $\tau \to l\gamma$ via the above-discussed mixing into the $\tau \leftrightarrow l$ dipole. Tensors are not considered in our tables, because $\tau \to l\gamma$ has already an excellent sensitivity to the operator coefficients. In Table 6.11 the direct "limits" on the product of $\tau \leftrightarrow l$ dimension six vectors arising from $\tau \to 3l$ searches are compared with the sensitivity of $Br(\mu \to e\gamma) < 10^{-14}$.

coefficients	$B^{(c)}_{\tau\leftrightarrow e}B^{(c)}_{\tau\leftrightarrow\mu}$	$B^{(f)}_{\mu\to e}$
$C^{e\tau tc}_{\ell u}C^{(1)\tau\mu 2t}_{\ell equ}$	—×—	1.2×10^{-7}
$C^{e\tau tc}_{\ell u}C^{(3)\tau\mu 2t}_{\ell equ}$	—×—	1×10^{-8}
$C^{\tau\mu 23}_{eq}C^{(1)e\tau 3c}_{\ell equ}$	$2.3\times10^{-3}(c)\times1.0\times10^{-2}(c)$	1.2×10^{-7}
$C^{\tau\mu 23}_{eq}C^{(3)e\tau 3c}_{\ell equ}$	$2.3\times10^{-3}(c)\times5.0\times10^{-3}(c)$	1×10^{-8}
$C^{\tau\mu tc}_{eu}C^{(1)e\tau 2t}_{\ell equ}$	—× —	1.2×10^{-7}
$C^{\tau\mu tc}_{eu}C^{(3)e\tau 2t}_{\ell equ}$	—× —	1×10^{-8}
$C^{(1)e\tau 23}_{\ell q}C^{(1)\tau\mu 3c}_{\ell equ}$	$2.3\times10^{-3}(c)\times9.0\times10^{-3}(c)$	1.2×10^{-7}
$C^{(3)e\tau 23}_{\ell q}C^{(1)\tau\mu 3c}_{\ell equ}$	$2.3\times10^{-3}(c)\times9.0\times10^{-3}(c)$	1×10^{-7}
$C^{(1)e\tau 23}_{\ell q}C^{(3)\tau\mu 3c}_{\ell equ}$	$2.3\times10^{-3}(c)\times6.4\times10^{-3}(c)$	1.2×10^{-7}
$C^{(3)e\tau 23}_{\ell q}C^{(3)\tau\mu 3c}_{\ell equ}$	$2.3\times10^{-3}(c)\times6.4\times10^{-3}(c)$	1×10^{-9}

Table 6.10: Similar to table 6.8, for $\mu \to e$ dimension eight tensor operators (see Eq. (6.49)) with a c quark bilinear. The sensitivity $B^{(f)}_{\mu\to e}$ arises from $\mu \to e\gamma$ with a branching ratio $Br(\mu \to e\gamma) \sim 10^{-14}$. The "limits" are on coefficients at $\Lambda_{\rm NP} \sim 4$ TeV.

coefficients	$B^{(c)}_{\tau\leftrightarrow e}B^{(c)}_{\tau\leftrightarrow\mu}$	$B^{(f)}_{\mu\to e}$
$C^{e\tau tt}_{\ell u}C^{\tau\mu 33}_{eq}$	$1.0\times10^{-2}(c)\times2.0\times10^{-2}(c)$	1.0×10^{-6}
$C^{(3)e\tau 33}_{\ell q}C^{\tau\mu tt}_{eu}$	$4.5\times10^{-3}(c)\times1.0\times10^{-2}(c)$	1.0×10^{-6}
$C^{(1)e\tau 33}_{\ell q}C^{\tau\mu tt}_{eu}$	$4.0\times10^{-2}(c)\times1.0\times10^{-2}(c)$	1.0×10^{-6}

Table 6.11: Similar to table 8, with the product of (current) direct limits $B^{(c)}_{\tau\leftrightarrow e}B^{(c)}_{\tau\leftrightarrow\mu}$ on pairs of $\tau \leftrightarrow l$ coefficients that mix to a $\mu \to e$ dimension eight tensor operator (see Eq. (6.49)) with two top quarks, upon which applies the limit $B_{\mu\to e}$. All the limits apply to the coefficients at $\Lambda_{\rm NP} \sim 4$ TeV. The limit $B^{(f)}_{\mu\to e}$ arises from $\mu \to e\gamma$ ($Br(\mu \to e\gamma) < 10^{-14}$), due to the large mixing of the top-tensor to the dipole, while the limits $B^{(c)}_{\tau\leftrightarrow l}$ are from the current upper limits on $Br(\tau \to 3l)$ given in Table 6.1. Future limits $B^{(f)}_{\tau\leftrightarrow e}B^{(f)}_{\tau\leftrightarrow\mu}$ are $\sim B^{(c)}_{\tau\leftrightarrow e}B^{(c)}_{\tau\leftrightarrow\mu}/10$.

6.4.1.3 $\mu \to e$ vectors

The remaining fish diagrams give mixing of two dimension six $\tau \leftrightarrow l$ SMEFT operators into dimension eight $\mu \to e$ vectors with first generation quarks. The sensitivities of $\mu \to e$ conversion and B decays on the product of the operator coefficients are summarized in Table 6.12 for lepton singlets and in Table 6.13 for lepton doublets. (The $\mu \to e$ conversion estimates assume an Aluminium target — see the beginning of Section 6.4.)

coefficients	$B^{(c)}_{\tau\leftrightarrow e}B^{(c)}_{\tau\leftrightarrow\mu}$	$B^{(f)}_{\mu\to e}$
$C^{e\tau 31}_{eq}C^{\tau\mu 13}_{eq}$	$2.3\times10^{-3}(c)\times1.5\times10^{-3}(c)$	2.5×10^{-9}
$C^{e\tau 13}_{eq}C^{\tau\mu 31}_{eq}$	$2.3\times10^{-3}(c)\times1.5\times10^{-3}(c)$	1×10^{-8}
$C^{e\tau tu}_{eu}C^{\tau\mu ut}_{eu}$	—×—	2.5×10^{-9}
$C^{e\tau ut}_{eu}C^{\tau\mu tu}_{eu}$	—×—	2.5×10^{-9}
$(C^{\tau ed3}_{\ell edq})^*C^{\tau\mu d3}_{\ell edq}$	$3.4\times10^{-4}(c)\times2.2\times10^{-4}(c)$	4×10^{-8}
$(C^{(1)\tau e1t}_{\ell equ})^*C^{(1)\tau\mu 1t}_{\ell equ}$	—×—	2×10^{-8}
$(C^{(1)\tau e3u}_{\ell equ})^*C^{(1)\tau\mu 3u}_{\ell equ}$	$5.8\times10^{-5}(c)\times4.3\times10^{-5}(c)$	4×10^{-8}
$(C^{(3)\tau e1t}_{\ell equ})^*C^{(3)\tau\mu 1t}_{\ell equ}$	—×—	1×10^{-10}
$(C^{(3)\tau e3u}_{\ell equ})^*C^{(3)\tau\mu 3u}_{\ell equ}$	$2.4\times10^{-4}(c)\times2.4\times10^{-4}(c)$	2.5×10^{-10}
$(C^{(1)\tau e1t}_{\ell equ})^*C^{(3)\tau\mu 1t}_{\ell equ}$	—×—	2×10^{-9}
$(C^{(3)\tau e1t}_{\ell equ})^*C^{(1)\tau\mu 1t}_{\ell equ}$	—×—	2×10^{-9}
$(C^{(1)\tau e3u}_{\ell equ})^*C^{(3)\tau\mu 3u}_{\ell equ}$	$5.8\times10^{-5}(c)\times2.4\times10^{-4}(c)$	4×10^{-9}
$(C^{(3)\tau e3u}_{\ell equ})^*C^{(1)\tau\mu 3u}_{\ell equ}$	$2.4\times10^{-4}(c)\times4.3\times10^{-5}(c)$	4×10^{-9}

Table 6.12: Similar to tables 6.8, for dimension eight $\mu \to e$ vector operators with SU(2) singlet leptons (see Eq.s (6.40)-(6.42)). .

coefficients	$B^{(c)}_{\tau\leftrightarrow e} B^{(c)}_{\tau\leftrightarrow \mu}$	$B^{(f)}_{\mu\to e}$
$C^{(1)e\tau 31}_{\ell q} C^{(1)\tau\mu 13}_{\ell q}$	$2.3\times10^{-3}(c)\times 1.5\times10^{-3}(c)$	1×10^{-8}
$C^{(1)e\tau 13}_{\ell q} C^{(1)\tau\mu 31}_{\ell q}$	$2.3\times10^{-3}(c)\times 1.5\times10^{-3}(c)$	2.5×10^{-9}
$C^{(3)e\tau 31}_{\ell q} C^{(3)\tau\mu 13}_{\ell q}$	$2.3\times10^{-3}(c)\times 1.5\times10^{-3}(c)$	2×10^{-9}
$C^{(3)e\tau 13}_{\ell q} C^{(3)\tau\mu 31}_{\ell q}$	$2.3\times10^{-3}(c)\times 1.5\times10^{-3}(c)$	2.5×10^{-9}
$C^{(3)e\tau 13}_{\ell q} C^{(1)\tau\mu 31}_{\ell q}$	$2.3\times10^{-3}(c)\times 1.5\times10^{-3}(c)$	2.5×10^{-9}
$C^{(1)e\tau 13}_{\ell q} C^{(3)\tau\mu 31}_{\ell q}$	$2.3\times10^{-3}(c)\times 1.5\times10^{-3}(c)$	2.5×10^{-9}
$C^{(3)e\tau 31}_{\ell q} C^{(1)\tau\mu 13}_{\ell q}$	$2.3\times10^{-3}(c)\times 1.5\times10^{-3}(c)$	1×10^{-8}
$C^{(1)e\tau 31}_{\ell q} C^{(3)\tau\mu 13}_{\ell q}$	$2.3\times10^{-3}(c)\times 1.5\times10^{-3}(c)$	1×10^{-8}
$C^{e\tau ut}_{\ell u} C^{\tau\mu tu}_{\ell u}$	—×—	1×10^{-8}
$C^{e\tau tu}_{\ell u} C^{\tau\mu ut}_{\ell u}$	—×—	2.5×10^{-9}
$(C^{(1)e\tau 3u}_{\ell equ})^* C^{(1)\mu\tau 3u}_{\ell equ}$	$4.5\times10^{-4}(c)\times 4.5\times10^{-4}(c)$	4×10^{-8}
$(C^{(1)e\tau 1t}_{\ell equ})^* C^{(1)\mu\tau 1t}_{\ell equ}$	—×—	4×10^{-8}
$(C^{(3)e\tau 3u}_{\ell equ})^* C^{(3)\mu\tau 3u}_{\ell equ}$	$1.8\times10^{-3}(c)\times 1.8\times10^{-3}(c)$	1.25×10^{-10}
$(C^{(3)e\tau 1t}_{\ell equ})^* C^{(3)\mu\tau 1t}_{\ell equ}$	—×—	1.25×10^{-10}
$(C^{(1)e\tau 1t}_{\ell equ})^* C^{(3)\mu\tau 1t}_{\ell equ}$	—×—	3×10^{-9}
$(C^{(1)e\tau 3u}_{\ell equ})^* C^{(3)\mu\tau 3u}_{\ell equ}$	$4.5\times10^{-5}(c)\times 1.8\times10^{-3}(c)$	1.6×10^{-9}
$(C^{(3)e\tau 1t}_{\ell equ})^* C^{(1)\mu\tau 1t}_{\ell equ}$	—×—	3×10^{-9}
$(C^{(3)e\tau 3u}_{\ell equ})^* C^{(1)\mu\tau 3u}_{\ell equ}$	$1.8\times10^{-3}(c)\times 4.5\times10^{-5}(c)$	1.6×10^{-9}

Table 6.13: Similar to tables 6.8, to generate $\mu \to e$ vector operators with a doublet lepton bilinear (see Eq.s (6.32)-(6.38)).

6.4.2 Higgs LFV couplings

In this section we discuss the sensitivities of $\mu \to e$ observables to dimension six Yukawa operators $\mathcal{O}_{eH}$ (Eq. (6.17)), and compare them with the upcoming direct limits imposed by $h \to \tau l$ decays. Pairs of Yukawa $\tau \leftrightarrow l$ operators contribute to various $\mu \to e$ interactions at dimension eight. They mix into penguins via the divergent diagrams of Figure 6.6c, which match onto the vector operators involved at tree-level in the $\mu \to e$ conversion and $\mu \to \bar{e}ee$ rates. In addition, dimension six Yukawas are inserted in the diagrams of Figures 6.7b and 6.7c-6.7d, that give matching contributions to the $\mu e \tau \tau$ tensor and dipole respectively. The matching conditions are written in Eq.s (6.89) and (6.90)-(6.91). $\mu \to e\gamma$ is marginally more sensitive to the $\mu e \tau \tau$ tensor than on the dipole; this is due to the large tensor-to-dipole mixing and the built-in y_μ Yukawa suppression in the dipole definition, which lead to the already discussed enhancement m_τ/m_μ. As a result, $\mu \to e\gamma$ is the most sensitive process, and an upcoming experimental reach of $Br(\mu \to e\gamma) \lesssim 10^{-14}$ gives :

$$\left|C_{eH}^{e\tau} C_{eH}^{\tau\mu}\right|, \left|C_{eH}^{\tau e} C_{eH}^{\mu\tau}\right| \lesssim 3 \times 10^{-9}. \tag{6.106}$$

In the charged lepton mass-eigenstate basis, the dimension six Yukawas induce flavour-changing interactions of 125 GeV-Higgs (see Eq. 6.88), so $h \to \tau l$ decays probe the off-diagonal coefficients $C_{eH}^{\tau l, l\tau}$. The most stringent upper limits on the rates are currently set by CMS [363], and ILC is expected to improve them by one order of magnitude [347]. The projected sensitivities to the branching ratios $Br(h \to \tau e) < 2.3 \times 10^{-4}$, $Br(h \to \tau\mu) < 2.4 \times 10^{-4}$ respectively lead to the bounds

$$\begin{aligned} \sqrt{\left|C_{eH}^{e\tau}\right|^2 + \left|C_{eH}^{\tau e}\right|^2} &< 3.2 \times 10^{-4} \\ \sqrt{\left|C_{eH}^{\tau\mu}\right|^2 + \left|C_{eH}^{\mu\tau}\right|^2} &< 3 \times 10^{-4}. \end{aligned} \tag{6.107}$$

The product of the direct limits is larger than $2\times$ the sensitivity of Eq. (6.106), so that $\mu \to e$ probe a region of parameter space that is beyond the reach of future LFV Higgs decays (see Figure 6.8).

6.5 Summary

The $\mu \to e$ experiments under construction are expected to improve the current branching ratio sensitivities by several orders of magnitude. In some cases the improvement is such that the upcoming experiments will be able to probe products $\mu \to \tau$ and $\tau \to e$ interactions beyond the reach of direct $\tau \leftrightarrow l$ searches (where $l \in \{e, \mu\}$). However, the relationship between $\tau \leftrightarrow l$ and $\mu \leftrightarrow e$ observables is generically model-dependent, as we discussed in Section 6.2.1. The goal of this paper is to retain the model-independent contributions to $\mu \to e$ processes from $\tau \leftrightarrow l$ lepton flavour change, although these may be subdominant. To do so, we assume that the New Physics responsible for $\tau \leftrightarrow l$ LFV is heavy ($\Lambda_{\rm NP} \gtrsim 4$ TeV) and we parameterise it with $\tau \leftrightarrow l$ dimension six operators in the "on-shell" operator basis of SMEFT. We briefly introduce our EFT formalism in section 6.2.2.

We insert $\mu \to \tau$ and $\tau \to e$ dimension six interactions $\mathcal{O}\left(1/\Lambda_{\rm NP}^2\right)$ in diagrams that generates $\mu \to e$ amplitudes at dimension eight $\mathcal{O}\left(1/\Lambda_{\rm NP}^4\right)$. We only compute the contributions that are

phenomenologically relevant, i.e within the reach of future experiments. Firstly, we focus on a subspace of dimension eight operators to which $\mu \to e$ observables are sensitive, as given in [2] and presented in Section 6.2.3. Secondly, in Section 6.2.5 we draw and estimate diagrams with two $\tau \leftrightarrow l$ dimension six interactions generating the above-mentioned dimension eight operators, and we disregard the contributions smaller than the upcoming experimental sensitivity.

Log-enhanced corrections to $\mu \to e$ dimension eight coefficients are the result of the $(\text{dimension } 6)^2 \to (\text{dimension } 8)$ mixing which appear in the Renormalization Group evolution, that we review in Section 6.2.2. Calculating this mixing present some technical challenges. The "on-shell" operator bases we use at dimension six and eight are reduced using the Equation of Motion (EOM), i.e do not contain operators that are related by applying the classical EOM on some field. In order to include the dimension 8 contributions that arise from using the EOM up to dimension 6 in reducing to the on-shell basis at dimension 6, we include some not-1PI diagrams in our calculations. This is more carefully discussed in Section 6.2.4.

In Section 6.3 we describe the calculation of the interesting contributions to $\mu \to e$ processes from $\tau \leftrightarrow l$ interactions, depicted in the diagrams of Figure 6.6 and Figure 6.7. Pairs of $\tau \leftrightarrow l$ operators are assumed to be generated at a New Physics scale $\Lambda_{\text{NP}} = 4$ TeV and mix into dimension eight $\mu \to e$ interactions when evolved down to the experimental scale of $\mu \to e$ observables. Between Λ_{NP} and m_W, the running is perfomed in SMEFT as described in section 6.3.1 and employing the RGEs solution of Eq. (6.10). The complete list of the $(\text{dimension } 6)^2 \to (\text{dimension } 8)$ anomalous dimensions that we obtained is given in Appendix D.2.

The dimension eight SMEFT operators that are generated in running are matched onto low energy interactions at m_W as described in Appendix C.2. We also include the contribution from pairs of $\tau \leftrightarrow l$ operators which generate $\mu \leftrightarrow e$ operators at tree level in matching, as discussed in section 6.3.2. Between m_W and the experimental scale Λ_{exp}, the running of low energy Wilson Coefficients is taken from [322], while we find that $\mu \to \tau \times \tau \to e$ RGEs mixing is negligible in the EFT below m_W, as discussed at the end of section 6.2.2.

We thus determined the sensitivity of $\mu \to e$ processes to products of $\tau \leftrightarrow l$ operator coefficients. Sensitivities represent the smallest absolute value that is experimentally detectable and are obtained by considering one non-zero pair of $\tau \leftrightarrow l$ operators at a time. They give a hyperbola in the $C^{[6]\tau\mu}$-$C^{[6]e\tau}$ plane of the dimension six coefficients (see Figure 6.8), outside which $\mu \to e$ observables can probe. In the same plane, direct $\tau \leftrightarrow l$ searches are sensitive to the region outside an ellipse. In Section 6.4 we discuss two examples where the hyperbola passes inside the ellipse: Section 6.4.1 shows that the contributions of fish diagrams (see Figure 6.6e-6.6f) to $\mu \to e$ observables allow to probe products of $\tau \leftrightarrow l$ coefficients involving third generation quarks. These same interactions contribute to the rate of LFV $B \to \tau(\nu_\tau)$ meson decays, which can directly probe the size of the Wilson Coefficients (The "limits" arising from the upper bounds on $B \to \tau(\nu_\tau)+\ldots$ are summarized in Appendix D.3). In most cases, we find that upcoming $\mu \to e$ experiments are sensitive to coefficients beyond the reach of future $B \to \tau(\nu_\tau)+\ldots$ searches. In Section 6.4.2, we study the sensitivity of upcoming $\mu \to e$ searches to products of LFV Higgs couplings, which overcomes the projected reach of the ILC to $h \to \tau^\pm l^\mp$.

In summary, we computed in SMEFT the contributions to $\mu \to e$ observables arising from $(\mu \to \tau) \times (\tau \to e)$ interactions. This required calculating a subset of the RGEs for dimension eight operators, so far missing in the literature. As a result, we obtained limits on products of $\tau \leftrightarrow l$ SMEFT coefficients assuming non-observation of $\mu \to e$ in future experiments. This can

give model-independent relations among $\mu \leftrightarrow e$, $\tau \leftrightarrow e$ and $\tau \leftrightarrow \mu$ LFV: in the event of a detected $\tau \leftrightarrow \mu$ signal, the non-observation of $\mu \leftrightarrow e$ would suggest that some $\tau \leftrightarrow e$ interactions are unlikely(if they occur, additional $\mu \leftrightarrow e$ interactions are required to obtain a cancellation in the $\mu \leftrightarrow e$ amplitude). This could provide theoretical guidance on where to search, or not, for $\tau \leftrightarrow e$.

We find that $\mu \to e$ processes have a good sensitivity to products of $\tau \leftrightarrow l$ operators that involve b quarks. These mediate leptonic flavour changing B decays, which are a promising avenue for New Physics in light of the recent anomalies. The R_{D^*} anomaly, where the experimental value is larger than the SM prediction and, as discussed in Section 6.4.1.2 (see Figure 6.11), can be fitted by increasing the rate of $B \to D^* \tau \nu$ with $\tau \leftrightarrow e$ operators. This is an example of the above-discussed relations that we can extrapolate from our calculation; the non-observation of $\mu \to e$ processes can identify values where $\tau \leftrightarrow \mu$ is unlikely to be seen.

Chapter 7

Conclusions and prospects

In this thesis, we assumed that new physics is heavy and parametrized its effects with the Standard Model Effective Field Theory. We focused on the operators that change the flavour of charged leptons because neutrino masses provide conclusive evidence that lepton flavour is not conserved, and because LFV processes expect a significant improvement in the already excellent experimental sensitivities.

We argued that the increasing precision of LFV experiments compels us to include extra contributions in the effective theory calculations. To reach this conclusion, in Chapter 5 we introduced a power counting scheme aimed at organising the (multiple) perturbative expansions in SMEFT and at identifying all the relevant contributions within the reach of future experiments. We express the loop, couplings and EFT expansion in terms of powers of a small parameter $\lambda \sim 0.2$ à la Wolfenstein. The state-of-the-art SMEFT calculations that are currently available include the complete one-loop running of dimension six operators, and partial results for the leading-order running of the dimension eight operators. We use our power counting scheme to assess if that is sufficient to fully parametrize LFV in the SMEFT. We find that the upcoming $\mu \to e$ data can be sensitive to some two-loop anomalous dimension (for NP scales up to $\Lambda_{\rm NP} \sim 100$ TeV) and to a subset of dimension eight operators of SMEFT (for NP scales $\Lambda_{\rm NP} \lesssim 20$ TeV). To partially account for the dimension eight amplitudes, in Appendix C.2 we calculate the matching of the relevant dimension eight subset onto the low energy $\mu \to e$ contact interactions.

The results of Chapter 5 can be used to motivate improved SMEFT calculations, such as some two-loop anomalous dimensions, which may be the subject of a future project.

The sensitivity of $\mu \to e$ experiments to dimension eight contributions is used to impose novel limits on dimension six operators that change the τ flavour. Diagrams with $\mu \to \tau$ and $\tau \to e$ vertices can contribute to $\mu \to e$ amplitudes. In some cases, the upcoming $\mu \to e$ experiment will be able to probe products of $\mu \to \tau$ and $\tau \to e$ interactions beyond the reach of dedicated $\tau \leftrightarrow l$ searches. We explore this in the SMEFT by calculating the renormalization group mixing of the product of two dimension six $\mu \to \tau$ and $\tau \to e$ operators into a $\mu \to e$ operator of the dimension eight subset identified in Chapter 5. The calculations are described in Chapter 6 and more details can be found in Appendix D. The running of the dimension eight operators is only partially known, and we computed a subset of dimension eight renormalization group equations for the first time.

We use the results to impose limits on the product of τ flavour changing operator coefficients that are stricter than the ones imposed by τ LFV searches. We show that this allows to probe region of parameter space that elude $\tau \leftrightarrow l$ direct searches, providing complementary information on τ flavour change using $\mu \to e$ observables. We show explicit examples on how this can be used to relate the lepton flavour transitions: an observation of a $\tau \leftrightarrow e$ process and a null result from $\mu \to e$ can give information on the size of the $\tau \leftrightarrow \mu$ couplings.

The complete effective parametrization of LFV advocated in this thesis can be used to study BSM models from a bottom-up perspective. A bottom-up calculation maps the experimental data at low energy into a combination of operator coefficients at the heavy physics scale and identifies the region of coefficient space where models should sit. It would be interesting to investigate whether a bottom-up analysis can give additional insight into how different models could be distinguished. This is a question that has been explored extensively with top-down calculations: LFV rates are calculated in terms of model parameters and the parameter space is scanned, with the hope of extrapolating correlations among LFV observables that could be checked against the experimental results. Unfortunately, scans are dependent on the adopted measure, and may not fully capture what models, which correspond to points in parameter space, can do.

A bottom-up analysis could provide a different and interesting perspective. Being agnostic on the specific value of the model parameters, and matching different models to the experimentally allowed space at the high scale, we could try to identify the correlation among observables that models cannot predict. Finding regions of the coefficient space that the model cannot reach may be a better-posed problem that does not rely on probable (but potentially unknowable) correlations, and that can assist in distinguishing models with LFV, as a detection in the forbidden regions can exclude them.

Chapter 8

Résumé en Français

Le Modèle Standard de la physique des particules a remarquablement réussi à expliquer les interactions des particules élémentaires découvertes. Le secteur électrofaible a été testé avec une très grande précision, tandis que les calculs perturbatifs, les approches effectives et les résultats de réseau ont fait de la QCD la description de la force forte. Le modèle standard a prédit l'existence et les propriétés de plusieurs particules, dont plus récemment le boson de Higgs, qui a été découvert au Large Hadron Collider en 2012.

Malgré ses succès, plusieurs constats et considérations théoriques appellent à une extension du Modèle Standard. Les masses et les oscillations des neutrinos, la matière noire et l'asymétrie entre la matière et l'antimatière, font partie des observations qui nécessitent une nouvelle physique. Ces énigmes non résolues motivent la recherche de la physique au-delà du Modèle Standard, qui pourrait éclairer ces questions fondamentales et ouvrir la voie à une compréhension plus profonde de la nature.

Les oscillations des neutrinos sont un phénomène expérimental bien établi qui nécessite une physique au-delà du modèle standard, car elles brisent les symétries de saveur des leptons du lagrangien du modèle standard. Une façon minimale d'étendre le MS pour s'accorder avec les observations consiste à introduire un fermion chiral droit léger pour donner aux neutrinos des masses de Dirac. Cependant, ce scénario est difficile à tester car il conduit à des courants neutres changeant la saveur des leptons extrêmement faibles.

De nouveaux états lourds ainsi que de nouvelles interactions sont nécessaires si les neutrinos sont des fermions de Majorana et/ou si le problème de masse des neutrinos est lié à d'autres questions ouvertes, conduisant à de potentielles processus observables qui changent la saveur des leptons chargés. Cette possibilité a suscité un grand effort expérimental pour rechercher des transitions violant la saveur des leptons, qui sont maintenant parmi les processus les mieux mesurés en physique des particules et devraient encore s'améliorer dans un avenir proche. La violation de la saveur des leptons (LFV) serait un signal prometteur de la nouvelle physique, qui pourrait faire la lumière sur le mécanisme expliquant les masses de neutrinos. De plus, c'est un outil puissant pour diriger la construction de modèles introduisant une nouvelle physique générique, puisque les symétries accidentelles du MS sont facilement violées une fois que de nouveaux états et interactions sont introduits. Les modèles qui tentent de résoudre diverses énigmes sont souvent contraints par l'exigence d'accord avec les résultats expérimentaux portant sur la LFV.

Les résultats inconcluants des expériences peuvent suggérer que nous sommes en présence d'un écart de masse, avec une nouvelle physique à apparaitrait à une échelle largement plus grande $\Lambda_{\rm NP} \gg v$. Si tel est le cas, le modèle standard peut être considéré comme le lagrangien renormalisable d'une théorie des champs effective où les états lourds ont été supprimés. L'effet de la physique lourde aux basses énergies peut être paramétré en termes d'interactions de contact entre les degrés de liberté légers, supprimées par les puissances de l'échelle lourde selon la dimension de l'opérateur.

Les observables peuvent être calculés dans la théorie effective en tant que fonctions des coefficients d'opérateur, et les expériences peuvent rechercher des preuves de leur présence.

Dans cette thèse, nous analysons les résultats expérimentaux actuels et à venir des recherches LFV dans la théorie du champ effectif du modèle standard (SMEFT). L'objectif est d'obtenir autant d'orientations théoriques que possible sur le paysage viable du LFV au-delà de la physique du modèle standard.

Les calculs EFT peuvent être envisagés dans une perspective descendante ou ascendante. Dans la perspective descendante, les degrés de liberté lourds sont supprimés de la théorie et les couplages et masses UV paramétrisent la taille des coefficients des opérateurs. Les observables sont calculés avec les opérateurs effectifs et reproduisent les prédictions du modèle au sein de l'erreur de troncature de l'EFT. Dans la perspective ascendante, les observables sont calculées dans la théorie effective la plus générale qui est cohérente avec les symétries, y compris chaque contribution d'opérateur qui pourrait être à la portée des expériences. Ce faisant, nous identifions la région de l'espace des coefficients où les modèles au-delà du MS devraient se tenir, ce qui pourrait donner un aperçu de la physique LFV. Dans les deux perspectives, avec l'amélioration exceptionnelle des sensibilités attendues pour la prochaine génération d'expériences (en particulier pour les transitions $\mu \to e$), les calculs théoriques devraient suivre le niveau de précision des observables LFV, incluant potentiellement des contributions souvent négligées dans les calculs théoriques effectifs. Ceux-ci peuvent inclure des diagrammes de boucle supérieure, ainsi que des opérateurs d'ordre supérieur dans l'expansion EFT.

Tout d'abord, nous introduisons un petit paramètre de comptage de puissance à la Wolfenstein pour évaluer si les calculs SMEFT de pointe, qui incluent les opérateurs de dimension six et leurs équations de groupe de renormalisation à une boucle, sont suffisants pour avoir une description efficace complète des observables LFV. Nous constatons que les recherches à venir de $\mu \to e$ peuvent être sensibles à quelques dizaines d'opérateurs de dimension huit, et à certains effets de dimensions anormales à deux boucles, pour les nouvelles échelles de physique inférieures à 20-100 TeV.
Nous nous appuyons sur ces résultats et explorons la sensibilité des recherches $\mu \to e$ aux interactions de changement de saveur $\tau \leftrightarrow e(\mu)$. Nous décrivons les interactions $\tau \leftrightarrow e(\mu)$ comme des opérateurs de dimension six dans le SM EFT, nous identifions des paires d'entre eux apportant des contributions intéressantes aux processus $\mu \to e$, et obtenons les dimensions anormales mélangeant ces paires vers des opérateurs $\mu \to e$ de dimension huit. La renormalisation de l'opérateur de dimension huit est quasiment inconnue, et nous avons calculé un sous-ensemble d'équations de groupe de renormalisation pour la première fois. Nous montrons que les prochaines expériences $\mu \to e$ pourraient permettre de sonder l'espace des paramètres au-delà de la portée des recherches actuelles et futures portant sur les transitions $\tau \to e(\mu)$, incluant les désintégration LFV du Higgs, du τ et des mésons B.

Appendices

Appendix A

$\mu \to e$ conversion in nuclei

A muon, when stopped in a material, can form a muonic atom with a nucleus of the target. While in a bound state, the muon can undergo two SM processes: decay in orbit, where an electron and an (anti-)neutrino are emitted, or muon capture, given by

$$\mu^- \; N(A,Z) \to \nu_\mu \; N'(A, Z-1) \tag{A.1}$$

where A, Z are, respectively, the mass and atomic number of the nucleus N. In the presence of LFV interactions that change muons to electrons, a muon can be captured by the nucleus without the emission of a neutrino

$$\mu^- \; N(A,Z) \to e^- \; N(A,Z). \tag{A.2}$$

in a processes known as $\mu \to e$ conversion in nuclei. After cascading down in energy levels, the ground state of the muonic atom is a 1s orbital with a binding energy E_b, and in the final state a monochromatic electron with energy $\sim m_\mu - E_b$ is emitted while the nucleus recoils. The SINDRUMII collaboration sets the upper limit $\Gamma(\mu N \to eN)/\Gamma_{capt} < 7 \times 10^{-13}$ [241] on the rate of $\mu \to e$ conversion with respect to the flavour conserving muon capture.

The state-of-the-art calculations for the conversion rate can be found in [142, 270]. In their notation, we describe coherent and spin-independent $\mu \to e$ conversion with LFV contact interactions among leptons and light quark currents

$$\begin{aligned} -\mathcal{L}_{conv} = 2\sqrt{2} G_F m_\mu (A_L \bar{e} \sigma^{\alpha\beta} P_L \mu F_{\alpha\beta} + A_R \bar{e} \sigma^{\alpha\beta} P_R \mu F_{\alpha\beta}) \\ + \frac{G_F}{\sqrt{2}} \sum_{q=u,d,s} \Big[(g_{LS(q)} \bar{e} P_L \mu + g_{RS(q)} \bar{e} P_R \mu) \bar{q} q \\ (g_{LV(q)} \bar{e} \gamma_\alpha P_L \mu + g_{RV(q)} \bar{e} \gamma_\alpha P_R \mu) \bar{q} \gamma^\alpha q \Big] + \text{h.c} \end{aligned}$$

where $F^{\alpha\beta}$ is the photon field tensor. Contributions that depend on the spin-state of the nucleus arise from contact interactions involving axial-vector, pseudo-scalar and tensor quark currents. The spin-independent rate is dominant because it is enhanced by the coherent sum over all nucleons. The effective Lagrangian at the quark-level can be match onto interactions involving nucleons via the following matrix elements

$$\langle N | \bar{q} \Gamma_K q | N \rangle = G_K^{(p,q)} \bar{p} \Gamma_K p \qquad \langle N | \bar{q} \Gamma_K q | N \rangle = G_K^{(n,q)} \bar{n} \Gamma_K n$$

where $\Gamma_S = 1, \Gamma_V = \gamma^\alpha$ and p, n label protons and neutrons, respectively. The vector coefficients are obtained by the quark content of the nucleon $G_V^{(p,u)} = G_V^{(n,d)} = 2$, $G_V^{(p,d)} = G_V^{(n,u)} = 1$, $G_V^{p(n),s} = 0$ while the scalar charges G_S are extrapolated with dispersive relations and lattice results [364, 365]. The wave function for the muon bound state is calculated by solving the Dirac equation in the

presence of the electric field of the nucleus, and is averaged over the proton and neutron densities. Defining $\tilde{g}^{(p)}_{XK} = \sum_q G^{(p,q)}_K g_{XK(q)}$ and $\tilde{g}^{(n)}_{XK} = \sum_q G^{(n,q)}_K g_{XK(q)}$, the conversion rate reads

$$\Gamma_{\mu N \to eN} = 2G_F^2 \left| A_L D + \tilde{g}^{(p)}_{LS} S^{(p)} + \tilde{g}^{(n)}_{LS} S^{(n)} + \tilde{g}^{(p)}_{LV} V^{(p)} + \tilde{g}^{(n)}_{LV} V^{(n)} \right|^2 + L \leftrightarrow R$$

where D, S, V are the overlap integrals in Equations (19)–(23) of [270], that involve proton/neutron densities and muon/electron wave functions. All the overlap integral scale with the atomic number $\sim Z$, giving the anticipated coherence factor Z^2 that enhances the spin-independent $\mu \to e$ conversion rate over the muon capture rate.

Appendix B

Calculation details

B.1 Integrals in Dimensional Regularization

We list here the $D-$dimensional integrals and identities used in the calculations presented in the text. The integral over Feynman parameters

$$\frac{1}{A_1 \dots A_n} = \int_0^1 dx_1 \dots dx_n \delta\left(\sum_i x_i - 1\right) \frac{(n-1)!}{\left(\sum_i x_i A_i\right)^n} \tag{B.1}$$

allows to reduce the loop integrals to

$$\int \frac{d^D k}{(2\pi)^D} \frac{1}{(k^2-\Delta)^n} = \frac{(-1)^n i}{(4\pi)^{D/2}} \frac{\Gamma\left(n-\frac{D}{2}\right)}{\Gamma(n)} \Delta^{D/2-n} \tag{B.2}$$

$$\int \frac{d^D k}{(2\pi)^D} \frac{k^2}{(k^2-\Delta)^n} = \frac{(-1)^{n-1} i}{(4\pi)^{D/2}} \frac{D}{2} \frac{\Gamma\left(n-\frac{D}{2}-1\right)}{\Gamma(n)} \Delta^{D/2-n+1} \tag{B.3}$$

$$\int \frac{d^D k}{(2\pi)^D} \frac{(k^2)^2}{(k^2-\Delta)^n} = \frac{(-1)^n i}{(4\pi)^{D/2}} \frac{D(D+2)}{4} \frac{\Gamma\left(n-\frac{D}{2}-2\right)}{\Gamma(n)} \Delta^{D/2-n+2} \tag{B.4}$$

Taking $D = 4 - 2\varepsilon$ space-time dimensions, we encounter $1/\varepsilon$ poles from the Γ function. The $\Gamma(x)$ function can be expanded around zero for $x > 0$ as

$$\Gamma(x) = \frac{1}{x} - \gamma_E + \mathcal{O}(x) \tag{B.5}$$

where $\gamma_E \sim 0.578$ is the Euler-Mascheroni constant. We often encounter the following product

$$\mu^{2\varepsilon} \frac{\Gamma(2-D/2)}{(4\pi)^{D/2}} M^{2(D/2-2)} \tag{B.6}$$

which can be expanded for small ε

$$\mu^{2\varepsilon} \frac{\Gamma(2-D/2)}{(4\pi)^{D/2}} M^{2(D/2-2)} = \frac{1}{(4\pi)^2} \left(\frac{1}{\varepsilon} + \log\left(\frac{\mu^2}{M^2}\right) - \gamma + \log 4\pi + \mathcal{O}(\varepsilon)\right). \tag{B.7}$$

In the modified subtraction scheme $\overline{\text{MS}}$, the renormalization scale is conveniently redefined $\mu = \overline{\mu} e^{\gamma_E/2}/(4\pi)^{1/2}$ to absorb the constant factors paired with the $1/\varepsilon$ pole

$$\frac{1}{(4\pi)^2} \left(\frac{1}{\varepsilon} + \log\left(\frac{\mu^2}{M^2}\right) - \gamma + \log 4\pi + \mathcal{O}(\varepsilon)\right) = \frac{1}{(4\pi)^2} \left(\frac{1}{\varepsilon} + \log\left(\frac{\overline{\mu}^2}{M^2}\right) + \mathcal{O}(\varepsilon)\right) \tag{B.8}$$

B.2 Fierz Identities

The space of matrices with two spinor indices in four space-time dimensions is 16-dimensional and is spanned by the basis

$$A = \{P_L, P_R, \gamma^\mu P_L, \gamma^\mu P_R, \sigma^{\mu\nu}\} \tag{B.9}$$

where $P_{L,R} = (1 \pm \gamma_5)/2$ are the chiral projectors and $\sigma^{\mu\nu} = i/2[\gamma^\mu, \gamma^\nu]$. A generic spinor matrix $M_{\alpha\beta}$ can be decomposed as a linear combination of the basis elements, and the coefficients can be identified by acting with the scalar product

$$\frac{1}{2}\operatorname{Tr}(X \cdot M) \quad \text{for } X \in A. \tag{B.10}$$

Acting on the basis elements, it is easy to show that

$$\begin{aligned} &\frac{1}{2}\operatorname{Tr}(P_X P_Y) = \delta_{XY} \qquad \frac{1}{2}\operatorname{Tr}(P_X \gamma_\mu P_Y) = 0 \qquad \frac{1}{2}\operatorname{Tr}(\gamma^\nu P_X \gamma_\mu P_Y) = \delta^\nu_\mu \delta_{XY} \\ &\frac{1}{2}\operatorname{Tr}(P_X \sigma^{\mu\nu}) = 0 \qquad \frac{1}{2}\operatorname{Tr}(\gamma_\alpha P_X \sigma^{\mu\nu}) = 0 \qquad \frac{1}{2}\operatorname{Tr}(\sigma_{\alpha\beta}\sigma^{\mu\nu}) = 2(\delta^\mu_\alpha \delta^\nu_\beta - \delta^\mu_\beta \delta^\nu_\alpha) \end{aligned} \tag{B.11}$$

The results in Eq. (B.11) can be used to derive the Fierz identities for four-fermion products. For instance, considering

$$(\overline{\psi_1}\gamma^\mu P_L \psi_2)(\overline{\psi_3}\gamma_\mu P_R \psi_4) \tag{B.12}$$

we can isolate the two index spinor matrix

$$M = \gamma^\mu P_L \psi_2 \overline{\psi_3} \gamma_\mu P_R. \tag{B.13}$$

Acting with the scalar product, the only non-zero trace is given by $1/2\operatorname{Tr}(P_R M)$:

$$\frac{1}{2}\operatorname{Tr}\big(P_R \gamma^\mu P_L \psi_2 \overline{\psi_3} \gamma_\mu P_R\big) = -\frac{1}{2}(\overline{\psi_3}\gamma^\mu \gamma_\mu P_L \psi_2) = -2(\overline{\psi_3} P_L \psi_2) \tag{B.14}$$

with the $-$ sign arising from the anti-commutation of the Grassmann numbers ψ_2, ψ_3. As a result, M is

$$M = -2(\overline{\psi_3} P_L \psi_2) P_R \tag{B.15}$$

which substituted back in Eq. (B.12) gives

$$(\overline{\psi_1}\gamma^\mu P_L \psi_2)(\overline{\psi_3}\gamma_\mu P_R \psi_4) = -2(\overline{\psi_1} P_R \psi_4)(\overline{\psi_3} P_L \psi_2) \tag{B.16}$$

One can similarly prove the following identities

$$(\overline{\psi_1}\gamma^\mu P_X \psi_2)(\overline{\psi_3}\gamma_\mu P_X \psi_4) = (\overline{\psi_1}\gamma^\mu P_X \psi_4)(\overline{\psi_3}\gamma_\mu P_X \psi_2) \tag{B.17}$$

$$(\overline{\psi_1} P_X \psi_2)(\overline{\psi_3} P_X \psi_4) = -\frac{1}{2}(\overline{\psi_1} P_X \psi_4)(\overline{\psi_3} P_X \psi_2) - \frac{1}{8}(\overline{\psi_1}\sigma^{\mu\nu} P_X \psi_4)(\overline{\psi_3}\sigma_{\mu\nu} P_X \psi_2) \tag{B.18}$$

$$(\overline{\psi_1}\sigma^{\mu\nu} P_X \psi_2)(\overline{\psi_3}\sigma_{\mu\nu} P_X \psi_4) = \frac{1}{2}(\overline{\psi_1}\sigma^{\mu\nu} P_X \psi_4)(\overline{\psi_3}\sigma_{\mu\nu} P_X \psi_2) - 6(\overline{\psi_1} P_X \psi_4)(\overline{\psi_3} P_X \psi_2) \tag{B.19}$$

We can use this technique to reduce fermion bilinears with multiple insertion of γ matrices. In the calculation of section 4.2.1, we encountered the four-fermion product

$$(\overline{\psi_1}\gamma^\mu \gamma^\alpha \gamma^\nu P_L \psi_2)(\overline{\psi_3}\gamma_\mu \gamma_\alpha \gamma_\nu P_L \psi_4). \tag{B.20}$$

Since

$$P_L\psi_2\overline{\psi_3}P_R = -\frac{1}{2}(\overline{\psi_3}\gamma_\rho P_L\psi_2)\gamma^\rho P_L, \tag{B.21}$$

we find

$$\begin{aligned}(\overline{\psi_1}\gamma^\mu\gamma^\alpha\gamma^\nu P_L\psi_2)(\overline{\psi_3}\gamma_\mu\gamma_\alpha\gamma_\nu P_L\psi_4) &= -\frac{1}{2}(\overline{\psi_3}\gamma_\rho P_L\psi_2)(\overline{\psi_1}\gamma^\mu\gamma^\alpha\gamma^\nu\gamma^\rho\gamma_\mu\gamma_\alpha\gamma_\nu P_L\psi_4)\\ &= (\overline{\psi_3}\gamma_\rho P_L\psi_2)(\overline{\psi_1}\gamma^\rho\gamma^\nu\gamma^\alpha\gamma_\alpha\gamma_\nu P_L\psi_4)\\ &= 16(\overline{\psi_3}\gamma_\rho P_L\psi_2)(\overline{\psi_1}\gamma^\rho P_L\psi_4)\\ &= 16(\overline{\psi_1}\gamma_\rho P_L\psi_2)(\overline{\psi_3}\gamma^\rho P_L\psi_4)\end{aligned} \tag{B.22}$$

where in the second line we have used the contraction of gamma matrices $\gamma^\mu\gamma^\alpha\gamma^\nu\gamma^\rho\gamma_\mu = -2\gamma^\rho\gamma^\nu\gamma^\alpha$. Likewise, we find

$$\begin{aligned}(\overline{\psi_1}\gamma^\mu\gamma^\alpha\gamma^\nu P_L\psi_2)(\overline{\psi_3}\gamma_\nu\gamma_\alpha\gamma_\mu P_L\psi_4) &= -\frac{1}{2}(\overline{\psi_3}\gamma_\rho P_L\psi_2)(\overline{\psi_1}\gamma^\mu\gamma^\alpha\gamma^\nu\gamma^\rho\gamma_\nu\gamma_\alpha\gamma_\mu P_L\psi_4)\\ &= 4(\overline{\psi_3}\gamma_\rho P_L\psi_2)(\overline{\psi_1}\gamma^\rho P_L\psi_4)\\ &= 4(\overline{\psi_1}\gamma_\rho P_L\psi_2)(\overline{\psi_3}\gamma^\rho P_L\psi_4)\end{aligned} \tag{B.23}$$

having used the identity $\gamma_\alpha\gamma_\mu\gamma^\alpha = -2\gamma_\mu$ thrice.

Appendix C

Appendix for Chapter 5

C.1 Some LFV Operators of dimension eight

Section 5.3.1 showed that $\mu \leftrightarrow e$ processes can be sensitive to some SMEFT operators of dimension eight, if these have O(1) coefficients at $\Lambda_{\rm NP} \gtrsim 4$ TeV. This appendix lists the relevant operators, following the notation of [308].

The LFV operators given here are required to match onto low energy operators involved in the processes of Table 5.3, so derivative operators, and those involving more than four particles at low energy, are neglected. In addition, operators of the form $\mu_H^2 \times$ dimension six, where μ_H^2 is the Higgs mass^2 term in the Lagrangian, are neglected because in matching onto operators below m_W, the potential minimisation condition relates μ_H^2 to $H^\dagger H$. Furthermore, we restrict our list to operators that are $\mu \leftrightarrow e$ flavour changing but flavour diagonal in the two other fermion legs, as the low energy observables constrain operator with this flavour structure.

The four-fermion operators of dimension eight can be obtained by adding two Higgs fields to dimension six four-fermion operators, or by multiplying two renormalizable Lagrangian terms. Dimension six operators can be multiplied by the singlet product $(H^\dagger H)$, but the Higgses can also contract with specific doublets; when the Higgs gets a vev, this feature induces a low-energy operator involving only some SU(2) partners. For instance, the dimension eight operator

$$(\bar{\ell}_\alpha \tilde{H} \gamma_\rho \tilde{H}^\dagger \ell_\beta)(\bar{q}\gamma^\rho q) \to (\overline{\nu}_\alpha \gamma_\rho \nu_\beta)(\overline{u}\gamma^\rho u + \overline{d}\gamma^\rho d) \quad .$$

This operator induces "Non-Standard neutrino Interactions" [343], which can be searched for at neutrino experiments, without inducing tree-level flavour-change among charged leptons. Exploiting SU(2) identities, these operators can be expressed as linear combinations of dim6$\times(H^\dagger H)$ and the following operator

$$(\bar{\ell}_\alpha \tau^I \gamma_\rho \ell_\beta)(\bar{q}\gamma^\rho q)(H^\dagger \tau^I H).$$

Adopting the convention of [308], we retain the triplet contractions in the operator basis. Since we are interested in the contribution of dimension eight operators to LFV observables, we organize the operator list according to whether a dimension six version exists or does not exist.

We display operators with "standard" flavour indices and we don't include the permutations that will be matched to the same low energy interaction, as discussed in Appendix C.2.

C.1.1 Dimension eight not present at dimension six

C.1.1.1 Four-fermion

SU(2) invariance and its chiral nature forbid SMEFT dimension six counterparts of some four-fermion contact interaction of the QCD∗QED invariant Lagrangian, forcing their appearance at

dimension eight. In the case of four-fermion operators with four-lepton legs these are the tensor operators

$$\mathcal{O}^{(4)e\mu kk}_{L^2E^2H^2} = (\bar{l}_e H\sigma^{\alpha\beta} e_\mu)(\bar{l}_k H\sigma_{\alpha\beta} e_k)$$

where $k \in \{e,\mu,\tau\}$. They can be related to the scalars $\mathcal{O}^{(3)ijkl}_{L^2E^2H^2} = (\bar{l}_i He_j)(\bar{l}_k He_l)$ of the basis [308] thanks to the following Fierz identity

$$\mathcal{O}^{(4)e\mu kk}_{L^2E^2H^2} = -8\mathcal{O}^{(3)ekk\mu}_{L^2E^2H^2} - 4\mathcal{O}^{(3)e\mu kk}_{L^2E^2H^2}.$$

Given that the tensors mix with the dipole, we retain both operators in the matching conditions of Appendix C.2, keeping in mind that we can remove the redundancy by means of the above identity.

For four-fermion interaction involving two-lepton and two-quark legs, the dimension eight operators that do not arise at dimension six are

$$\mathcal{O}^{(3)e\mu nn}_{LEDQH^2} = (\bar{\ell}_e He_\mu)(\bar{q}_n Hd_n) \qquad \mathcal{O}^{(4)e\mu nn}_{LEDQH^2} = (\bar{\ell}_e\sigma^{\alpha\beta} He_\mu)(\bar{q}_n\sigma_{\alpha\beta} Hd_n)$$
$$\mathcal{O}^{(5)e\mu nn}_{LEQUH^2} = (\bar{\ell}_e He_\mu)(\bar{u}_n\tilde{H}^\dagger q_n).$$

where n is a quark generation index. In this case, the scalar and tensor operator for down-type quarks are independent and cannot be related by means of Fierz identities.

C.1.1.2 Two-lepton operators

Two-lepton and two-gauge boson operators firstly appear at dimension eight

$$\begin{aligned}
\mathcal{O}^{(1)e\mu}_{LEG^2H} &= (\bar{\ell}_e He_\mu)G^A_{\alpha\beta}G^{A\alpha\beta} & \mathcal{O}^{(2)e\mu}_{LEG^2H} &= (\bar{\ell}_e He_\mu)G^A_{\alpha\beta}\tilde{G}^{A\alpha\beta}\\
\mathcal{O}^{(1)e\mu}_{LEW^2H} &= (\bar{\ell}_e He_\mu)W^I_{\alpha\beta}W^{I\alpha\beta} & \mathcal{O}^{(2)e\mu}_{LEW^2H} &= (\bar{\ell}_e He_\mu)W^I_{\alpha\beta}\tilde{W}^{I\alpha\beta}\\
\mathcal{O}^{(1)e\mu}_{LEB^2H} &= (\bar{\ell}_e He_\mu)B_{\alpha\beta}B^{\alpha\beta} & \mathcal{O}^{(2)e\mu}_{LEB^2H} &= (\bar{\ell}_e He_\mu)B_{\alpha\beta}\tilde{B}^{\alpha\beta}\\
\mathcal{O}^{(1)e\mu}_{LEWBH} &= (\bar{\ell}_e\tau^I He_\mu)B^{\alpha\beta}W^I_{\alpha\beta} & \mathcal{O}^{(2)e\mu}_{LEWBH} &= (\bar{\ell}_e\tau^I He_\mu)B_{\alpha\beta}\tilde{W}^{I\alpha\beta}
\end{aligned}$$

and provide the leading order matching contribution to the dimension seven two-photon $\mathcal{O}_{FF,Y} = (\bar{e}P_Y\mu)F_{\alpha\beta}F^{\alpha\beta}$,$\mathcal{O}_{F\tilde{F},Y} = (\bar{e}P_Y\mu)F_{\alpha\beta}\tilde{F}^{\alpha\beta}$ and two-gluon $\mathcal{O}_{GG,Y} = (\bar{e}P_Y\mu)G^A_{\alpha\beta}G^{A\alpha\beta}$, $\mathcal{O}_{G\tilde{G},Y} = (\bar{e}P_Y\mu)G^A_{\alpha\beta}\tilde{G}^{A\alpha\beta}$ operators of the low energy Lagrangian, whose coefficients are constrained by searches of $\mu \to e$ conversion in nuclei.

C.1.2 Dimension eight operators present at dimension six

C.1.2.1 Four-fermion

The four-fermion operators with four lepton legs that also appear at dimension six are

$$\begin{aligned}
\mathcal{O}^{(1)e\mu kk}_{L^4H^2} &= (\bar{\ell}_e\gamma^\alpha\ell_\mu)(\bar{\ell}_k\gamma_\alpha\ell_k)(H^\dagger H) & \mathcal{O}^{(2)e\mu kk}_{L^4H^2} &= (\bar{\ell}_e\gamma^\alpha\ell_\mu)(\bar{\ell}_k\tau^I\gamma_\alpha\ell_k)(H^\dagger\tau^I H)\\
\mathcal{O}^{(1)e\mu kk}_{L^2E^2H^2} &= (\bar{\ell}_e\gamma^\alpha\ell_\mu)(\bar{e}_k\gamma_\alpha e_k)(H^\dagger H) & \mathcal{O}^{(2)e\mu kk}_{L^2E^2H^2} &= (\bar{\ell}_e\tau^I\gamma^\alpha\ell_\mu)(\bar{e}_k\gamma_\alpha e_k)(H^\dagger\tau^I H)\\
\mathcal{O}^{e\mu kk}_{E^4H^2} &= (\bar{e}_e\gamma^\alpha e_\mu)(\bar{e}_k\gamma_\alpha e_k)(H^\dagger H),
\end{aligned}$$

where $k = e, \mu, \tau$.

In addition, the four-fermion operators containing two-lepton and two-quark legs are:

$$\mathcal{O}^{(1)e\mu nn}_{L^2Q^2H^2} = (\bar{\ell}_e\gamma^\alpha\ell_\mu)(\bar{q}_n\gamma_\alpha q_n)(H^\dagger H) \qquad \mathcal{O}^{(2)e\mu nn}_{L^2Q^2H^2} = (\bar{\ell}_e\tau^I\gamma^\alpha\ell_\mu)(\bar{q}_n\gamma_\alpha q_n)(H^\dagger\tau^I H)$$
$$\mathcal{O}^{(3)e\mu nn}_{L^2Q^2H^2} = (\bar{\ell}_e\tau^I\gamma^\alpha\ell_\mu)(\bar{q}_n\tau^I\gamma_\alpha q_n)(H^\dagger H) \qquad \mathcal{O}^{(4)e\mu nn}_{L^2Q^2H^2} = (\bar{\ell}_e\gamma^\mu\ell_\mu)(\bar{q}_n\tau^I\gamma_\mu q_n)(H^\dagger\tau^I H)$$
$$\mathcal{O}^{(5)e\mu nn}_{L^2Q^2H^2} = \varepsilon^{IJK}(\bar{\ell}_e\tau^I\gamma^\mu\ell_\mu)(\bar{q}_n\tau^J\gamma_\mu q_n)(H^\dagger\tau^K H) \qquad \mathcal{O}^{(1)e\mu nn}_{L^2U^2H^2} = (\bar{\ell}_e\gamma^\alpha\ell_\mu)(\bar{u}_n\gamma_\mu u_n)(H^\dagger H)$$
$$\mathcal{O}^{(2)e\mu nn}_{L^2U^2H^2} = (\bar{\ell}_e\tau^I\gamma^\alpha\ell_\mu)(\bar{u}_k\gamma_\alpha u_l)(H^\dagger\tau^I H) \qquad \mathcal{O}^{(1)e\mu nn}_{L^2D^2H^2} = (\bar{\ell}_e\gamma^\alpha\ell_\mu)(\bar{d}_k\gamma_\alpha d_l)(H^\dagger H)$$
$$\mathcal{O}^{(2)e\mu nn}_{L^2D^2H^2} = (\bar{\ell}_e\tau^I\gamma^\alpha\ell_\mu)(\bar{d}_n\gamma_\alpha d_n)(H^\dagger\tau^I H) \qquad \mathcal{O}^{(1)e\mu nn}_{E^2Q^2H^2} = (\bar{e}_e\gamma^\alpha e_\mu)(\bar{q}_n\gamma_\alpha q_n)(H^\dagger H)$$
$$\mathcal{O}^{(2)e\mu nn}_{E^2Q^2H^2} = (\bar{e}_e\gamma^\alpha e_\mu)(\bar{q}_n\tau^I\gamma_\alpha q_n)(H^\dagger\tau^I H) \qquad \mathcal{O}^{e\mu nn}_{E^2U^2H^2} = (\bar{e}_e\gamma^\alpha e_\mu)(\bar{u}_n\gamma_\alpha u_n)(H^\dagger H)$$
$$\mathcal{O}^{e\mu nn}_{E^2D^2H^2} = (\bar{e}_e\gamma^\alpha e_\mu)(\bar{d}_n\gamma_\alpha d_n)(H^\dagger H) \qquad \mathcal{O}^{(1)e\mu nn}_{LEDQH^2} = (\bar{\ell}_e e_\mu)(\bar{d}_n q_n)(H^\dagger H)$$
$$\mathcal{O}^{(2)e\mu nn}_{LEDQH^2} = (\bar{\ell}_e e_\mu)\tau^I(\bar{d}_n q_n)(H^\dagger\tau^I H) \qquad \mathcal{O}^{(1)e\mu nn}_{LEQUH^2} = (\bar{\ell}_e e_\mu)\varepsilon(\bar{q}_n u_n)(H^\dagger H)$$
$$\mathcal{O}^{(2)e\mu nn}_{LEQUH^2} = (\bar{\ell}_e e_\mu)\tau^I\varepsilon(\bar{q}_n u_n)(H^\dagger\tau^I H) \qquad \mathcal{O}^{(3)e\mu nn}_{LEQUH^2} = (\bar{\ell}_e\sigma^{\alpha\beta}e_\mu)\varepsilon(\bar{q}_n\sigma_{\alpha\beta}u_n)(H^\dagger H)$$
$$\mathcal{O}^{(4)e\mu nn}_{LEQUH^2} = (\bar{\ell}_e\sigma^{\alpha\beta}e_j)\tau^I\varepsilon(\bar{q}_n\sigma_{\alpha\beta}u_n)(H^\dagger\tau^I H)$$

where $n = 1, 2, 3$ runs over the quark generation space.

C.1.2.2 Two-lepton operators

Two-lepton operators include the eight dimensional dipoles

$$\mathcal{O}^{(1)e\mu}_{LEWH^3} = (\bar{\ell}_e\tau^I H\sigma^{\alpha\beta}e_\mu)W^I_{\alpha\beta}(H^\dagger H)$$
$$\mathcal{O}^{(2)e\mu}_{LEWH^3} = (\bar{\ell}_e H\sigma^{\alpha\beta}e_\mu)W^I_{\alpha\beta}(H^\dagger\tau^I H)$$
$$\mathcal{O}^{e\mu}_{LEBH^3} = (\bar{\ell}_i H\sigma^{\alpha\beta}e_j)B_{\alpha\beta}(H^\dagger H)$$

and the following operators

$$\mathcal{O}^{(1)e\mu}_{L^2H^4D} = i(\bar{\ell}_e\gamma^\alpha\ell_\mu)(H^\dagger\overleftrightarrow{D}_\alpha H)(H^\dagger H) \qquad \mathcal{O}^{(2)e\mu}_{L^2H^4D} = i(\bar{\ell}_e\tau^I\gamma^\alpha\ell_\mu)[(H^\dagger\overleftrightarrow{D}^I_\alpha H)(H^\dagger H) + (H^\dagger\overleftrightarrow{D}_\alpha H)(H^\dagger\tau^I H)]$$
$$\mathcal{O}^{e\mu}_{E^2H^4D} = i(\bar{e}_e\gamma^\alpha e_\mu)(H^\dagger\overleftrightarrow{D}_\alpha H)(H^\dagger H) \qquad \mathcal{O}^{e\mu}_{LEH^5} = (\bar{\ell}_e H e_\mu)(H^\dagger H)^2,$$

where

$$iH^\dagger\overleftrightarrow{D}_\mu H \equiv iH^\dagger(D_\mu H) - i(D_\mu H^\dagger)H$$
$$iH^\dagger\overleftrightarrow{D}^I_\mu H \equiv iH^\dagger\tau^I(D_\mu H) - i(D_\mu H^\dagger)\tau^I H.$$

Following Electroweak Spontaneous Symmetry Breaking, the second set of operators are matched onto four fermion contact interactions at low energy, after integrating out the heavy Z, h bosons at m_W.

C.2 Tree matching at m_W with LFV operators to dimension eight

This section presents the tree level matching conditions at m_W of $\mu \leftrightarrow e$ flavour-changing SMEFT operators, including the dimension eight operators listed in the previous section, but neglecting double-insertions of dimension six operators. The operator basis below m_W is given in the notation of [322], and reproduced in section 4.3.2.

C.2.1 Dipoles and two-photon(gluon)

Below m_W, there are the dipole operators of two chiralities, and operators with two photons or two gluons. Above m_W, there is a dimension six dipole operator for hypercharge, and another one for SU(2).

Since the photon is the combination $A_\mu = \cos\theta_W B_\mu + \sin\theta_W W^3_\mu \equiv c_W B_\mu + s_W W^3_\mu$, the low energy dipole coefficient (on the left) is matched onto the dimension six and eight SMEFT dipoles (on the right) as

$$C^{e\mu}_{D,R} = c_W \left(C^{e\mu}_{EB} + \frac{v^2}{y_\mu \Lambda^2_{\rm NP}} C^{e\mu}_{LEBH^3} \right) - s_W \left[C^{e\mu}_{EW} + \frac{v^2}{y_\mu \Lambda^2_{\rm NP}} \left(C^{e\mu}_{LEWH^3(1)} + C^{e\mu}_{LEWH^3(2)} \right) \right]$$
$$C^{e\mu}_{D,L} = c_W \left(C^{\mu e*}_{EB} + \frac{v^2}{y_\mu \Lambda^2_{\rm NP}} C^{\mu e*}_{LEBH^3} \right) - s_W \left[C^{\mu e*}_{EW} + \frac{v^2}{y_\mu \Lambda^2_{\rm NP}} \left(C^{\mu e*}_{LEWH^3(1)} + C^{\mu e*}_{LEWH^3(2)} \right) \right]$$

where the $-$ sign is due to the τ^3 matrix. In addition, since matching "at tree level" mean tree-level in the low-energy theory, loop diagrams in the theory above m_W composed of heavy particles can be included. We follow [352], and retain the two-loop Barr-Zee diagrams, in which a Higgs leg connects a W or t loop with the neutral Higgs flavour changing vertex of eq. (5.6), and the one loop $Z-$exchange diagram where one Z vertex is flavour changing. The former give the matching condition

$$\Delta C^{e\mu}_{D,L}(m_W) \simeq -C^{\mu e*}_{EH}(m_W) \left[\frac{e\alpha}{16\pi^3 y_\mu} \left(Q_t^2 N_c Y_t^2 - \frac{7}{2} \right) \right] \simeq C^{\mu e*}_{EH}(m_W) \left[\frac{e\alpha}{8\pi^3 y_\mu} \right], \tag{C.1}$$

while the latter give

$$\begin{aligned} \Delta C^{e\mu}_{D,L}(m_W) &\simeq \frac{e}{16\pi^2} g^e_L C^{e\mu}_{HE}(m_W) \\ \Delta C^{e\mu}_{D,R}(m_W) &\simeq \frac{e}{16\pi^2} g^e_R \left(C^{e\mu}_{HL(1)}(m_W) + C^{e\mu}_{HL(3)}(m_W) \right), \end{aligned} \tag{C.2}$$

where g^e_L, g^e_R are defined in the Feynman rule for Z couplings to leptons $-i\frac{g}{2c_W}(g^e_L P_L + g^e_R P_R)$ as $g^e_R = 2s^2_W$, and $g^e_L = -1 + 2s^2_W$.

For the two-photon and two-gluon operators the matching conditions are

$$C^{e\mu}_{FF,R} = \frac{v}{\Lambda_{\rm NP}}\left(c_W^2 C^{e\mu}_{LEB^2H(1)} - s_W c_W C^{e\mu}_{LEWBH(1)} + s_W^2 C^{e\mu}_{LEW^2H(1)}\right) \tag{C.3}$$

$$C^{e\mu}_{FF,L} = \frac{v}{\Lambda_{\rm NP}}\left(c_W^2 C^{\mu e*}_{LEB^2H(1)} - s_W c_W C^{\mu e*}_{LEWBH(1)} + s_W^2 C^{\mu e*}_{LEW^2H(1)}\right) \tag{C.4}$$

$$C^{e\mu}_{F\tilde{F},R} = \frac{v}{\Lambda_{\rm NP}}\left(c_W^2 C^{e\mu}_{LEB^2H(2)} - s_W c_W C^{e\mu}_{LEWBH(2)} + s_W^2 C^{e\mu}_{LEW^2H(2)}\right) \tag{C.5}$$

$$C^{e\mu}_{F\tilde{F},L} = \frac{v}{\Lambda_{\rm NP}}\left(c_W^2 C^{\mu e*}_{LEB^2H(2)} - s_W c_W C^{\mu e*}_{LEWBH(2)} + s_W^2 C^{\mu e*}_{LEW^2H(2)}\right) \tag{C.6}$$

$$C^{e\mu}_{GG,R} = \frac{v}{\Lambda_{\rm NP}} C^{e\mu}_{LEG^2H(1)} \qquad C^{e\mu}_{GG,L} = \frac{v}{\Lambda_{\rm NP}} C^{\mu e*}_{LEG^2H(1)} \tag{C.7}$$

$$C^{e\mu}_{G\tilde{G},R} = \frac{v}{\Lambda_{\rm NP}} C^{e\mu}_{LEG^2H(2)} \qquad C^{e\mu}_{G\tilde{G},L} = \frac{v}{\Lambda_{\rm NP}} C^{\mu e*}_{LEG^2H(2)} \tag{C.8}$$

C.2.2 Four-Lepton

SMEFT operators with four-fermion legs are matched onto four-fermion contact interactions in the low-energy effective theory as Electroweak symmetry is spontaneously broken and the Higgs doublet is replaced by its vacuum expectation value. In addition, given that the interesting LFV operators are $\mu \leftrightarrow e$ flavour changing but otherwise flavour diagonal, two-lepton $\mu \leftrightarrow e$ operators can be connected to a renormalizable vertex exchanging an h or a Z, generating an effective four-fermion interaction when the heavy SM bosons are integrated out at the Electroweak scale.

As discussed in the text, a flavour changing vertex with the h Higgs boson appears as the SMEFT operators $\mathcal{O}_{EH}$ and $\mathcal{O}_{LEH^5}$ contribute to the leptons mass

$$[m_e]^{ij} = v\left([Y_e]^{ij} - C^{ij}_{EH}\frac{v^2}{\Lambda^2_{\rm NP}} - C^{ij}_{LEH^5}\frac{v^4}{\Lambda^4_{\rm NP}}\right), \tag{C.9}$$

so that in the charged leptons mass basis the Yukawa coupling is off-diagonal

$$\frac{h}{\sqrt{2}}\bar{e}^i P_R e^j\left([Y_e]^{ij} - 3C^{ij}_{EH}\frac{v^2}{\Lambda^2_{\rm NP}} - 5C^{ij}_{LEH^5}\frac{v^4}{\Lambda^4_{\rm NP}}\right) = \frac{h}{\sqrt{2}}\bar{e}^i P_R e^j\left([m_e]^{ij} - 2C^{ij}_{EH}\frac{v^2}{\Lambda^2_{\rm NP}} - 4C^{ij}_{LEH^5}\frac{v^4}{\Lambda^4_{\rm NP}}\right) \tag{C.10}$$

and the LFV Feynman rule with the neutral Higgs reads

$$-i\sqrt{2}\bar{e}^i P_R e^j\left(C^{ij}_{EH}\frac{v^2}{\Lambda^2_{\rm NP}} + 2C^{ij}_{LEH^5}\frac{v^4}{\Lambda^4_{\rm NP}}\right) \tag{C.11}$$

In SMEFT there are more distinct flavour structures which are matched into the same low energy operators: for example $\mathcal{O}^{e\mu ff}_{LL}$, $\mathcal{O}^{ffe\mu}_{LL}$, $\mathcal{O}^{f\mu ef}_{LL}$ and $\mathcal{O}^{eff\mu}_{LL}$ all match onto the below-m_W LFV operator $\mathcal{O}^{e\mu ff}_{LL}$. In the following, we suppress these permutations for brevity, and write

$$C^{e\mu ff}_{\text{low energy}} = C^{e\mu ff}_{\rm SMEFT} + \text{perm.}$$

to indicate that these different flavour structures are to be summed on the right side of the matching

conditions. These are:

$$C^{e\mu\ell\ell}_{V,RR} = C^{e\mu\ell\ell}_{EE} + C^{e\mu}_{HE} g^e_R + \frac{v^2}{\Lambda^2_{\rm NP}} \left(C^{e\mu\ell\ell}_{E^4H^2} + C^{e\mu}_{E^2H^4D} g^e_R \right) + \text{perm.} \tag{C.12}$$

$$C^{e\mu\ell\ell}_{V,LR} = C^{e\mu\ell\ell}_{LE} + (C^{e\mu}_{HL,3} + C^{e\mu}_{HL,1}) g^e_R + \frac{v^2}{\Lambda^2_{\rm NP}} \left[C^{e\mu ll}_{L^2E^2H^2(1)} + C^{e\mu ll}_{L^2E^2H^2(2)} + \left(C^{e\mu}_{L^2H^4D(1)} + 2C^{e\mu}_{L^2H^4D(2)} \right) g^e_R \right]$$

$$C^{e\mu\ell\ell}_{V,RL} = C^{\ell\ell e\mu}_{LE} + C^{e\mu}_{HE} g^e_L + \frac{v^2}{\Lambda^2_{\rm NP}} \left[C^{\ell\ell e\mu}_{L^2E^2H^2(1)} + C^{\ell\ell e\mu}_{L^2E^2H^2(2)} + C^{e\mu}_{E^2H^4D} g^e_L \right] \tag{C.13}$$

$$C^{e\mu\ell\ell}_{V,LL} = C^{e\mu\ell\ell}_{LL} + (C^{e\mu}_{HL,3} + C^{e\mu}_{HL,1}) g^e_L + \frac{v^2}{\Lambda^2_{\rm NP}} \left[C^{e\mu\ell\ell}_{L^4H^2(1)} + C^{e\mu\ell\ell}_{L^4H^2(2)} + \left(C^{e\mu}_{L^2H^4D(1)} + C^{e\mu}_{L^2H^4D(2)} \right) g^e_L \right] + \text{perm.}$$

$$C^{e\mu\ell\ell}_{S,RR} = -\frac{m_\ell C^{e\mu}_{EH} v}{m_h^2} + \frac{v^2}{\Lambda^2_{\rm NP}} \left(C^{e\mu\ell\ell}_{L^2E^2H^2(3)} - 2\frac{m_\ell C^{e\mu}_{LEH^5} v}{m_h^2} \right) + \text{perm.} \tag{C.14}$$

$$C^{e\mu\tau\tau}_{S,LR} = -2C^{\tau\mu e\tau}_{LE} - \frac{m_\tau C^{\mu e*}_{EH} v}{m_h^2} - \frac{v^2}{\Lambda^2_{\rm NP}} \left[2 \left(C^{\tau\mu e\tau}_{L^2E^2H^2(1)} + C^{\tau\mu e\tau}_{L^2E^2H^2(2)} \right) + 2\frac{m_\tau C^{\mu e*}_{LEH^5} v}{m_h^2} \right] \tag{C.15}$$

$$C^{e\mu\tau\tau}_{S,RL} = -2C^{e\tau\tau\mu}_{LE} - \frac{m_\tau C^{e\mu}_{EH} v}{m_h^2} - \frac{v^2}{\Lambda^2_{\rm NP}} \left[2 \left(C^{e\tau\tau\mu}_{L^2E^2H^2(1)} + C^{e\tau\tau\mu}_{L^2E^2H^2(2)} \right) + 2\frac{m_\tau C^{e\mu}_{LEH^5} v}{m_h^2} \right] \tag{C.16}$$

$$C^{e\mu\ell\ell}_{S,LL} = -\frac{m_\ell C^{\mu e*}_{EH} v}{m_h^2} + \frac{v^2}{\Lambda^2_{\rm NP}} \left(C^{\mu e\ell\ell*}_{L^2E^2H^2(3)} - 2\frac{m_\ell C^{\mu e*}_{LEH^5} v}{m_h^2} \right) + \text{perm.} \tag{C.17}$$

$$C^{e\mu\tau\tau}_{T,RR} = \frac{v^2}{\Lambda^2_{\rm NP}} C^{e\mu\tau\tau}_{L^2E^2H^2(4)} \tag{C.18}$$

$$C^{e\mu\tau\tau}_{T,LL} = \frac{v^2}{\Lambda^2_{\rm NP}} C^{\mu e\tau\tau*}_{L^2E^2H^2(4)} \tag{C.19}$$

where $\ell \in \{e, \mu, \tau\}$. We see that lepton tensors are matched at tree level only at dimension eight, and also that dimension eight operators could be significant for LL or RR scalars, where the dimension six contribution is Yukawa-suppressed.

C.2.3 Two-lepton two-quark

Given that the low energy constraints are expressed in the quark mass eigenstate basis, in the "bottom up" approach adopted here, the CKM matrix will act on SMEFT operator coefficients in the matching conditions. As we work in the u_L-basis, a CKM weighted sum will appear in matching d_L operators.(The CKM matrix is here written as V, rather than the previously used V_{CKM}.)

Tree-level matching SMEFT dimension six and eight coefficients (on the right) onto low energy

coefficients (on the left) results in:

$$
\begin{aligned}
C_{LL}^{e\mu u_n u_n} &= C_{LQ(1)}^{e\mu nn} - C_{LQ(3)}^{e\mu nn} + g_L^u (C_{HL(1)}^{e\mu} + C_{HL(3)}^{e\mu}) \\
&+ \frac{v^2}{\Lambda_{\rm NP}^2}\left[C_{L^2Q^2H^2(1)}^{e\mu nn} + C_{L^2Q^2H^2(2)}^{e\mu nn} - C_{L^2Q^2H^2(3)}^{e\mu nn} - C_{L^2Q^2H^2(4)}^{e\mu nn} + \left(C_{L^2H^4D(1)}^{e\mu} + 2C_{L^2H^4D(2)}^{e\mu}\right) g_L^u\right] \\
C_{LL}^{e\mu d_n d_n} &= \sum_{jk} V_{jn} V_{kn}^* (C_{LQ(1)}^{e\mu jk} + C_{LQ(3)}^{e\mu jk}) + g_L^d (C_{HL(1)}^{e\mu} + C_{HL(3)}^{e\mu}) \\
&+ \frac{v^2}{\Lambda_{\rm NP}^2}\Bigg[\sum_{jk} V_{jn} V_{kn}^* \left(C_{L^2Q^2H^2(1)}^{e\mu jk} + C_{L^2Q^2H^2(2)}^{e\mu jk} + C_{L^2Q^2H^2(3)}^{e\mu jk} + C_{L^2Q^2H^2(4)}^{e\mu jk}\right) \\
&+ \left(C_{L^2H^4D(1)}^{e\mu} + 2C_{L^2H^4D(2)}^{e\mu}\right) g_L^d\Bigg] \qquad \text{(C.20)} \\
C_{RR}^{e\mu u_n u_n} &= C_{EU}^{e\mu nn} + g_R^u C_{HE}^{e\mu} + \frac{v^2}{\Lambda_{\rm NP}^2}\left(C_{E^2U^2H^2}^{e\mu nn} + C_{E^2H^4D}^{e\mu} g_R^u\right) \qquad \text{(C.21)} \\
C_{RR}^{e\mu d_n d_n} &= C_{ED}^{e\mu nn} + g_R^d C_{HE}^{e\mu} + \frac{v^2}{\Lambda_{\rm NP}^2}\left(C_{E^2D^2H^2}^{e\mu nn} + C_{E^2H^4D}^{e\mu} g_R^d\right) \qquad \text{(C.22)} \\
C_{LR}^{e\mu u_n u_n} &= C_{LU}^{e\mu nn} + g_R^u (C_{HL(1)}^{e\mu} + C_{HL(3)}^{e\mu}) \\
&+ \frac{v^2}{\Lambda_{\rm NP}^2}\left[C_{L^2U^2H^2(1)}^{e\mu nn} + C_{L^2U^2H^2(2)}^{e\mu nn} + \left(C_{L^2H^4D(1)}^{e\mu} + 2C_{L^2H^4D(2)}^{e\mu}\right) g_R^u\right] \qquad \text{(C.23)} \\
C_{LR}^{e\mu d_n d_n} &= C_{LD}^{e\mu nn} + g_R^d (C_{HL(1)}^{e\mu} + C_{HL(3)}^{e\mu}) \\
&+ \frac{v^2}{\Lambda_{\rm NP}^2}\left[C_{L^2D^2H^2(1)}^{e\mu nn} + C_{L^2D^2H^2(2)}^{e\mu nn} + \left(C_{L^2H^4D(1)}^{e\mu} + 2C_{L^2H^4D(2)}^{e\mu}\right) g_R^d\right] \qquad \text{(C.24)} \\
C_{RL}^{e\mu u_n u_n} &= C_{EQ}^{e\mu nn} + g_L^u C_{HE}^{e\mu} + \frac{v^2}{\Lambda_{\rm NP}^2}\left[C_{E^2Q^2(1)}^{e\mu nn} - C_{E^2Q^2(2)}^{e\mu nn} + C_{E^2H^4D}^{e\mu} g_L^u\right] \qquad \text{(C.25)} \\
C_{RL}^{e\mu d_n d_n} &= \sum_{jk} V_{jn} V_{kn}^* C_{EQ}^{e\mu jk} + g_L^d C_{HE}^{e\mu} + \frac{v^2}{\Lambda_{\rm NP}^2}\left[\sum_{jk} V_{jn} V_{kn}^* \left(C_{E^2Q^2(1)}^{e\mu jk} + C_{E^2Q^2(2)}^{e\mu jk}\right) + C_{E^2H^4D}^{e\mu} g_L^d\right] \qquad \text{(C.26)}
\end{aligned}
$$

$$C_{S,LL}^{e\mu u_n u_n} = -C_{LEQU}^{*\mu enn} - \frac{m_{u_n} v}{m_h^2} C_{EH}^{\mu e*} - \frac{v^2}{\Lambda_{\rm NP}^2}\left(C_{LEQUH^2(1)}^{\mu enn*} + C_{LEQUH^2(2)}^{\mu enn*} + 2\frac{m_{u_n} v}{m_h^2} C_{LEH^5}^{\mu e*}\right) \tag{C.27}$$

$$C_{S,LL}^{e\mu d_n d_n} = -\frac{m_{d_n} v}{m_h^2} C_{EH}^{\mu e*} + \frac{v^2}{\Lambda_{\rm NP}^2}\left(\sum_j V_{jn}^* C_{LEQDH^2(3)}^{\mu ejn*} - 2\frac{m_{d_n} v}{m_h^2} C_{LEH^5}^{\mu e*}\right) \tag{C.28}$$

$$C_{S,RR}^{e\mu u_n u_n} = -C_{LEQU}^{e\mu nn} - \frac{m_{u_n} v}{m_h^2} C_{EH}^{e\mu} - \frac{v^2}{\Lambda_{\rm NP}^2}\left(C_{LEQUH^2(1)}^{e\mu nn} + C_{LEQUH^2(2)}^{e\mu nn} + 2\frac{m_{u_n} v}{m_h^2} C_{LEH^5}^{e\mu}\right) \tag{C.29}$$

$$C_{S,RR}^{e\mu d_n d_n} = -\frac{m_{d_n} v}{m_h^2} C_{EH}^{e\mu} + \frac{v^2}{\Lambda_{\rm NP}^2}\left(\sum_j V_{jn} C_{LEQDH^2(3)}^{e\mu jn} - 2\frac{m_{d_n} v}{m_h^2} C_{LEH^5}^{e\mu}\right) \tag{C.30}$$

$$C_{S,LR}^{e\mu u_n u_n} = -\frac{m_{u_n} v}{m_h^2} C_{EH}^{\mu e*} - \frac{v^2}{\Lambda_{\rm NP}^2}\left(2\frac{m_{u_n} v}{m_h^2} C_{LEH^5}^{\mu e*} - C_{LEQUH^2(5)}^{\mu enn*}\right) \tag{C.31}$$

$$C_{S,LR}^{e\mu d_n d_n} = \sum_j V_{jn} C_{LEDQ}^{*\mu enj} - \frac{m_{d_n} v}{m_h^2} C_{EH}^{\mu e*} + \frac{v^2}{\Lambda_{\rm NP}^2}\left[\sum_j V_{jn}\left(C_{LEQDH^2(1)}^{\mu enj*} + C_{LEQDH^2(2)}^{\mu enj*}\right) - 2\frac{m_{d_n} v}{m_h^2} C_{LEH^5}^{\mu e*}\right]$$

$$C_{S,RL}^{e\mu u_n u_n} = -\frac{m_{u_n} v}{m_h^2} C_{EH}^{e\mu} - \frac{v^2}{\Lambda_{\rm NP}^2}\left(2\frac{m_{u_n} v}{m_h^2} C_{LEH^5}^{e\mu} - C_{LEQUH^2(5)}^{e\mu nn}\right) \tag{C.32}$$

$$C_{S,RL}^{e\mu d_n d_n} = \sum_j V_{jn}^* C_{LEDQ}^{e\mu nj} - \frac{m_{d_n} v}{m_h^2} C_{EH}^{e\mu} + \frac{v^2}{\Lambda_{\rm NP}^2}\left[\sum_j V_{jn}^*\left(C_{LEQDH^2(1)}^{e\mu nj} + C_{LEQDH^2(2)}^{e\mu nj}\right) - 2\frac{m_{d_n} v}{m_h^2} C_{LEH^5}^{e\mu}\right]$$

$$C_{T,LL}^{e\mu u_n u_n} = -C_{T,LEQU}^{*\mu enn} - \frac{v^2}{\Lambda_{\rm NP}^2}\left(C_{LEQUH^2(3)}^{\mu enn*} + C_{LEQUH^2(4)}^{\mu enn*}\right) \tag{C.33}$$

$$C_{T,RR}^{e\mu u_n u_n} = -C_{T,LEQU}^{e\mu nn} - \frac{v^2}{\Lambda_{\rm NP}^2}\left(C_{LEQUH^2(3)}^{e\mu nn} + C_{LEQUH^2(4)}^{e\mu nn}\right) \tag{C.34}$$

$$C_{T,RR}^{e\mu d_n d_n} = \frac{v^2}{\Lambda_{\rm NP}^2}\sum_j V_{jn} C_{LEQDH^2(5)}^{e\mu jn} \tag{C.35}$$

$$C_{T,LL}^{e\mu d_n d_n} = \frac{v^2}{\Lambda_{\rm NP}^2}\sum_j V_{jn}^* C_{LEQDH^2(5)}^{\mu ejn*} \tag{C.36}$$

where V is the CKM matrix, $u_n \in \{u, c\}$, $d_n \in \{d, s, b\}$, and

$$g_L^u = 1 - \frac{4}{3}s_W^2 \quad , \quad g_R^u = -\frac{4}{3}s_W^2 \quad , \quad g_L^d = -1 + \frac{2}{3}s_W^2 \quad , \quad g_R^d = \frac{2}{3}s_W^2 \quad . \tag{C.37}$$

As anticipated, the low energy LFV tensors involving $d-$type quarks are matched at tree level onto the SMEFT eight dimensional tensors. Dimension eight operators could also be relevant for LL, RR scalars with d quarks and RL, LR scalars with u quarks, as the dimension six contributions are suppressed by Yukawa couplings.

Appendix D

Appendix for Chapter 6

D.1 Feynman Rules

In this section we list the Feynman Rules for the interactions involved in the diagrams of section 6.3.1. Capital letters $I, J, L, K \ldots$ are used to label SU(2) indices, while lower-case letters i, j, l, k are generation indices. τ^a are the Pauli matrices and $\varepsilon_{12} = -\varepsilon_{21} = 1, \varepsilon_{11} = \varepsilon_{22} = 0$ is the anti-symmetric SU(2) tensor. The Feynman rules are obtained calculating by hand the iM amplitude of the tree-level processes.

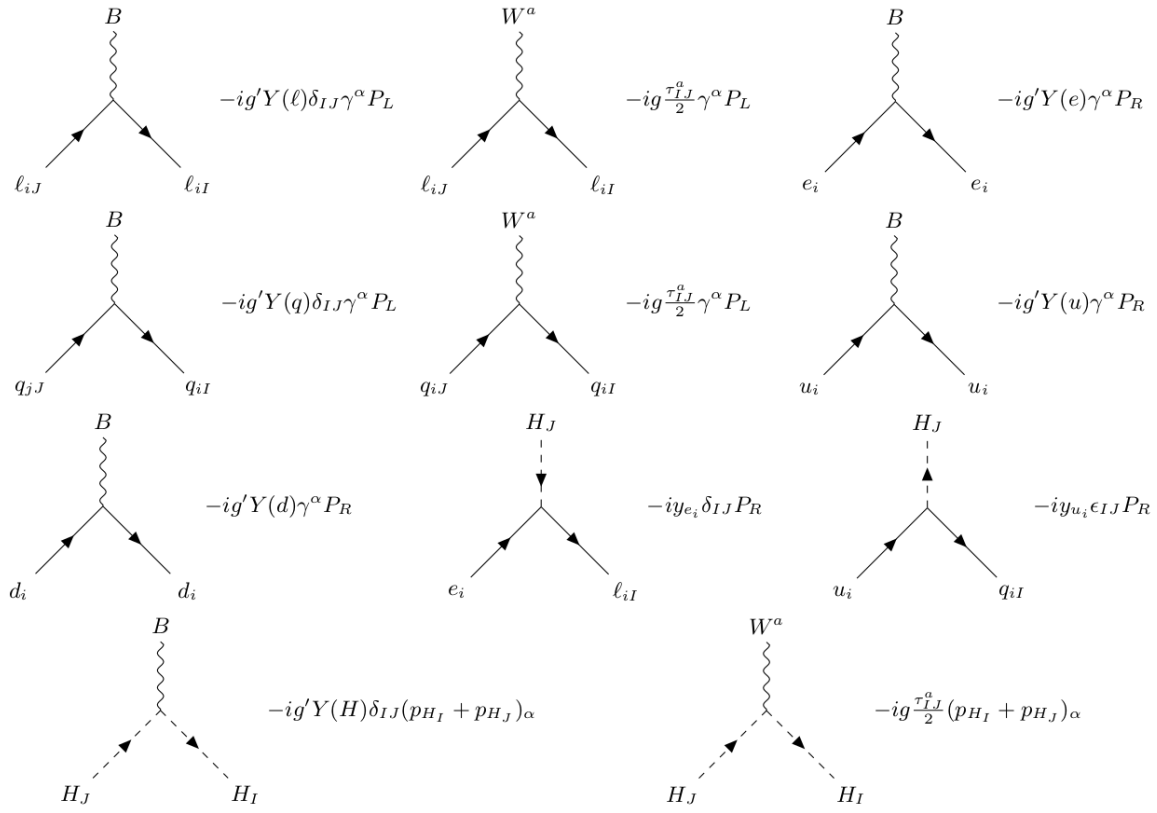

Figure D.1: Feynman rules for the dimension four interaction. The Higgs momenta follow the hypercharge arrow.

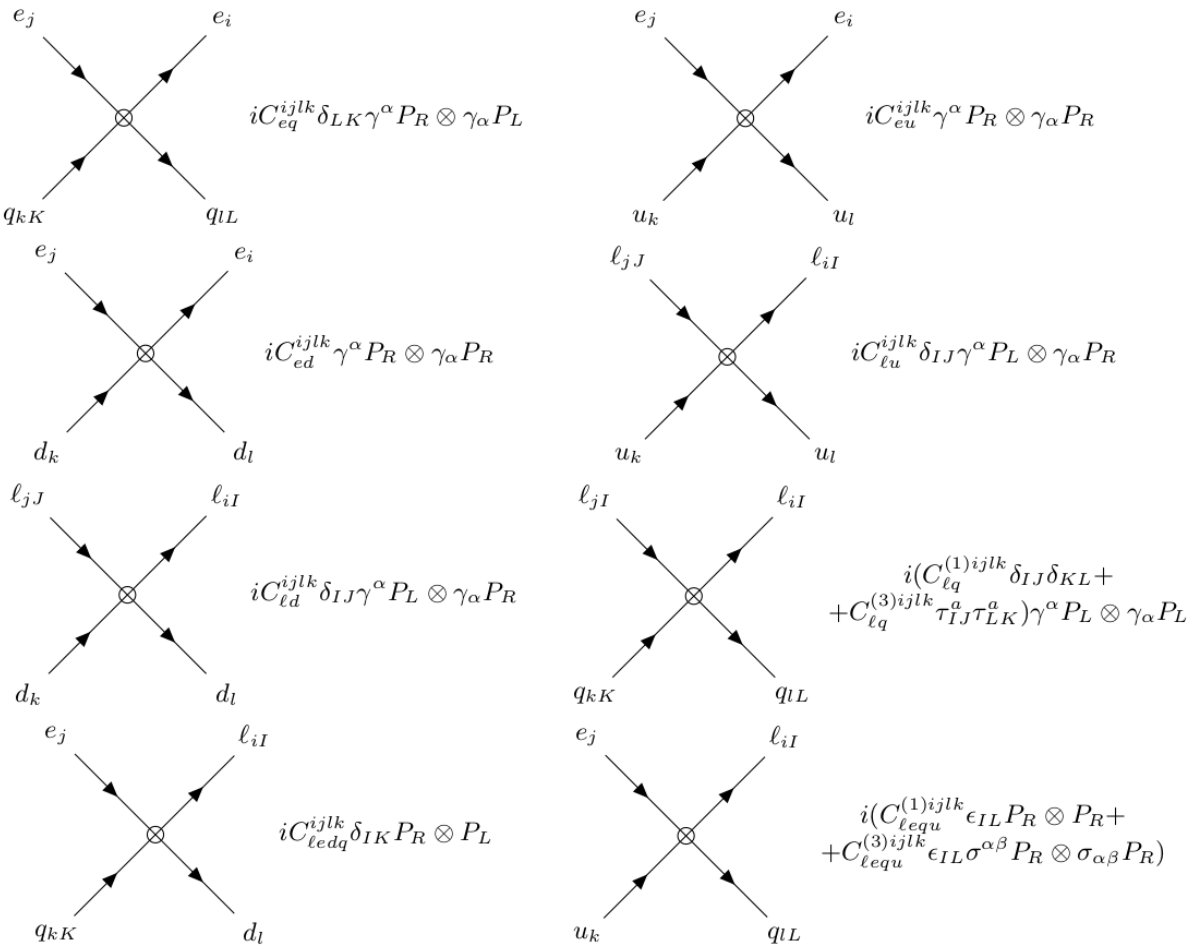

Figure D.2: Feynman rules for the dimension six SMEFT four-fermion interaction $4f_6$ of section 6.2.3. In the product $\Gamma_1 \otimes \Gamma_2$ the left matrix Γ_1 multiplies the lepton bilinear. Scalar and tensor with opposite chiralities have the same Feynman rules with conjugate coefficients and exchanged flavour indices within lepton and quark bilinears.

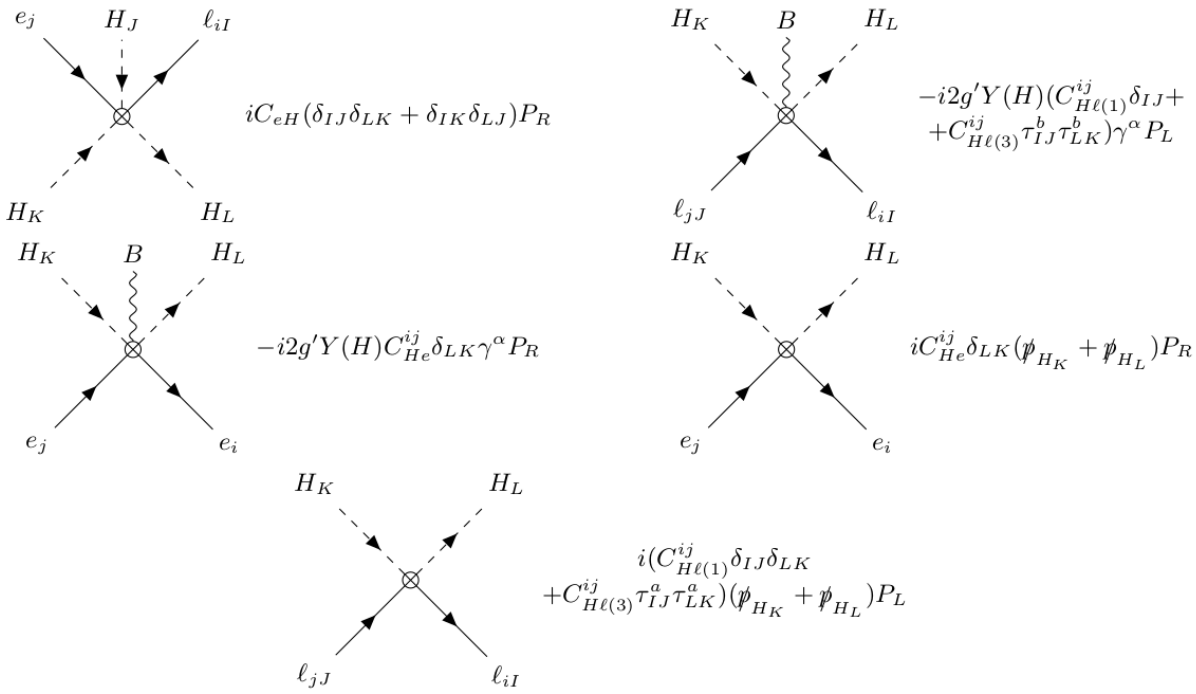

Figure D.3: Feynman rules for the dimension six SMEFT two fermion operators Y_6, P_6 of section 6.2.3. The Higgs momenta follow the hypercharge arrows.

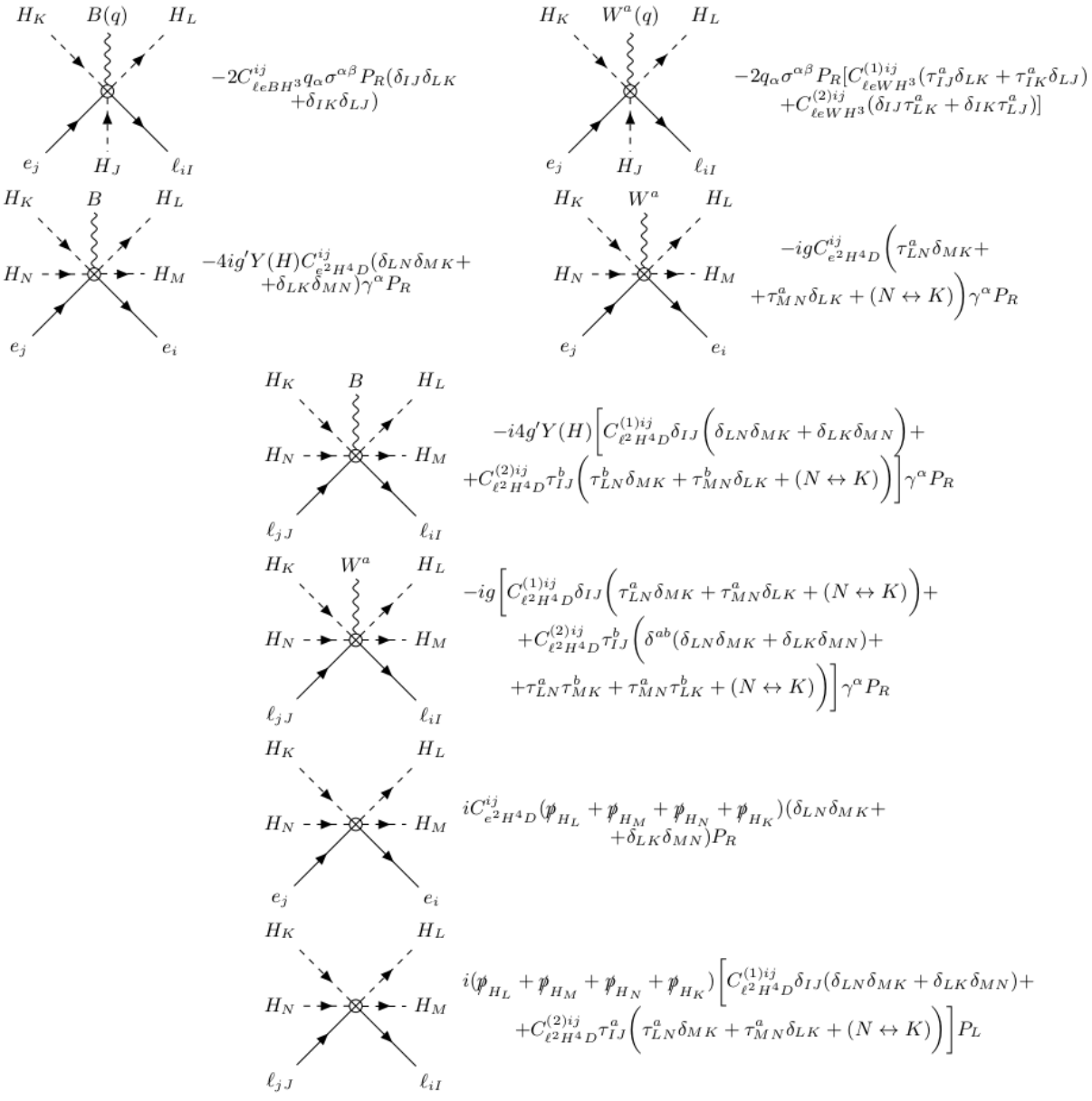

Figure D.4: Feynman rules for the dimension eight SMEFT two fermion operators D_8, P_8 of section 6.2.3. The Higgs momenta directions follow the hypercharge arrow, while the bosons momentum q is outgoing

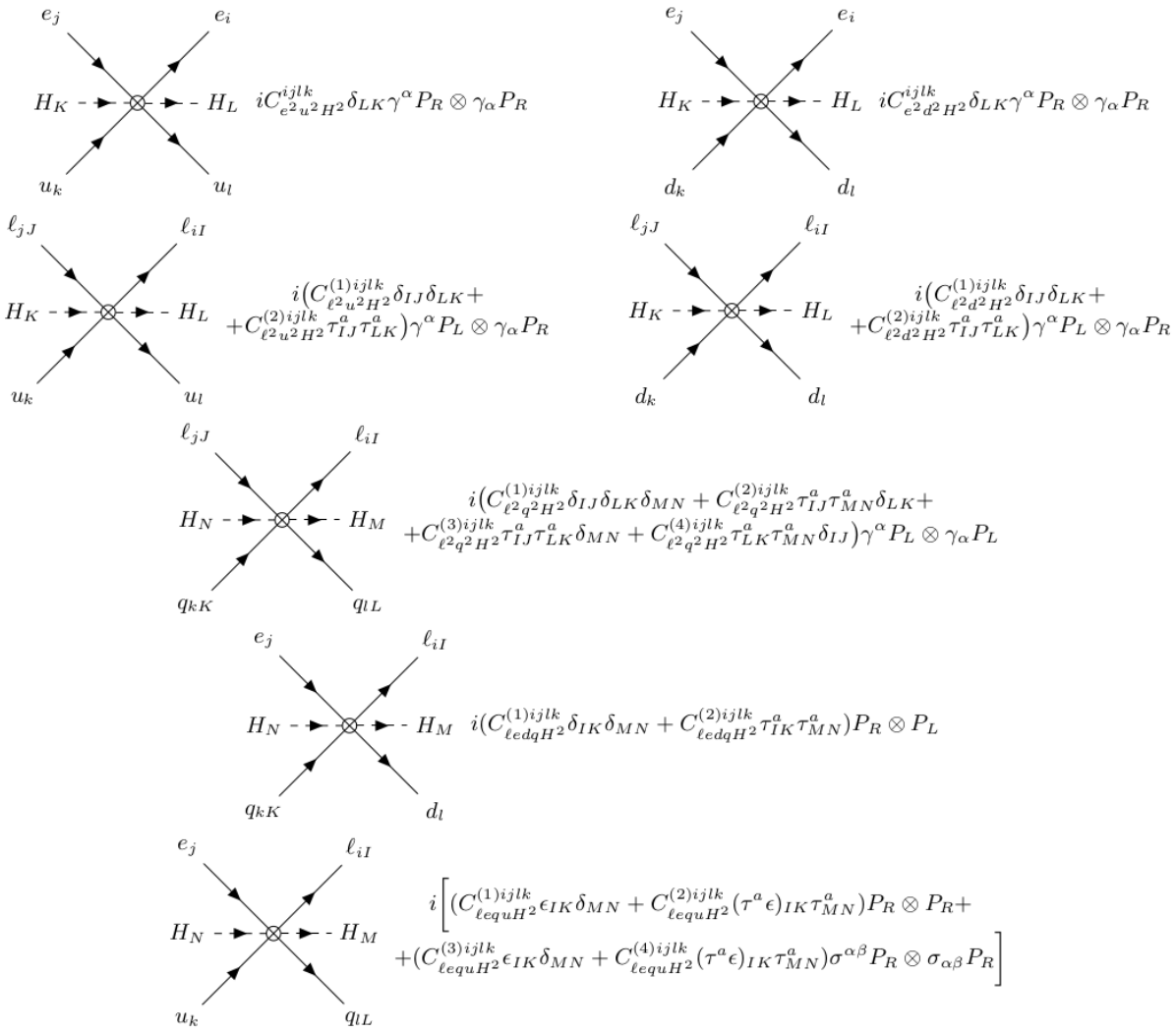

Figure D.5: Feynman rules for the dimension eight SMEFT four-fermion interactions $4f_8$ of section 6.2.3. We consider only the dimension eight operators involved in the diagrams of section 6.3.1.1. In the product $\Gamma_1\otimes\Gamma_2$ the left matrix Γ_1 multiplies the lepton bilinear. Scalar and tensor with opposite chiralities have the same Feynman rules with conjugate coefficients and exchanged flavour indices within lepton and quark bilinears.

D.2 Anomalous Dimensions

In this section we write the renormalization group equations for the mixing of a $\mu \to \tau$ dimension six operator, multiplied by a $\tau \to e$ dimension six operator, into a dimension eight $\mu \to e$ operator. These anomalous dimensions are generated by the diagrams of section 6.3.1.1. We conveniently present the RGEs divided in the "classes" introduced in the same section. The operator definitions can be found in section 6.2.3. The upper dot $\dot{C}$ on the Wilson coefficient indicate the logarithmic derivative with respect to the renormalization scale M. The anomalous dimensions are written for the dimension eight operators of Section 6.2.3, which are relevant for $\mu \to e$ processes that are otherwise flavour diagonal, although more general flavour structures can be obtained with the appropriate substitutions. For non-Hermitian operators such as $\mathcal{O}^{(1)}_{\ell equ H^2}$, we write the RGEs for the $\mu \to e$ operators $\mathcal{O}^{(1)e\mu ii}_{\ell equ H^2}, \mathcal{O}^{*(1)\mu eii}_{\ell equ H^2}$. This is to more explicitly show the $\tau \leftrightarrow l$ operator pairs upon which we obtain limits in section 6.4.

D.2.1 $4f_6 \times 4f_6 \to 4f_8$

Figure 6.6f shows the mixing $\propto y_t y_\tau$ of pairs of dimension six $\tau \to l$ operators into the dimension eight $\mu \to e$ tensor with top legs. We align $\tau \leftrightarrow e, \tau \leftrightarrow \mu$ Wilson coefficients respectively in row and column vectors to write the following anomalous dimensions, relevant for the $B_{\mu\to e}$ sensitivity of Table 6.11.

$$16\pi^2 \dot{C}^{(3)e\mu 3t}_{\ell equ H^2} = \begin{pmatrix} C^{e\tau tt}_{\ell u} & C^{(1)e\tau 33}_{\ell q} & C^{(3)e\tau 33}_{\ell q} & C^{(1)e\tau 3t}_{\ell equ} & C^{(3)e\tau 3t}_{\ell equ} \end{pmatrix} \begin{pmatrix} y_\tau y_t & 0 & 0 & 0 \\ 0 & -y_\tau y_t & 0 & 0 \\ 0 & y_\tau y_t & 0 & 0 \\ 0 & 0 & 0 & 3y_\tau y_t \\ 0 & 0 & 3y_\tau y_t & -8y_\tau y_t \end{pmatrix} \begin{pmatrix} C^{\tau\mu 33}_{eq} \\ C^{\tau\mu tt}_{eu} \\ C^{(1)\tau\mu 3t}_{\ell equ} \\ C^{(3)\tau\mu 3t}_{\ell equ} \end{pmatrix} \tag{D.1}$$

$$16\pi^2 \dot{C}^{*(3)\mu e3t}_{\ell equ H^2} = \begin{pmatrix} C^{\tau\mu tt}_{\ell u} & C^{(1)\tau\mu 33}_{\ell q} & C^{(3)\tau\mu 33}_{\ell q} & C^{*(1)\mu\tau 3t}_{\ell equ} & C^{*(3)\mu\tau 3t}_{\ell equ} \end{pmatrix} \begin{pmatrix} y_\tau y_t & 0 & 0 & 0 \\ 0 & -y_\tau y_t & 0 & 0 \\ 0 & y_\tau y_t & 0 & 0 \\ 0 & 0 & 0 & 3y_\tau y_t \\ 0 & 0 & 3y_\tau y_t & -8y_\tau y_t \end{pmatrix} \begin{pmatrix} C^{e\tau 33}_{eq} \\ C^{e\tau tt}_{eu} \\ C^{*(1)\tau e3t}_{\ell equ} \\ C^{*(3)\tau e3t}_{\ell equ} \end{pmatrix} \tag{D.2}$$

$$16\pi^2 \dot{C}^{(4)e\mu 3t}_{\ell equ H^2} = \begin{pmatrix} C^{e\tau tt}_{\ell u} & C^{(1)e\tau 33}_{\ell q} & C^{(3)e\tau 33}_{\ell q} & C^{(1)e\tau 3t}_{\ell equ} & C^{(3)e\tau 3t}_{\ell equ} \end{pmatrix} \begin{pmatrix} y_\tau y_t & 0 & 0 & 0 \\ 0 & -y_\tau y_t & 0 & 0 \\ 0 & -y_\tau y_t & 0 & 0 \\ 0 & 0 & 0 & y_\tau y_t \\ 0 & 0 & y_\tau y_t & 8y_\tau y_t \end{pmatrix} \begin{pmatrix} C^{\tau\mu 33}_{eq} \\ C^{\tau\mu tt}_{eu} \\ C^{(1)\tau\mu 3t}_{\ell equ} \\ C^{(3)\tau\mu 3t}_{\ell equ} \end{pmatrix} \tag{D.3}$$

$$16\pi^2\dot{C}^{*(4)\mu e3t}_{\ell equH^2} = \begin{pmatrix} C^{\tau\mu tt}_{\ell u} & C^{(1)\tau\mu 33}_{\ell q} & C^{(3)\tau\mu 33}_{\ell q} & C^{*(1)\mu\tau 3t}_{\ell equ} & C^{*(3)\mu\tau 3t}_{\ell equ} \end{pmatrix} \begin{pmatrix} y_\tau y_t & 0 & 0 & 0 \\ 0 & -y_\tau y_t & 0 & 0 \\ 0 & -y_\tau y_t & 0 & 0 \\ 0 & 0 & 0 & y_\tau y_t \\ 0 & 0 & y_\tau y_t & 8y_\tau y_t \end{pmatrix} \begin{pmatrix} C^{e\tau 33}_{eq} \\ C^{e\tau tt}_{eu} \\ C^{*(1)\tau e3t}_{\ell equ} \\ C^{*(3)\tau e3t}_{\ell equ} \end{pmatrix} \tag{D.4}$$

In Figure 6.6e we show a representative diagram with the double insertion of two-lepton two-quark $\tau \to l$ operators of dimension six, which renormalizes the coefficient of $\mu \to e$ dimension eight four fermion operators. The mixing is proportional to the square of the top Yukawa y_t^2. The RGEs for scalar and tensor with a up-singlet quark (the sensitivities of $\mu \to e$ processes that we obtain from this mixing are summarized in Tables 6.8 and 6.10) read

$$16\pi^2\dot{C}^{(1)e\mu ii}_{\ell equH^2} = \begin{pmatrix} C^{e\tau ti}_{\ell u} & C^{(1)e\tau ti}_{\ell equ} & C^{(3)e\tau 3i}_{\ell equ} & C^{(1)e\tau it}_{\ell equ} & C^{(3)e\tau it}_{\ell equ} & C^{(1)e\tau i3}_{\ell q} & C^{(3)e\tau i3}_{\ell q} \end{pmatrix} \begin{pmatrix} -2y_t^2 & -24y_t^2 & 0 & 0 & 0 & 0 \\ 0 & 0 & -y_t^2 & 0 & 0 & 0 \\ 0 & 0 & -12y_t^2 & 0 & 0 & 0 \\ 0 & 0 & 0 & 2y_t^2 & 0 & 0 \\ 0 & 0 & 0 & -24y_t^2 & 0 & 0 \\ 0 & 0 & 0 & 0 & y_t^2 & -12y_t^2 \\ 0 & 0 & 0 & 0 & -3y_t^2 & 36y_t^2 \end{pmatrix} \begin{pmatrix} C^{(1)\tau\mu it}_{\ell equ} \\ C^{(3)\tau\mu it}_{\ell equ} \\ C^{\tau\mu i3}_{eq} \\ C^{\tau\mu ti}_{eu} \\ C^{(1)\tau\mu 3i}_{\ell equ} \\ C^{(3)\tau\mu 3i}_{\ell equ} \end{pmatrix} \tag{D.5}$$

$$16\pi^2\dot{C}^{*(1)\mu eii}_{\ell equH^2} = \begin{pmatrix} C^{\tau\mu it}_{\ell u} & C^{*(1)\mu\tau 3i}_{\ell equ} & C^{*(3)\mu\tau 3i}_{\ell equ} & C^{*(1)\mu\tau it}_{\ell equ} & C^{*(3)\mu\tau it}_{\ell equ} & C^{(1)\tau\mu 3i}_{\ell q} & C^{(3)\tau\mu 3i}_{\ell q} \end{pmatrix} \begin{pmatrix} -2y_t^2 & -24y_t^2 & 0 & 0 & 0 & 0 \\ 0 & 0 & -y_t^2 & 0 & 0 & 0 \\ 0 & 0 & -12y_t^2 & 0 & 0 & 0 \\ 0 & 0 & 0 & 2y_t^2 & 0 & 0 \\ 0 & 0 & 0 & -24y_t^2 & 0 & 0 \\ 0 & 0 & 0 & 0 & y_t^2 & -12y_t^2 \\ 0 & 0 & 0 & 0 & -3y_t^2 & 36y_t^2 \end{pmatrix} \begin{pmatrix} C^{*(1)\tau eit}_{\ell equ} \\ C^{*(3)\tau eit}_{\ell equ} \\ C^{e\tau 3i}_{eq} \\ C^{e\tau it}_{eu} \\ C^{*(1)\tau e3i}_{\ell equ} \\ C^{*(3)\tau e3i}_{\ell equ} \end{pmatrix} \tag{D.6}$$

$$16\pi^2\dot{C}^{(2)e\mu ii}_{\ell equH^2} = \begin{pmatrix} C^{(1)e\tau 3i}_{\ell equ} & C^{(3)e\tau 3i}_{\ell equ} & C^{(1)e\tau i3}_{\ell q} & C^{(3)e\tau i3}_{\ell q} \end{pmatrix} \begin{pmatrix} -y_t^2 & 0 & 0 \\ -12y_t^2 & 0 & 0 \\ 0 & y_t^2 & -12y_t^2 \\ 0 & y_t^2 & -12y_t^2 \end{pmatrix} \begin{pmatrix} C^{\tau\mu i3}_{eq} \\ C^{(1)\tau\mu 3i}_{\ell equ} \\ C^{(3)\tau\mu 3i}_{\ell equ} \end{pmatrix} \tag{D.7}$$

$$16\pi^2\dot{C}^{*(2)\mu eii}_{\ell equH^2} = \begin{pmatrix} C^{*(1)\mu\tau 3i}_{\ell equ} & C^{*(3)\mu\tau 3i}_{\ell equ} & C^{(1)\tau\mu 3i}_{\ell q} & C^{(3)\tau\mu 3i}_{\ell q} \end{pmatrix} \begin{pmatrix} -y_t^2 & 0 & 0 \\ -12y_t^2 & 0 & 0 \\ 0 & y_t^2 & -12y_t^2 \\ 0 & y_t^2 & -12y_t^2 \end{pmatrix} \begin{pmatrix} C^{e\tau 3i}_{eq} \\ C^{*(1)\tau e3i}_{\ell equ} \\ C^{*(3)\tau e3i}_{\ell equ} \end{pmatrix} \tag{D.8}$$

$$16\pi^2\dot{C}^{(3)e\mu ii}_{\ell equ H^2} = \begin{pmatrix} C^{e\tau ti}_{\ell u} & C^{(1)e\tau 3i}_{\ell equ} & C^{(3)e\tau 3i}_{\ell equ} & C^{(1)e\tau it}_{\ell equ} & C^{(3)e\tau it}_{\ell equ} & C^{(1)e\tau i3}_{\ell q} & C^{(3)e\tau i3}_{\ell q} \end{pmatrix} \begin{pmatrix} -y_t^2/2 & -6y_t^2 & 0 & 0 & 0 & 0 \\ 0 & 0 & -y_t^2/4 & 0 & 0 & 0 \\ 0 & 0 & -3y_t^2 & 0 & 0 & 0 \\ 0 & 0 & 0 & -y_t^2/2 & 0 & 0 \\ 0 & 0 & 0 & 6y_t^2 & 0 & 0 \\ 0 & 0 & 0 & 0 & -y_t^2/4 & 3y_t^2 \\ 0 & 0 & 0 & 0 & 3y_t^2/4 & -9y_t^2 \end{pmatrix} \begin{pmatrix} C^{(1)\tau\mu it}_{\ell equ} \\ C^{(3)\tau\mu it}_{\ell equ} \\ C^{\tau\mu i3}_{eq} \\ C^{\tau\mu ti}_{eu} \\ C^{(1)\tau\mu 3i}_{\ell equ} \\ C^{(3)\tau\mu 3i}_{\ell equ} \end{pmatrix} \tag{D.9}$$

$$16\pi^2\dot{C}^{*(3)\mu eii}_{\ell equ H^2} = \begin{pmatrix} C^{\tau\mu it}_{\ell u} & C^{*(1)\mu\tau 3i}_{\ell equ} & C^{*(3)\mu\tau 3i}_{\ell equ} & C^{*(1)\mu\tau it}_{\ell equ} & C^{*(3)\mu\tau it}_{\ell equ} & C^{(1)\tau\mu 3i}_{\ell q} & C^{(3)\tau\mu 3i}_{\ell q} \end{pmatrix} \begin{pmatrix} -y_t^2/2 & -6y_t^2 & 0 & 0 & 0 & 0 \\ 0 & 0 & -y_t^2/4 & 0 & 0 & 0 \\ 0 & 0 & -3y_t^2 & 0 & 0 & 0 \\ 0 & 0 & 0 & -y_t^2/2 & 0 & 0 \\ 0 & 0 & 0 & 6y_t^2 & 0 & 0 \\ 0 & 0 & 0 & 0 & -y_t^2/4 & 3y_t^2 \\ 0 & 0 & 0 & 0 & 3y_t^2/4 & -9y_t^2 \end{pmatrix} \begin{pmatrix} C^{*(1)\tau eit}_{\ell equ} \\ C^{*(3)\tau eit}_{\ell equ} \\ C^{e\tau 3i}_{eq} \\ C^{e\tau it}_{eu} \\ C^{*(1)\tau e3i}_{\ell equ} \\ C^{*(3)\tau e3i}_{\ell equ} \end{pmatrix} \tag{D.10}$$

$$16\pi^2\dot{C}^{(4)e\mu ii}_{\ell equ H^2} = \begin{pmatrix} C^{(1)e\tau 3i}_{\ell equ} & C^{(3)e\tau 3i}_{\ell equ} & C^{(1)e\tau i3}_{\ell q} & C^{(3)e\tau i3}_{\ell q} \end{pmatrix} \begin{pmatrix} -y_t^2/4 & 0 & 0 \\ -3y_t^2 & 0 & 0 \\ 0 & -y_t^2/4 & 3y_t^2 \\ 0 & -y_t^2/4 & 3y_t^2 \end{pmatrix} \begin{pmatrix} C^{\tau\mu i3}_{eq} \\ C^{(1)\tau\mu 3i}_{\ell equ} \\ C^{(3)\tau\mu 3i}_{\ell equ} \end{pmatrix} \tag{D.11}$$

$$16\pi^2\dot{C}^{*(4)\mu eii}_{\ell equ H^2} = \begin{pmatrix} C^{*(1)\mu\tau 3i}_{\ell equ} & C^{*(3)\mu\tau 3i}_{\ell equ} & C^{(1)\tau\mu 3i}_{\ell q} & C^{(3)\tau\mu 3i}_{\ell q} \end{pmatrix} \begin{pmatrix} -y_t^2/4 & 0 & 0 \\ -3y_t^2 & 0 & 0 \\ 0 & -y_t^2/4 & 3y_t^2 \\ 0 & -y_t^2/4 & 3y_t^2 \end{pmatrix} \begin{pmatrix} C^{e\tau 3i}_{eq} \\ C^{*(1)\tau e3i}_{\ell equ} \\ C^{*(3)\tau e3i}_{\ell equ} \end{pmatrix}. \tag{D.12}$$

For scalars with a singlet down-quark (sensitivities in Table 6.9), the mixing is

$$16\pi^2\dot{C}^{(1)e\mu ii}_{\ell edq H^2} = \begin{pmatrix} C^{(1)e\tau i3}_{\ell q} & C^{(3)e\tau i3}_{\ell q} & C^{e\tau i3}_{\ledq} \end{pmatrix} \begin{pmatrix} -y_t^2 & 0 \\ -3y_t^2 & 0 \\ 0 & y_t^2 \end{pmatrix} \begin{pmatrix} C^{\tau\mu i3}_{\ell edq} \\ C^{\tau\mu 3i}_{eq} \end{pmatrix} \tag{D.13}$$

$$16\pi^2\dot{C}^{*(1)\mu eii}_{\ell edq H^2} = \begin{pmatrix} C^{(1)\tau\mu 3i}_{\ell q} & C^{(3)\tau\mu 3i}_{\ell q} & C^{*\mu\tau i3}_{\ell edq} \end{pmatrix} \begin{pmatrix} -y_t^2 & 0 \\ -3y_t^2 & 0 \\ 0 & y_t^2 \end{pmatrix} \begin{pmatrix} C^{*\tau ei3}_{\ell edq} \\ C^{e\tau i3}_{eq} \end{pmatrix} \tag{D.14}$$

$$16\pi^2\dot{C}^{(2)e\mu ii}_{\ell edqH^2} = \begin{pmatrix} C^{(1)e\tau i3}_{\ell q} & C^{(3)e\tau i3}_{\ell q} & C^{e\tau i3}_{\ell edq} \end{pmatrix} \begin{pmatrix} y_t^2 & 0 \\ -y_t^2 & 0 \\ 0 & -y_t^2 \end{pmatrix} \begin{pmatrix} C^{\tau\mu i3}_{\ell edq} \\ C^{\tau\mu 3i}_{eq} \end{pmatrix} \tag{D.15}$$

$$16\pi^2\dot{C}^{*(2)\mu eii}_{\ell edqH^2} = \begin{pmatrix} C^{(1)\tau\mu 3i}_{\ell q} & C^{(3)\tau\mu 3i}_{\ell q} & C^{*\mu\tau i3}_{\ell edq} \end{pmatrix} \begin{pmatrix} y_t^2 & 0 \\ -y_t^2 & 0 \\ 0 & -y_t^2 \end{pmatrix} \begin{pmatrix} C^{*\tau ei3}_{\ell edq} \\ C^{e\tau i3}_{eq} \end{pmatrix} \tag{D.16}$$

The anomalous dimensions for the mixing into $\mu \to e$ vectors with SU(2) lepton singlets are (sensitivities in Table 6.12)

$$16\pi^2\dot{C}^{(1)e\mu ii}_{e^2q^2H^2} = \begin{pmatrix} C^{e\tau 3i}_{eq} & C^{e\tau i3}_{eq} & C^{*(1)\tau eit}_{\ell equ} & C^{*(3)\tau eit}_{\ell equ} \end{pmatrix} \begin{pmatrix} -4y_t^2 & 0 & 0 & 0 \\ 0 & y_t^2 & 0 & 0 \\ 0 & 0 & -y_t^2/2 & -6y_t^2 \\ 0 & 0 & -6y_t^2 & -72y_t^2 \end{pmatrix} \begin{pmatrix} C^{\tau\mu i3}_{eq} \\ C^{\tau\mu 3i}_{eq} \\ C^{(1)\tau\mu it}_{\ell equ} \\ C^{(3)\tau\mu it}_{\ell equ} \end{pmatrix} \tag{D.17}$$

$$16\pi^2\dot{C}^{(2)e\mu ii}_{e^2q^2H^2} = \begin{pmatrix} C^{e\tau 3i}_{eq} & C^{e\tau i3}_{eq} \end{pmatrix} \begin{pmatrix} 4y_t^2 & 0 \\ 0 & -y_t^2 \end{pmatrix} \begin{pmatrix} C^{\tau\mu i3}_{eq} \\ C^{\tau\mu 3i}_{eq} \end{pmatrix} \tag{D.18}$$

$$16\pi^2\dot{C}^{e\mu ii}_{e^2u^2H^2} = \begin{pmatrix} C^{e\tau ti}_{eu} & C^{e\tau it}_{eu} & C^{*(1)\tau e3i}_{\ell equ} & C^{*(3)\tau e3i}_{\ell equ} \end{pmatrix} \begin{pmatrix} -2y_t^2 & 0 & 0 & 0 \\ 0 & 8y_t^2 & 0 & 0 \\ 0 & 0 & y_t^2/2 & -6y_t^2 \\ 0 & 0 & -6y_t^2 & 72y_t^2 \end{pmatrix} \begin{pmatrix} C^{\tau\mu it}_{eu} \\ C^{\tau\mu ti}_{eu} \\ C^{(1)\tau\mu 3i}_{\ell equ} \\ C^{(3)\tau\mu 3i}_{\ell equ} \end{pmatrix} \tag{D.19}$$

$$16\pi^2\dot{C}^{e\mu ii}_{e^2d^2H^2} = -\frac{y_t^2}{2} C^{*\tau ei3}_{\ell edq} C^{\tau\mu i3}_{\ell edq} \tag{D.20}$$

while for vectors with lepton doublets (sensitivities in Table 6.13) these are

$$16\pi^2\dot{C}^{(1)e\mu ii}_{\ell^2q^2H^2} = \begin{pmatrix} C^{(1)e\tau 3i}_{\ell q} & C^{(3)e\tau 3i}_{\ell q} & C^{(1)e\tau i3}_{\ell q} & C^{(3)e\tau i3}_{\ell q} & C^{(1)e\tau it}_{\ell equ} & C^{(3)e\tau it}_{\ell equ} \end{pmatrix} \begin{pmatrix} -y_t^2 & 0 & 0 & 0 & 0 & 0 \\ 0 & -3y_t^2 & 0 & 0 & 0 & 0 \\ 0 & 0 & 4y_t^2 & 0 & 0 & 0 \\ 0 & 0 & 0 & 12y_t^2 & 0 & 0 \\ 0 & 0 & 0 & 0 & y_t^2/4 & -3y_t^2 \\ 0 & 0 & 0 & 0 & -3y_t^2 & 36y_t^2 \end{pmatrix} \begin{pmatrix} C^{(1)\tau\mu i3}_{\ell q} \\ C^{(3)\tau\mu i3}_{\ell q} \\ C^{(1)\tau\mu 3i}_{\ell q} \\ C^{(3)\tau\mu 3i}_{\ell q} \\ C^{*(1)\mu\tau it}_{\ell equ} \\ C^{*(3)\mu\tau it}_{\ell equ} \end{pmatrix} \tag{D.21}$$

$$16\pi^2\dot{C}^{(2)e\mu ii}_{\ell^2q^2H^2} = \begin{pmatrix} C^{(1)e\tau ti}_{\ell q} & C^{(3)e\tau ti}_{\ell q} & C^{(1)e\tau it}_{\ell q} & C^{(3)e\tau it}_{\ell q} \end{pmatrix} \begin{pmatrix} 0 & y_t^2 & 0 & 0 \\ y_t^2 & -2y_t^2 & 0 & 0 \\ 0 & 0 & 0 & -4y_t^2 \\ 0 & 0 & -4y_t^2 & -8y_t^2 \end{pmatrix} \begin{pmatrix} C^{(1)\tau\mu i3}_{\ell q} \\ C^{(3)\tau\mu i3}_{\ell q} \\ C^{(1)\tau\mu 3i}_{\ell q} \\ C^{(3)\tau\mu 3i}_{\ell q} \end{pmatrix} \tag{D.22}$$

$$16\pi^2\dot{C}^{(3)e\mu ii}_{\ell^2q^2H^2} = \begin{pmatrix} C^{(1)e\tau 3i}_{\ell q} & C^{(3)e\tau 3i}_{\ell q} & C^{(1)e\tau i3}_{\ell q} & C^{(3)e\tau i3}_{\ell q} & C^{(1)e\tau it}_{\ell equ} & C^{(3)e\tau it}_{\ell equ} \end{pmatrix} \begin{pmatrix} 0 & -y_t^2 & 0 & 0 & 0 & 0 \\ -y_t^2 & -2y_t^2 & 0 & 0 & 0 & 0 \\ 0 & 0 & 0 & 4y_t^2 & 0 & 0 \\ 0 & 0 & 4y_t^2 & -8y_t^2 & 0 & 0 \\ 0 & 0 & 0 & 0 & -y_t^2/4 & 3y_t^2 \\ 0 & 0 & 0 & 0 & 3y_t^2 & -36y_t^2 \end{pmatrix} \begin{pmatrix} C^{(1)\tau\mu i3}_{\ell q} \\ C^{(3)\tau\mu i3}_{\ell q} \\ C^{(1)\tau\mu 3i}_{\ell q} \\ C^{(3)\tau\mu 3i}_{\ell q} \\ C^{*(1)\mu\tau it}_{\ell equ} \\ C^{*(3)\mu\tau it}_{\ell equ} \end{pmatrix} \tag{D.23}$$

$$16\pi^2\dot{C}^{(4)e\mu ii}_{\ell^2q^2H^2} = \begin{pmatrix} C^{(1)e\tau 3i}_{\ell q} & C^{(3)e\tau 3i}_{\ell q} & C^{(1)e\tau i3}_{\ell q} & C^{(3)e\tau i3}_{\ell q} \end{pmatrix} \begin{pmatrix} y_t^2 & 0 & 0 & 0 \\ & -y_t^2 & 0 & 0 \\ 0 & 0 & -4y_t^2 & 0 \\ 0 & 0 & 0 & 4y_t^2 \end{pmatrix} \begin{pmatrix} C^{(1)\tau\mu i3}_{\ell q} \\ C^{(3)\tau\mu i3}_{\ell q} \\ C^{(1)\tau\mu 3i}_{\ell q} \\ C^{(3)\tau\mu 3i}_{\ell q} \end{pmatrix} \tag{D.24}$$

$$16\pi^2\dot{C}^{(1)e\mu ii}_{\ell^2u^2H^2} = \begin{pmatrix} C^{e\tau ti}_{\ell u} & C^{e\tau it}_{\ell u} & C^{(1)e\tau 3i}_{\ell equ} & C^{(3)e\tau 3i}_{\ell equ} \end{pmatrix} \begin{pmatrix} -8y_t^2 & 0 & 0 & 0 \\ 0 & 2y_t^2 & 0 & 0 \\ 0 & 0 & -y_t^2/4 & -3y_t^2 \\ 0 & 0 & -3y_t^2 & -36y_t^2 \end{pmatrix} \begin{pmatrix} C^{\tau\mu it}_{\ell u} \\ C^{\tau\mu ti}_{\ell u} \\ C^{*(1)\mu\tau 3i}_{\ell equ} \\ C^{*(3)\mu\tau 3i}_{\ell equ} \end{pmatrix} \tag{D.25}$$

$$16\pi^2\dot{C}^{(2)e\mu ii}_{\ell^2u^2H^2} = \begin{pmatrix} C^{(1)e\tau 3i}_{\ell equ} & C^{(3)e\tau 3i}_{\ell equ} \end{pmatrix} \begin{pmatrix} -y_t^2/4 & -3y_t^2 \\ -3y_t^2 & -36y_t^2 \end{pmatrix} \begin{pmatrix} C^{*(1)\mu\tau 3i}_{\ell equ} \\ C^{*(3)\mu\tau 3i}_{\ell equ} \end{pmatrix} \tag{D.26}$$

$$16\pi^2\dot{C}^{(1)e\mu ii}_{\ell^2d^2H^2} = \frac{y_t^2}{4}C^{e\tau i3}_{\ell edq}C^{*\mu\tau i3}_{\ell edq} \qquad 16\pi^2\dot{C}^{(2)e\mu ii}_{\ell^2d^2H^2} = -\frac{y_t^2}{4}C^{e\tau i3}_{\ell edq}C^{*\mu\tau i3}_{\ell edq} \tag{D.27}$$

D.2.2 $P_6 \times 4f_6 \to 4f_8$

Dimension six $\tau \to l$ four fermion interactions renormalise $\mu \to e$ dimension eight operators via gauge loops where one vertex is a flavour changing penguin (Eq. (6.12)-(6.14)), as depicted in Figure 6.6d. One-particle-irreducible vertex corrections and "wavefunction-like" contributions (see section 6.2.4 for a discussion) give the following gauge invariant anomalous dimensions, where we align four-fermion interactions and penguins respectively in row and column vectors:

$$16\pi^2 \dot{C}^{(1)e\mu ii}_{\ell equH^2} = \begin{pmatrix} C^{(1)e\tau ii}_{\ell equ} & C^{(3)e\tau ii}_{\ell equ} & C^{(1)\tau\mu ii}_{\ell equ} & C^{(3)\tau\mu ii}_{\ell equ} \end{pmatrix} \begin{pmatrix} 3g'^2 & 0 & 0 \\ -20g'^2 & 0 & 0 \\ 0 & 6g'^2 & 0 \\ 0 & -20g'^2 & 36g'^2 \end{pmatrix} \begin{pmatrix} C^{\tau\mu}_{He} \\ C^{(1)e\tau}_{H\ell} \\ C^{(3)e\tau}_{H\ell} \end{pmatrix} \tag{D.28}$$

$$16\pi^2 \dot{C}^{*(1)\mu eii}_{\ell equH^2} = \begin{pmatrix} C^{*(1)\mu\tau ii}_{\ell equ} & C^{*(3)\mu\tau ii}_{\ell equ} & C^{*(1)\tau eii}_{\ell equ} & C^{*(3)\tau eii}_{\ell equ} \end{pmatrix} \begin{pmatrix} 3g'^2 & 0 & 0 \\ -20g'^2 & 0 & 0 \\ 0 & 6g'^2 & 0 \\ 0 & -20g'^2 & 36g'^2 \end{pmatrix} \begin{pmatrix} C^{e\tau}_{He} \\ C^{(1)\tau\mu}_{H\ell} \\ C^{(3)\tau\mu}_{H\ell} \end{pmatrix} \tag{D.29}$$

$$16\pi^2 \dot{C}^{(2)e\mu ii}_{\ell equH^2} = \begin{pmatrix} C^{(1)e\tau ii}_{\ell equ} & C^{(3)e\tau ii}_{\ell equ} & C^{(1)\tau\mu ii}_{\ell equ} & C^{(3)\tau\mu ii}_{\ell equ} \end{pmatrix} \begin{pmatrix} -3g'^2 & 0 & 0 \\ 12g'^2 & 0 & 0 \\ 0 & 0 & 6g'^2 \\ 0 & 12g^2 & -20g'^2 \end{pmatrix} \begin{pmatrix} C^{\tau\mu}_{He} \\ C^{(1)e\tau}_{H\ell} \\ C^{(3)e\tau}_{H\ell} \end{pmatrix} \tag{D.30}$$

$$16\pi^2 \dot{C}^{*(2)\mu eii}_{\ell equH^2} = \begin{pmatrix} C^{*(1)\mu\tau ii}_{\ell equ} & C^{*(3)\mu\tau ii}_{\ell equ} & C^{*(1)\tau eii}_{\ell equ} & C^{*(3)\tau eii}_{\ell equ} \end{pmatrix} \begin{pmatrix} -3g'^2 & 0 & 0 \\ 12g'^2 & 0 & 0 \\ 0 & 0 & 6g'^2 \\ 0 & 12g^2 & -20g'^2 \end{pmatrix} \begin{pmatrix} C^{e\tau}_{He} \\ C^{(1)\tau\mu}_{H\ell} \\ C^{(3)\tau\mu}_{H\ell} \end{pmatrix} \tag{D.31}$$

$$16\pi^2 \dot{C}^{(3)e\mu ii}_{\ell equH^2} = \begin{pmatrix} C^{(1)e\tau ii}_{\ell equ} & C^{(3)e\tau ii}_{\ell equ} & C^{(1)\tau\mu ii}_{\ell equ} & C^{(3)\tau\mu ii}_{\ell equ} \end{pmatrix} \begin{pmatrix} -5g'^2/12 & 0 & 0 \\ g'^2 & 0 & 0 \\ 0 & -5g'^2/12 & 3g^2/4 \\ 0 & -4g'^2 & -6g^2 \end{pmatrix} \begin{pmatrix} C^{\tau\mu}_{He} \\ C^{(1)e\tau}_{H\ell} \\ C^{(3)e\tau}_{H\ell} \end{pmatrix} \tag{D.32}$$

$$16\pi^2\dot{C}^{*(3)\mu eii}_{\ell equuH^2} = \begin{pmatrix} C^{*(1)\mu\tau ii}_{\ell equ} & C^{*(3)\mu\tau ii}_{\ell equ} & C^{*(1)\tau eii}_{\ell equ} & C^{*(3)\tau eii}_{\ell equ} \end{pmatrix} \begin{pmatrix} -5g'^2/12 & 0 & 0 \\ g'^2 & 0 & 0 \\ 0 & -5g'^2/12 & 3g^2/4 \\ 0 & -4g'^2 & -6g^2 \end{pmatrix} \begin{pmatrix} C^{e\tau}_{He} \\ C^{(1)\tau\mu}_{H\ell} \\ C^{(3)\tau\mu}_{H\ell} \end{pmatrix} \tag{D.33}$$

$$16\pi^2\dot{C}^{(4)e\mu ii}_{\ell equuH^2} = \begin{pmatrix} C^{(1)e\tau ii}_{\ell equ} & C^{(3)e\tau ii}_{\ell equ} & C^{(1)\tau\mu ii}_{\ell equ} & C^{(3)\tau\mu ii}_{\ell equ} \end{pmatrix} \begin{pmatrix} g^2/4 & 0 & 0 \\ 3g^2 & 0 & 0 \\ 0 & g^2/4 & -5g'^2/12 \\ 0 & -2g^2 & -4g'^2 \end{pmatrix} \begin{pmatrix} C^{\tau\mu}_{He} \\ C^{(1)e\tau}_{H\ell} \\ C^{(3)e\tau}_{H\ell} \end{pmatrix} \tag{D.34}$$

$$16\pi^2\dot{C}^{*(4)\mu eii}_{\ell equuH^2} = \begin{pmatrix} C^{*(1)\mu\tau ii}_{\ell equ} & C^{*(3)\mu\tau ii}_{\ell equ} & C^{*(1)\tau eii}_{\ell equ} & C^{*(3)\tau eii}_{\ell equ} \end{pmatrix} \begin{pmatrix} g^2/4 & 0 & 0 \\ 3g^2 & 0 & 0 \\ 0 & g^2/4 & -5g'^2/12 \\ 0 & -2g^2 & -4g'^2 \end{pmatrix} \begin{pmatrix} C^{e\tau}_{He} \\ C^{(1)\tau\mu}_{H\ell} \\ C^{(3)\tau\mu}_{H\ell} \end{pmatrix} \tag{D.35}$$

$$16\pi^2\dot{C}^{(1)e\mu ii}_{\ell edqH^2} = \begin{pmatrix} C^{e\tau ii}_{\ell edq} & C^{\tau\mu ii}_{\ell edq} \end{pmatrix} \begin{pmatrix} 3g'^2 & 0 \\ 0 & 6g'^2 \end{pmatrix} \begin{pmatrix} C^{\tau\mu}_{He} \\ C^{(1)e\tau}_{H\ell} \end{pmatrix} \tag{D.36}$$

$$16\pi^2\dot{C}^{*(1)\mu eii}_{\ell edqH^2} = \begin{pmatrix} C^{*\mu\tau ii}_{\ell edq} & C^{*\tau eii}_{\ell edq} \end{pmatrix} \begin{pmatrix} 3g'^2 & 0 \\ 0 & 6g'^2 \end{pmatrix} \begin{pmatrix} C^{e\tau}_{He} \\ C^{(1)\tau\mu}_{H\ell} \end{pmatrix} \tag{D.37}$$

$$16\pi^2\dot{C}^{(2)e\mu ii}_{\ell edqH^2} = \begin{pmatrix} C^{e\tau ii}_{\ell edq} & C^{\tau\mu ii}_{\ell edq} \end{pmatrix} \begin{pmatrix} -3g^2 & 0 \\ 0 & 6g'^2 \end{pmatrix} \begin{pmatrix} C^{\tau\mu}_{He} \\ C^{(3)e\tau}_{H\ell} \end{pmatrix} \tag{D.38}$$

$$16\pi^2\dot{C}^{*(2)\mu eii}_{\ell edqH^2} = \begin{pmatrix} C^{*\mu\tau ii}_{\ell edq} & C^{*\tau eii}_{\ell edq} \end{pmatrix} \begin{pmatrix} -3g^2 & 0 \\ 0 & 6g'^2 \end{pmatrix} \begin{pmatrix} C^{e\tau}_{He} \\ C^{(3)\tau\mu}_{H\ell} \end{pmatrix} \tag{D.39}$$

$$16\pi^2\dot{C}^{(1)e\mu ii}_{\ell^2q^2H^2} = \begin{pmatrix} C^{(1)e\tau ii}_{\ell q} & C^{(3)e\tau ii}_{\ell q} & C^{(1)\tau\mu ii}_{\ell q} & C^{(3)\tau\mu ii}_{\ell q} \end{pmatrix} \begin{pmatrix} g'^2 & 0 & 0 & 0 \\ 0 & 9g^2 & 0 & 0 \\ 0 & 0 & g'^2 & 0 \\ 0 & 0 & 0 & 9g^2 \end{pmatrix} \begin{pmatrix} C^{(1)\tau\mu}_{H\ell} \\ C^{(3)\tau\mu}_{H\ell} \\ C^{(1)e\tau}_{H\ell} \\ C^{(3)e\tau}_{H\ell} \end{pmatrix} \tag{D.40}$$

$$16\pi^2\dot{C}^{(2)e\mu ii}_{\ell^2q^2H^2} = \begin{pmatrix} C^{(1)e\tau ii}_{\ell q} & C^{(3)e\tau ii}_{\ell q} & C^{(1)\tau\mu ii}_{\ell q} & C^{(3)\tau\mu ii}_{\ell q} \end{pmatrix} \begin{pmatrix} 0 & g'^2 & 0 & 0 \\ 3g^2 & 0 & 0 & 0 \\ 0 & 0 & 0 & g'^2 \\ 0 & 0 & 3g^2 & 0 \end{pmatrix} \begin{pmatrix} C^{(1)\tau\mu}_{H\ell} \\ C^{(3)\tau\mu}_{H\ell} \\ C^{(1)e\tau}_{H\ell} \\ C^{(3)e\tau}_{H\ell} \end{pmatrix} \tag{D.41}$$

$$16\pi^2\dot{C}^{(3)e\mu ii}_{\ell^2q^2H^2} = \begin{pmatrix} C^{(1)e\tau ii}_{\ell q} & C^{(3)e\tau ii}_{\ell q} & C^{(1)\tau\mu ii}_{\ell q} & C^{(3)\tau\mu ii}_{\ell q} \end{pmatrix} \begin{pmatrix} 0 & 3g^2 & 0 & 0 \\ g'^2 & -10g^2 & 0 & 0 \\ 0 & 0 & 0 & 3g^2 \\ 0 & 0 & g'^2 & -10g^2 \end{pmatrix} \begin{pmatrix} C^{(1)\tau\mu}_{H\ell} \\ C^{(3)\tau\mu}_{H\ell} \\ C^{(1)e\tau}_{H\ell} \\ C^{(3)e\tau}_{H\ell} \end{pmatrix} \tag{D.42}$$

$$16\pi^2\dot{C}^{(4)e\mu ii}_{\ell^2q^2H^2} = \begin{pmatrix} C^{(1)e\tau ii}_{\ell q} & C^{(3)e\tau ii}_{\ell q} & C^{(1)\tau\mu ii}_{\ell q} & C^{(3)\tau\mu ii}_{\ell q} \end{pmatrix} \begin{pmatrix} 3g^2 & 0 & 0 & 0 \\ 0 & g'^2 & 0 & 0 \\ 0 & 0 & 3g^2 & 0 \\ 0 & 0 & 0 & g'^2 \end{pmatrix} \begin{pmatrix} C^{(1)\tau\mu}_{H\ell} \\ C^{(3)\tau\mu}_{H\ell} \\ C^{(1)e\tau}_{H\ell} \\ C^{(3)e\tau}_{H\ell} \end{pmatrix} \tag{D.43}$$

$$16\pi^2\dot{C}^{e\mu ii}_{e^2u^2H^2} = \begin{pmatrix} C^{e\tau ii}_{eu} & C^{\tau\mu ii}_{eu} \end{pmatrix} \begin{pmatrix} 4g'^2 & 0 \\ 0 & 4g'^2 \end{pmatrix} \begin{pmatrix} C^{\tau\mu}_{He} \\ C^{e\tau}_{He} \end{pmatrix} \tag{D.44}$$

$$16\pi^2\dot{C}^{e\mu ii}_{e^2d^2H^2} = \begin{pmatrix} C^{e\tau ii}_{ed} & C^{\tau\mu ii}_{ed} \end{pmatrix} \begin{pmatrix} -2g'^2 & 0 \\ 0 & -2g'^2 \end{pmatrix} \begin{pmatrix} C^{\tau\mu}_{He} \\ C^{e\tau}_{He} \end{pmatrix} \tag{D.45}$$

$$16\pi^2\dot{C}^{(1)e\mu ii}_{e^2q^2H^2} = \begin{pmatrix} C^{e\tau ii}_{eq} & C^{\tau\mu ii}_{eq} \end{pmatrix} \begin{pmatrix} -g'^2 & 0 \\ 0 & -g'^2 \end{pmatrix} \begin{pmatrix} C^{\tau\mu}_{He} \\ C^{e\tau}_{He} \end{pmatrix} \tag{D.46}$$

$$16\pi^2 \dot{C}^{(2)e\mu ii}_{e^2q^2H^2} = \begin{pmatrix} C^{e\tau ii}_{eq} & C^{\tau\mu ii}_{eq} \end{pmatrix} \begin{pmatrix} -3g^2 & 0 \\ 0 & -3g^2 \end{pmatrix} \begin{pmatrix} C^{\tau\mu}_{He} \\ C^{e\tau}_{He} \end{pmatrix} \tag{D.47}$$

$$16\pi^2 \dot{C}^{(1)e\mu ii}_{\ell^2u^2H^2} = \begin{pmatrix} C^{e\tau ii}_{\ell u} & C^{\tau\mu ii}_{\ell u} \end{pmatrix} \begin{pmatrix} -4g'^2 & 0 \\ 0 & -4g'^2 \end{pmatrix} \begin{pmatrix} C^{(1)\tau\mu}_{H\ell} \\ C^{(1)e\tau}_{H\ell} \end{pmatrix} \tag{D.48}$$

$$16\pi^2 \dot{C}^{(2)e\mu ii}_{\ell^2u^2H^2} = \begin{pmatrix} C^{e\tau ii}_{\ell u} & C^{\tau\mu ii}_{\ell u} \end{pmatrix} \begin{pmatrix} -4g'^2 & 0 \\ 0 & -4g'^2 \end{pmatrix} \begin{pmatrix} C^{(3)\tau\mu}_{H\ell} \\ C^{(3)e\tau}_{H\ell} \end{pmatrix} \tag{D.49}$$

$$16\pi^2 \dot{C}^{(1)e\mu ii}_{\ell^2d^2H^2} = \begin{pmatrix} C^{e\tau ii}_{\ell d} & C^{\tau\mu ii}_{\ell d} \end{pmatrix} \begin{pmatrix} 2g'^2 & 0 \\ 0 & 2g'^2 \end{pmatrix} \begin{pmatrix} C^{(1)\tau\mu}_{H\ell} \\ C^{(1)e\tau}_{H\ell} \end{pmatrix} \tag{D.50}$$

$$16\pi^2 \dot{C}^{(2)e\mu ii}_{\ell^2d^2H^2} = \begin{pmatrix} C^{e\tau ii}_{\ell d} & C^{\tau\mu ii}_{\ell d} \end{pmatrix} \begin{pmatrix} 2g'^2 & 0 \\ 0 & 2g'^2 \end{pmatrix} \begin{pmatrix} C^{(3)\tau\mu}_{H\ell} \\ C^{(3)e\tau}_{H\ell} \end{pmatrix} \tag{D.51}$$

D.2.3 $Y_6 \times Y_6 \to P_8$

We here write the RGEs for the mixing of two dimension six $\tau \to l$ Yukawa (Eq. (6.17)) into the the dimension eight $\mu \to e$ penguins (Eq. (6.43)). More details can be found in section 6.3.1.1 of the text.

$$16\pi^2 \dot{C}^{e\mu}_{e^2H^4D} = -C^{\tau\mu}_{eH} C^{*\tau e}_{eH} \tag{D.52}$$

$$16\pi^2 \dot{C}^{(1)e\mu}_{\ell^2H^4D} = \frac{1}{2} C^{*\mu\tau}_{eH} C^{e\tau}_{eH} \qquad 16\pi^2 \dot{C}^{(2)e\mu}_{\ell^2H^4D} = \frac{1}{4} C^{*\mu\tau}_{eH} C^{e\tau}_{eH} \tag{D.53}$$

D.3 Limits from B Decays

In the body of the paper, we saw that $\mu \leftrightarrow e$ processes have a good sensitivity to products of $\tau \leftrightarrow l$ coefficients which both involve a top quark, via the fish diagram of Figure 6.6 e). When the top quark is in an doublet, these same $\tau \leftrightarrow l$ coefficients mediate B decays, which is discussed in this section.

We set limits on the $\tau \leftrightarrow l$ coefficients from their contributions to leptonic and semi-leptonic B decays. They can induce "neutral current" processes, such as $B_d \to \tau^{\pm} l^{\mp}$, which are absent in the SM, and also contribute to "charged current" decays such as $B^+ \to \bar{\tau}\nu$, to which the SM does contribute but with a different-flavoured neutrino. Since our coefficients are lepton-flavour-changing, they cannot interfere with the Standard Model, so neccessarily increase the Branching Ratios with respect to their SM expectation. This makes it difficult to fit the current B anomalies with LFV operators, because many of the anomalies are experimental deficits with respect to the SM predictions.

The list of decays that are included is given in table D.1, along with the value of the Branching Ratio(BR) which we use to extract limits (A coefficient at its upper limit gives this BR). For processes where the SM contribution is negligeable, this value is the the experimental 95% C.L. upper bound on the BR. In the case of SM processes where prediction $\approx$ observation, this value is the SM prediction + theory uncertainty + 2σ experimental uncertainty. This definition is used because we would like to remove the SM part and require that the flavour-changing interactions contribute less than the remainder. However, it can occur that the SM prediction exceeds the experimental observation (as in some "B anomalies").

To extrapolate the limits we obtain from current experimental constraints into the future, we suppose a factor of 10 improvement in the experimental sensitivity (and in the theoretical precision), such that the future limits will be a factor of ~ 3 better.

Our limits are obtained using Flavio [360]. The limits obtained from two-body leptonic decays were checked analytically, using the well-known formula for the rate as a function of operator coefficients at the experimental scale m_b:

$$\Gamma(B_0 \to \bar{\tau}\mu) = \frac{E_\mu^2 f_B^2}{16\pi v^4}\Big\{(|C_{V,LX}^{db\mu\tau}|^2 + |C_{V,RX}^{db\mu\tau}|^2)(E_\tau - E_\mu) + (|C_{S,RX}^{db\mu\tau}|^2 + |C_{S,LX}^{db\mu\tau}|^2)\frac{m_B^2}{m_b^2}(E_\tau + E_\mu) + ...\Big\} \tag{D.54}$$

where "..." are cross-terms and m_μ is neglected. A numerical limit can be obtained by, for instance, comparing to the experimental rate for $B^+ \to \bar{\tau}\nu$.

The coefficients are run from $m_b \to \Lambda_{\rm NP} = 4$ TeV with the one-loop RGEs of QCD (which shrinks scalar coefficients by a factor $\sim 3/5$), with tree-level matching to SMEFT operators when passing m_W. Electroweak running is neglected, except in the case of tensor to scalar mixing in SMEFT[1] (where $C_S(m_W) \sim 0.3 C_T(\Lambda_{\rm NP})$), which for instance, mixes single-top tensors $\mathcal{O}_{\ell equ}^{(3)\tau e3u}$ into scalars that induce $B^+ \to \bar{e}\nu$.

[1] The tensor to scalar mixing below m_W in QED is negligeable for "charged-current" tensors involving a b and a ν.

coefficient	limit	process	BR
$C_{eq}^{e\tau 32}$,$C_{\ell q}^{(1)e\tau 32} + C_{\ell q}^{(3)e\tau 32}$	2.3×10^{-3}(c)	$B^+ \to K + \tau^\pm e^\mp$	$< 4.4 \times 10^{-5}$ [366]
$C_{eq}^{e\tau 31}$,$C_{\ell q}^{(1)e\tau 31} + C_{\ell q}^{(3)e\tau 31}$	2.3×10^{-3}(c)	$B_d^0 \to \tau^\pm e^\mp$	$< 3.0 \times 10^{-5}$ [367]
$C_{eq}^{\mu\tau 32}$,$C_{\ell q}^{(1)\mu\tau 32} + C_{\ell q}^{(3)\mu\tau 32}$	2.3×10^{-3}(c)	$B_s^0 \to \tau^\pm \mu^\mp$	$< 4.3 \times 10^{-5}$ [368]
$C_{eq}^{\mu\tau 31}$,$C_{\ell q}^{(1)\mu\tau 31} + C_{\ell q}^{(3)\mu\tau 31}$	1.5×10^{-3}(c)	$B_d^0 \to \tau^\pm \mu^\mp$	$< 1.2 \times 10^{-5}$ [368]
$C_{\ell edq}^{e\tau d3}$, $C_{\ell edq}^{\tau e d3}$	3.4×10^{-4}(c)	$B_d^0 \to e^\pm \tau^\mp$	$< 3.0 \times 10^{-5}$ [367]
$C_{\ell edq}^{\mu\tau d3}$, $C_{\ell edq}^{\tau\mu d3}$	2.2×10^{-4}(c)	$B_d^0 \to \mu^\pm \tau^\mp$	$< 1.2 \times 10^{-5}$ [368]
$C_{\ell edq}^{\mu\tau s3}$, $C_{\ell edq}^{\tau\mu s3}$	3.3×10^{-4}(c)	$B_s^0 \to \mu^\pm \tau^\mp$	$< 4.3 \times 10^{-5}$ [368]
$C_{\ell equ}^{(1)l\tau 3u}$	4.5×10^{-4}(c)	$B^- \to \tau\bar{\nu}$	1.4×10^{-4} [360,369]
$C_{\ell equ}^{(1)\tau e 3u}$	5.8×10^{-5}(c)	$B^- \to e\bar{\nu}$	$\leq 1.2 \times 10^{-6}$ [370]
$C_{\ell equ}^{(1)\tau\mu 3u}$	4.3×10^{-5}(c)	$B^- \to \mu\bar{\nu}$	$\leq 1.0 \times 10^{-6}$ [371]
$C_{\ell equ}^{(1)l\tau 3c}$	1.0×10^{-2}(c)	$B_c^- \to \tau\bar{\nu}$	0.1 [360]
$C_{\ell equ}^{(1)\tau e 3c}$	9.0×10^{-3}(c)	$B_d^0 \to De\bar{\nu}$	$\leq 3.0 \times 10^{-2}$ [360]
$C_{\ell equ}^{(1)\tau\mu 3c}$	9.0×10^{-3}(c)	$B_d^0 \to D\mu\bar{\nu}$	$\leq 3.1 \times 10^{-2}$ [360]
$C_{\ell equ}^{(3)l\tau 3u}$	1.8×10^{-3}(c)	$B^- \to \tau\bar{\nu}$	1.4×10^{-4} [360,369]
$C_{\ell equ}^{(3)\tau e 3u}$	2.4×10^{-4}(c)	$B^- \to e\bar{\nu}$	$\leq 1.2 \times 10^{-6}$ [370]
$C_{\ell equ}^{(3)\tau\mu 3u}$	1.8×10^{-4}(c)	$B^- \to \mu\bar{\nu}$	$\leq 1.0 \times 10^{-6}$ [371]
$C_{\ell equ}^{(3)l\tau 3c}$	5.0×10^{-3}(c)	$R_{\tau/l}(B \to D^* l\bar{\nu})$	0.28 [360]
$C_{\ell equ}^{(3)\tau e 3c}$	5.3×10^{-3}(c)	$B_d^0 \to D^* e\bar{\nu}$	$\leq 7.3 \times 10^{-2}$ [360]
$C_{\ell equ}^{(3)\tau\mu 3c}$	6.4×10^{-3}(c)	$B_d^0 \to D^*\mu\bar{\nu}$	$\leq 7.7 \times 10^{-2}$ [360]

Table D.1: Current limits (c) on $\tau \leftrightarrow e$ and $\tau \leftrightarrow \mu$ coefficients of SMEFT operators, at 4 TeV, arising from the B decays given in the third column. The limits saturate the Branching Ratio given in the last column (which may not be the cited experimental limit, see discussion in Appendix D.3). Limits on vector coefficients apply for permuted lepton and quark flavour indices, scalars apply as given.

D.4 Table of Sensitivities

coefficients	$B^{(f)}_{\tau\leftrightarrow e}B^{(f)}_{\tau\leftrightarrow\mu}$	$B^{(f)}_{\mu\to e}$
$C^{(1)e\tau 1u}_{\ell equ}C^{\tau\mu}_{He}$	$8.3\times10^{-5}(f)\times1.2\times10^{-4}(f)$	5×10^{-9}
$\boldsymbol{C^{(3)e\tau 1u}_{\ell equ}C^{\tau\mu}_{He}}$	$7.7\times10^{-5}(f)\times1.2\times10^{-4}(f)$	2×10^{-9}
$(C^{(1)\tau e1u}_{\ell equ})^*C^{\tau\mu}_{H\ell(1)}$	$8.3\times10^{-5}(f)\times1.0\times10^{-4}(f)$	1×10^{-8}
$\boldsymbol{(C^{(3)\tau e1u}_{\ell equ})^*C^{\tau\mu}_{H\ell(1)}}$	$7.7\times10^{-5}(f)\times1.0\times10^{-4}(f)$	2×10^{-9}
$(C^{(1)\tau e1u}_{\ell equ})^*C^{\tau\mu}_{H\ell(3)}$	$8.3\times10^{-5}(f)\times1.0\times10^{-4}(f)$	1×10^{-8}
$\boldsymbol{(C^{(3)\tau e1u}_{\ell equ})^*C^{\tau\mu}_{H\ell(3)}}$	$7.7\times10^{-5}(f)\times1.0\times10^{-4}(f)$	3×10^{-10}
$C^{e\tau d1}_{\ell edq}C^{\tau\mu}_{He}$	$8.3\times10^{-5}(f)\times1.2\times10^{-4}(f)$	5×10^{-9}
$(C^{\tau ed1}_{\ell edq})^*C^{\tau\mu}_{H\ell(1)}$	$8.3\times10^{-5}(f)\times1.0\times10^{-4}(f)$	1×10^{-8}
$(C^{\tau ed1}_{\ell edq})^*C^{\tau\mu}_{H\ell(3)}$	$8.3\times10^{-5}(f)\times1.0\times10^{-4}(f)$	1×10^{-8}

Table D.2: Pair of $\tau\leftrightarrow l$ penguin and four fermion dimension six operators that generate $\mu\to e$ scalar/tensor dimension eight operators with a singlet u and d quark. The future (f) "limits" $B^{(f)}_{\tau\leftrightarrow l}$ on $\tau\leftrightarrow l$ vectors and scalars are from the upper bounds on the LFV decays $\tau\to l\rho(\eta)$ and $\tau\to\pi l$ respectively (adapted from [322]). The limits on penguins follow from their contribution to four-lepton vector interactions $\tau\to 3l$. The same bound applies to the dimension six operators with $\mu\leftrightarrow e$ interchanged. The sensitivities $B^{(f)}_{\mu\to e}$ arise from future $\mu\to e$ conversion. Bolded pairs indicate that the sensitivity of $\mu\to e$ is better than the one arising from direct $\tau\leftrightarrow l$ searches (see Eq. (6.100)).

coefficients	$B^{(f)}_{\tau\leftrightarrow e}B^{(f)}_{\tau\leftrightarrow\mu}$	$B^{(f)}_{\mu\to e}$
$C^{e\tau uu}_{eu}C^{\tau\mu}_{He}$	$2.4\times10^{-4}(f)\times1.1\times10^{-4}(f)$	4.6×10^{-8}
$C^{e\tau dd}_{ed}C^{\tau\mu}_{He}$	$2.4\times10^{-4}(f)\times1.1\times10^{-4}(f)$	8.2×10^{-8}
$C^{(1)e\tau 11}_{\ell q}C^{\tau\mu}_{H\ell(1)}$	$7.0\times10^{-4}(f)\times1.\times10^{-4}(f)$	1×10^{-7}
$C^{(1)e\tau 11}_{\ell q}C^{\tau\mu}_{H\ell(3)}$	$7.0\times10^{-4}(f)\times1.\times10^{-4}(f)$	8.5×10^{-8}
$C^{(3)e\tau 11}_{\ell q}C^{\tau\mu}_{H\ell(1)}$	$1.2\times10^{-4}(f)\times1.\times10^{-4}(f)$	1×10^{-8}
$\boldsymbol{C^{(3)e\tau 11}_{\ell q}C^{\tau\mu}_{H\ell(3)}}$	$1.2\times10^{-4}(f)\times1.\times10^{-4}(f)$	3.2×10^{-9}

Table D.3: Similar to Table D.2 but with product of penguin and four-fermion dimension six operators that mix into $\mu\to e$ vectors at dimension eight.

Bibliography

[1] M. Ardu and G. Pezzullo, *Introduction to Charged Lepton Flavor Violation*, *Universe* **8** (2022) 299 [2204.08220]. (Cited on pages 2 and 24.)

[2] M. Ardu and S. Davidson, *What is Leading Order for LFV in SMEFT?*, *JHEP* **08** (2021) 002 [2103.07212]. (Cited on pages 2 and 134.)

[3] M. Ardu, S. Davidson and M. Gorbahn, *Sensitivity of $\mu \to e$ processes to τ flavor change*, *Phys. Rev. D* **105** (2022) 096040 [2202.09246]. (Cited on page 2.)

[4] M. Ardu and F. Kirk, *A viable $L_e - L_\mu$ model with $\mu \to e$ violation*, *Eur. Phys. J. C* **83** (2023) 394 [2205.02254]. (Cited on page 3.)

[5] M. Ardu, G. Isidori and M. Pesut, *Semi-inclusive Lepton Flavor Universality ratio in $b \to s\ell^+\ell^-$ transitions*, *Phys. Rev. D* **106** (2022) 093008 [2207.12420]. (Cited on page 3.)

[6] P. A. M. Dirac, *Quantum theory of emission and absorption of radiation*, *Proc. Roy. Soc. Lond. A* **114** (1927) 243. (Cited on page 5.)

[7] F. J. Dyson, *The radiation theories of tomonaga, schwinger, and feynman*, *Phys. Rev.* **75** (1949) 486. (Cited on page 5.)

[8] E. Fermi, *Tentativo di una teoria dell'emissione dei raggi beta*, *Ric. Sci.* **4** (1933) 491. (Cited on page 5.)

[9] C. L. Cowan, F. Reines, F. B. Harrison, H. W. Kruse and A. D. McGuire, *Detection of the free neutrino: A Confirmation*, *Science* **124** (1956) 103. (Cited on page 5.)

[10] G. Danby, J. M. Gaillard, K. A. Goulianos, L. M. Lederman, N. B. Mistry, M. Schwartz et al., *Observation of High-Energy Neutrino Reactions and the Existence of Two Kinds of Neutrinos*, *Phys. Rev. Lett.* **9** (1962) 36. (Cited on page 5.)

[11] J. Schwinger, *A theory of the fundamental interactions*, *Annals of Physics* **2** (1957) 407. (Cited on page 5.)

[12] T. D. Lee and C. N. Yang, *Possible nonlocal effects in μ decay*, *Phys. Rev.* **108** (1957) 1611. (Cited on page 5.)

[13] S. A. Bludman, *On the universal Fermi interaction*, *Nuovo Cim.* **9** (1958) 433. (Cited on page 5.)

[14] S. L. Glashow, *Partial Symmetries of Weak Interactions*, *Nucl. Phys.* **22** (1961) 579. (Cited on page 5.)

[15] A. Salam and J. C. Ward, *Electromagnetic and weak interactions*, *Phys. Lett.* **13** (1964) 168. (Cited on page 5.)

[16] S. Weinberg, *A Model of Leptons*, *Phys. Rev. Lett.* **19** (1967) 1264. (Cited on page 5.)

[17] F. Englert and R. Brout, *Broken symmetry and the mass of gauge vector mesons*, *Phys. Rev. Lett.* **13** (1964) 321. (Cited on page 5.)

[18] P. W. Higgs, *Broken symmetries and the masses of gauge bosons*, *Phys. Rev. Lett.* **13** (1964) 508. (Cited on page 5.)

[19] F. Hasert, S. Kabe, W. Krenz and J. V. et al., *Observation of neutrino-like interactions without muon or electron in the gargamelle neutrino experiment*, *Physics Letters B* **46** (1973) 138. (Cited on page 6.)

[20] C. M. G. Lattes, G. P. S. Occhialini and C. F. Powell, *Observations on the Tracks of Slow Mesons in Photographic Emulsions. 2*, *Nature* **160** (1947) 486. (Cited on page 6.)

[21] G. D. Rochester and C. C. Butler, *Evidence for the Existence of New Unstable Elementary Particles*, *Nature* **160** (1947) 855. (Cited on page 6.)

[22] J. Steinberger, W. K. H. Panofsky and J. Steller, *Evidence for the production of neutral mesons by photons*, *Phys. Rev.* **78** (1950) 802. (Cited on page 6.)

[23] M. Gell-Mann, *Isotopic spin and new unstable particles*, *Phys. Rev.* **92** (1953) 833. (Cited on page 6.)

[24] M. Gell-Mann, *A schematic model of baryons and mesons*, *Physics Letters* **8** (1964) 214. (Cited on page 6.)

[25] G. Zweig, *An SU(3) model for strong interaction symmetry and its breaking. Version 2*, in *DEVELOPMENTS IN THE QUARK THEORY OF HADRONS. VOL. 1. 1964 - 1978*, D. B. Lichtenberg and S. P. Rosen, eds., pp. 22–101, (2, 1964). (Cited on page 6.)

[26] N. Cabibbo, *Unitary symmetry and leptonic decays*, *Phys. Rev. Lett.* **10** (1963) 531. (Cited on page 6.)

[27] O. W. Greenberg, *Spin and Unitary Spin Independence in a Paraquark Model of Baryons and Mesons*, *Phys. Rev. Lett.* **13** (1964) 598. (Cited on page 6.)

[28] D. J. Gross and F. Wilczek, *Ultraviolet Behavior of Nonabelian Gauge Theories*, *Phys. Rev. Lett.* **30** (1973) 1343. (Cited on page 6.)

[29] H. D. Politzer, *Reliable Perturbative Results for Strong Interactions?*, *Phys. Rev. Lett.* **30** (1973) 1346. (Cited on page 6.)

[30] S. L. Glashow, J. Iliopoulos and L. Maiani, *Weak interactions with lepton-hadron symmetry*, *Phys. Rev. D* **2** (1970) 1285. (Cited on pages 7 and 10.)

[31] J. J. Aubert, U. Becker, P. J. Biggs, J. Burger, M. Chen, G. Everhart et al., *Experimental observation of a heavy particle j*, *Phys. Rev. Lett.* **33** (1974) 1404. (Cited on page 7.)

[32] J. E. Augustin, A. M. Boyarski, M. Breidenbach, F. Bulos, J. T. Dakin, G. J. Feldman et al., *Discovery of a narrow resonance in e^+e^- annihilation*, *Phys. Rev. Lett.* **33** (1974) 1406. (Cited on page 7.)

[33] S. Weinberg, *Effects of a neutral intermediate boson in semileptonic processes*, *Phys. Rev. D* **5** (1972) 1412. (Cited on page 7.)

[34] M. L. Perl et al., *Evidence for Anomalous Lepton Production in e+ - e- Annihilation*, *Phys. Rev. Lett.* **35** (1975) 1489. (Cited on page 7.)

[35] E288 collaboration, *Observation of a Dimuon Resonance at 9.5-GeV in 400-GeV Proton-Nucleus Collisions*, *Phys. Rev. Lett.* **39** (1977) 252. (Cited on page 7.)

[36] CDF collaboration, *Observation of top quark production in $\bar{p}p$ collisions*, *Phys. Rev. Lett.* **74** (1995) 2626 [hep-ex/9503002]. (Cited on page 7.)

[37] M. Kobayashi and T. Maskawa, *CP Violation in the Renormalizable Theory of Weak Interaction*, *Prog. Theor. Phys.* **49** (1973) 652. (Cited on page 7.)

[38] UA1 collaboration, *Experimental Observation of Isolated Large Transverse Energy Electrons with Associated Missing Energy at $\sqrt{s} = 540$ GeV*, *Phys. Lett. B* **122** (1983) 103. (Cited on page 7.)

[39] UA1 collaboration, *Experimental Observation of Lepton Pairs of Invariant Mass Around 95-GeV/c**2 at the CERN SPS Collider*, *Phys. Lett. B* **126** (1983) 398. (Cited on page 7.)

[40] ATLAS collaboration, *Observation of a new particle in the search for the Standard Model Higgs boson with the ATLAS detector at the LHC*, *Phys. Lett. B* **716** (2012) 1 [1207.7214]. (Cited on page 7.)

[41] CMS collaboration, *Observation of a New Boson at a Mass of 125 GeV with the CMS Experiment at the LHC*, *Phys. Lett. B* **716** (2012) 30 [1207.7235]. (Cited on page 7.)

[42] Super-Kamiokande collaboration, *Review of Nucleon Decay Searches at Super-Kamiokande*, in *51st Rencontres de Moriond on EW Interactions and Unified Theories*, pp. 437–444, 2016, 1605.03235. (Cited on page 8.)

[43] S. L. Adler, *Axial-vector vertex in spinor electrodynamics*, *Phys. Rev.* **177** (1969) 2426. (Cited on page 8.)

[44] J. S. Bell and R. Jackiw, *A PCAC puzzle: $\pi^0 \to \gamma\gamma$ in the σ model*, *Nuovo Cim. A* **60** (1969) 47. (Cited on page 8.)

[45] W. A. Bardeen, *Anomalous Currents in Gauge Field Theories*, *Nucl. Phys. B* **75** (1974) 246. (Cited on page 9.)

[46] A. Belavin, A. Polyakov, A. Schwartz and Y. Tyupkin, *Pseudoparticle solutions of the yang-mills equations*, *Physics Letters B* **59** (1975) 85. (Cited on page 9.)

[47] Particle Data Group collaboration, *Review of Particle Physics*, *PTEP* **2022** (2022) 083C01. (Cited on pages 9, 83 and 85.)

[48] L. Wolfenstein, *Parametrization of the Kobayashi-Maskawa Matrix*, *Phys. Rev. Lett.* **51** (1983) 1945. (Cited on pages 10 and 79.)

[49] A. J. Buras, M. E. Lautenbacher and G. Ostermaier, *Waiting for the top quark mass, K+ —> pi+ neutrino anti-neutrino, B(s)0 - anti-B(s)0 mixing and CP asymmetries in B decays*, *Phys. Rev. D* **50** (1994) 3433 [hep-ph/9403384]. (Cited on page 10.)

[50] CKMfitter Group collaboration, *CP violation and the CKM matrix: Assessing the impact of the asymmetric B factories*, *Eur. Phys. J. C* **41** (2005) 1 [hep-ph/0406184]. (Cited on page 10.)

[51] Particle Data Group collaboration, *Review of Particle Physics*, *PTEP* **2022** (2022) 083C01. (Cited on pages 10, 12, 14 and 15.)

[52] A. Hocker, H. Lacker, S. Laplace and F. Le Diberder, *A New approach to a global fit of the CKM matrix*, *Eur. Phys. J. C* **21** (2001) 225 [hep-ph/0104062]. (Cited on page 10.)

[53] C. Jarlskog, *Commutator of the quark mass matrices in the standard electroweak model and a measure of maximal* CP *nonconservation*, *Phys. Rev. Lett.* **55** (1985) 1039. (Cited on page 11.)

[54] R. Davis, Jr., D. S. Harmer and K. C. Hoffman, *Search for neutrinos from the sun*, *Phys. Rev. Lett.* **20** (1968) 1205. (Cited on page 11.)

[55] B. T. Cleveland, T. Daily, R. Davis, Jr., J. R. Distel, K. Lande, C. K. Lee et al., *Measurement of the solar electron neutrino flux with the Homestake chlorine detector*, *Astrophys. J.* **496** (1998) 505. (Cited on page 11.)

[56] SAGE collaboration, *Solar neutrino flux measurements by the Soviet-American Gallium Experiment (SAGE) for half the 22 year solar cycle*, *J. Exp. Theor. Phys.* **95** (2002) 181 [astro-ph/0204245]. (Cited on page 11.)

[57] GALLEX collaboration, *GALLEX solar neutrino observations: Results for GALLEX IV*, *Phys. Lett. B* **447** (1999) 127. (Cited on page 11.)

[58] GNO collaboration, *Complete results for five years of GNO solar neutrino observations*, *Phys. Lett. B* **616** (2005) 174 [hep-ex/0504037]. (Cited on page 11.)

[59] SAGE collaboration, *Measurement of the solar neutrino capture rate with gallium metal. III: Results for the 2002–2007 data-taking period*, *Phys. Rev. C* **80** (2009) 015807 [0901.2200]. (Cited on page 11.)

[60] J. N. Bahcall, W. F. Huebner, S. H. Lubow, P. D. Parker and R. K. Ulrich, *Standard solar models and the uncertainties in predicted capture rates of solar neutrinos*, *Rev. Mod. Phys.* **54** (1982) 767. (Cited on page 11.)

[61] J. N. Bahcall, A. M. Serenelli and S. Basu, *New solar opacities, abundances, helioseismology, and neutrino fluxes*, *Astrophys. J. Lett.* **621** (2005) L85 [astro-ph/0412440]. (Cited on page 11.)

[62] A. M. Serenelli, W. C. Haxton and C. Pena-Garay, *Solar models with accretion. I. Application to the solar abundance problem*, *Astrophys. J.* **743** (2011) 24 [1104.1639]. (Cited on page 11.)

[63] SNO collaboration, *Direct evidence for neutrino flavor transformation from neutral current interactions in the Sudbury Neutrino Observatory*, *Phys. Rev. Lett.* **89** (2002) 011301 [nucl-ex/0204008]. (Cited on page 11.)

[64] Super-Kamiokande collaboration, *Evidence for oscillation of atmospheric neutrinos*, *Phys. Rev. Lett.* **81** (1998) 1562 [hep-ex/9807003]. (Cited on page 11.)

[65] KamLAND collaboration, *First results from KamLAND: Evidence for reactor anti-neutrino disappearance*, *Phys. Rev. Lett.* **90** (2003) 021802 [hep-ex/0212021]. (Cited on page 11.)

[66] Borexino collaboration, *First real time detection of Be-7 solar neutrinos by Borexino*, *Phys. Lett. B* **658** (2008) 101 [0708.2251]. (Cited on page 11.)

[67] MINOS collaboration, *Measurement of Neutrino and Antineutrino Oscillations Using Beam and Atmospheric Data in MINOS*, *Phys. Rev. Lett.* **110** (2013) 251801 [1304.6335]. (Cited on page 11.)

[68] J. Schechter and J. W. F. Valle, *Comment on the lepton mixing matrix*, *Phys. Rev. D* **21** (1980) 309. (Cited on page 11.)

[69] J. Schechter and J. W. F. Valle, *Neutrino masses in su(2) $\bigotimes$ u(1) theories*, *Phys. Rev. D* **22** (1980) 2227. (Cited on page 11.)

[70] Z. Maki, M. Nakagawa and S. Sakata, *Remarks on the unified model of elementary particles*, *Prog. Theor. Phys.* **28** (1962) 870. (Cited on page 11.)

[71] B. Pontecorvo, *Inverse beta processes and nonconservation of lepton charge*, *Zh. Eksp. Teor. Fiz.* **34** (1957) 247. (Cited on page 11.)

[72] E. K. Akhmedov and A. Y. Smirnov, *Paradoxes of neutrino oscillations*, *Phys. Atom. Nucl.* **72** (2009) 1363 [0905.1903]. (Cited on page 12.)

[73] E. Akhmedov, *Quantum mechanics aspects and subtleties of neutrino oscillations*, in *International Conference on History of the Neutrino: 1930-2018*, 1, 2019, 1901.05232. (Cited on page 12.)

[74] L. Wolfenstein, *Neutrino oscillations in matter*, *Phys. Rev. D* **17** (1978) 2369. (Cited on page 12.)

[75] S. Mikheyev and A. Smirnov, *Resonant neutrino oscillations in matter*, *Progress in Particle and Nuclear Physics* **23** (1989) 41. (Cited on page 12.)

[76] M. C. Gonzalez-Garcia, M. Maltoni and T. Schwetz, *NuFIT: Three-Flavour Global Analyses of Neutrino Oscillation Experiments*, *Universe* **7** (2021) 459 [2111.03086]. (Cited on page 13.)

[77] P. F. de Salas, D. V. Forero, S. Gariazzo, P. Martínez-Miravé, O. Mena, C. A. Ternes et al., *2020 global reassessment of the neutrino oscillation picture*, *JHEP* **02** (2021) 071 [2006.11237]. (Cited on page 13.)

[78] N. Cabibbo, *Time reversal violation in neutrino oscillation*, *Physics Letters B* **72** (1978) 333. (Cited on page 13.)

[79] S. Bilenky, J. Hošek and S. Petcov, *On the oscillations of neutrinos with dirac and majorana masses*, *Physics Letters B* **94** (1980) 495. (Cited on page 13.)

[80] V. Barger, K. Whisnant and R. J. N. Phillips, CP *nonconservation in three-neutrino oscillations*, *Phys. Rev. Lett.* **45** (1980) 2084. (Cited on page 13.)

[81] GERDA collaboration, *Final Results of GERDA on the Search for Neutrinoless Double-β Decay*, *Phys. Rev. Lett.* **125** (2020) 252502 [2009.06079]. (Cited on page 14.)

[82] KamLAND-Zen collaboration, *Search for Majorana Neutrinos near the Inverted Mass Hierarchy Region with KamLAND-Zen*, *Phys. Rev. Lett.* **117** (2016) 082503 [1605.02889]. (Cited on page 14.)

[83] I. Esteban, M. C. Gonzalez-Garcia, A. Hernandez-Cabezudo, M. Maltoni and T. Schwetz, *Global analysis of three-flavour neutrino oscillations: synergies and tensions in the determination of θ_{23}, δ_{CP}, and the mass ordering*, *JHEP* **01** (2019) 106 [1811.05487]. (Cited on page 14.)

[84] F. Zwicky, *Die Rotverschiebung von extragalaktischen Nebeln*, *Helv. Phys. Acta* **6** (1933) 110. (Cited on page 15.)

[85] K. C. Freeman, *On the disks of spiral and SO Galaxies*, *Astrophys. J.* **160** (1970) 811. (Cited on page 15.)

[86] V. C. Rubin and W. K. Ford, Jr., *Rotation of the Andromeda Nebula from a Spectroscopic Survey of Emission Regions*, *Astrophys. J.* **159** (1970) 379. (Cited on page 15.)

[87] Planck collaboration, *Planck 2018 results. VI. Cosmological parameters*, *Astron. Astrophys.* **641** (2020) A6 [1807.06209]. (Cited on pages 15 and 24.)

[88] G. Steigman, *Primordial Nucleosynthesis in the Precision Cosmology Era*, *Ann. Rev. Nucl. Part. Sci.* **57** (2007) 463 [0712.1100]. (Cited on page 15.)

[89] A. D. Sakharov, *Violation of cp invariance, c asymmetry, and baryon asymmetry of the universe*, *Soviet Physics Uspekhi* **34** (1991) 392. (Cited on page 15.)

[90] M. B. Gavela, P. Hernandez, J. Orloff and O. Pene, *Standard model CP violation and baryon asymmetry*, *Mod. Phys. Lett. A* **9** (1994) 795 [hep-ph/9312215]. (Cited on page 16.)

[91] P. Huet and E. Sather, *Electroweak baryogenesis and standard model CP violation*, *Phys. Rev. D* **51** (1995) 379 [hep-ph/9404302]. (Cited on page 16.)

[92] M. Gavela, M. Lozano, J. Orloff and O. Pène, *Standard model cp-violation and baryon asymmetry (i). zero temperature*, *Nuclear Physics B* **430** (1994) 345. (Cited on page 16.)

[93] M. B. Gavela, P. Hernandez, J. Orloff, O. Pene and C. Quimbay, *Standard model CP violation and baryon asymmetry. Part 2: Finite temperature*, *Nucl. Phys. B* **430** (1994) 382 [hep-ph/9406289]. (Cited on page 16.)

[94] K. Kajantie, M. Laine, K. Rummukainen and M. E. Shaposhnikov, *Is there a hot electroweak phase transition at $m_H \gtrsim m_W$?*, *Phys. Rev. Lett.* **77** (1996) 2887 [hep-ph/9605288]. (Cited on page 16.)

[95] F. Karsch, T. Neuhaus, A. Patkos and J. Rank, *Critical Higgs mass and temperature dependence of gauge boson masses in the SU(2) gauge Higgs model*, *Nucl. Phys. B Proc. Suppl.* **53** (1997) 623 [hep-lat/9608087]. (Cited on page 16.)

[96] M. Gurtler, E.-M. Ilgenfritz and A. Schiller, *Where the electroweak phase transition ends*, *Phys. Rev. D* **56** (1997) 3888 [hep-lat/9704013]. (Cited on page 16.)

[97] K. Rummukainen, M. Tsypin, K. Kajantie, M. Laine and M. E. Shaposhnikov, *The Universality class of the electroweak theory*, *Nucl. Phys. B* **532** (1998) 283 [hep-lat/9805013]. (Cited on page 16.)

[98] M. D'Onofrio and K. Rummukainen, *Standard model cross-over on the lattice*, *Phys. Rev. D* **93** (2016) 025003 [1508.07161]. (Cited on page 16.)

[99] CMS collaboration, *A measurement of the Higgs boson mass in the diphoton decay channel*, *Phys. Lett. B* **805** (2020) 135425 [2002.06398]. (Cited on page 16.)

[100] ATLAS collaboration, *Measurement of the Higgs boson mass in the $H \to ZZ^* \to 4\ell$ decay channel using 139 fb^{-1} of $\sqrt{s} = 13$ TeV pp collisions recorded by the ATLAS detector at the LHC*, 2207.00320. (Cited on page 16.)

[101] J. M. Cline, *Baryogenesis*, in *Les Houches Summer School - Session 86: Particle Physics and Cosmology: The Fabric of Spacetime*, 9, 2006, hep-ph/0609145. (Cited on page 16.)

[102] S. Davidson, E. Nardi and Y. Nir, *Leptogenesis*, *Phys. Rept.* **466** (2008) 105 [0802.2962]. (Cited on page 16.)

[103] G. 't Hooft, *Naturalness, chiral symmetry, and spontaneous chiral symmetry breaking*, *NATO Sci. Ser. B* **59** (1980) 135. (Cited on page 16.)

[104] Y. A. Golfand and E. P. Likhtman, *Extension of the Algebra of Poincare Group Generators and Violation of p Invariance*, *JETP Lett.* **13** (1971) 323. (Cited on page 16.)

[105] D. V. Volkov and V. P. Akulov, *Is the Neutrino a Goldstone Particle?*, *Phys. Lett. B* **46** (1973) 109. (Cited on page 16.)

[106] J. Wess and B. Zumino, *Supergauge Transformations in Four-Dimensions*, *Nucl. Phys. B* **70** (1974) 39. (Cited on page 16.)

[107] J. Wess and B. Zumino, *Supergauge Invariant Extension of Quantum Electrodynamics*, *Nucl. Phys. B* **78** (1974) 1. (Cited on page 16.)

[108] S. Ferrara and B. Zumino, *Supergauge Invariant Yang-Mills Theories*, *Nucl. Phys. B* **79** (1974) 413. (Cited on page 16.)

[109] C. Csáki and P. Tanedo, *Beyond the Standard Model*, in *2013 European School of High-Energy Physics*, pp. 169–268, 2015, DOI [1602.04228]. (Cited on page 16.)

[110] C. Callan, R. Dashen and D. Gross, *The structure of the gauge theory vacuum*, *Physics Letters B* **63** (1976) 334. (Cited on page 17.)

[111] S. Weinberg, *The quantum theory of fields. Vol. 2: Modern applications*. Cambridge University Press, 8, 2013, 10.1017/CBO9781139644174. (Cited on page 17.)

[112] C. Abel et al., *Measurement of the Permanent Electric Dipole Moment of the Neutron*, *Phys. Rev. Lett.* **124** (2020) 081803 [2001.11966]. (Cited on page 17.)

[113] R. Crewther, P. Di Vecchia, G. Veneziano and E. Witten, *Chiral estimate of the electric dipole moment of the neutron in quantum chromodynamics*, *Physics Letters B* **88** (1979) 123. (Cited on page 17.)

[114] V. Baluni, CP-*nonconserving effects in quantum chromodynamics*, *Phys. Rev. D* **19** (1979) 2227. (Cited on page 17.)

[115] R. D. Peccei and H. R. Quinn, CP *conservation in the presence of pseudoparticles*, *Phys. Rev. Lett.* **38** (1977) 1440. (Cited on page 17.)

[116] R. D. Peccei and H. R. Quinn, *Constraints imposed by* CP *conservation in the presence of pseudoparticles*, *Phys. Rev. D* **16** (1977) 1791. (Cited on page 17.)

[117] S. Weinberg, *A new light boson?*, *Phys. Rev. Lett.* **40** (1978) 223. (Cited on page 17.)

[118] F. Wilczek, *Problem of strong p and t invariance in the presence of instantons*, *Phys. Rev. Lett.* **40** (1978) 279. (Cited on page 17.)

[119] C. Vafa and E. Witten, *Parity conservation in quantum chromodynamics*, *Phys. Rev. Lett.* **53** (1984) 535. (Cited on page 17.)

[120] M. Dine, W. Fischler and M. Srednicki, *A simple solution to the strong cp problem with a harmless axion*, *Physics Letters B* **104** (1981) 199. (Cited on page 18.)

[121] J. E. Kim, *Weak-interaction singlet and strong* CP *invariance*, *Phys. Rev. Lett.* **43** (1979) 103. (Cited on page 18.)

[122] M. Shifman, A. Vainshtein and V. Zakharov, *Can confinement ensure natural cp invariance of strong interactions?*, *Nuclear Physics B* **166** (1980) 493. (Cited on page 18.)

[123] J. Preskill, M. B. Wise and F. Wilczek, *Cosmology of the Invisible Axion*, *Phys. Lett. B* **120** (1983) 127. (Cited on page 18.)

[124] M. Dine and W. Fischler, *The Not So Harmless Axion*, *Phys. Lett. B* **120** (1983) 137. (Cited on page 18.)

[125] L. F. Abbott and P. Sikivie, *A Cosmological Bound on the Invisible Axion*, *Phys. Lett. B* **120** (1983) 133. (Cited on page 18.)

[126] L. Di Luzio, M. Giannotti, E. Nardi and L. Visinelli, *The landscape of QCD axion models*, *Phys. Rept.* **870** (2020) 1 [2003.01100]. (Cited on page 18.)

[127] A. Nelson, *Naturally weak cp violation*, *Physics Letters B* **136** (1984) 387. (Cited on page 18.)

[128] S. M. Barr, *Solving the strong* CP *problem without the peccei-quinn symmetry*, *Phys. Rev. Lett.* **53** (1984) 329. (Cited on page 18.)

[129] S. M. Barr, *Natural class of non-peccei-quinn models*, *Phys. Rev. D* **30** (1984) 1805. (Cited on page 18.)

[130] C. Froggatt and H. Nielsen, *Hierarchy of quark masses, cabibbo angles and cp violation*, *Nuclear Physics B* **147** (1979) 277. (Cited on pages 18 and 79.)

[131] K. S. Babu and T. Enkhbat, *Fermion mass hierarchy and electric dipole moments*, *Nucl. Phys. B* **708** (2005) 511 [hep-ph/0406003]. (Cited on page 18.)

[132] G. D'Ambrosio, G. F. Giudice, G. Isidori and A. Strumia, *Minimal flavor violation: An Effective field theory approach*, *Nucl. Phys. B* **645** (2002) 155 [hep-ph/0207036]. (Cited on pages 19 and 79.)

[133] F. Feruglio, *Pieces of the Flavour Puzzle*, *Eur. Phys. J. C* **75** (2015) 373 [1503.04071]. (Cited on page 19.)

[134] T. Aoyama, N. Asmussen, M. Benayoun, J. Bijnens, T. Blum, M. Bruno et al., *The anomalous magnetic moment of the muon in the standard model*, *Physics Reports* **887** (2020) 1. (Cited on page 19.)

[135] Muon g-2 collaboration, *Measurement of the Positive Muon Anomalous Magnetic Moment to 0.46 ppm*, *Phys. Rev. Lett.* **126** (2021) 141801 [2104.03281]. (Cited on page 19.)

[136] Muon g-2 collaboration, *Final Report of the Muon E821 Anomalous Magnetic Moment Measurement at BNL*, *Phys. Rev. D* **73** (2006) 072003 [hep-ex/0602035]. (Cited on page 19.)

[137] S. Borsanyi et al., *Leading hadronic contribution to the muon magnetic moment from lattice QCD*, *Nature* **593** (2021) 51 [2002.12347]. (Cited on page 19.)

[138] Extended Twisted Mass collaboration, *Lattice calculation of the short and intermediate time-distance hadronic vacuum polarization contributions to the muon magnetic moment using twisted-mass fermions*, *Phys. Rev. D* **107** (2023) 074506 [2206.15084]. (Cited on page 19.)

[139] M. Cè et al., *Window observable for the hadronic vacuum polarization contribution to the muon g-2 from lattice QCD*, *Phys. Rev. D* **106** (2022) 114502 [2206.06582]. (Cited on page 19.)

[140] Heavy Flavor Averaging Group, HFLAV collaboration, *Averages of b-hadron, c-hadron, and τ-lepton properties as of 2021*, *Phys. Rev. D* **107** (2023) 052008 [2206.07501]. (Cited on page 19.)

[141] LHCb collaboration, *Test of lepton universality in $b \to s\ell^+\ell^-$ decays*, 2212.09152. (Cited on page 20.)

[142] Y. Kuno and Y. Okada, *Muon decay and physics beyond the standard model*, *Rev. Mod. Phys.* **73** (2001) 151 [hep-ph/9909265]. (Cited on pages 24, 25, 30, 36, 74, 84, 103 and 143.)

[143] R. Bernstein and P. S. Cooper, *Charged lepton flavor violation: An experimenter's guide*, *Physics Reports* **532** (2013) 27–64. (Cited on pages 24, 39 and 46.)

[144] L. Calibbi and G. Signorelli, *Charged lepton flavour violation: An experimental and theoretical introduction*, *Rivista del Nuovo Cimento* **41** (2018) 71–172. (Cited on pages 24, 39 and 44.)

[145] F. Cei and D. Nicolò, *Lepton flavour violation experiments*, *Advances in High Energy Physics* **532** (2014) . (Cited on page 24.)

[146] M. Lindner, M. Platscher and F. S. Queiroz, *A Call for New Physics : The Muon Anomalous Magnetic Moment and Lepton Flavor Violation*, *Phys. Rept.* **731** (2018) 1 [1610.06587]. (Cited on page 24.)

[147] M. E. Peskin and D. V. Schroeder, *An Introduction to quantum field theory*. Addison-Wesley, Reading, USA, 1995. (Cited on page 25.)

[148] T. P. Cheng and L. F. Li, *Gauge theory of elementary particle physics*. Oxford University Press, Oxford, UK, 1984. (Cited on pages 25 and 27.)

[149] S. T. Petcov, *The Processes $\mu \to e + \gamma, \mu \to e + \overline{e}, \nu' \to \nu + \gamma$ in the Weinberg-Salam Model with Neutrino Mixing*, *Sov. J. Nucl. Phys.* **25** (1977) 340. (Cited on page 26.)

[150] S. M. Bilenky, S. T. Petcov and B. Pontecorvo, *Lepton Mixing, mu -> e + gamma Decay and Neutrino Oscillations*, *Phys. Lett. B* **67** (1977) 309. (Cited on page 26.)

[151] W. J. Marciano and A. I. Sanda, *Exotic Decays of the Muon and Heavy Leptons in Gauge Theories*, *Phys. Lett. B* **67** (1977) 303. (Cited on page 26.)

[152] B. W. Lee, S. Pakvasa, R. E. Shrock and H. Sugawara, *Muon and Electron Number Nonconservation in a V-A Gauge Model*, *Phys. Rev. Lett.* **38** (1977) 937. (Cited on page 26.)

[153] B. W. Lee and R. E. Shrock, *Natural Suppression of Symmetry Violation in Gauge Theories: Muon - Lepton and Electron Lepton Number Nonconservation*, *Phys. Rev. D* **16** (1977) 1444. (Cited on page 26.)

[154] A. Denner, H. Eck, O. Hahn and J. Kublbeck, *Feynman rules for fermion number violating interactions*, *Nucl. Phys. B* **387** (1992) 467. (Cited on page 26.)

[155] W. Grimus and L. Lavoura, *The Seesaw mechanism at arbitrary order: Disentangling the small scale from the large scale*, *JHEP* **11** (2000) 042 [hep-ph/0008179]. (Cited on pages 26 and 27.)

[156] P. Minkowski, $\mu \to e\gamma$ *at a Rate of One Out of* 10^9 *Muon Decays?*, *Phys. Lett. B* **67** (1977) 421. (Cited on page 26.)

[157] S. Antusch, C. Biggio, E. Fernandez-Martinez, M. B. Gavela and J. Lopez-Pavon, *Unitarity of the Leptonic Mixing Matrix*, *JHEP* **10** (2006) 084 [hep-ph/0607020]. (Cited on page 27.)

[158] Xing, Zhi-zhong and Zhang, Di, *Radiative decays of charged leptons as constraints of unitarity polygons for active-sterile neutrino mixing and cp violation*, *Eur. Phys. J. C* **80** (2020) 1134. (Cited on page 27.)

[159] F. Vissani, *Do experiments suggest a hierarchy problem?*, *Phys. Rev. D* **57** (1998) 7027 [hep-ph/9709409]. (Cited on page 27.)

[160] M. C. Gonzalez-Garcia, A. Santamaria and J. W. F. Valle, *Isosinglet Neutral Heavy Lepton Production in Z Decays and Neutrino Mass*, *Nucl. Phys. B* **342** (1990) 108. (Cited on page 27.)

[161] M. C. Gonzalez-Garcia and J. W. F. Valle, *Fast Decaying Neutrinos and Observable Flavor Violation in a New Class of Majoron Models*, *Phys. Lett. B* **216** (1989) 360. (Cited on page 27.)

[162] F. F. Deppisch and A. Pilaftsis, *Lepton Flavour Violation and theta(13) in Minimal Resonant Leptogenesis*, *Phys. Rev. D* **83** (2011) 076007 [1012.1834]. (Cited on page 27.)

[163] A. Ibarra, E. Molinaro and S. T. Petcov, *Low Energy Signatures of the TeV Scale See-Saw Mechanism*, *Phys. Rev. D* **84** (2011) 013005 [1103.6217]. (Cited on page 27.)

[164] D. N. Dinh and S. T. Petcov, *Lepton Flavor Violating τ Decays in TeV Scale Type I See-Saw and Higgs Triplet Models*, *JHEP* **09** (2013) 086 [1308.4311]. (Cited on page 27.)

[165] A. Abada, C. Biggio, F. Bonnet, M. B. Gavela and T. Hambye, *Low energy effects of neutrino masses*, *JHEP* **12** (2007) 061 [0707.4058]. (Cited on page 28.)

[166] D. Zhang and S. Zhou, *Complete one-loop matching of the type-I seesaw model onto the Standard Model effective field theory*, *JHEP* **09** (2021) 163 [2107.12133]. (Cited on page 28.)

[167] X. Li, D. Zhang and S. Zhou, *One-loop matching of the type-II seesaw model onto the Standard Model effective field theory*, *JHEP* **04** (2022) 038 [2201.05082]. (Cited on page 28.)

[168] T. Hambye, *CLFV and the origin of neutrino masses*, *Nucl. Phys. B Proc. Suppl.* **248-250** (2014) 13 [1312.5214]. (Cited on page 28.)

[169] E. Ma, *Verifiable radiative seesaw mechanism of neutrino mass and dark matter*, *Phys. Rev. D* **73** (2006) 077301 [hep-ph/0601225]. (Cited on page 29.)

[170] J. Kubo, E. Ma and D. Suematsu, *Cold Dark Matter, Radiative Neutrino Mass, $\mu \to e\gamma$, and Neutrinoless Double Beta Decay*, *Phys. Lett. B* **642** (2006) 18 [hep-ph/0604114]. (Cited on page 29.)

[171] D. Aristizabal Sierra, J. Kubo, D. Restrepo, D. Suematsu and O. Zapata, *Radiative seesaw: Warm dark matter, collider and lepton flavour violating signals*, *Phys. Rev. D* **79** (2009) 013011 [0808.3340]. (Cited on page 29.)

[172] D. Suematsu, T. Toma and T. Yoshida, *Reconciliation of CDM abundance and mu —> e gamma in a radiative seesaw model*, *Phys. Rev. D* **79** (2009) 093004 [0903.0287]. (Cited on page 29.)

[173] T. Toma and A. Vicente, *Lepton Flavor Violation in the Scotogenic Model*, *JHEP* **01** (2014) 160 [1312.2840]. (Cited on pages 29 and 31.)

[174] E. Arganda and M. J. Herrero, *Testing supersymmetry with lepton flavor violating tau and mu decays*, *Phys. Rev. D* **73** (2006) 055003 [hep-ph/0510405]. (Cited on page 30.)

[175] A. Vicente and C. E. Yaguna, *Probing the scotogenic model with lepton flavor violating processes*, *JHEP* **02** (2015) 144 [1412.2545]. (Cited on page 31.)

[176] A. Zee, *Quantum numbers of majorana neutrino masses*, *Nuclear Physics* **264** (1986) 99. (Cited on page 31.)

[177] K. Babu, *Model of "calculable" majorana neutrino masses*, *Physics Letters B* **203** (1988) 132. (Cited on page 31.)

[178] J. Herrero-Garcia, M. Nebot, N. Rius and A. Santamaria, *The Zee–Babu model revisited in the light of new data*, *Nucl. Phys. B* **885** (2014) 542 [1402.4491]. (Cited on page 31.)

[179] M. Nebot, J. F. Oliver, D. Palao and A. Santamaria, *Prospects for the Zee-Babu Model at the CERN LHC and low energy experiments*, *Phys. Rev. D* **77** (2008) 093013 [0711.0483]. (Cited on page 31.)

[180] D. Aristizabal Sierra and M. Hirsch, *Experimental tests for the Babu-Zee two-loop model of Majorana neutrino masses*, *JHEP* **12** (2006) 052 [hep-ph/0609307]. (Cited on page 31.)

[181] Y. Cai, J. Herrero-García, M. A. Schmidt, A. Vicente and R. R. Volkas, *From the trees to the forest: a review of radiative neutrino mass models*, *Front. in Phys.* **5** (2017) 63 [1706.08524]. (Cited on page 31.)

[182] G. C. Branco, P. M. Ferreira, L. Lavoura, M. N. Rebelo, M. Sher and J. P. Silva, *Theory and phenomenology of two-Higgs-doublet models*, *Phys. Rept.* **516** (2012) 1 [1106.0034]. (Cited on page 31.)

[183] S. Davidson and H. E. Haber, *Basis-independent methods for the two-Higgs-doublet model*, *Phys. Rev. D* **72** (2005) 035004 [hep-ph/0504050]. (Cited on page 32.)

[184] S. Davidson, $\mu \to e\gamma$ *in the 2HDM: an exercise in EFT*, *Eur. Phys. J. C* **76** (2016) 258 [1601.01949]. (Cited on pages 32 and 33.)

[185] ATLAS collaboration, *Cross-section measurements of the Higgs boson decaying into a pair of τ-leptons in proton-proton collisions at $\sqrt{s} = 13$ TeV with the ATLAS detector*, *Phys. Rev. D* **99** (2019) 072001 [1811.08856]. (Cited on pages 33 and 83.)

[186] CMS collaboration, *Observation of the Higgs boson decay to a pair of τ leptons with the CMS detector*, *Phys. Lett. B* **779** (2018) 283 [1708.00373]. (Cited on pages 33 and 83.)

[187] J. F. Gunion and H. E. Haber, *The CP conserving two Higgs doublet model: The Approach to the decoupling limit*, *Phys. Rev. D* **67** (2003) 075019 [hep-ph/0207010]. (Cited on page 33.)

[188] J. L. Diaz-Cruz and J. J. Toscano, *Lepton flavor violating decays of Higgs bosons beyond the standard model*, *Phys. Rev. D* **62** (2000) 116005 [hep-ph/9910233]. (Cited on page 33.)

[189] S. Kanemura, T. Ota and K. Tsumura, *Lepton flavor violation in Higgs boson decays under the rare tau decay results*, *Phys. Rev. D* **73** (2006) 016006 [hep-ph/0505191]. (Cited on page 33.)

[190] ATLAS collaboration, *Search for the decays of the Higgs boson $H \to ee$ and $H \to e\mu$ in pp collisions at $\sqrt{s} = 13$ TeV with the ATLAS detector*, . (Cited on pages 33, 34, 40 and 99.)

[191] CMS Collaboration collaboration, *Search for lepton-flavor violating decays of the higgs boson in the $\mu\tau$ and $e\tau$ final states in proton-proton collisions at $\sqrt{s} = 13$ TeV*, *Phys. Rev. D* **104** (2021) 032013. (Cited on pages 33, 34, 40 and 99.)

[192] J. D. Bjorken and S. Weinberg, *A Mechanism for Nonconservation of Muon Number*, *Phys. Rev. Lett.* **38** (1977) 622. (Cited on pages 33 and 79.)

[193] R. Diaz, R. Martinez and J. A. Rodriguez, *Lepton flavor violation in the two Higgs doublet model type III*, *Phys. Rev. D* **63** (2001) 095007 [hep-ph/0010149]. (Cited on page 33.)

[194] R. A. Diaz, R. Martinez and J. A. Rodriguez, *Phenomenology of lepton flavor violation in 2HDM(3) from (g-2)(mu) and leptonic decays*, *Phys. Rev. D* **67** (2003) 075011 [hep-ph/0208117]. (Cited on page 33.)

[195] D. Chang, W. S. Hou and W.-Y. Keung, *Two loop contributions of flavor changing neutral Higgs bosons to mu —> e gamma*, *Phys. Rev. D* **48** (1993) 217 [hep-ph/9302267]. (Cited on pages 33 and 121.)

[196] P. Paradisi, *Higgs-mediated e —> mu transitions in II Higgs doublet model and supersymmetry*, *JHEP* **08** (2006) 047 [hep-ph/0601100]. (Cited on page 33.)

[197] R. Harnik, J. Kopp and J. Zupan, *Flavor Violating Higgs Decays*, *JHEP* **03** (2013) 026 [1209.1397]. (Cited on pages 33 and 34.)

[198] T. P. Cheng and M. Sher, *Mass-matrix ansatz and flavor nonconservation in models with multiple higgs doublets*, *Phys. Rev. D* **35** (1987) 3484. (Cited on page 34.)

[199] S. P. Martin, *A Supersymmetry primer*, *Adv. Ser. Direct. High Energy Phys.* **18** (1998) 1 [hep-ph/9709356]. (Cited on page 34.)

[200] S. Weinberg, *The quantum theory of fields. Vol. 3: Supersymmetry*. Cambridge University Press, 6, 2013. (Cited on page 34.)

[201] A. Bilal, *Introduction to supersymmetry*, hep-th/0101055. (Cited on page 34.)

[202] S. Coleman and J. Mandula, *All possible symmetries of the s matrix*, *Phys. Rev.* **159** (1967) 1251. (Cited on page 34.)

[203] R. Haag, J. T. Łopuszański and M. Sohnius, *All possible generators of supersymmetries of the s-matrix*, *Nuclear Physics B* **88** (1975) 257. (Cited on page 34.)

[204] ATLAS Collaboration collaboration, *Search for squarks and gluinos in final states with jets and missing transverse momentum using 36 fb^{-1} of $\sqrt{s} = 13$ TeV pp collision data with the ATLAS detector*, tech. rep., CERN, Geneva, Apr, 2017. (Cited on page 35.)

[205] CMS collaboration, *Search for new phenomena with the M_{T2} variable in the all-hadronic final state produced in proton–proton collisions at $\sqrt{s} = 13$ TeV*, *Eur. Phys. J. C* **77** (2017) 710 [1705.04650]. (Cited on page 35.)

[206] ATLAS collaboration, *Search for a scalar partner of the top quark in the jets plus missing transverse momentum final state at $\sqrt{s}$=13 TeV with the ATLAS detector*, *JHEP* **12** (2017) 085 [1709.04183]. (Cited on page 35.)

[207] A. H. Chamseddine, R. Arnowitt and P. Nath, *Locally supersymmetric grand unification*, *Phys. Rev. Lett.* **49** (1982) 970. (Cited on page 35.)

[208] R. Barbieri, S. Ferrara and C. A. Savoy, *Gauge models with spontaneously broken local supersymmetry*, *Physics Letters B* **119** (1982) 343. (Cited on page 35.)

[209] J. Hisano, T. Moroi, K. Tobe and M. Yamaguchi, *Exact event rates of lepton flavor violating processes in supersymmetric SU(5) model*, *Phys. Lett. B* **391** (1997) 341 [hep-ph/9605296]. (Cited on page 36.)

[210] R. Barbieri, L. J. Hall and A. Strumia, *Violations of lepton flavor and CP in supersymmetric unified theories*, *Nucl. Phys. B* **445** (1995) 219 [hep-ph/9501334]. (Cited on page 36.)

[211] CMS Collaboration collaboration, *Search for electroweak production of charginos and neutralinos in multilepton final states in pp collision data at $\sqrt{s} = 13$ TeV*, tech. rep., CERN, Geneva, 2017. (Cited on page 36.)

[212] J. Hisano, T. Moroi, K. Tobe and M. Yamaguchi, *Lepton-flavor violation via right-handed neutrino yukawa couplings in the supersymmetric standard model*, *Phys. Rev. D* **53** (1996) 2442. (Cited on pages 36 and 37.)

[213] J. Hisano and D. Nomura, *Solar and atmospheric neutrino oscillations and lepton flavor violation in supersymmetric models with the right-handed neutrinos*, *Phys. Rev. D* **59** (1999) 116005 [hep-ph/9810479]. (Cited on page 36.)

[214] J. R. Ellis, M. E. Gomez, G. K. Leontaris, S. Lola and D. V. Nanopoulos, *Charged lepton flavor violation in the light of the Super-Kamiokande data*, *Eur. Phys. J. C* **14** (2000) 319 [hep-ph/9911459]. (Cited on page 36.)

[215] J. A. Casas and A. Ibarra, *Oscillating neutrinos and $\mu \to e, \gamma$*, *Nucl. Phys. B* **618** (2001) 171 [hep-ph/0103065]. (Cited on pages 36 and 37.)

[216] L. Calibbi, A. Faccia, A. Masiero and S. K. Vempati, *Lepton flavour violation from SUSY-GUTs: Where do we stand for MEG, PRISM/PRIME and a super flavour factory*, *Phys. Rev. D* **74** (2006) 116002 [hep-ph/0605139]. (Cited on pages 36 and 37.)

[217] L. Calibbi, D. Chowdhury, A. Masiero, K. M. Patel and S. K. Vempati, *Status of supersymmetric type-I seesaw in SO(10) inspired models*, *JHEP* **11** (2012) 040 [1207.7227]. (Cited on pages 36 and 37.)

[218] M. Hirsch, F. R. Joaquim and A. Vicente, *Constrained SUSY seesaws with a 125 GeV Higgs*, *JHEP* **11** (2012) 105 [1207.6635]. (Cited on page 36.)

[219] J. L. Evans, K. Kadota and T. Kuwahara, *Revisiting Flavor and CP Violation in Supersymmetric $SU(5)$ with Right-Handed Neutrinos*, *Phys. Rev. D* **98** (2018) 075030 [1807.08234]. (Cited on page 36.)

[220] K. Hirao and T. Moroi, *Leptonic CP and flavor violations in SUSY GUT with right-handed neutrinos*, *Phys. Rev. D* **104** (2021) 035038 [2102.04070]. (Cited on page 36.)

[221] S. Davidson and A. Ibarra, *Determining seesaw parameters from weak scale measurements?*, *JHEP* **09** (2001) 013 [hep-ph/0104076]. (Cited on page 37.)

[222] I. Masina and C. A. Savoy, *On power and complementarity of the experimental constraints on seesaw models*, *Phys. Rev. D* **71** (2005) 093003 [hep-ph/0501166]. (Cited on page 37.)

[223] T. M. Collaboration, *Search for the lepton flavour violating decay $\mu^+ \to e^+\gamma$ with the full dataset of the meg experiment*, 2016. (Cited on pages 37, 40, 42, 43, 83, 85 and 99.)

[224] A. M. Baldini, V. Baranov et al., *The search for $\mu^+ \to e^+\gamma$ with 10^{-14} sensitivity: The upgrade of the meg experiment*, *Symmetry* **13** (2021) . (Cited on pages 37, 42, 43, 85 and 99.)

[225] E. Kou, P. Urquijo, W. Altmannshofer et al., *The Belle II Physics Book*, *Progress of Theoretical and Experimental Physics* **2019** (2019) [https://academic.oup.com/ptep/article-pdf/2019/12/123C01/32693980/ptz106.pdf]. (Cited on pages 37 and 54.)

[226] L. Calibbi, I. Galon, A. Masiero, P. Paradisi and Y. Shadmi, *Charged Slepton Flavor post the 8 TeV LHC: A Simplified Model Analysis of Low-Energy Constraints and LHC SUSY Searches*, *JHEP* **10** (2015) 043 [1502.07753]. (Cited on page 37.)

[227] L. E. Ibáñez and G. G. Ross, *Discrete gauge symmetries and the origin of baryon and lepton number conservation in supersymmetric versions of the standard model*, *Nuclear Physics B* **368** (1992) 3. (Cited on page 38.)

[228] R. Barbier et al., *R-parity violating supersymmetry*, *Phys. Rept.* **420** (2005) 1 [hep-ph/0406039]. (Cited on page 38.)

[229] D. Ambrose, C. Arroyo, M. Bachman, D. Connor, M. Eckhause, S. Graessle et al., *New limit on muon and electron lepton number violation from $k_l^0 \to \mu^{\pm} e^{\mp}$ decay*, *Physical Review Letters* **81** (1998) 5734–5737. (Cited on pages 38 and 40.)

[230] D. Choudhury and P. Roy, *New constraints on lepton nonconserving R-parity violating couplings*, *Phys. Lett. B* **378** (1996) 153 [hep-ph/9603363]. (Cited on page 38.)

[231] K. Arndt, H. Augustin et al., *Technical design of the phase i mu3e experiment*, *Nuclear Instruments and Methods in Physics Research Section A: Accelerators, Spectrometers, Detectors and Associated Equipment* **1014** (2021) 165679. (Cited on pages 38, 44, 85 and 99.)

[232] F. W. on behalf of the Mu3e collaboration, *The Mu3e experiment*, *SciPost Phys. Proc.* (2021) 20. (Cited on pages 38, 44 and 45.)

[233] A. de Gouvea, S. Lola and K. Tobe, *Lepton flavor violation in supersymmetric models with trilinear R-parity violation*, *Phys. Rev. D* **63** (2001) 035004 [hep-ph/0008085]. (Cited on page 38.)

[234] M. Chaichian and K. Huitu, *Constraints on r-parity violating interactions from $\mu \to e\gamma$*, *Physics Letters B* **384** (1996) 157. (Cited on page 38.)

[235] F. Tahir, M. Sadiq, M. Anwar Mughal and K. Ahmed, *Bounds on R-parity violating SUSY Yukawa couplings from semileptonic decays of baryons*, *Phys. Lett. B* **439** (1998) 316 [hep-ph/9807445]. (Cited on page 38.)

[236] K. Huitu, J. Maalampi, M. Raidal and A. Santamaria, *New constraints on R-parity violation from mu e conversion in nuclei*, *Phys. Lett. B* **430** (1998) 355 [hep-ph/9712249]. (Cited on page 38.)

[237] H. K. Dreiner, K. Nickel, F. Staub and A. Vicente, *New bounds on trilinear R-parity violation from lepton flavor violating observables*, *Phys. Rev. D* **86** (2012) 015003 [1204.5925]. (Cited on page 38.)

[238] H. K. Dreiner, M. Kramer and B. O'Leary, *Bounds on R-parity violating supersymmetric couplings from leptonic and semi-leptonic meson decays*, *Phys. Rev. D* **75** (2007) 114016 [hep-ph/0612278]. (Cited on page 38.)

[239] U. Bellgardt, G. Otter, R. Eichler, L. Felawka, C. Niebuhr, H. Walter et al., *Search for the decay $\mu^+ \to e^+ e^- e^+$*, *Nuclear Physics B* **299** (1988) 1. (Cited on pages 40, 44, 85 and 99.)

[240] C. Dohmen, K.-D. Groth et al., *Test of lepton-flavour conservation in $\mu \to e$ conversion on titanium*, *Physics Letters B* **317** (1993) 631. (Cited on page 40.)

[241] B. W. H. et al. (SINDRUM II Collaboration), *A search for muon to electron conversion in muonic gold*, *Eur. Phys. J. C* **47** (2006) . (Cited on pages 40, 48 and 143.)

[242] J. Kaulard, C. Dohmen, H. Haan, W. Honecker, D. Junker, G. Otter et al., *Improved limit on the branching ratio of $\mu^- \to e^+$ conversion on titanium*, *Physics Letters B* **422** (1998) 334. (Cited on pages 40 and 50.)

[243] B. Aubert, Y. Karyotakis, J. P. Lees, V. Poireau, E. Prencipe, X. Prudent et al., *Searches for lepton flavor violation in the decays $\tau^\pm \to e^\pm\gamma$ and $\tau^\pm \to \mu^\pm\gamma$*, *Physical Review Letters* **104** (2010) . (Cited on pages 40, 52, 85 and 99.)

[244] K. Hayasaka, K. Inami, Y. Miyazaki, K. Arinstein, V. Aulchenko, T. Aushev et al., *Search for lepton-flavor-violating τ decays into three leptons with 719 million produced*, *Physics Letters B* **687** (2010) 139–143. (Cited on pages 40, 53, 85 and 99.)

[245] Y. Miyazaki, I. Adachi et al., *Search for lepton flavor violating τ^- decays into $l - \eta$, $l - \eta'$ and $l - \pi^0$*, *Physics Letters B* **648** (2007) 341–350. (Cited on pages 40, 85 and 99.)

[246] B. Aubert, M. Bona, D. Boutigny, F. Couderc, Y. Karyotakis, J. P. Lees et al., *Search for lepton flavor violating decays $\tau^\pm \to l^\pm\pi^0, l^\pm\eta, l^\pm\eta'$*, *Physical Review Letters* **98** (2007) . (Cited on page 40.)

[247] Y. Miyazaki, H. Aihara, K. Arinstein, V. Aulchenko, A. Bakich, V. Balagura et al., *Search for lepton-flavor-violating τ decays into a lepton and a vector meson*, *Physics Letters B* **699** (2011) 251–257. (Cited on pages 40, 85 and 99.)

[248] E. Abouzaid, M. Arenton, A. R. Barker et al., *Search for lepton-flavor-violating decays of the neutral kaon*, *Physical Review Letters* **100** (2008) . (Cited on page 40.)

[249] A. Sher, R. Appel et al., *Improved upper limit on the decay $k^+ \to \pi^+\mu^+e^-$*, *Physical Review D* **72** (2005) . (Cited on page 40.)

[250] M. Ablikim, M. N. Achasov, O. Albayrak, D. J. Ambrose, F. F. An, Q. An et al., *Search for the lepton flavor violation process $j/\psi \to e\mu$ at besiii*, *Physical Review D* **87** (2013) . (Cited on page 40.)

[251] M. Ablikim, M. Achasov et al., *Search for the charged lepton flavor violating decay $j/\psi \to e\tau$*, *Physical Review D* **103** (2021) . (Cited on page 40.)

[252] M. Ablikim, J. Bai, Y. Ban et al., *Search for the lepton flavor violation processes*, *Physics Letters B* **598** (2004) 172–177. (Cited on page 40.)

[253] R. Aaij, B. Adeva, M. Adinolfi, C. Adrover, A. Affolder, Z. Ajaltouni et al., *Search for the lepton-flavor-violating decays $b_s^0 \to e^\pm\mu^\mp$ and $b^0 \to e^\pm\mu^\mp$*, *Physical Review Letters* **111** (2013) . (Cited on page 40.)

[254] B. Aubert, M. Bona, Y. Karyotakis, J. P. Lees, V. Poireau, X. Prudent et al., *Searches for the decays $b^0 \to l^\pm \tau^\mp$ and $b^+ \to l^+ \nu$ $(l = e, \mu)$ using hadronic tag reconstruction*, *Physical Review D* **77** (2008) . (Cited on page 40.)

[255] R. Aaij, C. Abellán Beteta et al., *Search for the lepton-flavor-violating decays $b_s^0 \to \tau^\pm \mu^\mp$ and $b^0 \to \tau^\pm \mu^\mp$*, *Physical Review Letters* **123** (2019) . (Cited on page 40.)

[256] B. Aubert, R. Barate, M. Bona, D. Boutigny, F. Couderc, Y. Karyotakis et al., *Measurements of branching fractions, rate asymmetries, and angular distributions in the rare decays $b \to k l^+ l^-$ and $b \to k^* l^+ l^-$*, *Physical Review D* **73** (2006) . (Cited on page 40.)

[257] J. P. Lees, V. Poireau, V. Tisserand, J. Garra Tico, E. Grauges, D. A. Milanes et al., *Search for the decay modes $b^\pm \to h^\pm \tau l$*, *Physical Review D* **86** (2012) . (Cited on page 40.)

[258] G. Aad, B. Abbott, J. Abdallah, S. Abdel Khalek, O. Abdinov, R. Aben et al., *Search for the lepton flavor violating decay $z \to e\mu$ in pp collisions at $\sqrt{s}$=8 tev with the atlas detector*, *Physical Review D* **90** (2014) . (Cited on page 40.)

[259] OPAL Collaboration collaboration, *A search for lepton flavour violating z^0 decays*, *Phys. C - Particles and Fields* **67** (1995) 555. (Cited on page 40.)

[260] OPAL Collaboration collaboration, *Search for lepton flavour number violating z^0 decays*, *Phys C - Particles and Fields* **73** (1997) 243. (Cited on page 40.)

[261] E. P. Hincks and B. Pontecorvo, *Search for gamma-radiation in the 2.2-microsecond meson decay process*, *Phys. Rev.* **73** (1948) 257. (Cited on page 39.)

[262] T. Prokscha, E. Morenzoni and others., *A new high-intensity, low-momentum muon beam for the generation of low-energy muons at psi*, in *HFI/NQI 2004*, (Berlin, Heidelberg), pp. 812–815, Springer Berlin Heidelberg, 2005. (Cited on page 39.)

[263] M. Aiba, A. Amato, A. Antognini et al., *Science case for the new high-intensity muon beams himb at psi*, 2021. (Cited on page 39.)

[264] S. Cook, R. D'Arcy, A. Edmonds, M. Fukuda, K. Hatanaka, Y. Hino et al., *Delivering the world's most intense muon beam*, *Physical Review Accelerators and Beams* **20** (2017) . (Cited on page 39.)

[265] R. D. Bolton, M. D. Cooper, J. S. Frank et al., *Search for rare muon decays with the crystal box detector*, *Phys. Rev. D; (United States)* **38:7** (1988) . (Cited on page 41.)

[266] MEGA Collaboration collaboration, *New limit for the lepton-family-number nonconserving decay $\mu^+ \to e^+ \gamma$*, *Phys. Rev. Lett.* **83** (1999) 1521. (Cited on pages 41 and 42.)

[267] G. SIGNORELLI and O. behalf of the MEG collaboration, *The liquid xenon scintillation calorimeter of the meg experiment: Operation of a large prototype*, in *Calorimetry in Particle Physics*, pp. 281–286, https://www.worldscientific.com/doi/pdf/10.1142/9789812701978_0034, DOI. (Cited on page 42.)

[268] W. Bertl, S. Egli, R. Eichler, R. Engfer, L. Felawka, C. Grab et al., *Search for the decay $\mu^+ \to e^+e^-e^+$*, *Nuclear Physics B* **260** (1985) 1. (Cited on page 45.)

[269] H. Augustin, N. Berger, C. Blattgerste et al., *Performance of the large scale HV-CMOS pixel sensor MuPix8*, *Journal of Instrumentation* **14** (2019) C10011. (Cited on page 46.)

[270] R. Kitano, M. Koike and Y. Okada, *Detailed calculation of lepton flavor violating muon electron conversion rate for various nuclei*, *Phys. Rev. D* **66** (2002) 096002 [hep-ph/0203110]. (Cited on pages 46, 143 and 144.)

[271] R. Szafron and A. Czarnecki, *Bound muon decay spectrum in the leading logarithmic accuracy*, *Physical Review D* **94** (2016) . (Cited on page 47.)

[272] TWIST Collaboration collaboration, *Decay of negative muons bound in ^{27}Al*, *Phys. Rev. D* **80** (2009) 052012. (Cited on page 47.)

[273] R. M. Dzhilkibaev and V. M. Lobashev, *The solenoid muon capture system for the melc experiment*, *Beam Dynamics and Technology Issues for mu+ mu- Colliders: Proceedings of the 9th ICFA Advanced Beam Dynamics Workshop, Oct. 15-20 1995, Montauk* (1995) . (Cited on page 48.)

[274] J. L. Popp, *The meco experiment: A search for lepton flavor violation in muonic atom*, *Nucl. Instrum. Meth. A* **472** (2000) 354. (Cited on page 48.)

[275] L. Bartoszek, E. Barnes, J. P. Miller et al., *Mu2e technical design report*, 2015. (Cited on pages 48, 85 and 99.)

[276] G. Pezzullo, *The Mu2e Tracker*, *PoS* **ICHEP2018** (2019) 542. (Cited on page 48.)

[277] N. Atanov, V. Baranov et al., *Design and status of the mu2e crystal calorimeter*, *IEEE Transactions on Nuclear Science* **65** (2018) 2073. (Cited on page 48.)

[278] R. Abramishvili, G. Adamov, R. R. Akhmetshin, A. Allin, J. C. Angélique, V. Anishchik et al., *Comet phase-i technical design report*, *Progress of Theoretical and Experimental Physics* **2020** (2020) . (Cited on pages 49 and 50.)

[279] N. Teshima, *Status of the deeme experiment, an experimental search for μ-e conversion at j-parc mlf*, 2019. (Cited on pages 49 and 50.)

[280] N. Teshima, M. Aoki, Y. Higashino, H. Ikeuchi, K. Komukai, D. Nagao et al., *Development of a multiwire proportional chamber with good tolerance to burst hits*, *Nuclear Instruments and Methods in Physics Research Section A: Accelerators, Spectrometers, Detectors and Associated Equipment* **999** (2021) 165228. (Cited on page 49.)

[281] M. Lee and M. MacKenzie, *Muon to positron conversion*, *Universe* **8** (2022) . (Cited on page 50.)

[282] B. Aubert, others, S. Saremi et al., *The babar detector: Upgrades, operation and performance*, *Nuclear Instruments and Methods in Physics Research Section A: Accelerators, Spectrometers, Detectors and Associated Equipment* **729** (2013) 615. (Cited on pages 50 and 52.)

[283] A. Abashian, K. Gotow et al., *The belle detector*, *Nuclear Instruments and Methods in Physics Research Section A: Accelerators, Spectrometers, Detectors and Associated Equipment* **479** (2002) 117. (Cited on pages 50 and 52.)

[284] T. L. Collaboration, A. A. Alves, L. M. A. Filho et al., *The LHCb detector at the LHC*, *Journal of Instrumentation* **3** (2008) S08005. (Cited on page 50.)

[285] S. Banerjee, M. Chrząszcz, K. Hayasaka, H. Hayashii, A. Lusiani, M. Roney et al., *Hflav-tau 2018 report*, 2019. (Cited on page 51.)

[286] K. Uno, K. Hayasaka, K. Inami, I. Adachi, H. Aihara, D. M. Asner et al., *Search for lepton-flavor-violating tau-lepton decays to $l\gamma$ at belle*, *Journal of High Energy Physics* **2021** (2021) . (Cited on page 53.)

[287] Belle-II collaboration, *Prospects for τ Lepton Physics at Belle II*, 1906.08950. (Cited on page 53.)

[288] J. P. Lees, V. Poireau, E. Prencipe, V. Tisserand, J. Garra Tico, E. Grauges et al., *Limits on τ lepton-flavor violating decays into three charged leptons*, *Physical Review D* **81** (2010) . (Cited on page 53.)

[289] G. Aad, B. Abbott, J. Abdallah, O. Abdinov, R. Aben, M. Abolins et al., *Probing lepton flavour violation via neutrinoless $\tau \longrightarrow 3\mu$ decays with the atlas detector*, *The European Physical Journal C* **76** (2016) . (Cited on page 54.)

[290] LHCb collaboration, *Search for the lepton flavour violating decay $\tau^- \to \mu^-\mu^+\mu^-$*, *JHEP* **02** (2015) 121 [1409.8548]. (Cited on page 54.)

[291] A. M. Sirunyan, A. Tumasyan, W. Adam, F. Ambrogi, T. Bergauer, M. Dragicevic et al., *Search for the lepton flavor violating decay $\tau \to 3\mu$ in proton-proton collisions at $\sqrt{s} = 13$ tev*, *Journal of High Energy Physics* **2021** (2021) . (Cited on page 54.)

[292] T. Appelquist and J. Carazzone, *Infrared singularities and massive fields*, *Phys. Rev. D* **11** (1975) 2856. (Cited on page 58.)

[293] S. Davidson, P. Gambino, M. Laine, M. Neubert and C. Salomon, eds., *Proceedings, Les Houches summer school: EFT in Particle Physics and Cosmology: Les Houches (Chamonix Valley), France, July 3-28, 2017*, vol. 108 of *Lecture Notes of the Les Houches Summer School*. Oxford University Press, Oxford, 4, 2020, 10.1093/oso/9780198855743.001.0001. (Cited on page 59.)

[294] A. J. Buras, *Weak Hamiltonian, CP violation and rare decays*, in *Les Houches Summer School in Theoretical Physics, Session 68: Probing the Standard Model of Particle Interactions*, pp. 281–539, 6, 1998, hep-ph/9806471. (Cited on pages 59 and 79.)

[295] H. Georgi, *Effective field theory*, *Ann. Rev. Nucl. Part. Sci.* **43** (1993) 209. (Cited on page 59.)

[296] M. D. Schwartz, *Quantum Field Theory and the Standard Model*. Cambridge University Press, 3, 2014. (Cited on page 59.)

[297] L. Silvestrini, *Effective Theories for Quark Flavour Physics*, 1905.00798. (Cited on pages 59 and 79.)

[298] A. V. Manohar, *Introduction to Effective Field Theories*, 1804.05863. (Cited on page 62.)

[299] S. Weinberg, *Baryon and Lepton Nonconserving Processes*, *Phys. Rev. Lett.* **43** (1979) 1566. (Cited on page 71.)

[300] L. Lehman and A. Martin, *Hilbert Series for Constructing Lagrangians: expanding the phenomenologist's toolbox*, *Phys. Rev. D* **91** (2015) 105014 [1503.07537]. (Cited on page 71.)

[301] B. Henning, X. Lu, T. Melia and H. Murayama, *Hilbert series and operator bases with derivatives in effective field theories*, *Commun. Math. Phys.* **347** (2016) 363 [1507.07240]. (Cited on page 71.)

[302] L. Lehman and A. Martin, *Low-derivative operators of the Standard Model effective field theory via Hilbert series methods*, *JHEP* **02** (2016) 081 [1510.00372]. (Cited on page 71.)

[303] B. Henning, X. Lu, T. Melia and H. Murayama, *2, 84, 30, 993, 560, 15456, 11962, 261485, ...: Higher dimension operators in the SM EFT*, *JHEP* **08** (2017) 016 [1512.03433]. (Cited on page 71.)

[304] W. Buchmuller and D. Wyler, *Effective Lagrangian Analysis of New Interactions and Flavor Conservation*, *Nucl. Phys. B* **268** (1986) 621. (Cited on pages 71, 81 and 102.)

[305] B. Grzadkowski, M. Iskrzynski, M. Misiak and J. Rosiek, *Dimension-Six Terms in the Standard Model Lagrangian*, *JHEP* **10** (2010) 085 [1008.4884]. (Cited on pages 71, 72, 81, 102 and 110.)

[306] L. Lehman, *Extending the Standard Model Effective Field Theory with the Complete Set of Dimension-7 Operators*, *Phys. Rev. D* **90** (2014) 125023 [1410.4193]. (Cited on page 71.)

[307] Y. Liao and X.-D. Ma, *Renormalization Group Evolution of Dimension-seven Baryon- and Lepton-number-violating Operators*, *JHEP* **11** (2016) 043 [1607.07309]. (Cited on page 71.)

[308] C. W. Murphy, *Dimension-8 operators in the Standard Model Eective Field Theory*, *JHEP* **10** (2020) 174 [2005.00059]. (Cited on pages 71, 81, 88, 102, 149 and 150.)

[309] H.-L. Li, Z. Ren, J. Shu, M.-L. Xiao, J.-H. Yu and Y.-H. Zheng, *Complete set of dimension-eight operators in the standard model effective field theory*, *Phys. Rev. D* **104** (2021) 015026 [2005.00008]. (Cited on pages 71, 88 and 102.)

[310] E. E. Jenkins, A. V. Manohar and P. Stoffer, *Low-Energy Effective Field Theory below the Electroweak Scale: Operators and Matching*, *JHEP* **03** (2018) 016 [1709.04486]. (Cited on page 73.)

[311] W. Dekens and P. Stoffer, *Low-energy effective field theory below the electroweak scale: matching at one loop*, *JHEP* **10** (2019) 197 [1908.05295]. (Cited on pages 73 and 103.)

[312] S. Hamoudou, J. Kumar and D. London, *Dimension-8 SMEFT matching conditions for the low-energy effective field theory*, *JHEP* **03** (2023) 157 [2207.08856]. (Cited on page 73.)

[313] E. E. Jenkins, A. V. Manohar and P. Stoffer, *Low-Energy Effective Field Theory below the Electroweak Scale: Anomalous Dimensions*, *JHEP* **01** (2018) 084 [1711.05270]. (Cited on page 73.)

[314] S. Davidson, M. Gorbahn and M. Leak, *Majorana neutrino masses in the renormalization group equations for lepton flavor violation*, *Phys. Rev. D* **98** (2018) 095014 [1807.04283]. (Cited on pages 73 and 103.)

[315] E. E. Jenkins, A. V. Manohar and M. Trott, *Renormalization Group Evolution of the Standard Model Dimension Six Operators I: Formalism and lambda Dependence*, *JHEP* **10** (2013) 087 [1308.2627]. (Cited on pages 73, 102 and 103.)

[316] E. E. Jenkins, A. V. Manohar and M. Trott, *Renormalization Group Evolution of the Standard Model Dimension Six Operators II: Yukawa Dependence*, *JHEP* **01** (2014) 035 [1310.4838]. (Cited on pages 73 and 103.)

[317] R. Alonso, E. E. Jenkins, A. V. Manohar and M. Trott, *Renormalization Group Evolution of the Standard Model Dimension Six Operators III: Gauge Coupling Dependence and Phenomenology*, *JHEP* **04** (2014) 159 [1312.2014]. (Cited on pages 73 and 103.)

[318] S. Davidson and M. Gorbahn, *Charged lepton flavor change and nonstandard neutrino interactions*, *Phys. Rev. D* **101** (2020) 015010 [1909.07406]. (Cited on pages 73, 88 and 103.)

[319] L. V. Silva, *Effects of squared four-fermion operators of the Standard Model Effective Field Theory on meson mixing*, 2201.03038. (Cited on pages 73 and 103.)

[320] M. Chala, G. Guedes, M. Ramos and J. Santiago, *Towards the renormalisation of the Standard Model effective field theory to dimension eight: Bosonic interactions I*, *SciPost Phys.* **11** (2021) 065 [2106.05291]. (Cited on pages 73 and 103.)

[321] S. Das Bakshi, M. Chala, A. Díaz-Carmona and G. Guedes, *Towards the renormalisation of the Standard Model effective field theory to dimension eight: bosonic interactions II*, *Eur. Phys. J. Plus* **137** (2022) 973 [2205.03301]. (Cited on page 73.)

[322] S. Davidson, *Completeness and complementarity for $\mu \to e\gamma$ $\mu \to e\bar{e}e$ and $\mu A \to eA$*, *JHEP* **02** (2021) 172 [2010.00317]. (Cited on pages 73, 74, 75, 76, 83, 84, 85, 86, 87, 122, 123, 126, 127, 134 and 152.)

[323] A. Crivellin, S. Davidson, G. M. Pruna and A. Signer, *Renormalisation-group improved analysis of $\mu \to e$ processes in a systematic effective-field-theory approach*, *JHEP* **05** (2017) 117 [1702.03020]. (Cited on pages 75, 80, 86, 87, 91 and 103.)

[324] V. Cirigliano, S. Davidson and Y. Kuno, *Spin-dependent $\mu \to e$ conversion*, *Phys. Lett. B* **771** (2017) 242 [1703.02057]. (Cited on pages 75 and 76.)

[325] S. Davidson, Y. Kuno and A. Saporta, *"Spin-dependent" $\mu \to e$ conversion on light nuclei*, *Eur. Phys. J. C* **78** (2018) 109 [1710.06787]. (Cited on pages 75 and 76.)

[326] S. Davidson, Y. Kuno, Y. Uesaka and M. Yamanaka, *Probing $\mu e \gamma\gamma$ contact interactions with $\mu \to e$ conversion*, *Phys. Rev. D* **102** (2020) 115043 [2007.09612]. (Cited on pages 75 and 89.)

[327] M. Hoferichter, J. Menéndez and F. Noël, *Improved limits on lepton-flavor-violating decays of light pseudoscalars via spin-dependent $\mu \to e$ conversion in nuclei*, 2204.06005. (Cited on page 76.)

[328] S. Davidson, Y. Kuno and M. Yamanaka, *Selecting $\mu \to e$ conversion targets to distinguish lepton flavour-changing operators*, *Phys. Lett. B* **790** (2019) 380 [1810.01884]. (Cited on page 76.)

[329] S. Davidson and A. Saporta, *Constraints on $2\ell 2q$ operators from $\mu - e$ flavour-changing meson decays*, *Phys. Rev. D* **99** (2019) 015032 [1807.10288]. (Cited on pages 76, 84 and 85.)

[330] T. Husek, K. Monsalvez-Pozo and J. Portoles, *Lepton-flavour violation in hadronic tau decays and $\mu - \tau$ conversion in nuclei*, *JHEP* **01** (2021) 059 [2009.10428]. (Cited on page 76.)

[331] M. Bordone, O. Catà and T. Feldmann, *Effective Theory Approach to New Physics with Flavour: General Framework and a Leptoquark Example*, *JHEP* **01** (2020) 067 [1910.02641]. (Cited on page 79.)

[332] T. Huber, E. Lunghi, M. Misiak and D. Wyler, *Electromagnetic logarithms in $\bar{B} \to X_s l^+ l^-$*, *Nucl. Phys. B* **740** (2006) 105 [hep-ph/0512066]. (Cited on page 79.)

[333] S. Herrlich and U. Nierste, *Evanescent operators, scheme dependences and double insertions*, *Nucl. Phys. B* **455** (1995) 39 [hep-ph/9412375]. (Cited on pages 81 and 103.)

[334] G. F. Giudice and O. Lebedev, *Higgs-dependent Yukawa couplings*, *Phys. Lett. B* **665** (2008) 79 [0804.1753]. (Cited on page 82.)

[335] CMS collaboration, *Evidence for Higgs boson decay to a pair of muons*, *JHEP* **01** (2021) 148 [2009.04363]. (Cited on page 83.)

[336] ATLAS collaboration, *A search for the dimuon decay of the Standard Model Higgs boson with the ATLAS detector*, *Phys. Lett. B* **812** (2021) 135980 [2007.07830]. (Cited on page 83.)

[337] CMS collaboration, *Search for lepton flavour violating decays of the Higgs boson to $\mu\tau$ and $e\tau$ in proton-proton collisions at $\sqrt{s} = 13$ TeV*, *JHEP* **06** (2018) 001 [1712.07173]. (Cited on page 83.)

[338] ATLAS collaboration, *Search for lepton-flavour-violating decays of the Higgs and Z bosons with the ATLAS detector*, *Eur. Phys. J. C* **77** (2017) 70 [1604.07730]. (Cited on page 83.)

[339] SINDRUM II collaboration, *A Search for muon to electron conversion in muonic gold*, *Eur. Phys. J. C* **47** (2006) 337. (Cited on pages 85 and 99.)

[340] COMET collaboration, *Conceptual design report for experimental search for lepton flavor violating mu- - e- conversion at sensitivity of 10**(-16) with a slow-extracted bunched proton beam (COMET)*, . (Cited on pages 85 and 99.)

[341] Belle-II collaboration, *The Belle II Physics Book*, *PTEP* **2019** (2019) 123C01 [1808.10567]. (Cited on pages 85, 99 and 111.)

[342] Y. K. et al. (PRISM collaboration), *An Experimental Search for a $\mu \to e$ Conversion at Sensitivity of the Order of $^{-18}$ with a Highly Intense Muon Source: PRISM, J-PARC LOI*, *unpublished* (2006) . (Cited on page 84.)

[343] Y. Farzan and M. Tortola, *Neutrino oscillations and Non-Standard Interactions*, *Front. in Phys.* **6** (2018) 10 [1710.09360]. (Cited on pages 88 and 149.)

[344] M. Ciuchini, E. Franco, L. Reina and L. Silvestrini, *Leading order QCD corrections to b —> s gamma and b —> s g decays in three regularization schemes*, *Nucl. Phys. B* **421** (1994) 41 [hep-ph/9311357]. (Cited on pages 89, 91 and 103.)

[345] A. Czarnecki, W. J. Marciano and A. Vainshtein, *Refinements in electroweak contributions to the muon anomalous magnetic moment*, *Phys. Rev. D* **67** (2003) 073006 [hep-ph/0212229]. (Cited on page 91.)

[346] L. V. Silva, S. Jäger and K. Leslie, *Using dipole processes to constrain the flavour of four-fermion effective interactions*, *PoS* **ICHEP2020** (2021) 434 [2012.05630]. (Cited on pages 91 and 95.)

[347] Q. Qin, Q. Li, C.-D. Lü, F.-S. Yu and S.-H. Zhou, *Charged lepton flavor violating Higgs decays at future e^+e^- colliders*, *Eur. Phys. J. C* **78** (2018) 835 [1711.07243]. (Cited on pages 99, 111 and 133.)

[348] V. Cirigliano, K. Fuyuto, C. Lee, E. Mereghetti and B. Yan, *Charged Lepton Flavor Violation at the EIC*, *JHEP* **03** (2021) 256 [2102.06176]. (Cited on page 99.)

[349] S. M. Etesami, R. Jafari, M. M. Najafabadi and S. Tizchang, *Searching for lepton flavor violating interactions at future electron-positron colliders*, *Phys. Rev. D* **104** (2021) 015034 [2107.00545]. (Cited on page 99.)

[350] M. Chala and A. Titov, *Neutrino masses in the Standard Model effective field theory*, *Phys. Rev. D* **104** (2021) 035002 [2104.08248]. (Cited on page 103.)

[351] R. Kitano, M. Koike and Y. Okada, *Detailed calculation of lepton flavor violating muon electron conversion rate for various nuclei*, *Phys. Rev. D* **66** (2002) 096002 [hep-ph/0203110]. (Cited on pages 103 and 127.)

[352] S. Davidson, $\mu \to e\gamma$ *and matching at* m_W, *Eur. Phys. J. C* **76** (2016) 370 [1601.07166]. (Cited on pages 103 and 152.)

[353] H. Simma, *Equations of motion for effective Lagrangians and penguins in rare B decays*, *Z. Phys. C* **61** (1994) 67 [hep-ph/9307274]. (Cited on page 109.)

[354] T. Hahn, *Generating Feynman diagrams and amplitudes with FeynArts 3*, *Comput. Phys. Commun.* **140** (2001) 418 [hep-ph/0012260]. (Cited on page 115.)

[355] A. Alloul, N. D. Christensen, C. Degrande, C. Duhr and B. Fuks, *FeynRules 2.0 - A complete toolbox for tree-level phenomenology*, *Comput. Phys. Commun.* **185** (2014) 2250 [1310.1921]. (Cited on page 115.)

[356] E. E. Jenkins, A. V. Manohar and M. Trott, *Renormalization Group Evolution of the Standard Model Dimension Six Operators II: Yukawa Dependence*, *JHEP* **01** (2014) 035 [1310.4838]. (Cited on pages 117 and 130.)

[357] J. D. Bjorken, K. D. Lane and S. Weinberg, *The Decay mu -> e + gamma in Models with Neutral Heavy Leptons*, *Phys. Rev. D* **16** (1977) 1474. (Cited on page 121.)

[358] D. Chang, W. S. Hou and W.-Y. Keung, *Two loop contributions of flavor changing neutral Higgs bosons to mu —> e gamma*, *Phys. Rev. D* **48** (1993) 217 [hep-ph/9302267]. (Cited on page 122.)

[359] S. Davidson, *Completeness and complementarity for* $\mu \to e\gamma\mu \to e\bar{e}e$ *and* $\mu A \to eA$, *JHEP* **02** (2021) 172 [2010.00317]. (Cited on page 175.)

[360] D. M. Straub, *flavio: a Python package for flavour and precision phenomenology in the Standard Model and beyond*, 1810.08132. (Cited on pages 127, 129, 173 and 174.)

[361] R.-X. Shi, L.-S. Geng, B. Grinstein, S. Jäger and J. Martin Camalich, *Revisiting the new-physics interpretation of the* $b \to c\tau\nu$ *data*, *JHEP* **12** (2019) 065 [1905.08498]. (Cited on page 129.)

[362] HFLAV collaboration, *Averages of b-hadron, c-hadron, and* τ*-lepton properties as of 2018*, *Eur. Phys. J. C* **81** (2021) 226 [1909.12524]. (Cited on page 129.)

[363] CMS Collaboration collaboration, *Search for lepton-flavor violating decays of the Higgs boson in the* $\mu\tau$ *and* $e\tau$ *final states in proton-proton collisions at* $\sqrt{s} = 13$ TeV, *Phys. Rev. D* **104** (2021) 032013. (Cited on page 133.)

[364] M. Hoferichter, J. Ruiz de Elvira, B. Kubis and U.-G. Meißner, *High-Precision Determination of the Pion-Nucleon* σ *Term from Roy-Steiner Equations*, *Phys. Rev. Lett.* **115** (2015) 092301 [1506.04142]. (Cited on page 143.)

[365] P. Junnarkar and A. Walker-Loud, *Scalar strange content of the nucleon from lattice QCD*, *Phys. Rev. D* **87** (2013) 114510 [1301.1114]. (Cited on page 143.)

[366] BaBar collaboration, *A search for the decay modes $B^{+-} \to h^{+-}\tau^{+-}l$*, *Phys. Rev. D* **86** (2012) 012004 [1204.2852]. (Cited on page 174.)

[367] BaBar collaboration, *Searches for the decays $B^0 \to \ell^{\pm}\tau^{\mp}$ and $B^+ \to \ell^+\nu$ (l=e, μ) using hadronic tag reconstruction*, *Phys. Rev. D* **77** (2008) 091104 [0801.0697]. (Cited on page 174.)

[368] LHCb collaboration, *Search for the lepton-flavour-violating decays $B_s^0 \to \tau^{\pm}\mu^{\mp}$ and $B^0 \to \tau^{\pm}\mu^{\mp}$*, *Phys. Rev. Lett.* **123** (2019) 211801 [1905.06614]. (Cited on page 174.)

[369] Particle Data Group collaboration, *Review of Particle Physics*, *PTEP* **2020** (2020) 083C01. (Cited on page 174.)

[370] Belle collaboration, *A Search for the rare leptonic decays B+ —> mu+ nu(mu) and B+ —> e+ nu(nu)*, *Phys. Lett. B* **647** (2007) 67 [hep-ex/0611045]. (Cited on page 174.)

[371] Belle collaboration, *Search for $B^+ \to \mu^+\nu_\mu$ and $B^+ \to \mu^+ N$ with inclusive tagging*, *Phys. Rev. D* **101** (2020) 032007 [1911.03186]. (Cited on page 174.)